

สารบัญชี้แจงแอลฟาคลูโคไซด์จากอนุพันธ์อะมิโนไซคลิทอลที่มีหมู่แทนที่ตำแหน่งไนโตรเจน
และการสังเคราะห์ CJ-16,264



นางสาววิศุชญญา วรระลัย

จุฬาลงกรณ์มหาวิทยาลัย

CHULALONGKORN UNIVERSITY

บทคัดย่อและแฟ้มข้อมูลฉบับเต็มของวิทยานิพนธ์ตั้งแต่ปีการศึกษา 2554 ที่ให้บริการในคลังปัญญาจุฬาฯ (CUIR)
เป็นแฟ้มข้อมูลของนิสิตเจ้าของวิทยานิพนธ์ ที่ส่งผ่านทางบัณฑิตวิทยาลัย

The abstract and full text of theses from the academic year 2011 in Chulalongkorn University Intellectual Repository (CUIR)
are the thesis authors' files submitted through the University Graduate School.

วิทยานิพนธ์นี้เป็นส่วนหนึ่งของการศึกษาตามหลักสูตรปริญญาวิทยาศาสตรดุษฎีบัณฑิต

สาขาวิชาเคมี ภาควิชาเคมี

คณะวิทยาศาสตร์ จุฬาลงกรณ์มหาวิทยาลัย

ปีการศึกษา 2557

ลิขสิทธิ์ของจุฬาลงกรณ์มหาวิทยาลัย

α -GLUCOSIDASE INHIBITORS FROM *N*-SUBSTITUTED AMINOCYCLITOL DERIVATIVES
AND TOTAL SYNTHESIS OF CJ-16,264

Miss Wisuttaya Worawalai



A Dissertation Submitted in Partial Fulfillment of the Requirements
for the Degree of Doctor of Philosophy Program in Chemistry

Department of Chemistry

Faculty of Science

Chulalongkorn University

Academic Year 2014

Copyright of Chulalongkorn University

Thesis Title	α -GLUCOSIDASE INHIBITORS FROM N-SUBSTITUTED AMINOCYCLITOL DERIVATIVES AND TOTAL SYNTHESIS OF CJ-16,264
By	Miss Wisuttaya Worawalai
Field of Study	Chemistry
Thesis Advisor	Assistant Professor Preecha Phuwapraisirisan, Ph.D.
Thesis Co-Advisor	Assistant Professor Sumrit Wacharasindhu, Ph.D.

Accepted by the Faculty of Science, Chulalongkorn University in Partial Fulfillment of the Requirements for the Doctoral Degree

.....Dean of the Faculty of Science
(Professor Supot Hannongbua, Dr.rer.nat.)

THESIS COMMITTEE

.....Chairman
(Assistant Professor Warinthorn Chavasiri, Ph.D.)

.....Thesis Advisor
(Assistant Professor Preecha Phuwapraisirisan, Ph.D.)

.....Thesis Co-Advisor
(Assistant Professor Sumrit Wacharasindhu, Ph.D.)

.....Examiner
(Assistant Professor Aroonsiri Shitangkoon, Ph.D.)

.....Examiner
(Associate Professor Paitoon Rashatasakhon, Ph.D.)

.....External Examiner
(Professor Apichart Suksamran, Ph.D.)

.....External Examiner
(Poonsakdi Ploypradith, Ph.D.)

.....External Examiner
(Professor Emmanuel Theodorakis, Ph.D.)

วิทยุชญา วรเวทย์ : สารยับยั้งแอลฟาไกลูโคซิเดสจากอนุพันธ์อะมิโนไซคลิทอลที่มีหมู่แทนที่ตำแหน่งไนโตรเจนและการสังเคราะห์ CJ-16,264 (**α** -GLUCOSIDASE INHIBITORS FROM *N*-SUBSTITUTED AMINOCYCLITOL DERIVATIVES AND TOTAL SYNTHESIS OF CJ-16,264) อ.ที่ปรึกษาวิทยานิพนธ์หลัก: ปรีชา ภูวไพโรศิรกาล, อ.ที่ปรึกษาวิทยานิพนธ์ร่วม: สัมฤทธิ์ วัชรสินธุ์, หน้า.

ในงานวิจัยนี้ได้สังเคราะห์สารออกฤทธิ์ยับยั้งเอนไซม์แอลฟาไกลูโคซิเดส คือสารประกอบ *condurotol F* inositols และ อนุพันธ์อะมิโนเคอร์ชิตอล (*N*-substituted aminoquercitols) จากสารตั้งต้น (+)-*proto*-quercitol ซึ่งเป็นสารที่แยกได้จากธรรมชาติ ด้วยความเหมาะสมทางด้านสเตอริโอเคมีของ (+)-*proto*-quercitol นี้ จึงส่งผลให้ปฏิกิริยาการปกป้องหมู่ไฮดรอกซิลของสารประกอบนี้เกิดขึ้นอย่างมีความจำเพาะ ซึ่งจะนำไปสู่การดัดแปรหมู่ฟังก์ชันที่เหลือเป็นผลิตภัณฑ์เป้าหมาย ได้อย่างมีประสิทธิภาพ กล่าวคือ ได้ผลผลิตในปริมาณที่สูง และใช้ขั้นตอนในการสังเคราะห์น้อย จากผลการทดสอบฤทธิ์ยับยั้งเอนไซม์แอลฟาไกลูโคซิเดสของสารสังเคราะห์ทั้งหมดนี้ พบว่าสารประกอบ *condurotol F* มีฤทธิ์ยับยั้งเอนไซม์แอลฟาไกลูโคซิเดสที่มาจากยีสต์ได้ดีที่สุด ด้วยค่า IC_{50} เท่ากับ 86.1 ไมโครโมลาร์ ซึ่งจะมีฤทธิ์ยับยั้งเอนไซม์ได้ดีกว่ายารักษาโรคเบาหวาน acarbose ประมาณ 5 เท่า และในทางตรงกันข้าม อนุพันธ์อะมิโนเคอร์ชิตอล สามารถยับยั้งเอนไซม์แอลฟาไกลูโคซิเดสที่มาจากลำไส้เล็กของหนูได้ดีที่สุด และเมื่อเปรียบเทียบกับสารในกลุ่มนี้ทั้งหมด พบว่าสารประกอบ 5-1 และ 5-9 ซึ่งเป็นสารที่มีโครงสร้างคล้ายกับยารักษาโรคเบาหวาน voglibose นั้น แสดงการออกฤทธิ์ยับยั้งเอนไซม์มอลเตสได้ดีที่สุด

สำหรับการศึกษากลไกการยับยั้งเอนไซม์ชนิดนี้ของอนุพันธ์อะมิโนเคอร์ชิตอล ที่มีฤทธิ์ดีที่สุด พบว่าอนุพันธ์อะมิโนเคอร์ชิตอลเป็นสารยับยั้งแบบแข่งขัน ซึ่งจะแสดงบทบาทในการยับยั้งแบบเดียวกับยารักษาโรคเบาหวาน ซึ่งจากผลดังกล่าวนี้ ทำให้ผู้วิจัยสนใจที่จะศึกษาเกี่ยวกับ molecular docking ต่อเพื่อต้องการทราบในรายละเอียดเกี่ยวกับการจับกันระหว่างอนุพันธ์อะมิโนเคอร์ชิตอลกับเอนไซม์มอลเตสที่บริเวณเร่ง และจากการศึกษาแล้วพบว่า หมู่ไฮดรอกซิลที่อยู่วงไซโคลเฮกเซนและอะตอมของไนโตรเจน สามารถเกิดพันธะไฮโดรเจนกับหมู่อะมิโนของเอนไซม์ได้ นอกจากนี้หมู่อะมิโนของอนุพันธ์อะมิโนเคอร์ชิตอล อาจมีส่วนช่วยในการออกฤทธิ์ยับยั้งเอนไซม์ได้เช่นกัน นอกจากนี้ การศึกษาเกี่ยวกับ 3D-QSAR ของอนุพันธ์อะมิโนเคอร์ชิตอลสามารถสรุปได้ว่า หมู่ที่เมื่อต่อกับอะตอมไนโตรเจนของอนุพันธ์อะมิโนเคอร์ชิตอลแล้วสามารถช่วยเสริมฤทธิ์การยับยั้งเอนไซม์แอลฟาไกลูโคซิเดสได้ดี คือหมู่ที่มีขั้วปานกลางและไม่เกาะเกาะมาก ดังเช่นที่พบในสารประกอบ 5-1 และ 5-9 ดังนั้นสารประกอบชนิดนี้จึงน่าจะมีโอกาสพัฒนาไปเป็นยารักษาโรคเบาหวานได้ในอนาคต

นอกจากนี้ในงานวิจัยนี้ยังได้รายงานเป็นครั้งแรกเกี่ยวกับการสังเคราะห์ (total synthesis) สารประกอบ 1-*epi*-CJ-16,264 ซึ่งเป็นสารธรรมชาติที่มีฤทธิ์ด้านการเจริญเติบโตของเชื้อแบคทีเรีย (antibiotic) โดยใช้สารประกอบ citronellal ซึ่งเป็นสารที่หาซื้อได้ง่าย และราคาถูก ใช้เป็นสารตั้งต้นในการสังเคราะห์ครั้งนี้ ขั้นตอนที่สำคัญในการสังเคราะห์คือการเกิด *cis*-decalin โดยผ่านปฏิกิริยาที่มีความจำเพาะ *exo*-selective IMDA และปฏิกิริยา boron-mediated Reformatsky ส่งผลให้ได้ผลิตภัณฑ์ในปริมาณมาก

ภาควิชา เคมี	ลายมือชื่อนิสิต
สาขาวิชา เคมี	ลายมือชื่อ อ.ที่ปรึกษาหลัก
ปีการศึกษา 2557	ลายมือชื่อ อ.ที่ปรึกษาร่วม

5273855923 : MAJOR CHEMISTRY

KEYWORDS: (+)-PROTO-QUERCITOL / CONDURITOL F / N-SUBSTITUTED AMINOQUERCITOLS / α -GLUCOSIDASE INHIBITORS / TOTAL SYNTHESIS / CJ-16,264

WISUTTAYA WORAWALAI: α -GLUCOSIDASE INHIBITORS FROM N-SUBSTITUTED AMINOCYCLITOL DERIVATIVES AND TOTAL SYNTHESIS OF CJ-16,264. ADVISOR: ASST. PROF. PREECHA PHUWAPRAIRISAN, Ph.D., CO-ADVISOR: ASST. PROF. SUMRIT WACHARASINDHU, Ph.D., pp.

An efficient synthesis of α -glucosidase inhibitors; conduritol and its analogues, and *N*-substituted aminoquercitols, from naturally available (+)-*proto*-quercitol was investigated. Proper configuration of (+)-*proto*-quercitol perfectly set up for regioselective protection of hydroxyl group which was further functionalized into various α -glucosidase inhibitors in a straightforward manner. This synthetic method provided a concise synthesis of α -glucosidase inhibitors in a large quantity. From this investigation, over 40 new *N*-substituted aminoquercitols and conduritol analogues were synthesized. Among them, (+)-conduritol F was the most potent type I α -glucosidase inhibitor with an IC_{50} value of 86.1 μ M, which is five times greater than the standard antidiabetic drug, Acarbose. On the other hand, a series of *N*-substituted aminoquercitols showed highly improved inhibition against rat intestinal maltase (type II α -glucosidase). Of all synthesized compounds, 5-1 and 5-9 were the most active inhibitors against rat intestinal maltase, which had potency similar to the most effective antidiabetic drug, Voglibose. Kinetic study of *N*-substituted aminoquercitols indicated that they retarded maltase function in a competitive manner. A molecular docking study suggested that the hydrogen bonding, from hydroxyl groups at aminoquercitol moiety and *N*-alkyl side chain with the key residues in the rat maltase active site, played an important role in molecular interactions. In addition, the -NH group might also form the hydrogen bond within the active site of enzyme. 3D-QSAR study emphasized structural features around *N*-substituted part of aminoquercitol derivatives as the α -glucosidase inhibitory activity. The resulting contour maps from the 3D-QSAR models provide a good insight into the molecular features relevant to the biological activity for this series, suggesting that the less steric and hydrophilic groups at *N*-position of aminoquercitol could increase activity. This is the first report on molecular docking and 3D-QSAR modeling for a series of *N*-substituted aminoquercitols toward the modeled rat intestinal maltase. Compounds 5-1 and 5-9 therefore represent a new class of promising compounds that can improve α -glucosidase inhibitory activity.

Moreover, the diastereoselective total synthesis of antibiotic CJ-16,264 analogue (1-*epi*-CJ-16,264) has been completed in 18 steps from commercially available citronellal. The key steps involved an *exo*-selective IMDA reaction of macrolactone to furnish the *cis*-decalin scaffold and boron-mediated Reformatsky reaction affording the full CJ-16,264 skeleton in high yield with exquisite stereoselectivity.

Department: Chemistry

Field of Study: Chemistry

Academic Year: 2014

Student's Signature

Advisor's Signature

Co-Advisor's Signature

ACKNOWLEDGEMENTS

I wish to express my deep gratitude to my advisor, Assistant Professor Dr. Preecha Phuwapraisirisan and co-advisor, Assistant Professor Dr. Sumrit Wacharasindhu for their generous assistance, kind guidance and encouragement throughout the course of this research.

My appreciation is also expressed to Professor Dr. Emmanuel A. Theodorakis for welcoming me into his laboratory, for his benevolent assistance, guidance, and unconditional support that I have received during my internship at University of California, San Diego.

I also would like to sincerely thank Associate Professor Dr. Pornthep Sompornpisut for his kind assistance, advice, and for all of his tireless efforts in computational study.

I would like to gratefully acknowledge the committees, Assistant Professor Dr. Warinthorn Chavasiri, Assistant Professor Dr. Aroonsiri Shitangkoon, Associate Professor Dr. Paitoon Rashatasakhon, Professor Dr. Apichart Suksamram and Dr. Poonsakdi Ploypradith for their comments, guidance and extending cooperation over my presentation.

I would like to express my gratitude to Natural Products Research Unit, Department of Chemistry, Faculty of Science, Chulalongkorn University for providing the chemicals and facilities throughout the course of study.

A deep affectionate gratitude is acknowledged to my family for their understanding, encouragement and support throughout the education course and I would like to give special thanks to Dr. Henry Korman, Dr. Oraphin Chantarasriwong, Dr. Jirapast Sichaem, Dr. Jing Xu, Michelle Lacoske, Celso Rezende, and Mr. Eakkaphon Rattanangkool for their technical assistance and for all of the unforgettable memories. Moreover, I would like to thank all of my friends in the laboratory for their friendships and help during the course of my graduate research.

CONTENTS

	Page
THAI ABSTRACT	iv
ENGLISH ABSTRACT	v
ACKNOWLEDGEMENTS	vi
CONTENTS	vii
LIST OF TABLES	xi
LIST OF FIGURES	xii
LIST OF SCHEMES	xv
LIST OF ABBREVIATIONS	xvii
CHAPTER I INTRODUCTION.....	1
1.1 Diabetes mellitus (DM).....	1
1.2 α -Glucosidase inhibitors	3
1.3 Synthesis of α -glucosidase inhibitors.....	7
1.3.1 Synthesis of conduritols and their analogues	7
1.3.2 Synthesis of aminocyclitol derivatives	11
CHAPTER II CONCISE SYNTHESIS OF (+)-CONDURITOL F AND INOSITOL ANALOGUES FROM NATURALLY AVAILABLE (+)- <i>proto</i> -QUERCITOL AND THEIR GLUCOSIDASE INHIBITORY ACTIVITY	20
2.1 Improvement for extraction and isolation of (+)- <i>proto</i> -quercitol	20
2.2 Synthesis of conduritol F and inositols.....	21
2.3 α -Glucosidase inhibitory effect	23
2.4 Conclusion.....	24
2.5 Experimental section	25
2.5.1 General experimental procedures	25

	Page
2.5.2 Plant material.....	25
2.5.3 Isolation of (+)- <i>proto</i> -quercitol (1-47)	25
2.5.4 Synthesis of (+)-conduritol F and inositols	26
2.5.5 α -Glucosidase inhibition assay.....	29
2.5.5.1 Chemicals and equipment.....	29
2.5.5.2 Procedure	29
CHAPTER III SYNTHESIS OF NEW <i>N</i> -SUBSTITUTED AMINOQUERCITOLS FROM NATURALLY AVAILABLE (+)- <i>proto</i> -QUERCITOL AND THEIR α -GLUCOSIDASE INHIBITORY ACTIVITY	32
3.1 Synthesis of <i>N</i> -substituted aminoquercitols	32
3.2 α -Glucosidase inhibitory activity of <i>N</i> -substituted aminoquercitols	35
3.3 Kinetic study and a possible mechanism underlying the maltase inhibition of <i>N</i> -substituted aminoquercitols.....	38
3.4 Conclusion.....	40
3.5 Experimental section	41
3.5.1 General experimental procedures	41
3.5.2 Synthesis of <i>N</i> -acyl aminoquercitols	41
3.5.3 Synthesis of <i>N</i> -alkyl aminoquercitols	46
3.5.3.1 General procedure for reductive amination.....	46
3.5.3.2 General procedure for deprotection.....	53
3.5.4 α -Glucosidase inhibition assay.....	59
3.5.5 Measurement of kinetic constants.....	60
CHAPTER IV AMINE-LINKED DIQUERCITOLS AS NEW α -GLUCOSIDASE INHIBITORS	61
4.1 Synthesis of amine-linked diquercitols	62

	Page
4.2 α -Glucosidase inhibitory activity.....	67
4.3 Conclusion.....	68
4.4 Experimental section	69
4.4.1 General experimental procedures	69
4.4.2 Synthesis of amine-linked diquercitols	69
4.4.2.1 General procedure for reductive amination.....	69
4.4.3 α -Glucosidase inhibition assay.....	71
CHAPTER V NEW α -GLUCOSIDASE INHIBITORS FROM NATURALLY AVAILABLE (+)- <i>proto</i> -QUERCITOL: SYNTHESIS, KINETIC AND COMPUTATIONAL PREDICTION.....	72
5.1 Synthesis of <i>N</i> -substituted aminoquercitols and voglibose-like compounds	72
5.2 α -Glucosidase inhibitory activity and kinetic analysis	76
5.3 Molecular docking of synthesized compounds with rat intestinal maltase.....	80
5.4 3D-QSAR analysis	85
5.5 Conclusion.....	90
5.6 Experimental section	91
5.6.1 General experimental procedures	91
5.6.2 Synthesis of <i>N</i> -substituted aminoquercitols	91
5.6.2.1 General procedure for reductive amination.....	91
5.6.2.2 General procedure for deprotection of all synthesized compounds	99
5.6.3 α -Glucosidase inhibition assay.....	104
5.6.4 Measurement of kinetic constant	104
5.6.5 Homology modeling and validation.....	104

	Page
5.6.6 Molecular docking.....	105
5.6.7 3D-QSAR Models.....	105
CHAPTER VI DIASTEREOSELECTIVE TOTAL SYNTHESIS OF CJ-16,264 ANALOGUES.....	107
6.1 Introduction	107
6.1.1 Isolation and biological activity of pyrrolizidinones.....	107
6.1.2 Synthetic strategies towards pyrrolizidinones	109
6.2 Total synthesis of CJ-16,264 analogues	112
6.2.1 Retrosynthesis of CJ-16,264 diastereomers (6-1a).....	112
6.2.2 Synthesis of racemic tricyclic iodolactone (6-9)	113
6.2.3 Synthesis of the key intermediate seco-acid (\pm)-6-24	114
6.2.4 Macrocyclization optimization.....	115
6.2.5 Synthesis of decalin aldehyde (\pm)-6-10	118
6.2.6 Studies toward completion of the synthesis of CJ-16,264 analogues ...	120
6.3 Conclusion.....	124
6.4 Experimental section	124
6.4.1 General experimental procedures.....	124
6.4.2 Total synthesis of CJ-16,264 analogues.....	125
CHAPTER VII CONCLUSION	137
REFERENCES	141
APPENDIX.....	149
VITA.....	241

LIST OF TABLES

Table	Page
2.1 α -Glucosidase inhibitory effect of cyclitols 1-47 , 2-4 , 2-6a , and 2-6b	24
3.2 α -Glucosidase inhibitory effect of <i>N</i> -substituted aminoquercitols.....	36
3.3 Inhibitory effect against rat intestinal maltase and kinetic parameters of 3-6 , 3-34 , 3-40	40
4.1 α -Glucosidase inhibitory effect of synthesized compounds	68
5.1 Reaction conditions and yields for reductive amination	74
5.2 α -Glucosidase inhibitory effect of <i>N</i> -substituted aminoquercitols.....	77
5.3 IC_{50} and K_i values of 5-9	80
5.4 IC_{50} , and Vina docking scores of synthesized compounds with rat maltase	84
5.5 Statistical results of CoMFA and CoMSIA models	86
5.6 Experimental and predicted activities of the test set.....	87
6.1 Study of HWE cyclization of (±)-6-41	117
6.2 Study of macrolactonization of seco acid (±)-6-24	118

LIST OF FIGURES

Figure	Page
1.1	Insulin signaling in peripheral cells..... 1
1.2	Causes of diabetes: insufficient insulin for type 1 DM and insulin resistant for type 2 DM..... 2
1.3	Digestion of starch in the small intestine by α -glucosidase enzyme. 4
1.4	Transition states of (a) natural substrate and the corresponding potent transition state-analogue inhibitors (b) miglitol and (c) conduritols, with α -glucosidase at the active site. 6
1.5	Structures of digestive α -glucosidase inhibitors. 7
1.6	Structures of certain natural cyclitols..... 8
1.7	Structures of conduritols..... 9
1.8	Structures of isomeric inositols..... 9
1.9	Structures of natural aminocyclitols..... 12
3.1	Inhibition trends of selected <i>N</i> -acyl (3-4 – 3-7 and 3-9 – 3-12) and <i>N</i> -alkyl (3-29 – 3-32 and 3-33 – 3-36) aminoquercitols against rat intestinal maltase..... 37
3.2	Lineweaver-Burk plots for inhibitory activity against rat intestinal maltase. (a) <i>N</i> -acyl aminoquercitol 3-6 , (b) <i>N</i> -alkyl aminoquercitol 3-34 , (c) <i>N,N</i> -dialkyl aminoquercitol 3-40 and (d) secondary replots of slope vs. [I] from a primary Lineweaver-Burk plot for the determination of K_i 39
4.1	Structures of <i>N</i> -linked dicyclitols..... 61
4.2	Partial ^1H NMR spectra of 4-4 and 4-6 (CDCl_3) focusing on signals of methylene protons ($\text{H}_2\text{-6}$ and $\text{H}_2\text{-6}'$)..... 66

Figure	Page
5.1 (a) Preparation of oxazolidinone derivative 5-25 ; (b) Selected NOESY correlations of 5-25	76
5.2 Lineweaver-Burk plots for inhibitory activity of 5-9 against rat intestinal: (a) maltase; (b) sucrase. Inset: secondary replots of slope vs. $[I]$ from a primary Lineweaver-Burk plot for the determination of K_i	79
5.3 (a) Homology model of the rat intestinal N-terminal domain of maltase-glucoamylase (rat-ntMGAM) and (b) Structural superimposition between the crystal and docked miglitol (RMSD = 0.48 Å). The figure also shows the conserved residues important for the binding of the inhibitor in the active site of rat-ntMGAM and hu-ntMGAM (number in parentheses). The dashed lines illustrate atom pairs within hydrogen bond distances.....	81
5.4 (a) The superimposed lowest energy conformations of all ligands (5-1 , 5-9 , 5-13 – 5-22 , and 5-24) obtained by docking at active site of the modeled rat intestinal maltase. Interactions of amino acid residues with (b) 5-9 and (c) the superimposition of 5-20 , 5-21 , and 5-22 . The surrounding conserved residues and ligand molecules are in stick representation. Hydrogen bonds are depicted by dashed lines.	83
5.5 Plots between the experimental and predicted biological activities of training (filled square) and test set (filled circle): (a) CoMFA plot and (b) CoMSIA plot.....	86
5.6 The stdev* coeff. contour maps. (a) and (b) represent CoMFA steric and electrostatic, respectively. (c) to (g) represent CoMSIA steric, electrostatic, hydrophobic, hydrogen bond donor, and hydrogen bond acceptor, respectively. Steric field is represented by green and yellow contour maps. Electrostatic field is represented by blue and red contour maps. Hydrophobic field is represented by yellow and white contour maps. Hydrogen bond donor field is represented by cyan and purple contour maps. Hydrogen bond acceptor field is represented by magenta and red	

Figure	Page
contour maps. All the contours represented the default 80% and 20% level contributions for favorable and unfavorable regions, respectively.	89
6.1 Structures of pyrrolizidinone antibiotics CJ-16,264, UCS1025A, and UCS1025B	109
6.2 Reformatsky-type approach to 6-2 by Danishefsky.	110
6.3 Hoye's approach to (±)-6-2	110
6.4 Possible true structures of CJ-16,264.	112
6.5 Selected NOESY correlations of (±)-6-30 . For clarity, certain H atoms are omitted.	120
6.6 Possible structures of products from Reformatsky reaction.	121



LIST OF SCHEMES

Scheme	Page
1.1	Synthesis of conduritols C and E and <i>neo</i> -inositol from bromobenzene. 11
1.2	Synthesis of valioline from (-)-quinic acid..... 13
1.3	Synthesis of valienamine from <i>myo</i> -inositol..... 14
1.4	Synthesis of aminocyclitol 1-35 from (-)- <i>vibo</i> -quercitol..... 15
1.5	Preparation of <i>N</i> -benzylated valienamines from their parent valienamine. 17
1.6	Synthesis of sugar-amines 1-44a – 1-44e 17
1.7	Synthesis of sugar-amides 1-46a – 1-46e 18
2.1	Comparison of the isolation procedure of (+)- <i>proto</i> -quercitol from the stems of <i>Arfeuillea arborescens</i> between a) previous [36] and b) present procedure. 20
2.2	Synthesis of 2-2 21
2.3	Synthesis of (+)-conduritol F (2-4)..... 22
2.4	Synthesis of inositols 2-6a and 2-6b 23
2.5	Hydrolysis by yeast α -glucosidase..... 29
2.6	Hydrolysis of rat intestinal α -glucosidase 30
3.1	Synthesis of <i>N</i> -acyl aminoquercitols..... 33
3.2	Synthesis of <i>N</i> -alkyl aminoquercitols..... 35
4.1	Synthetic strategy of target amine-liked diquercitols (4-5 and 4-7)..... 62
4.2	Synthesis of aminoquercitols 3-1a and 3-2a . <i>Reagents and conditions</i> : (a) Me ₂ C(OMe) ₂ , DMF, <i>p</i> -TsOH; (b) MeSO ₂ Cl, Et ₃ N, DMAP; (c) NaN ₃ , DMF, 15-crown-5-ether, 100 °C; (d) LiAlH ₄ ; (e) Ac ₂ O, DMSO; (f) TFA, THF..... 63
4.3	Synthesis of 4-5 64

Scheme	Page
4.4	Synthesis of 4-7 65
4.5	Proposed mechanistic formations of 4-5 and 4-7 67
5.1	Synthesis of <i>N</i> -substituted aminoquercitols..... 75
5.2	Synthesis of 5-24 75
6.1	Synthetic strategy of target CJ-16,264 analogues (6-1a)..... 113
6.2	Synthesis of racemic tricyclic iodolactone (6-9)..... 114
6.3	Synthesis of seco-acid (±)- 6-24 115
6.4	Preparation of phosphonate aldehyde (±)- 6-41 116
6.5	Synthesis of decalin aldehyde (±)- 6-10 119
6.6	BET ₃ mediated Reformatsky-type coupling of (±)- 6-9 and (±)- 6-10 120
6.7	Completion for the synthesis of 6-1a 122
6.8	Preparation of (±)- 6-36 from (±)- 6-33 123

LIST OF ABBREVIATIONS

acetone- d_6	deuterated acetone
brd	broad doublet (NMR)
brs	broad singlet (NMR)
calcd	calculated
^{13}C NMR	carbon-13 nuclear magnetic resonance
CDCl_3	deuterated chloroform
CD_3OD	deuterated methanol
COSY	correlated spectroscopy
CoMFA	comparative molecular field analysis
CoMSIA	comparative molecular similarity indices analysis
D_2O	deuterium oxide
DMF	<i>N,N</i> -dimethylformamide
DMAP	4-(dimethylamino)pyridine
DM	diabetes mellitus
ddd	doublet of doublet of doublet (NMR)
dt	doublet of triplet (NMR)
d	doublet (NMR)
dd	doublet of doublet (NMR)
2D NMR	two dimensional nuclear magnetic resonance
1D NMR	one dimensional nuclear magnetic resonance
ESIMS	electrospray ionization mass spectrometry
equiv	equivalent (s)

GLUT-4	glucose transporter 4
g	gram (s)
^1H NMR	proton nuclear magnetic resonance
Hz	Hertz
HRESIMS	high resolution electrospray ionization mass spectrum
HIV	human immunodeficiency virus
h	hour (s)
IC50	concentration that required for 50% inhibition in vitro
IDDM	insulin-dependent diabetes mellitus
J	coupling constant
mg	milligram (s)
mL	milliliter (s)
mmol	millimole (s)
m/z	mass per charge
m	multiplet (NMR)
MsCl	mesyl chloride
M.W.	molecular weight
M	molar
NIDDM	non-insulin-dependent diabetes mellitus
PNP-G	<i>p</i> -nitrophenyl- α -D-glucopyranoside
PLS	partial least squares
rt	room temperature
s	singlet (NMR)
TFA	trifluoroacetic acid

THF	tetrahydrofuran
TMS	tetramethylsilane
TsOH	<i>p</i> -toluenesulfonic acid
TLC	thin layer chromatography
U	unit
UV	ultraviolet
δ	chemical shift
δ_C	chemical shift of carbon
δ_H	chemical shift of proton
$^{\circ}\text{C}$	degree Celsius
ν_{max}	maximum wave number
μL	microliter (s)
μM	micromolar (s)
% yield	percentage yield
$[\alpha]_D$	specific optical rotation

CHAPTER I

INTRODUCTION

1.1 Diabetes mellitus (DM)

Diabetes mellitus is a syndrome consisting of metabolic, vascular, and neuropathic components that are interrelated. It actually is a group of metabolic diseases characterized by hyperglycemia arising as a consequence of a relative or absolute deficiency of insulin secretion, resistance to insulin action, or both [1].

Insulin is a hormone produced by the pancreas. It is secreted directly into the bloodstream to regulate the sugar (glucose) levels in the body. When the person eats or drinks, food is digested into glucose, which is absorbed into the bloodstream and stimulates the pancreas to produce insulin. Thus, glucose is transported into the cells when insulin binds to insulin receptor, which straddles the cell membrane of many cells (Figure 1.1) [2].

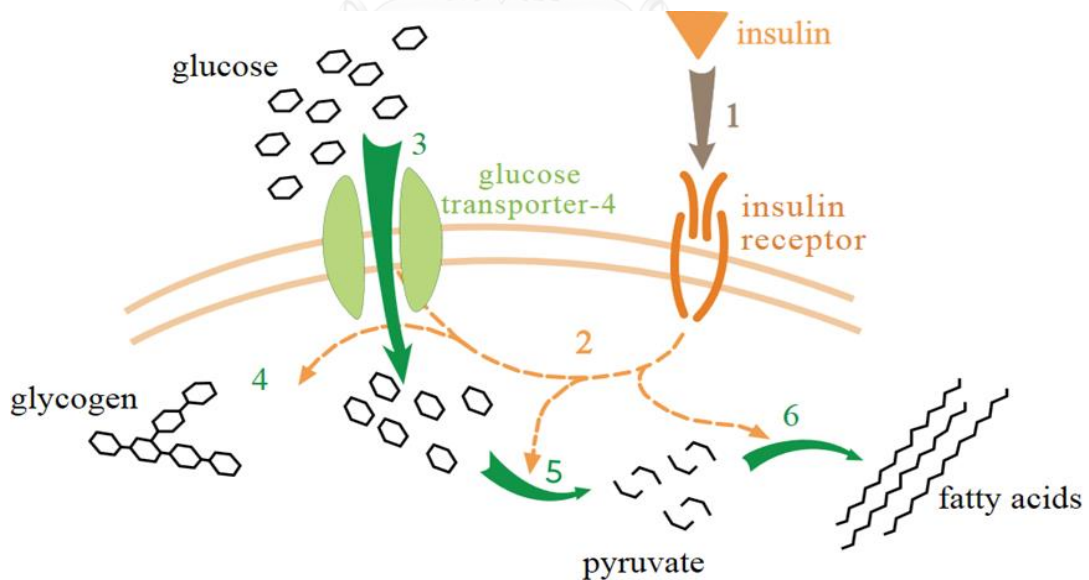


Figure 1.1 Insulin signaling in peripheral cells [2].

The lack of effective insulin action leads to alterations of carbohydrate, fat, and protein metabolism. As the chronic hyperglycemia of diabetes, diabetic patients may suffer from the tragic ravages of long-term damage, dysfunction, and failure of

various organs, especially eyes, kidneys, nerves, heart, and blood vessels. Although several pathogenic processes may be involved in the development of diabetes, the vast majority of cases are classified into two main categories: type 1 and type 2 diabetes, as illustrated in Figure 1.2 [3].

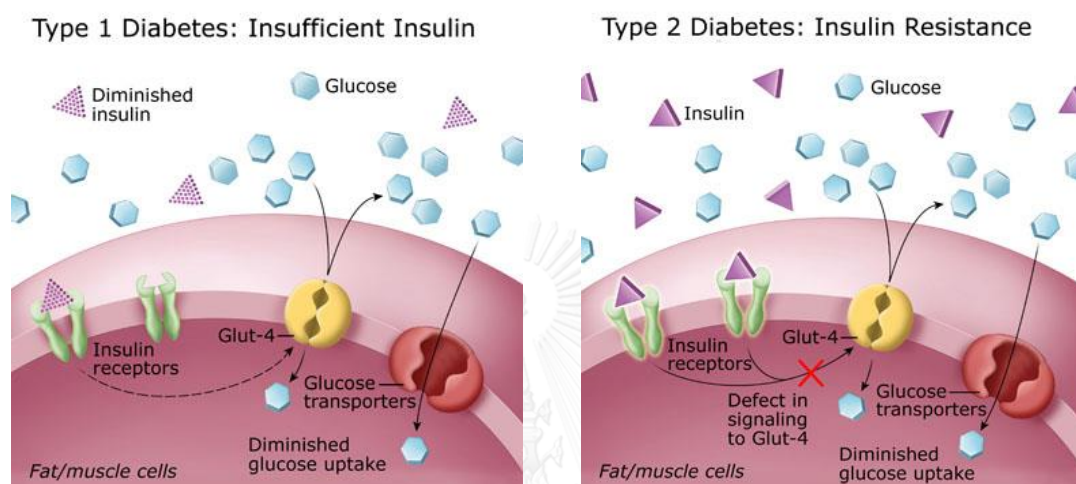


Figure 1.2 Causes of diabetes: insufficient insulin for type 1 DM and insulin resistant for type 2 DM (www.dtc.ucsf.edu/types-of-diabetes).

Type 1 DM is characterized by the loss of insulin-secreting capacity due to selective autoimmune destruction of the pancreatic β -cells, leading to a deficiency of insulin (Figure 1.2). Without the presence of insulin, many of the body's cells cannot take glucose from the blood and therefore the body uses other sources of energy. This type of DM comprises approximately 5% to 10% of all people with DM. People with type 1 DM require insulin injection to compensate for their body's lack of insulin [4].

Type 2 DM, the more common type, is characterized by a relative insulin deficiency and is associated with insulin resistance in the peripheral tissues (Figure 1.2). As a result, the body is less able to take up glucose from the blood, causing hyperglycemia as well as vascular, nerve and renal complications. This type of DM comprises approximately 90% to 95% of all diabetes patients. It usually occurs in

adult, in addition to young people. In all probability, the causes of type 2 DM lie in environmental and lifestyle factors. Prominence among these factors is obesity, and approximately 50% to 90% of all patients with type 2 DM are obese [5]. Recently, the prevalence of type 2 DM throughout the world is increasing at an alarming rate. There are over 173 million people worldwide with type 2 DM. The main complications of type 2 DM are associated with the cardiovascular disease, resulting in excess morbidity and mortality [6, 7].

There are several approaches for treatment of type 2 DM. Each approach works in different ways to lower blood glucose levels. In the early stages, many people with type 2 DM can control their blood glucose levels by diet, exercise, and weight loss. Most importantly, an efficient therapeutic approach for treatment of type 2 DM is to delay the postprandial hyperglycemia by retarding the rate of carbohydrate digestion through the inhibition of α -glucosidase [8].

1.2 α -Glucosidase inhibitors

α -Glucosidases (isomaltase, maltase, and sucrase), spreading in the brush border of the small intestine, are the glycoside hydrolases which selectively hydrolyses α -1,4-glycosidic bond of starch to glucose (Figure 1.3). The mechanism of enzymatic glycoside hydrolysis occurs via transition state which involved the formation of oxocarbenium ion [9-11] (Figure 1.4a). Inhibition of these enzymes by α -glucosidase inhibitors retards the rate of carbohydrates digestion and delays glucose absorption, resulting in the lower blood glucose levels.

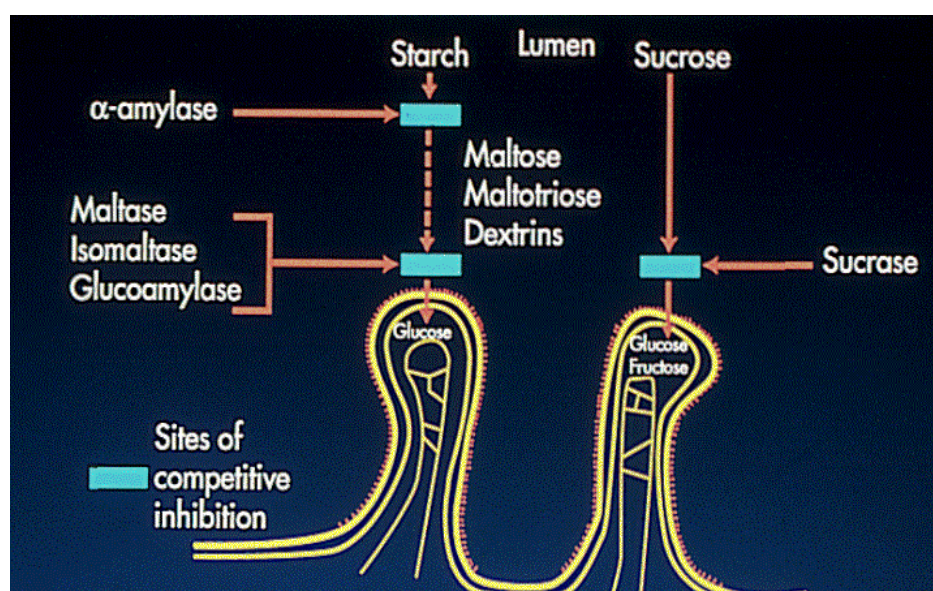
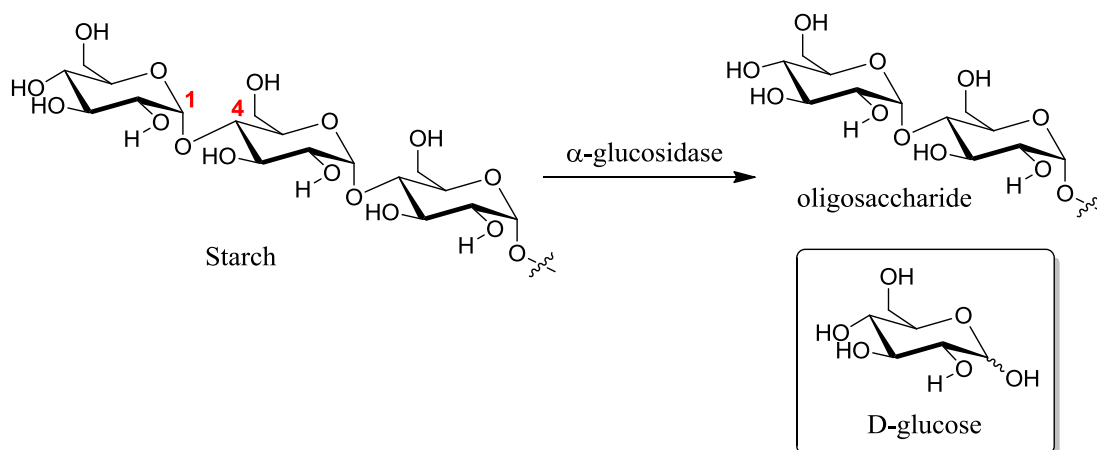


Figure 1.3 Digestion of starch in the small intestine by α -glucosidase enzyme [11].

α -Glucosidase inhibitors are a class of oral antidiabetic agents that have been utilized for the treatment of type 2 diabetes and associated complications for about 20 years. Currently three drugs (acarbose, miglitol, and voglibose) belonging to this category are in the market and have shown effective clinical use [12]. Moreover, the α -glucosidase inhibitors not only reduced blood glucose levels, but also showed antiviral, anticancer and anti-HIV activity [13].

Acarbose (Precose[®] or Glucobay[®], **1-1**) (Figure 1.5), a prominent α -glucosidase inhibitor, is a pseudotetrasaccharide containing a 4-amino-4,6-dideoxy-glucose unit connected with two glucose residues (forming maltose), which was first isolated from

soil bacteria *Actinoplanes* sp [14]. Acarbose is a strong competitive inhibitor against α -glucosidase. It was effective in carbohydrate loading tests in rats and healthy volunteer, reducing postprandial blood glucose and increasing insulin secretion [11].

1-Deoxynojirimycin (DNJ, **1-2**) was isolated from the roots of mulberry tree [15]. Despite the excellent α -glucosidase inhibitory activity in vitro, its efficacy in vivo was only moderate. Therefore, a large number of DNJ derivatives were prepared in the expectation of increasing the in vivo activity. Thus, miglitol (Glyset[®], **1-3**) was discovered as the effective inhibitor in an *in vivo* model, which showed reducing postprandial blood glucose levels.

Voglibose (Basen[®], **1-4**), which has a high inhibitory activity against sucrase and maltase, has been employed in Japan for the treatment of diabetes since 1994. It was synthesized from valioline (1-5) via reductive amination with dihydroxy acetone. In current studies based on α -glucosidase inhibitory activity, it showed 20 to 30 times higher potency than acarbose [11].

From a structural point of view, most of antidiabetic drugs are a group of aminocyclitols or carbasugars [16]. The inhibitory effect of antidiabetic drugs (aminocyclitols) revealed that the carbohydrate mimics containing nitrogen are protonated in the active site and act as glycoside inhibitors because of their ability to mimic the shape or charge of the presumed transition state for enzymatic glycoside hydrolysis [11, 17] (Figure 1.4b). In addition, conduritols, other kinds of carbasugars having cyclohexene moiety, can also inhibit the enzyme by mimicking a half-chair conformation of the substrate [11] (Figure 1.4c). As mentioned above, α -glucosidase inhibitors therefore displayed competitive inhibition.

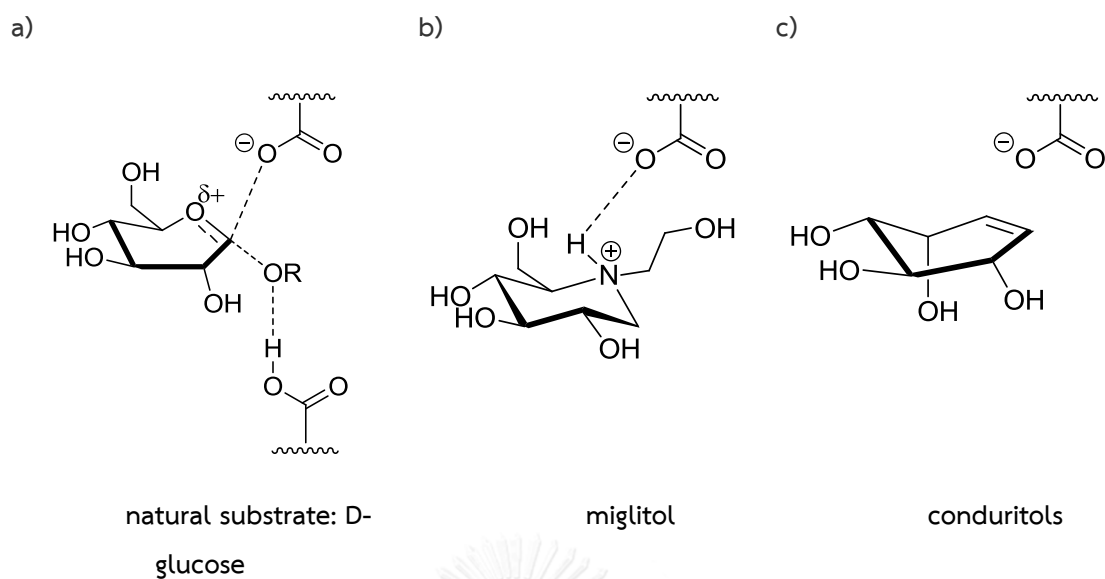


Figure 1.4 Transition states of (a) natural substrate and the corresponding potent transition state-analogue inhibitors (b) miglitol and (c) conduritols, with α -glucosidase at the active site.

To date, α -glucosidase inhibitors are attractive target compounds because of their therapeutic potential in the treatment of a variety of carbohydrate-mediated diseases such as cancer, viral infection, diabetes, etc [18]. Of the several α -glucosidase inhibitors, groups of conduritols and aminocyclitols have been studied intensively in the design and synthesis for the enhancement of their α -glucosidase inhibitory activity [19, 20].

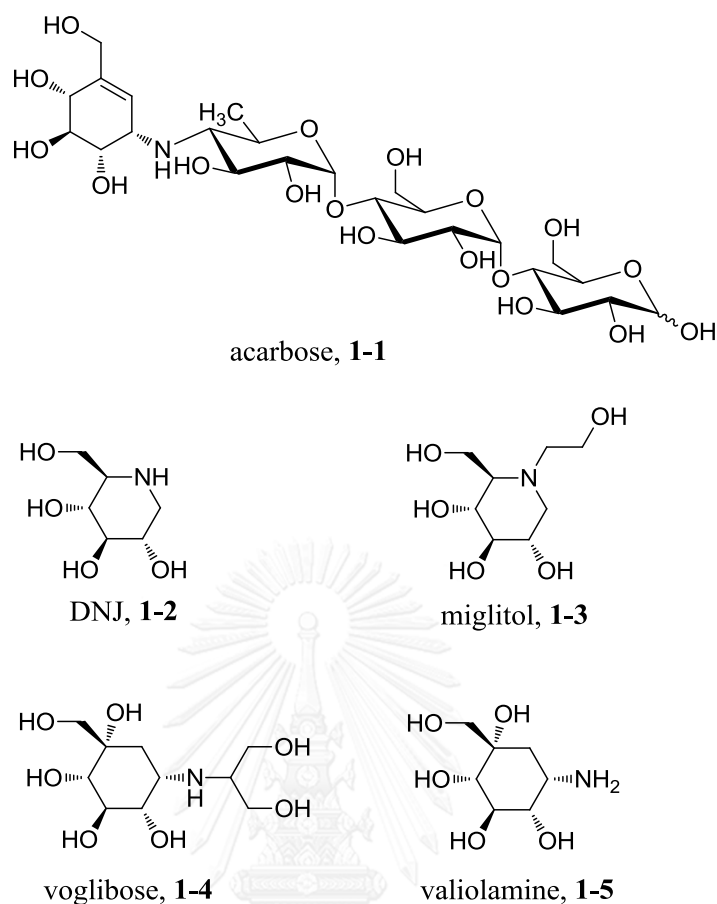


Figure 1.5 Structures of digestive α -glucosidase inhibitors.

1.3 Synthesis of α -glucosidase inhibitors

1.3.1 Synthesis of conduritols and their analogues

Cyclitols are defined as polyhydroxy-substituted cycloalkenes or cycloalkanes that are classified into four major groups, namely conduritols, quercitols, inositols, and quinic acids [20] (Figure 1.6). Cyclitols have attracted considerable attention from the synthetic community because of their significant biological properties. For example, narciclasine is an amino conduritol derivative which is a potential antitumor agent [21]. Bromoconduritol-B potentially inhibit several glucosidase enzymes [22]. *myo*-Inositol is an ingredient in food supplements [23] (Figure 1.6).

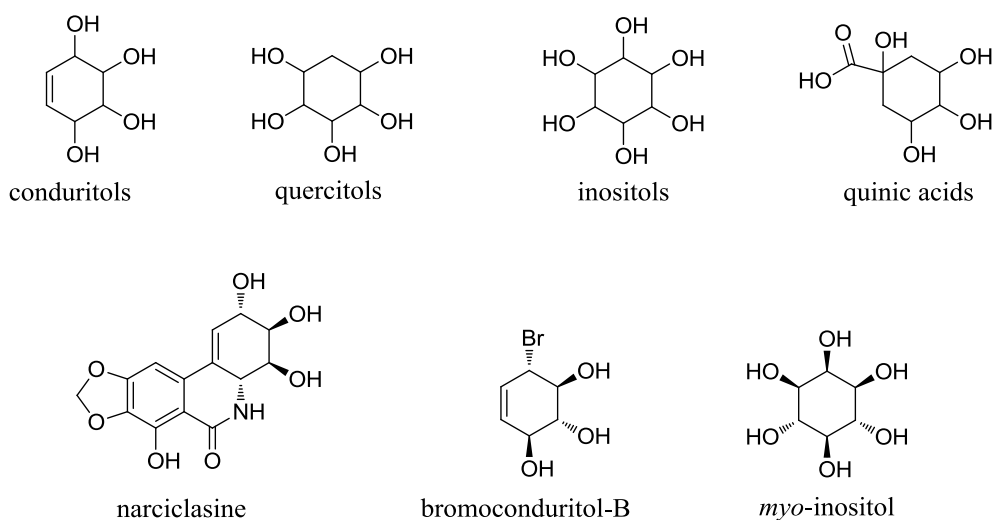


Figure 1.6 Structures of certain natural cyclitols.

Conduritols were first isolated in 1908 from the bark of *Marsdenia condurango* [24]. They are cyclitol derivatives possessing four contiguous hydroxyl groups on the cyclohexene ring (Figure 1.7). The presence of four stereogenic C-atoms allows them to exist in six different configurations. There are ten possible stereoisomers; four enantiomeric pairs (conduritols B, C, E and F) and two meso-forms (conduritols A and D).

Inositols are a group of cyclitols, in which cyclohexane ring is fully substituted by six hydroxyl groups. There are nine possible isomers. Five are known as naturally occurring inositols namely *myo*-, *chiro*-, *scyllo*-, *muco*-, and *neo*-inositols and the unnaturally occurring isomers are *cis*-, *epi*-, and *allo*-inositols (Figure 1.8).

Interest in conduritols and their analogues have been amplified due to synthetic challenge and the presence of a variety of biological activities such as antifeedant, antibiotics, antileukemics and growth-regulation. Currently, as a vital motif in potent anticancer narciclasine and antidiabetic conduritol A, facile and efficient synthetic approaches have been developed to produce optically pure conduritols in a large quantity [25]. Many syntheses of conduritols and their analogues, particularly inositols, were described in current literatures [20, 26]; in

which bromobenzenes have always been utilized as starting material. Particular syntheses of conduritols and inositols are summarized in Scheme 1.1.

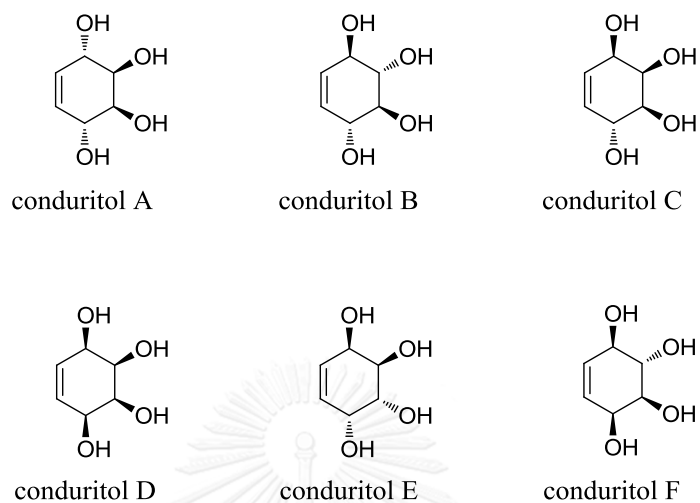


Figure 1.7 Structures of conduritols.

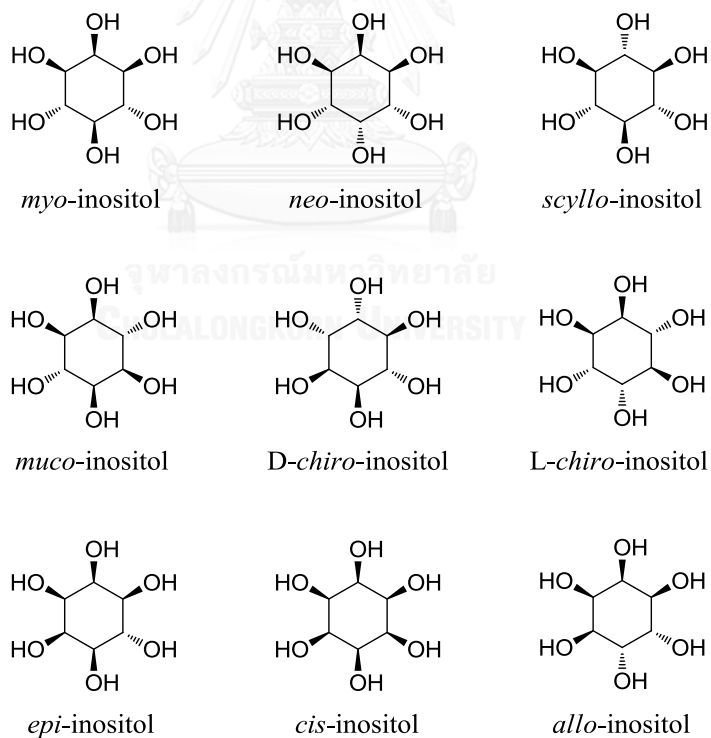
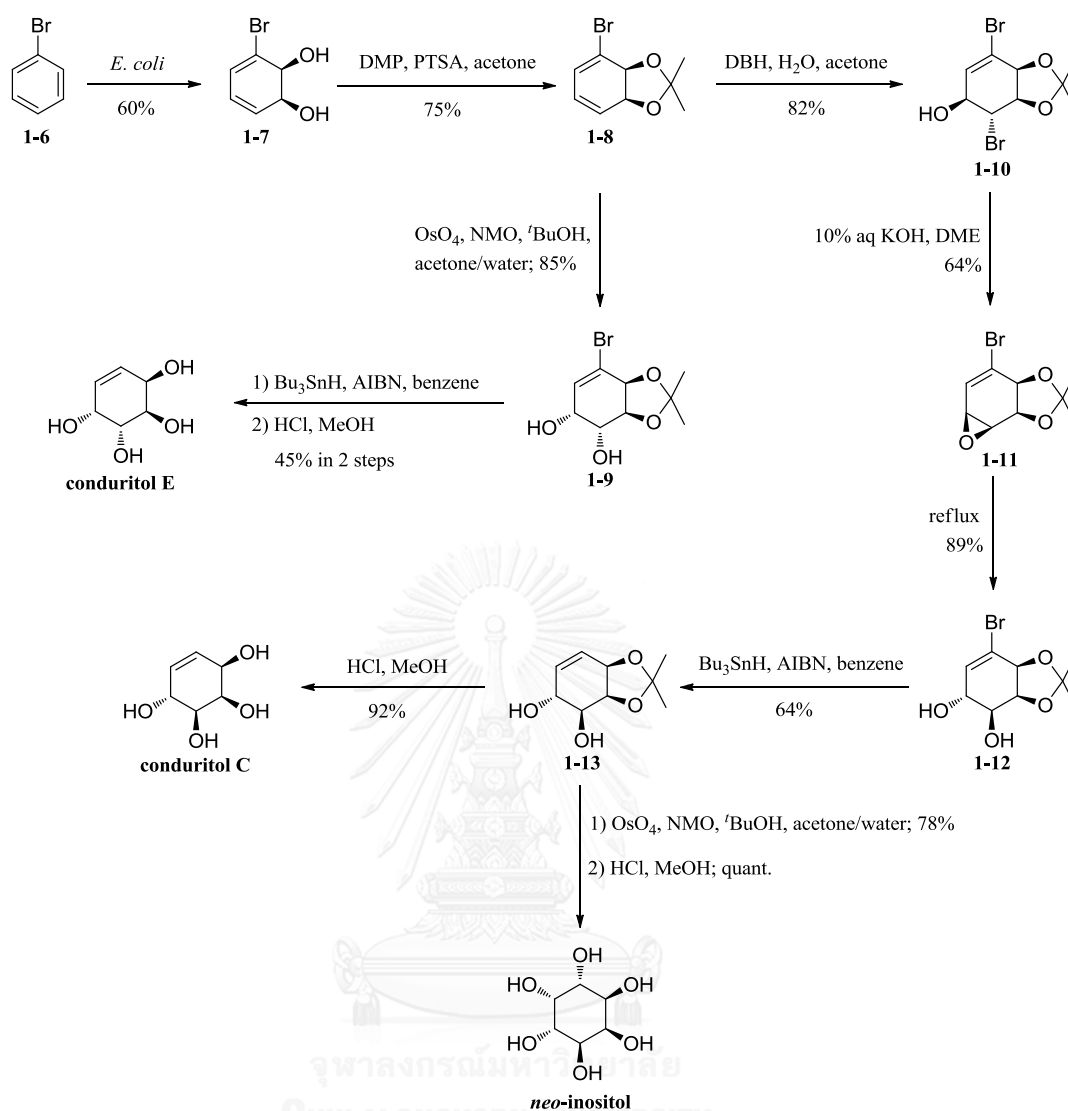


Figure 1.8 Structures of isomeric inositols.

The traditional method for the synthesis of conduritol and inositol analogues is the chemoenzymatic biooxidation of aromatic compounds, which provide the various conduritol and inositol derivatives.

Conduritol E was synthesized by the enzymatic oxidation of bromobenzene **1-6** in five steps (Scheme 1.1). *E. coli* was used for this conversion to afford the diene-*cis*-diol **1-7**. The resulting diol was therefore protected as the acetonide followed by dihydroxylation using OsO₄ to obtain diol **1-9**. Debromination of **1-9** and subsequent acetonide deprotection provided conduritol E. Moreover, the protected diene-*cis*-diol **1-8** can also be converted to conduritol C and *neo*-inositol in five and six steps, respectively. Initially, the reaction of **1-8** with 1,3-dibromo-5,5-dimethylhydantoin in acetone/water gave bromohydrin **1-10**. Next, treatment of **1-10** under basic condition led to the formation of *trans*-diol **1-12** through epoxide **1-11**. Reduction of the vinyl bromide gave olefin **1-13**, which was deprotected by HCl to afford conduritol C, or was dihydroxylated in the presence of OsO₄ followed by acetonide deprotection to give *neo*-inositol.

Although several conduritols and inositols have been principally prepared through microbial and photo-oxidations of halogenated benzene, vicinal-diols obtained after oxidation inevitably existed as a mixture of two or more stereoisomers. Therefore, preparation of conduritols and inositols from optically pure starting materials is likely to be a method of choice to circumvent such problems.



Scheme 1.1 Synthesis of conduritol C and E and *neo*-inositol from bromobenzene.

1.3.2 Synthesis of aminocyclitol derivatives

Aminocyclitols is broadly defined as a cycloalkane polyol encompassing amino group or incorporating nitrogen atom into the ring. Because their structures are closely similar to sugars, aminocyclitols are also regarded as amino-carbasugars [19]. Moreover, aminocyclitols are a group of natural products possessing significant relevance in medicinal chemistry as they are structural components of a variety of antibiotics and glucosidase inhibitors (Figure 1.9). Due to their close structural resemblance to sugars, aminocyclitols are also expected to act as carbohydrate mimics, which can be developed as inhibitors of glucosidase-related biological

processes such as viral infection, cancer development and diabetes mellitus (DM) [27].

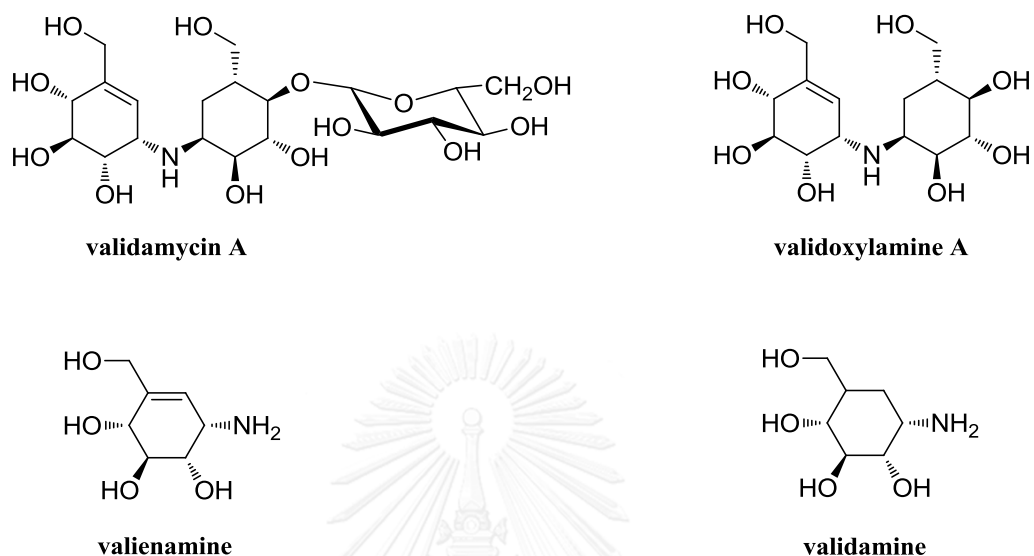


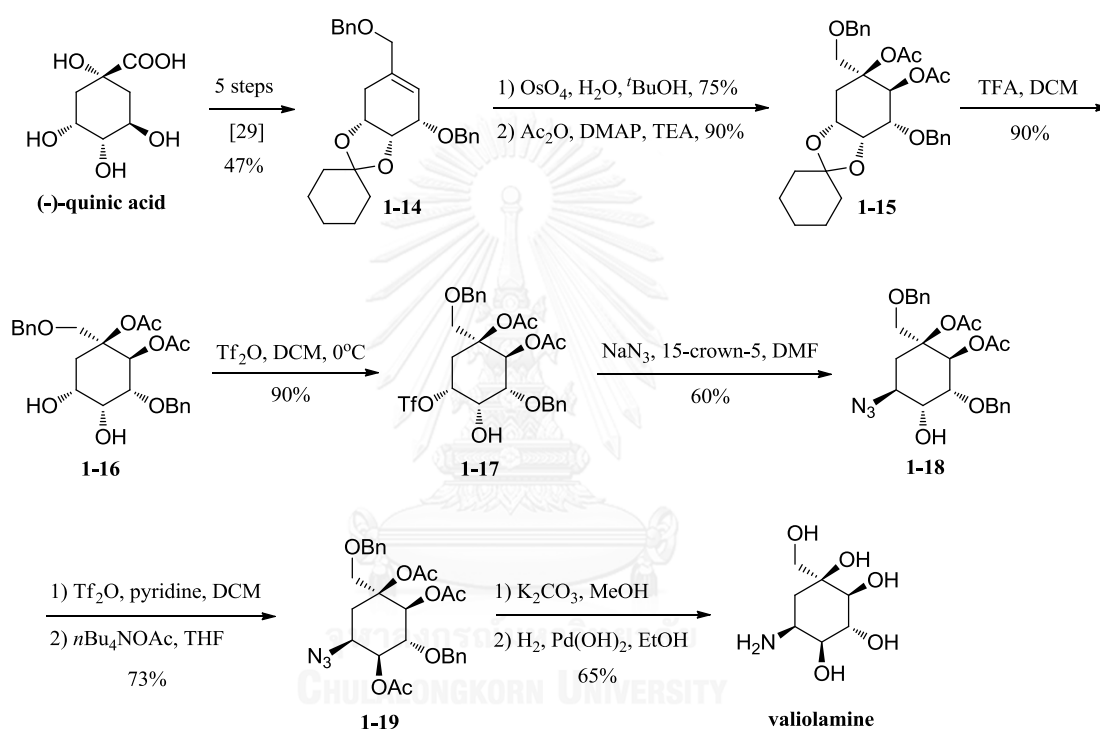
Figure 1.9 Structures of natural aminocyclitols.

More recently, the syntheses of aminocyclitols have attracted considerable interest and the synthetic approaches have been developed. A variety of synthetic methodologies for aminocyclitols were described in a current literature [19], in which the key steps involved intramolecular cyclizations, rearrangements, and nucleophilic substitution reactions.

Noticeably, most synthetic approaches employed cyclitols as a chiral pool of starting materials [19] instead of ordinary monosaccharides because they provided a shortcut to the target molecules.

Quinic acid is one of natural chiral pool materials frequently applied for the synthesis of several pharmacological drugs, which include aminocyclitol analogues. Synthesis of valioline and its diastereomers from (-)-quinic acid was reported by Shing and Wan [28]. Initially, (-)-quinic acid could be converted into alkene **1-14** in five steps with an overall yield of 47%. Dihydroxylation using OsO_4 followed by protection with acetic anhydride provided diacetate **1-15**. Acidic removal of the

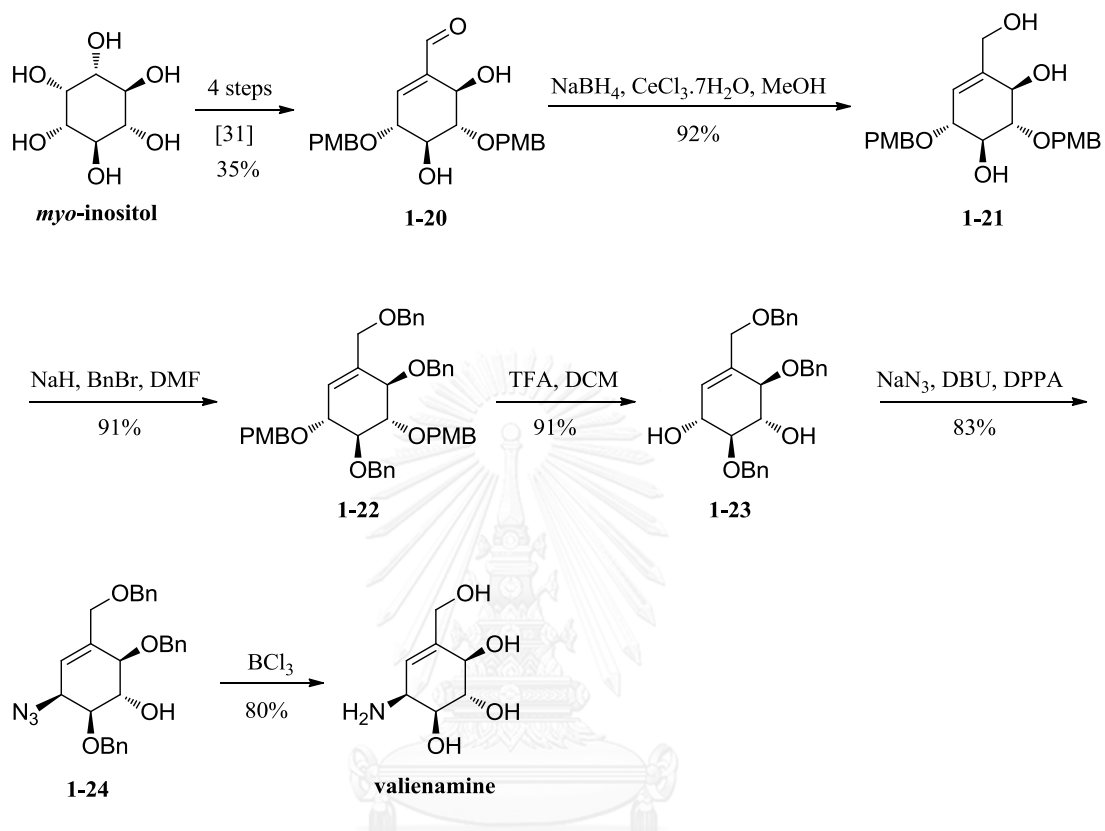
cyclohexylidene acetal in **1-15** gave diol **1-16**. Next, azide **1-18** was prepared by selective esterification of **1-16** using triflic anhydride followed by azidolysis using NaN_3 . Triflylation of the alcohol **1-18** and subsequent nucleophilic displacement with $n\text{Bu}_4\text{NOAc}$ furnished azido triacetate **1-19**. Finally, deacetylation and azide reduction with concurrent hydrogenolysis of the benzyl ethers of **1-19** then provided valiolamine (Scheme 1.2).



Scheme 1.2 Synthesis of valiolamine from (-)-quinic acid.

Moreover, inositols were also used as the starting material for the synthesis of aminocyclitols. Total synthesis of valienamine from *myo*-inositol was reported by Mondal and co-workers (Scheme 1.3) [29]. Initially, the enal **1-20** was prepared, in 35% yield, from commercially available *myo*-inositol in four steps [31]. Luche reduction of the α,β -unsaturated aldehyde **1-20** provided triol **1-21** in good yield. Benzoylation of triol **1-21** furnished the tribenzyl ether **1-22**. Acidic hydrolysis of **1-22** gave diol **1-23** in 91% yield. Diol **1-23**, on Mitsunobu reaction using

diphenylphosphorylazide (DPPA) and DBU, afforded the azide **1-24** regioselectively in good yield. Finally, valienamine was obtained from **1-24** via deprotection and reduction using BCl_3 .

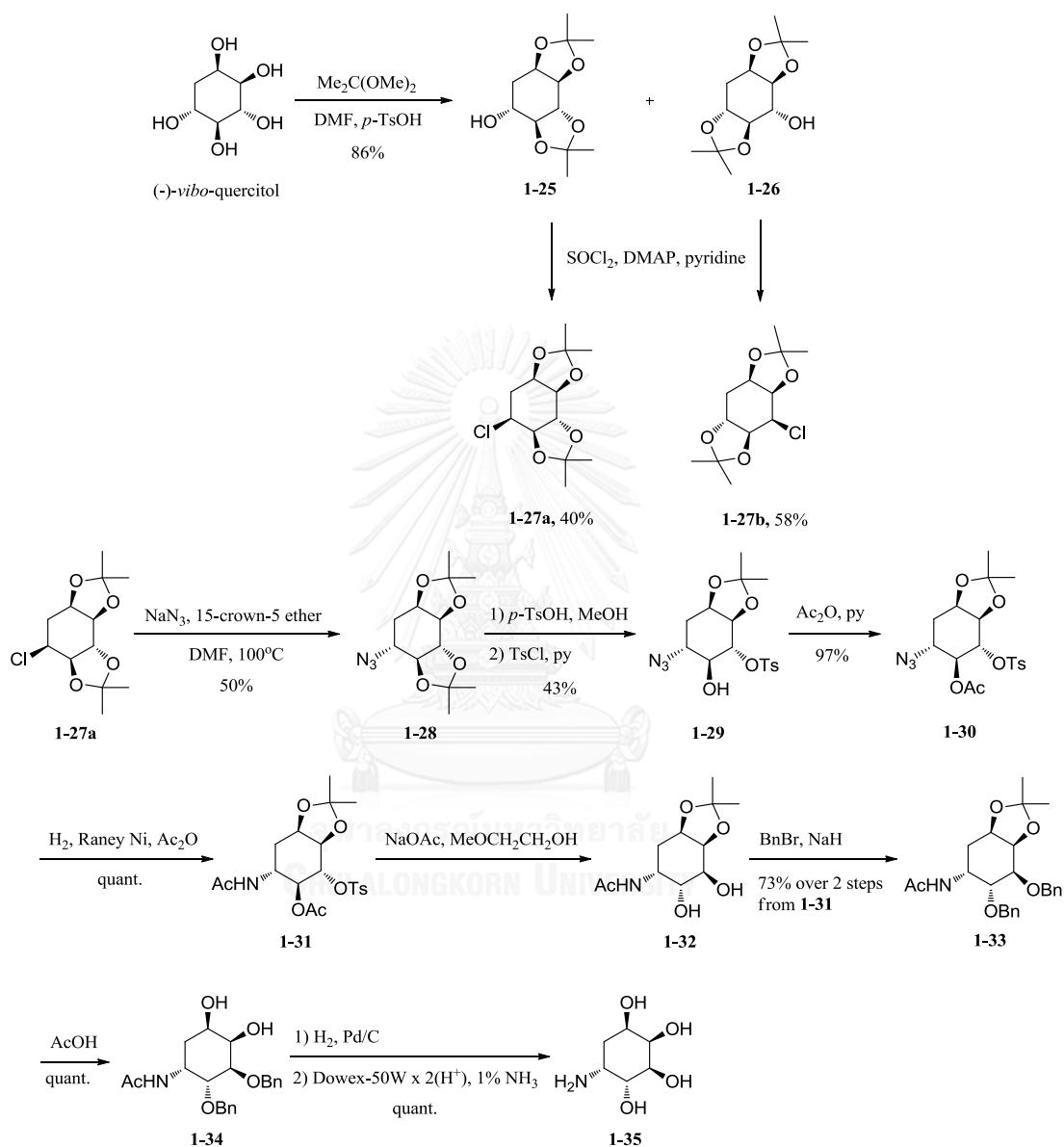


Scheme 1.3 Synthesis of valienamine from *myo*-inositol.

CHULALONGKORN UNIVERSITY

Furthermore, several syntheses of aminocyclitols have been accomplished using cyclohexanepentols or trivially called quercitols as starting components. In fact, quercitol has 16 possible stereoisomers in its family. Of all isomers, there are only (+)-*proto*-, (-)-*proto*-, and (-)-*vibo*-quercitols being encountered abundantly in nature [30]. The synthesis of aminocyclitol starting from (-)-*vibo*-quercitol was described by Ogawa [31]. 5-Amino-1,2,3,4-cyclohexanetetrol (**1-35**) was prepared from (-)-*vibo*-quercitol. Firstly, protection of (-)-*vibo*-quercitol with 2,2-dimethoxypropane gave an inseparable mixture of 1,2:3,4- and 1,2:4,5-di-*O*-isopropylidene derivatives (**1-25** and **1-26**) in 86% yield. The mixture was treated with thionyl chloride in the presence of DMAP in pyridine, giving two chloro compounds **1-27a** (40%) and **1-27b** (58%).

Further transformations of **1-27a** into the aminocyclitol **1-35** involved azidolysis, tosylation, acetylation, hydrogenation, and deprotection (Scheme 1.4).



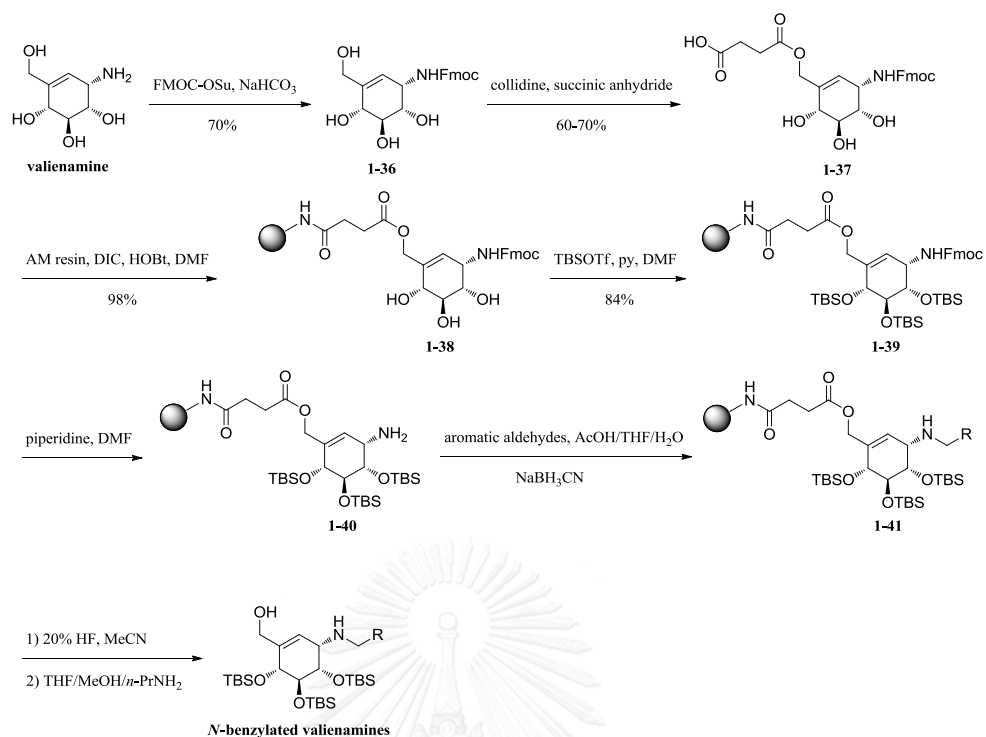
Scheme 1.4 Synthesis of aminocyclitol **1-35** from *(-)-vibo-querцитол*.

In addition, at present, a series of aminocyclitol derivatives have been studied on their potential for the enhancement of glucosidase inhibitory activity by modifying the free amino groups with a variety of hydrophobic and hydrophilic moieties [32-34].

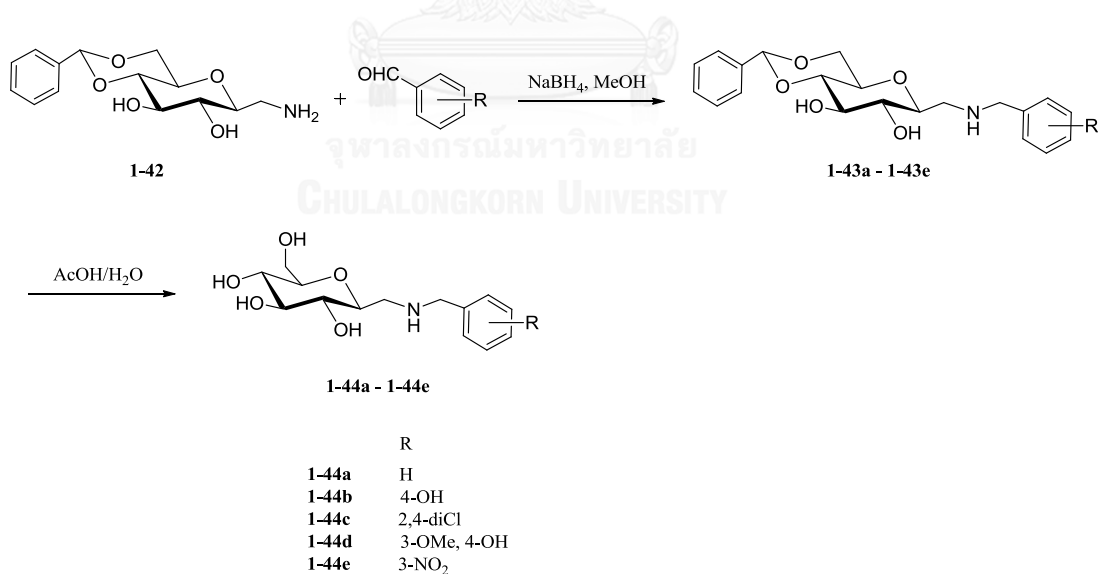
Many groups have reported the α -glucosidase inhibitory effect of *N*-substituted aminocyclitol series and concluded that the potent α -glucosidase inhibitors were developed from their parent aminocyclitols. Some of experimental evidences were described in a literature review [35]. Therefore, the synthesis of *N*-substituted aminocyclitol derivatives would lead to the discovery of new glucosidase inhibitors.

In 2006, Łysek and co-workers have prepared new *N*-benzylated valienamines *via* a solid-phase synthesis [36]. Firstly, valienamine was converted to its Fmoc derivative **1-36** (Scheme 1.5). The selective acylation of **1-36** with succinic anhydride and collidine as catalyst provided the desired **1-37** in good yield. Next, the acid **1-37** was linked to an aminomethylated polystyrene resin *via* amide formation to give **1-38** in good yield. Three hydroxyl groups of **1-38** were then protected as silyl ethers using TBSOTf to obtain **1-39**, in which the Fmoc was deprotected using piperidine to give **1-40**. Reductive amination of amine **1-40** with various aromatic aldehydes in the presence of NaBH₃CN and acid followed by resin deprotection furnished *N*-benzylated valienamine derivatives. All synthesized compounds were evaluated for α -glucosidase inhibitory activity and the result showed that most *N*-substituted valienamines have significantly improved inhibitory activity toward α -glucosidases.

Another synthesis of *N*-substituted aminocyclitol derivatives using their parent as starting material was elaborated by Bian and co-workers [34]. They reported the preparation of *N*-substituted aminomethyl- β -D-glucopyranoside and their α -glucosidase inhibitory activity. The target compounds were divided into two series: the amino and amide sugar analogues. Both series were prepared from 1-aminomethyl-4,6-*O*-benzylidene- β -D-glucopyranoside (**1-42**) *via* reductive amination (Scheme 1.6) or acylation (Scheme 1.7), respectively. Next, all synthesized compounds were evaluated *in vitro* against yeast and rat intestinal α -glucosidase. Most of them displayed α -glucosidase inhibition greater than their parent **1-42**. Of all synthesized compounds, **1-46a** (IC₅₀ = 2.3 μ M) and **1-46e** (IC₅₀ = 5.1 μ M) were the most potent inhibitors against yeast α -glucosidase and rat intestinal maltase, respectively.



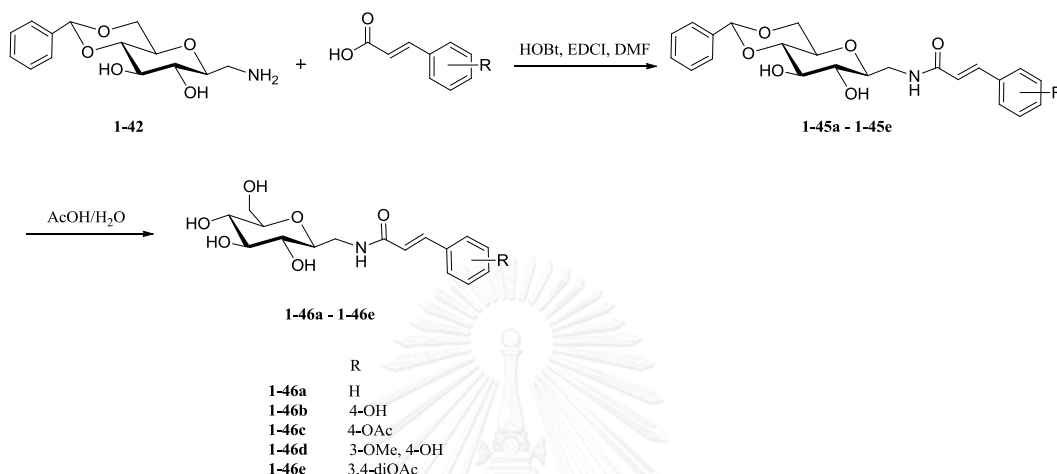
Scheme 1.5 Preparation of *N*-benzylated valienamines from their parent valienamine.



Scheme 1.6 Synthesis of sugar-amines **1-44a** – **1-44e**.

However, synthesis of α -glucosidase inhibitors using cyclitols as chiral substrates have also encountered some problems associated with multi-step

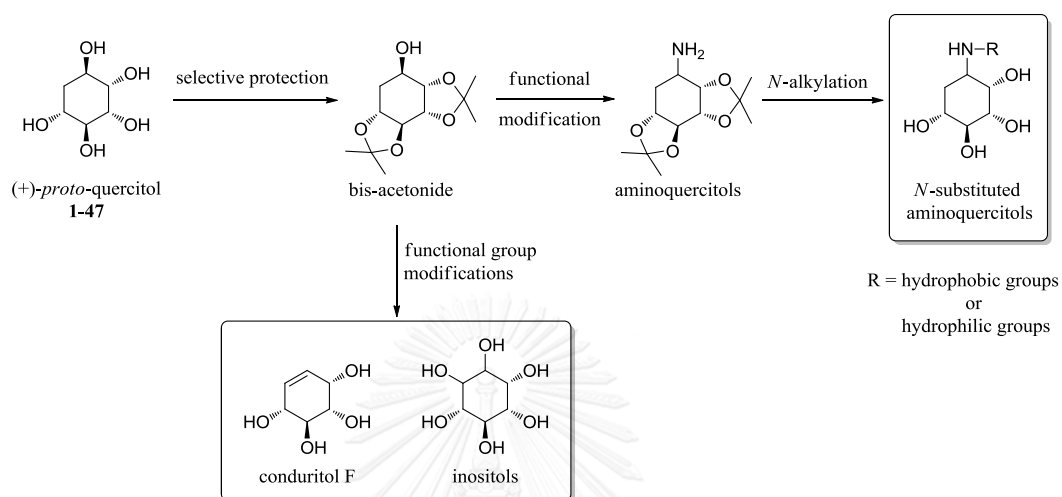
synthesis and the generation of undesired byproducts, leading to difficult separation and lower yield of the desired products. Therefore, in order to access various α -glucosidase inhibitors, selection of the suitable starting material and excellent synthesis design are crucial.



Scheme 1.7 Synthesis of sugar-amides **1-46a** – **1-46e**.

In this research, we used (+)-*proto*-quercitol as a starting material because it is likely to be a potential candidate for large scale synthesis. Due to its proper configuration, exclusive formation of single bis-acetonide is critical to obtain desired products in excellent yield with high optical purity. This postulation was proved by our previous investigation on the synthesis of α -glucosidase inhibitors [36]. Importantly, many previous data suggested that the potent α -glucosidase inhibitors were developed from their parent by functional group modifications. With this interesting information, we herein focus on the discovery of various α -glucosidase inhibitors starting from naturally available (+)-*proto*-quercitol (**1-47**). As the main point of this research, we describe the synthesis of *N*-substituted aminoquercitols derived from their parent aminoquercitols by the introduction of hydrophobic or hydrophilic moieties at the nitrogen atom. In addition, we describe the preparation of conduritol and its analogues by modifying on the quercitol core. α -Glucosidase

inhibitory activity and kinetic analysis of the synthesized compounds were also studied.



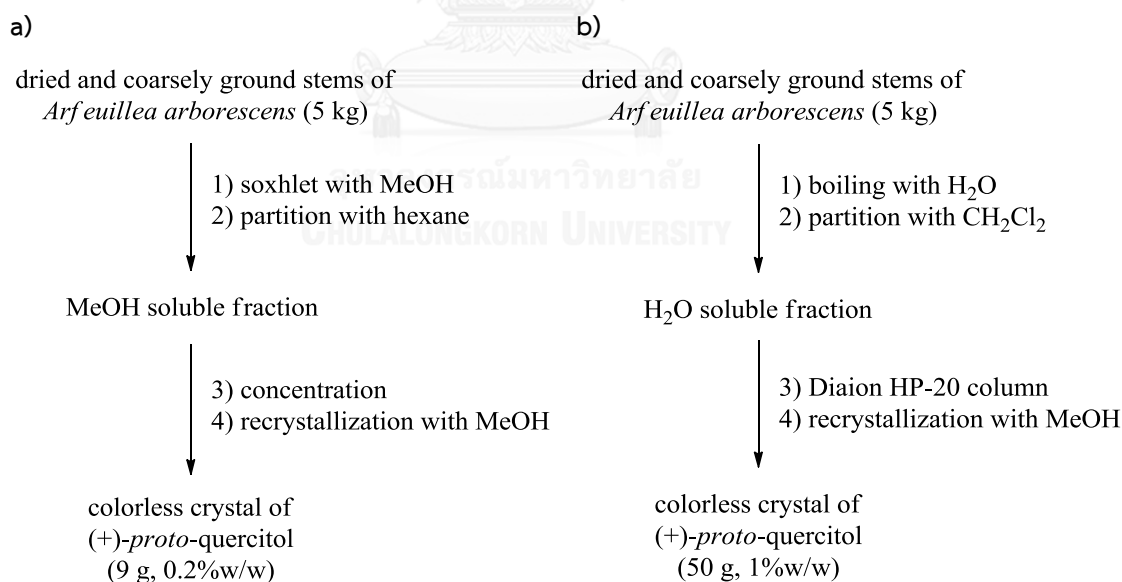
Scope of this research

จุฬาลงกรณ์มหาวิทยาลัย
CHULALONGKORN UNIVERSITY

CHAPTER II
CONCISE SYNTHESIS OF (+)-CONDURITOL F AND INOSITOL ANALOGUES
FROM NATURALLY AVAILABLE (+)-*proto*-QUERCITOL AND THEIR
GLUCOSIDASE INHIBITORY ACTIVITY

2.1 Improvement for extraction and isolation of (+)-*proto*-quercitol

In this work, we developed an efficient method to isolate (+)-*proto*-quercitol from stems of *Arfeuillea arborescens* using hot water (Scheme 2.1b). The aqueous fraction, after partition with CH₂Cl₂, was purified by Diaion HP-20 column using H₂O as solvent system followed by recrystallization with MeOH to afford the desired quercitol as colorless crystals. This method could be applied to yield multiple grams of enantiomerically pure (+)-*proto*-quercitol (1% yield). It was also environmentally friendly as water was mainly used during extraction and isolation.

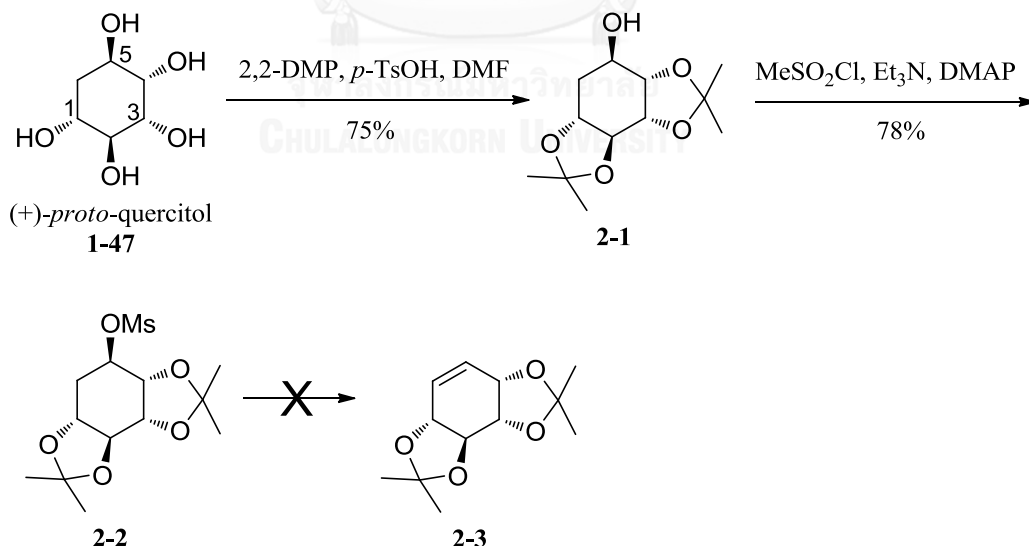


Scheme 2.1 Comparison of the isolation procedure of (+)-*proto*-quercitol from the stems of *Arfeuillea arborescens* between a) previous [36] and b) present procedure.

2.2 Synthesis of conduritol F and inositols

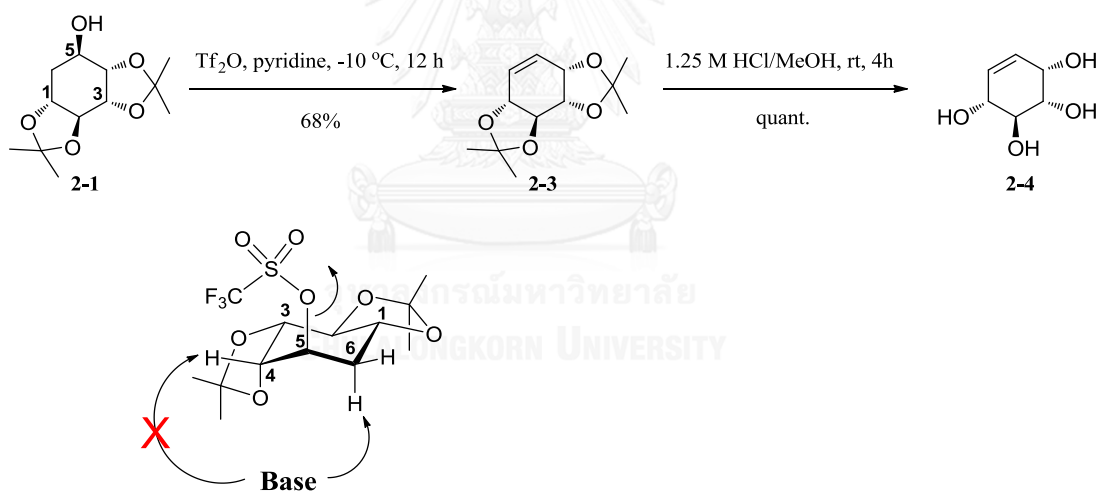
Conduritol F (**2-4**) was our first target because of its prominent α -glucosidase inhibitory activity and low natural abundance. Regardless of the presence of an unsaturation in conduritol F and one additional hydroxyl group in (+)-*proto*-quercitol, their gross structure and relative configuration are identical. Thus, dehydration of starting material would readily generate the desired product.

With starting material **1-47** in hand, the bis-diol moiety was then preferentially protected as the corresponding acetonide to provide the desired compound **2-1** in an excellent yield (Scheme 2.2). Since one hydroxyl group remains unprotected, it was thus activated with mesyl chloride to afford mesylate ester **2-2** in 78% yield. Unfortunately, elimination of **2-2** using various bases such as DBU, pyridine, and *t*-BuOK, in the hope that it would be converted to the protected conduritol **2-3**, was unsuccessful. More than 80% of **2-2** was recovered along with **2-3** in less than 5%. We hypothesized that the mesyl group may not be a sufficiently good leaving group under these conditions.



Scheme 2.2 Synthesis of **2-2**.

Having failed the elimination reaction of **2-2** under basic conditions, we turned our focus on olefin formation directly *via* bis-acetonide **2-1** using strong dehydrating agents such as thionyl chloride, phosphorus oxychloride, Martin's reagent and trifluoromethanesulfonic anhydride. Treatment of **2-1** with SOCl_2 or POCl_3 in pyridine resulted in complex mixtures along with only trace amount of the desired alkene **2-3**. Moreover, Martin's sulfurane dehydrating agent was also employed in dry toluene under reflux but an inseparable mixture along with 50% of starting material were recovered. Fortunately, dehydration of **2-1** took place smoothly upon addition of Tf_2O in pyridine at $-10\text{ }^\circ\text{C}$, affording the protected conduritol F (**2-3**) as the sole product (Scheme 2.3). This alternative route not only provided us a short-step conversion of (+)-*proto*-quercitol to conduritol F but also generated the desired product without any congeners.

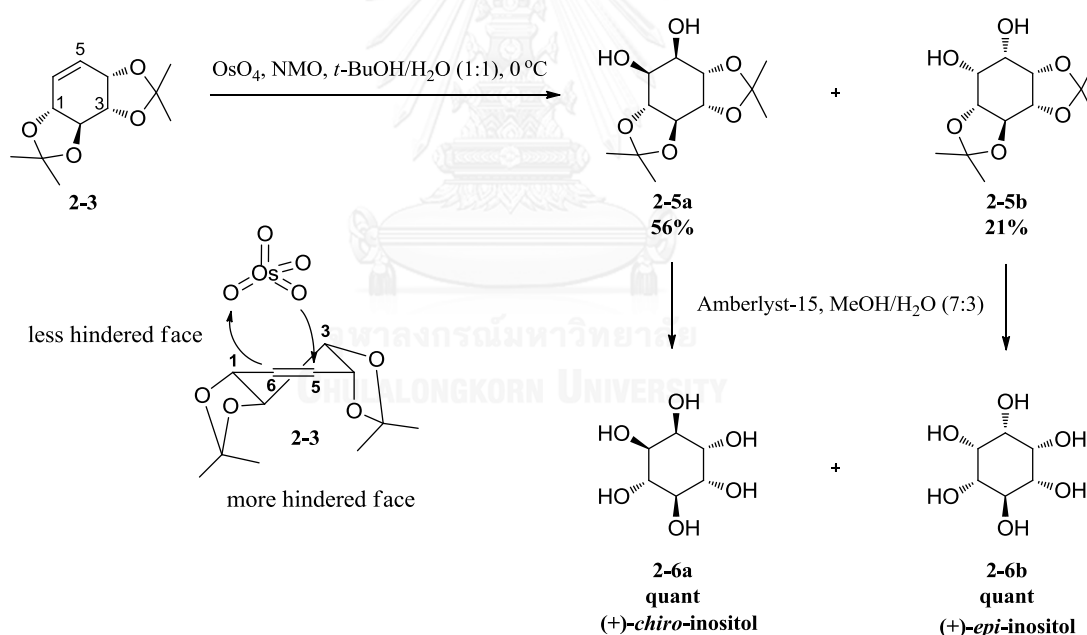


Scheme 2.3 Synthesis of (+)-conduritol F (**2-4**).

The specificity of this elimination step is possibly attributed to steric effect. The bulky acetonide may block the proton abstraction at C-4 whereas *trans*-diaxial orientation of H-6_{ax} and the leaving group trifluoromethanesulfonyl facilitates E2 pathway, hence generating protected alkene **2-3** (Scheme 2.3). Eventually, conduritol F (**2-4**) was obtained by deprotection of **2-3** with methanolic HCl. The NMR data and

specific rotation (+79.5, c 1.12, MeOH) of our prepared conduritol F were completely identical to those previously reported [37, 38], confirming the absolute configuration as (+)-conduritol F.

The success in preparing optically pure (+)-conduritol F allowed us to access other cyclitols. The protected conduritol **2-3** could serve as a chiral building block for single-step conversion to inositol derivatives. Dihydroxylation of **2-3** using OsO₄ led to the formation of readily separable 3:1 diastereomeric inositols **2-5a** and **2-5b** in 77% yield (Scheme 2.4). The selective formation of **2-5a** over **2-5b** could be rationalized by preferential osmylation on the less hindered face of alkene. Consequently, **2-5a** and **2-5b** were deprotected by Amberlyst-15 to quantitatively afford (+)-*chiro*-inositol (**2-6a**) and (+)-*epi*-inositol (**2-6b**), respectively.



Scheme 2.4 Synthesis of inositols **2-6a** and **2-6b**.

2.3 α -Glucosidase inhibitory effect

(+)-Conduritol F (**2-4**) and inositols (**2-6a** and **2-6b**) including (+)-*proto*-quercitol (**1-47**) were evaluated for α -glucosidase inhibitory activity using enzymes

from two different sources; baker's yeast (type I) and rat small intestine (type II) [36, 39].

From the inhibition results, all synthesized compounds selectively inhibited α -glucosidase from baker's yeast, in which **2-4** displayed highest inhibition with an IC_{50} value of 86.1 μ M (Table 2.1). A potent inhibitory effect (6–16 times) of **2-4** over its corresponding diols, (+)-*chiro*-inositol (**2-6a**) and (+)-*epi*-inositol (**2-6b**), indicated that a half-chair conformation of cyclohexene moiety is more critical in binding active site of the enzyme (Figure 1.4c) than additional dihydroxy groups. This observation was also supported by a very low inhibition of (+)-*proto*-quercitol (**1-47**), a hydroxylated cyclitol of **2-4**. However, all cyclitols evaluated did not inhibit maltase and sucrase, type II α -glucosidases from rat small intestine.

Table 2.1 α -Glucosidase inhibitory effect of cyclitols **1-47**, **2-4**, **2-6a**, and **2-6b**

Cyclitol	IC_{50} (μ M)		
	Baker's yeast	Maltase ^a	Sucrase ^a
1-47	NI ^b	NI	NI
2-4	86.1 \pm 0.5	NI	NI
2-6a	1256.1 \pm 1.7	NI	NI
2-6b	475.7 \pm 0.9	NI	NI
Acarbose	403.9 \pm 0.4	1.50 \pm 0.14	2.38 \pm 0.02

^a α -Glucosidase was obtained from rat small intestine.

^b NI, no inhibition, inhibitory effect less than 30% at 10 mg/mL for baker's yeast and at 1 mg/mL for maltase and sucrase.

2.4 Conclusion

In summary, we have simply and efficiently achieved short synthesis for (+)-conduritol F and inositols, (+)-*chiro*- and (+)-*epi*-inositols, from naturally available (+)-*proto*-quercitol. A key step involves dehydration of protected (+)-*proto*-quercitol (**2-1**) after addition of Tf_2O in pyridine, therefore taking totally three steps to produce

optically pure conduritol F in excellent yield. Furthermore, our method also provided rapid access to the corresponding dihydroxy analogues, (+)-*chiro*- and (+)-*epi*-inositols. A potent inhibition of conduritol F, selectively against type I α -glucosidase, over related compounds as well as antidiabetic drug acarbose suggested that its half-chair conformation is critical for exerting inhibition.

2.5 Experimental section

2.5.1 General experimental procedures

All moisture-sensitive reactions were carried out under a nitrogen atmosphere. All solvents were distilled prior to use. Mass spectra were measured by ESI-MS and high resolution (HR)-ESI-MS. ^1H and ^{13}C NMR spectra were recorded (CDCl_3 , D_2O , and CD_3OD as solvent) at 400 and 100 MHz, respectively, on a Varian Mercury⁺ 400 NMR spectrometer using tetramethylsilane (TMS) as an internal standard. Chemical shifts are reported in ppm downfield from TMS. Optical rotations were measured on a Perkin-Elmer 341 polarimeter using a cell with 1 mL capacity and a 10 cm path length. Analytical thin layer chromatography (TLC) was performed on pre-coated Merck silica gel 60 F₂₅₄ plates (0.25 mm thick layer) and visualized by potassium permanganate as the detecting agent. Column chromatography was performed using Merck silica gel 60 (70-230 mesh).

2.5.2 Plant material

The stems of *Arfeuillea arborescens* were purchased from Chao-Krom-Per, a Thai medical plant shop, Bangkok, Thailand, in October, 2009.

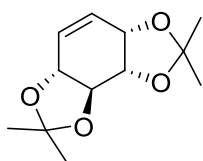
2.5.3 Isolation of (+)-*proto-quercitol* (1-47)

Ground stems (5 kg) of *A. arborescens* were boiled with water (4 L) for 3 h. The decoction was filtered and partitioned twice with equal volume of CH_2Cl_2 . The aqueous layer was loaded onto a column chromatography filled with wet Diaion HP-20 (1 kg) and excessively eluted with H_2O (10 L). The combined aqueous elutes were

lyophilized to afford white powder, which was subsequently purified by crystallization using hot MeOH, providing (+)-*proto*-quercitol (50 g, 1% w/w) as a colorless crystal.

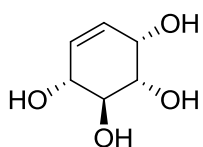
2.5.4 Synthesis of (+)-conduritol F and inositols

Protected conduritol F (2-3)



A solution of bis-acetonide **2-1** (207.8 mg, 0.85 mmol) in pyridine (8 mL) was cooled to -10 °C. Trifluoromethanesulfonic anhydride (430 μ L, 2.6 mmol) was added dropwise under nitrogen. After stirring for 12 h, the reaction was quenched by adding H₂O and extracted with EtOAc (3 \times 10 mL). The combined organic layers were washed with brine, dried over anhydrous Na₂SO₄ and concentrated under reduced pressure. The crude product was purified by silica gel column chromatography (10% EtOAc-hexane) to give **2-3** (130.0 mg, 68%) as a white solid; ¹H NMR (CDCl₃, 400 MHz) δ 6.13 (d, *J* = 10.0 Hz, 1H), 5.75 (dt, *J* = 10.0, 2.4 Hz, 1H), 4.76 (dd, *J* = 7.6, 1.6 Hz, 1H), 4.33 (t, *J* = 9.2 Hz, 1H), 4.00 (d, *J* = 8.8 Hz, 1H), 3.48 (t, *J* = 8.8 Hz, 1H), 1.46 (s, 3H), 1.40 (s, 3H), 1.38 (s, 3H), 1.31 (s, 3H); ¹³C NMR (CDCl₃, 100 MHz) δ 128.5, 125.6, 112.7, 110.5, 81.4, 74.9, 74.7, 74.6, 27.3, 26.8, 26.7, 24.6.

(+)-Conduritol F (2-4)



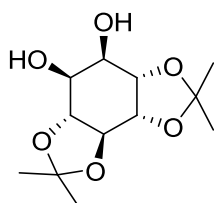
A solution of protected conduritol F (**2-3**) (17.3 mg, 0.08 mmol) in 1.25 M methanolic HCl (1 mL) was stirred at room temperature for 4 h. The reaction mixture was evaporated to dryness to give **2-4** (15 mg, quantitative yield) as a colorless oil: $[\alpha]_D^{25} = +79.5$ (c 1.12, CH₃OH); ¹H NMR (CD₃OD, 400 MHz) δ 5.79 (ddd, *J* = 10.0, 4.8, 2.0 Hz, 1H), 5.72 (dd, *J* = 10.0, 2.0 Hz, 1H), 4.17 (t, *J* = 4.4 Hz, 1H), 3.94 (d, *J* = 7.6 Hz,

1H), 3.62 (dd, $J = 10.4, 7.6$ Hz, 1H), 3.43 (dd, $J = 10.4, 4.0$ Hz, 1H); ^{13}C NMR (CD_3OD , 100 MHz) δ 133.9, 128.1, 74.1, 73.9, 72.7, 68.1; HRESIMS m/z 169.0479 [$\text{M}+\text{Na}$] $^+$ (calcd for $\text{C}_6\text{H}_{10}\text{NaO}_4$, 169.0477). These spectroscopic data are identical to those reported previously [37, 38].

Dihydroxylation of protected conduritol F (2-3)

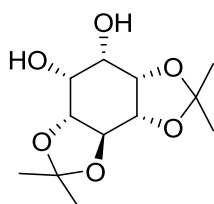
To a stirred solution of **2-3** (12.0 mg, 0.05 mmol) and 4-methylmorpholine *N*-oxide monohydrate (NMMO) (18 mg, 0.13 mmol) in 1:1 *t*-BuOH/ H_2O (1.2 mL) at 0 °C was added OsO_4 (2.5% w/v solution in *t*-BuOH, 108 μL , 0.01 mmol) dropwise. After stirring for 12 h, the reaction was quenched by adding $\text{Na}_2\text{S}_2\text{O}_5$, and extracted with EtOAc (3 \times 5 mL). The combined organic layers were washed with brine, dried over anhydrous Na_2SO_4 and concentrated under reduced pressure. The crude product was purified by silica gel column chromatography (50% EtOAc-hexane), giving two diastereoisomers **2-5a** and **2-5b** as white solids.

2-5a



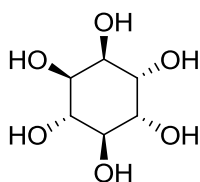
7.9 mg, 56%; ^1H NMR (CDCl_3 , 400 MHz) δ 4.31 (br d, $J = 6.0$ Hz, 2H), 4.15 (dd, $J = 4.8, 4.8$ Hz, 1H), 4.04 (dd, $J = 8.8, 4.8$ Hz, 1H), 3.66 (dd, $J = 8.8, 8.8$ Hz, 1H), 3.58 (m, 1H), 1.44 (s, 3H), 1.38 (s, 6H), 1.30 (s, 3H); ^{13}C NMR (CDCl_3 , 100 MHz) δ 112.1, 110.0, 78.7, 78.4, 77.2, 76.0, 70.8, 70.0, 27.9, 27.0, 26.9, 25.4.

2-5b



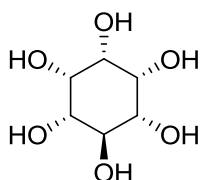
3.0 mg, 21%; ^1H NMR (CDCl_3 , 400 MHz) δ 4.32-4.38 (m, 2H), 4.13-4.15 (m, 2H), 3.89 (m, 1H), 3.23 (m, 1H), 1.49 (s, 3H), 1.40 (s, 3H), 1.38 (s, 3H), 1.31 (s, 3H).

(+)-*chiro*-inositol (2-6a)



To a solution of **2-5a** (7.9 mg, 0.03 mmol) in 70% MeOH- H_2O (1 mL) was added Amberlyst-15 (20 mg) and stirred at room temperature for 3 h. The resin was filtered off, washed with MeOH and the filtrate was concentrated under reduced pressure afforded **2-6a** (6.0 mg, quantitative yield) as a pale yellow oil: $[\alpha]_D^{25} = +81.9$ (c 0.45, H_2O); ^1H NMR (D_2O , 400 MHz) δ 3.81 (br s, 2H), 3.54 (br d, $J = 7.2$ Hz, 2H), 3.37 (br d, $J = 7.2$ Hz, 2H); ^{13}C NMR (D_2O , 100 MHz) δ 72.8, 71.7, 70.5; ESIMS m/z 134 (100% base peak) $[\text{M}-\text{H}_2\text{O}-\text{CO}]^-$ (calcd for $\text{C}_6\text{H}_{12}\text{O}_6$, 180). These spectroscopic data are identical to those reported previously [40].

(+)-*epi*-inositol (2-6b)



(+)-*epi*-inositol was prepared from **2-5b** (3.0 mg, 0.01 mmol) as described for the preparation of (+)-*chiro*-inositol, yielding (+)-*epi*-inositol (4 mg, quantitative yield) as a white solid: $[\alpha]_D^{25} = -36.0$ (c 0.27, H_2O); ^1H NMR (D_2O , 400 MHz) δ 3.86 (br s, 1H), 3.81 (br s, 1H), 3.53 (br s, 2H), 3.37 (dd, $J = 7.2, 2.4$ Hz, 1H), 3.28 (dd, $J = 9.6, 2.4$ Hz, 1H); ^{13}C NMR (D_2O , 100 MHz) δ 74.5, 72.8, 71.8, 71.7, 70.5; ESIMS m/z 134 (100% base peak) $[\text{M}-\text{H}_2\text{O}-\text{CO}]^-$ (calcd for $\text{C}_6\text{H}_{12}\text{O}_6$, 180). These spectroscopic data are identical to those reported previously [40].

2.5.5 α -Glucosidase inhibition assay

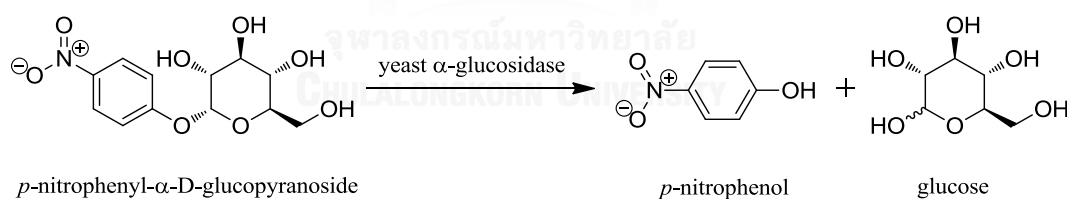
2.5.5.1 Chemicals and equipment

Sucrose, maltose, baker's yeast α -glucosidase, rat intestinal acetone powder, *p*-nitrophenyl- α -D-glucopyranoside, and glucose assay kit were purchased from Sigma-Aldrich (St. Louis, MO, USA). Acarbose was obtained from Bayer (Germany). Bio-Rad microplate reader model 3550 UV was used to measure the absorbance at 405, and 500 nm for the enzymatic reaction in the microplate assay.

2.5.5.2 Procedure

Baker's yeast α -glucosidase inhibitory activity

Yeast assay was performed using colorimetric method with some slight modifications. In brief, α -glucosidase hydrolyzed the substrate *p*-nitrophenyl- α -D-glucopyranoside to produce *p*-nitrophenol and glucose (Scheme 2.5). Thus, the inhibitory effect of the synthesized compounds against yeast enzyme was quantified by UV at 405 nm, in term of *p*-nitrophenol decline.



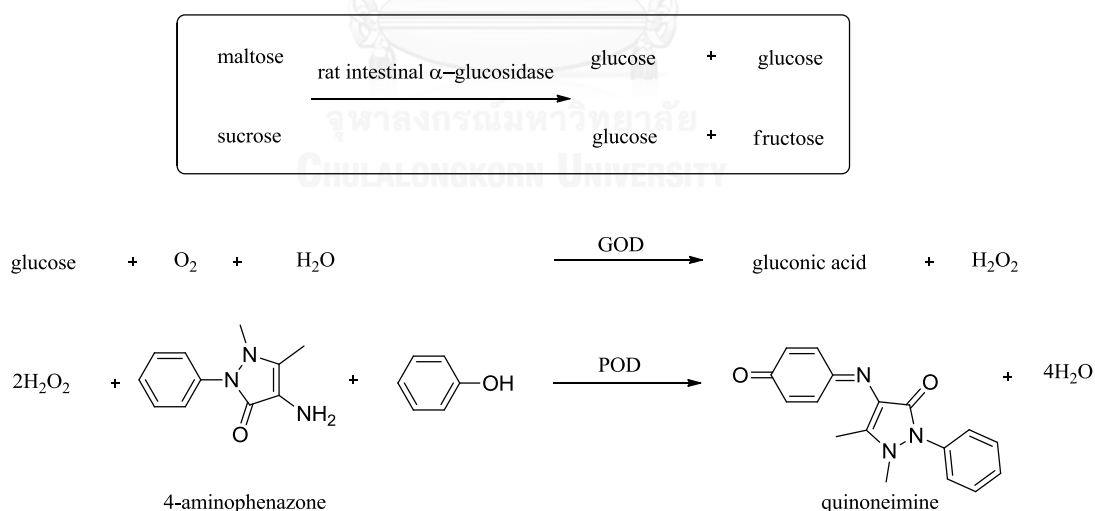
Scheme 2.5 Hydrolysis by yeast α -glucosidase.

The α -glucosidase inhibition assay was performed according to the slightly modified method of Wacharasindhu *et al* [36]. α -Glucosidase (0.1 U/mL) and substrate (1 mM *p*-nitrophenyl- α -D-glucopyranoside) were dissolved in 0.1 M phosphate buffer, pH 6.9. 10 μ L of synthesized compounds (1 mg/mL in DMSO) was pre-incubated with 40 μ L of α -glucosidase at 37 $^{\circ}$ C for 10 min. A 50 μ L substrate solution was then added to the reaction mixture and incubated at 37 $^{\circ}$ C for 20 min,

and terminated by adding 100 μL of 1 M Na_2CO_3 . Enzymatic activity was quantified by measuring the absorbance at 405 nm. The percentage inhibition of activity was calculated as $[(A_0 - A_1)/A_0] \times 100$, where A_0 is the absorbance without the sample, and A_1 is the absorbance with the sample. The IC_{50} value was determined from a plot of percentage inhibition versus sample concentration. Acarbose[®] was used as standard control and the experiment was performed in triplicate.

Rat intestinal α -glucosidase inhibitory activity

The amount of glucose can be determined indirectly via first the enzymatic oxidation in the presence of glucose oxidase (GOD) which concurrently produces hydrogen peroxide. The formed hydrogen peroxide then reacts with 4-aminophenazone and phenol under peroxidase (POD) as catalyst to give a red-violet quinoneimine dye as indicator. The inhibitory effect of the synthesized compounds against rat enzyme was quantified by UV at 500 nm, in term of quinoneimine decline (Scheme 2.6).



Scheme 2.6 Hydrolysis of rat intestinal α -glucosidase.

Rat intestinal α -glucosidase inhibitory activity was determined according to the modified method of Wikul *et al* [39]. The crude enzyme solution prepared from

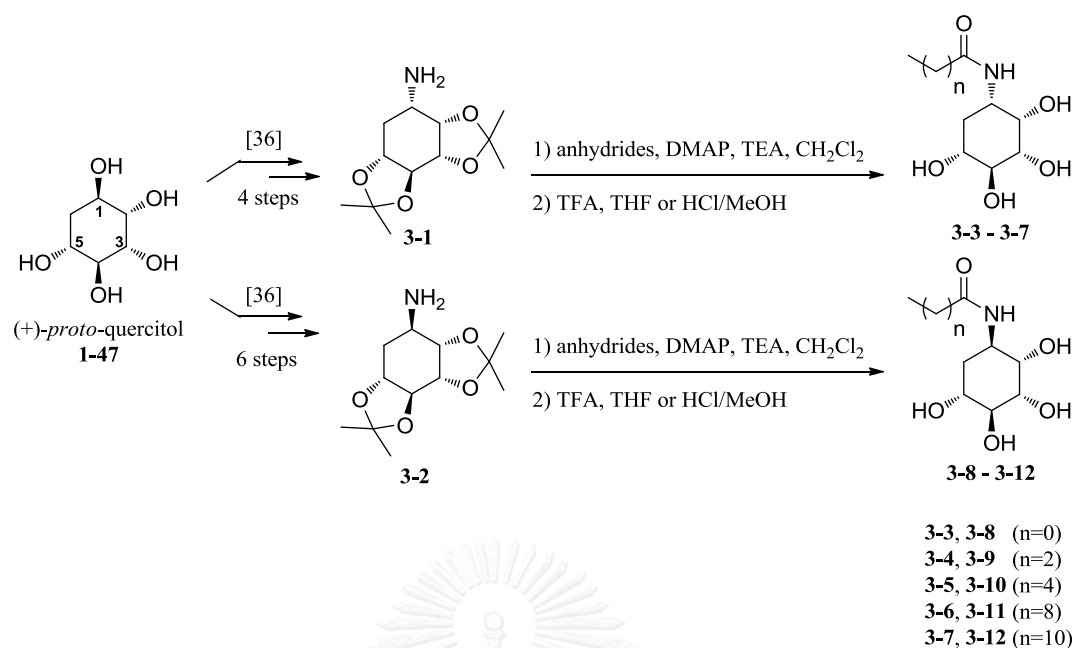
rat intestinal acetone powder was used as a source of maltase and sucrase. Rat intestinal acetone powder (1 g) was homogenized in 30 mL of 0.9% NaCl solution. After centrifugation (12,000 g × 30 min), the solution was subjected to assay. A 10 μL of the synthesized compounds (1 mg/mL in DMSO) was pre-incubated with crude enzyme solution (as maltase, 20 μL ; as sucrase, 20 μL , respectively) at 37 °C for 10 min. The substrate solution (maltose: 0.58 mM, 20 μL ; sucrose: 20 mM, 20 μL , respectively) in 0.1 M phosphate buffer (pH 6.9) was then added to the reaction mixture and incubated at 37 °C for 40 min. The mixture was heated in the oven at 80 °C for 15 min to stop the reaction. The concentration of glucose released from the reaction mixture was determined by the glucose oxidase method using a commercial glucose assay kit. The percent inhibition of the enzymatic activity was calculated as $[(A_0 - A_1)/A_0] \times 100$, where A_0 is the absorbance without the sample, and A_1 is the absorbance with the sample. The IC_{50} value was determined from a plot of percent inhibition versus sample concentration. Acarbose[®] was used as standard control and the experiment was performed in triplicate.

CHAPTER III
SYNTHESIS OF NEW *N*-SUBSTITUTED AMINOQUERCITOLS FROM
NATURALLY AVAILABLE (+)-*proto*-QUERCITOL AND THEIR α -
GLUCOSIDASE INHIBITORY ACTIVITY

In our previous report [36], we developed an efficient synthetic method for the construction of aminoquercitol framework starting from chiral building block (+)-*proto*-quercitol. This method provided a concise synthesis of aminoquercitols in excellent overall yield. With the success of our methodology in hand, we herein expand this approach to synthesize a new series of *N*-substituted aminoquercitols.

3.1 Synthesis of *N*-substituted aminoquercitols

After we obtained aminoquercitols **3-1** and **3-2** in hand, we began to synthesize the series of *N*-acyl aminoquercitols (**3-3** – **3-12**) as depicted in Scheme 3.1. With the aim of gaining information on structure–activity relationships, both aminoquercitols **3-1** and **3-2** were reacted with the corresponding anhydrides encompassing various alkyl chain lengths. This design was aimed at determining the optimal length of the aliphatic linker and also exploring the effect of the stereochemistry at C1 for glucosidase inhibition. After acylation, all products were deprotected with either TFA or HCl to afford the *N*-acyl derivatives **3-3** – **3-12** in fair to good yields (Scheme 3.1).



Scheme 3.1 Synthesis of *N*-acyl aminoquercitols.

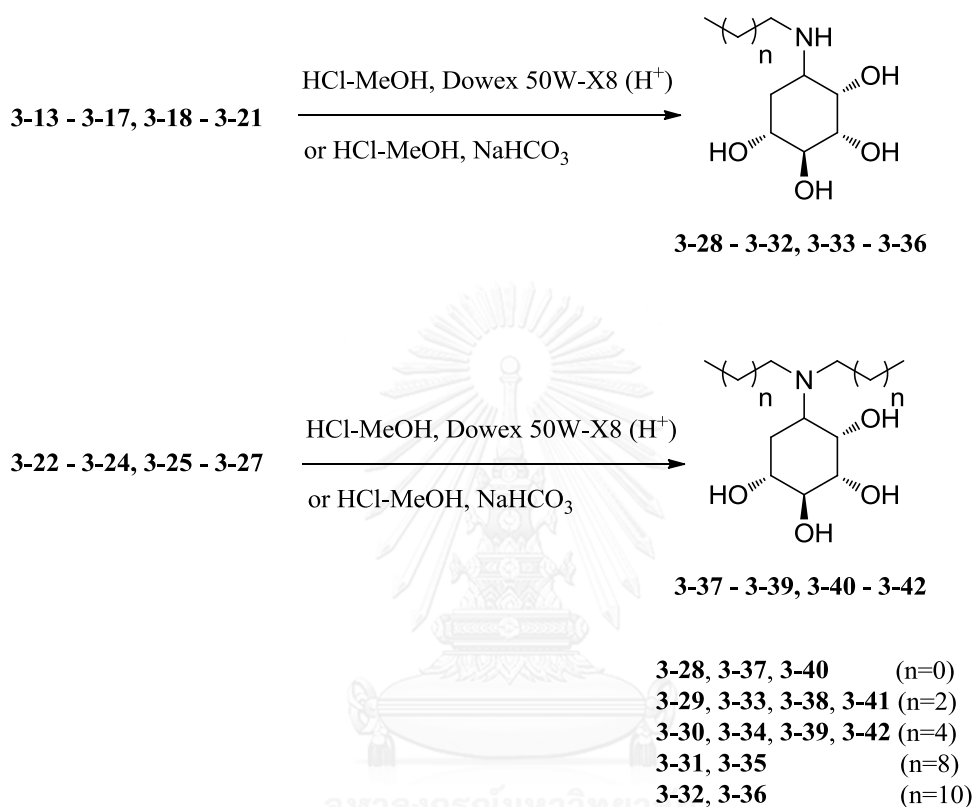
The search for more potent *N*-substituted aminoquercitols has prompted us to further prepare *N*-alkylated analogues **3-28** – **3-36**. Synthesis of these compounds involved reductive amination between aminoquercitols (**3-1** and **3-2**) and various alkyl aldehydes in the presence of NaBH₃CN as reducing agent and acids as catalyst. Notably, the numbers of methylenes in this series were equal to the *N*-acylated analogues (**3-3** – **3-12**). This is for comparative purpose. Surprisingly, treatment of **3-1** with acetaldehyde in the presence of acetic acid as catalyst did not provide the desired secondary amine **3-13** but yielded the tertiary amine **3-22** as the sole product in 48% yield (Table 3.1). The dialkylation of amines is commonly encountered due to the occurrence of a second reductive amination mediated by AcOH [41]. To circumvent this problem, reductive amination of **3-1** with acetaldehyde was carried out in the presence of mild Lewis acid such as Ti(O^{*i*}Pr)₄, therefore producing the desired monoalkylated product **3-13** together with dialkylated product **3-22** in a ratio of 3 : 1. Even though the selectivity of this transformation is not impressive, it offers compound diversity, which possibly provides additional information about the structural requirement for glucosidase

inhibitory activity. Thus, similar chemistry was applied for the synthesis of monoalkylated analogues and dialkylated analogues from the corresponding amines **3-1** and **3-2**. Reductive amination of **3-1** and **3-2** with various aldehydes in the presence of NaBH_3CN and catalysts such as either acetic acid or titanium isopropoxide afforded protected monoalkylated (**3-13** – **3-21**) and dialkylated aminoquercitols **3-22** – **3-27** (Table 3.1).

Table 3.1 Reaction conditions for reductive amination

Amine	Aldehyde (n)	Acid	Isolated yield (%)	
			2° amine	3° amine
3-1	0	AcOH	-	3-22 (48%)
3-1	0	$\text{Ti}(\text{O}^i\text{Pr})_4$	3-13 (29%)	3-22 (11%)
3-1	2	AcOH	3-14 (34%)	3-23 (51%)
3-1	4	AcOH	3-15 (51%)	3-24 (38%)
3-1	8	AcOH	3-16 (60%)	-
3-1	10	AcOH	3-17 (50%)	-
3-2	0	AcOH	-	3-25 (45%)
3-2	2	AcOH	-	3-26 (57%)
3-2	2	$\text{Ti}(\text{O}^i\text{Pr})_4$	3-18 (14%)	3-26 (26%)
3-2	4	AcOH	-	3-27 (91%)
3-2	4	$\text{Ti}(\text{O}^i\text{Pr})_4$	3-19 (54%)	3-27 (16%)
3-2	8	AcOH	3-20 (67%)	-
3-2	10	AcOH	3-21 (32%)	-

Finally, cleavage of the two acetonide protecting groups in **3-13** – **3-27** under acidic conditions generated the target *N*-alkylated analogues **3-28** – **3-42** in good yields (Scheme 3.2).



Scheme 3.2 Synthesis of *N*-alkyl aminoquercitols.

3.2 α -Glucosidase inhibitory activity of *N*-substituted aminoquercitols

All target compounds were evaluated for α -glucosidase inhibitory activity using enzymes from two different sources; baker's yeast (type I) and rat intestine (type II), and the results are illustrated in Table 3.2. Generally, *N*-acyl and *N*-alkyl aminoquercitols displayed weak (IC_{50} 150–2300 μ M) to no inhibition against α -glucosidase from baker's yeast. The inhibitory activity of *N*-acyl aminoquercitols (**3-3** – **3-7** and **3-8** – **3-12**) tends to decrease with the extension of chain length, which was supported by the similar results of *N,N*-dialkyl aminoquercitols (**3-37** – **3-39** and **3-40** – **3-42**). We supposed that the greater hydrophobicity from the alkyl chain

caused a reduction in inhibitory effect. Of all synthesized compounds, **3-8** showed the highest inhibition with an IC_{50} value of 150 μ M, which was three-fold more active than acarbose.

Table 3.2 α -Glucosidase inhibitory effect of *N*-substituted aminoquercitols

Compound	IC_{50} (μ M)			Compound	IC_{50} (μ M)		
	Baker's yeast	Maltase ^a	Sucrase ^a		Baker's yeast	Maltase ^a	Sucrase ^a
3-1a	2,890	5.8	7.3	3-30	NI	2.5	NI
3-2a	12.5	4.4	6.8	3-31	NI	2.0	410
3-3	270	180	NI ^b	3-32	NI	1.9	NI
3-4	NI	38	NI	3-33	1200	57	NI
3-5	NI	4.2	NI	3-34	400	0.24	NI
3-6	NI	2.0	NI	3-35	NI	0.41	NI
3-7	NI	10	NI	3-36	NI	1.5	NI
3-8	150	5.3	5.3	3-37	1600	21	360
3-9	1200	19	4.7	3-38	2300	24	36
3-10	1700	3.8	6.1	3-39	NI	32	120
3-11	NI	3.5	NI	3-40	1600	5.0	NI
3-12	NI	7.4	NI	3-41	1800	7.6	NI
3-28	NI	NI	NI	3-42	NI	48	NI
3-29	NI	290	NI	Acarbose[®]	480	1.5	2.3

^a α -glucosidase was obtained from rat small intestine.

^b No inhibition (inhibitory effect < 30% at 10 mg/mL for baker's yeast and at 1 mg/mL for maltase and sucrase)

As for type II α -glucosidases, *N*-substituted aminoquercitols inhibited maltase more selectively than sucrase, varying from low (IC_{50} 180–290 μ M) to high (IC_{50} 0.24–0.41 μ M) potency. Generally, the inhibitory effect increased according to chain length; the maximum inhibitions were observed where *n* was 4 and 8 (Figure 3.1). From the *N*-acyl and *N*-alkyl series, **3-6** (*n* = 8) and **3-34** (*n* = 4) were the most potent

maltase inhibitors with IC_{50} values of 2.0 and 0.24 μM , respectively. However, the inhibitory effect dropped significantly (2–5 times) when n reached 10. With a given n , the *N*-alkyl series were likely to be more potent than their corresponding *N*-acyl analogues. In addition to the aforementioned factors, a relationship between configuration of C-1 and inhibitory effect was also observed. *N*-Alkyl aminoquercitols **3-33** – **3-35**, all prepared from **3-2**, apparently exerted stronger inhibition than their corresponding epimers **3-29** – **3-31**, generated from **3-1**. However, the configuration of C-1 had no impact on the inhibitory activity of the *N*-acyl series. In our experiment, we discovered that **3-36** was equipotent to acarbose whereas **3-34** and **3-35** revealed higher inhibition.

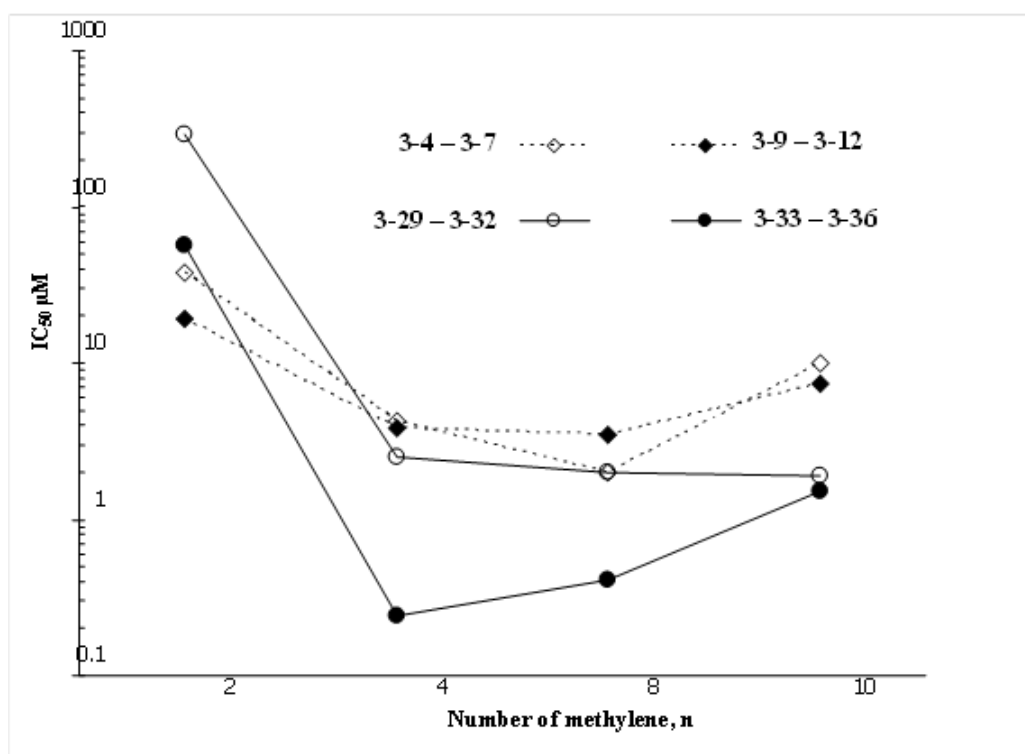


Figure 3.1 Inhibition trends of selected *N*-acyl (**3-4** – **3-7** and **3-9** – **3-12**) and *N*-alkyl (**3-29** – **3-32** and **3-33** – **3-36**) aminoquercitols against rat intestinal maltase.

In contrast to the *N*-acyl and *N*-alkyl series, the inhibitory activity of *N,N*-dialkyl aminoquercitols **3-40** – **3-42** (IC_{50} 5.0–48 μ M) depended largely on the steric hindrance of the alkyl groups whereas the inhibitory effect of the corresponding diastereomers **3-37** – **3-39** (IC_{50} 21–32 μ M) was comparable. Compared to the most potent *N*-alkyl aminoquercitol **3-34**, the corresponding *N,N*-dialkyl analogue **3-42** revealed approximately 200-fold weaker inhibition. A similar trend was also observed in tertiary *N*-alkylated arabinoiminofuranoses, whose inhibitions were approximately 10^2 -times less potent than their corresponding secondary amines [42].

3.3 Kinetic study and a possible mechanism underlying the maltase inhibition of *N*-substituted aminoquercitols

Apparently, *N*-substituted aminoquercitols selectively inhibited type II, particularly maltase, rather than type I α -glucosidase. Since rat intestinal maltase used in this experiment and that of humans are categorized into the same group [43, 44], an insight into how *N*-substituted aminoquercitols inhibit maltase function is required for further development in therapeutic application.

We therefore investigated the inhibitory mechanism of **3-6**, **3-34** and **3-40**, all of which were the most potent inhibitors and representatives of *N*-acyl, *N*-alkyl and *N,N*-dialkyl aminoquercitols, respectively. Lineweaver–Burk plots of the initial velocity versus substrate concentrations in the presence of different concentrations of the inhibitors gave a series of straight lines, all of which intersected at the *Y*-axis (Figure 3.2). The analysis revealed the increase in K_m values while V_{max} remained constant. This behavior indicated that **3-6**, **3-34** and **3-40** inhibited maltase in a competitive manner (Table 3.3) through forming enzyme–inhibitor (EI) complexes, the same as observed in the antidiabetic acarbose.

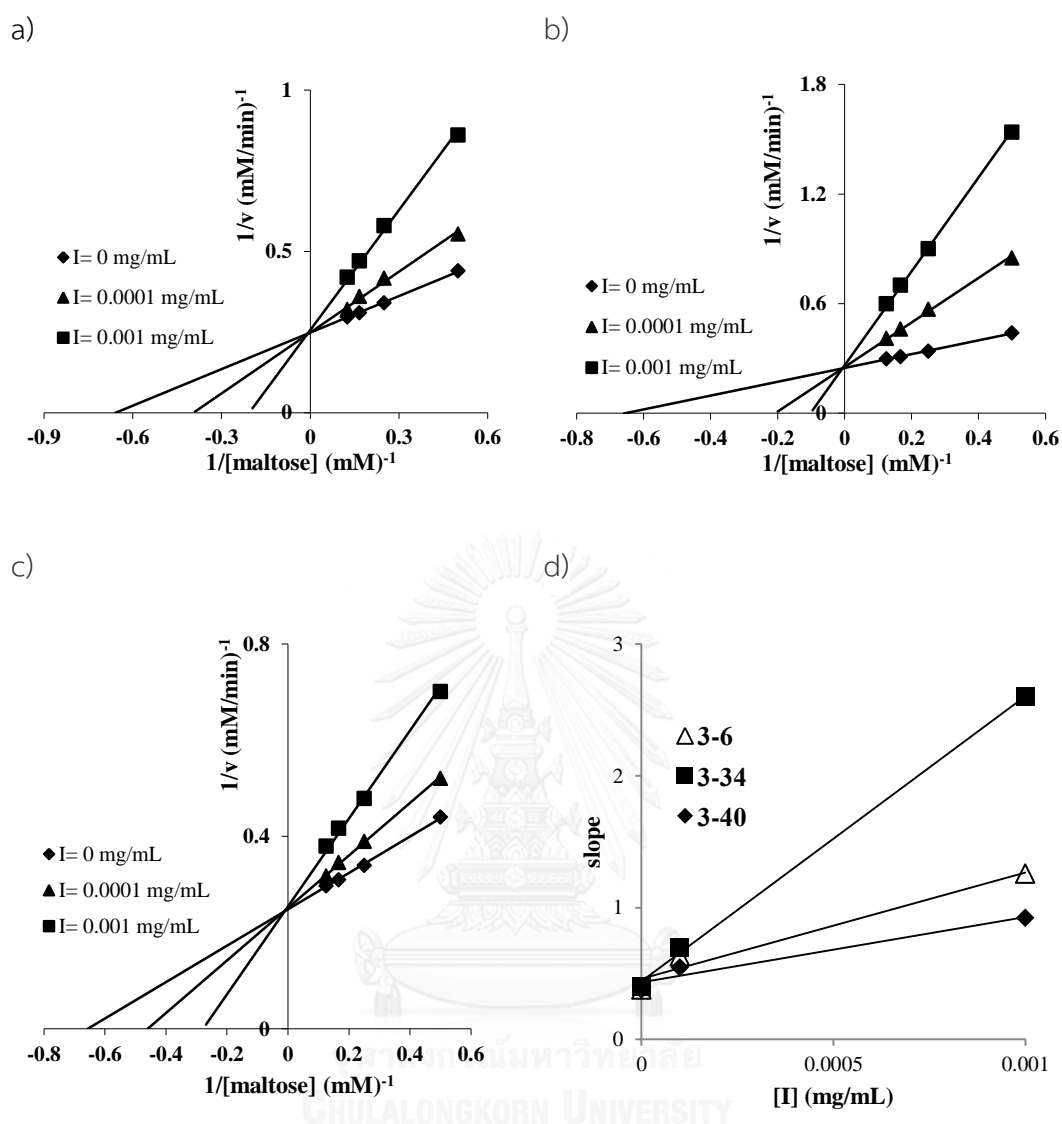


Figure 3.2 Lineweaver-Burk plots for inhibitory activity against rat intestinal maltase. (a) *N*-acyl aminoquercitol **3-6**, (b) *N*-alkyl aminoquercitol **3-34**, (c) *N,N*-dialkyl aminoquercitol **3-40** and (d) secondary replots of slope vs. $[I]$ from a primary Lineweaver-Burk plot for the determination of K_i .

To envisage the binding affinity between the *N*-substituted aminoquercitols and maltase, secondary replots were performed. The slopes of the lines in the Lineweaver-Burk relation *versus* inhibitor concentration in the secondary replot produced EI dissociation constants (K_i) of 1.5, 0.73 and 3.5 μM for **3-6**, **3-34** and **3-40** (Table 3.3), respectively. The higher K_i values of **3-6** and **3-40** over that of acarbose

indicated their weaker EI binding. In contrast, *N*-alkyl aminoquercitol **3-34** having a lower K_i obviously bound to maltase more tightly than acarbose. Due to its potent inhibitory effect and strong binding with maltase, **3-34** could serve as a new candidate for antidiabetic drug development through mainly retarding maltase function.

Table 3.3 Inhibitory effect against rat intestinal maltase and kinetic parameters of **3-6**, **3-34**, **3-40**

Compound	IC ₅₀ (μM)	K _i (μM)	Inhibition type
3-6	2.0	1.5	Competitive
3-34	0.24	0.73	Competitive
3-40	5.0	3.5	Competitive
Acarbose	1.5	0.99	Competitive

3.4 Conclusion

In summary, we first synthesized a series of *N*-acyl and *N*-alkyl aminoquercitols having different chain lengths from (+)-*proto*-quercitol. Evaluation of their α-glucosidase inhibition revealed that they selectively inhibited rat intestinal maltase (type II glucosidase) rather than yeast glucosidase (type I glucosidase). Of the compounds examined, *N*-alkyl aminoquercitols (**3-34** and **3-35**) having medium chains (C₆ and C₁₀) showed highly potent inhibition at sub-micromolar level (IC₅₀ 0.24 and 0.41 μM), whereas antidiabetic drug acarbose was 3–6 times less active (IC₅₀ 1.5 μM). Although *N*-alkylated aminocyclitols have been expected to exert an improved

inhibitory effect, against α -glucosidase, than their unsubstituted precursors, there have been few reports demonstrating the optimal chain length required for potent activity. Our findings also provided an insight into the importance of the hydrophobicity of medium alkyl chains ($\leq C_{10}$) in exerting inhibitory activity, possibly due to being a more preferred structure to fit into the binding site of enzyme.

In addition, the kinetic studies on the mechanism of α -glucosidase inhibition by particularly active compounds (**3-6**, **3-34** and **3-40**) showed competitive inhibition. More importantly, the most potent *N*-alkyl aminoquercitol **3-34** revealed stronger binding to maltase than acarbose. The synthesis of the new *N*-substituted aminoquercitols reported herein could provide necessary data on the structural requirement for designing other potent α -glucosidase inhibitors.

3.5 Experimental section

3.5.1 General experimental procedures

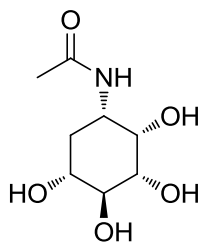
General experiments performed in this Chapter were similar to those described in Chapter 2.

3.5.2 Synthesis of *N*-acyl aminoquercitols

General procedure for synthesis of *N*-acyl-aminoquercitols **3-3** – **3-6**

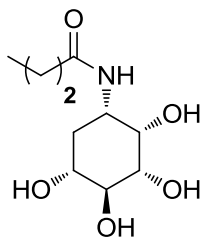
To a stirred solution of aminocyclitol **3-1** or **3-2** (0.14 mmol) in CH_2Cl_2 (1.4 mL) was added DMAP (ca. 1-2 mg) and TEA (1.09 mmol). After the clear solution was obtained, anhydride compounds (0.41 mmol) were added slowly, and the mixture was stirred at room temperature for 3 h. The reaction mixture was extracted with CH_2Cl_2 (3×10 mL), washed with brine, dried over anhydrous Na_2SO_4 , filtered and concentrated under reduced pressure. The crude product was treated with trifluoroacetic acid (0.74 mmol) in THF (2 mL) and stirred at room temperature for 4 h. The reaction mixture was evaporated to dryness, redissolved in EtOAc, and extracted with H_2O (3 × 10 mL). The combined aqueous layers were loaded onto Diaion HP-20 column and washed with H_2O followed by MeOH. Fractions eluted with H_2O were lyophilized to afford *N*-acyl aminoquercitols.

N-((1*S*,2*S*,3*S*,4*S*,5*R*)-2,3,4,5-tetrahydroxycyclohexyl)acetamide (3-3).



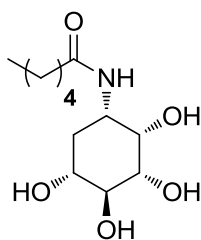
White solid (74%). ^1H NMR (D_2O , 400 MHz) δ 3.91 (br s, 1H, H-2), 3.80 (br d, $J = 12.0$ Hz, 1H, H-1), 3.42-3.50 (m, 3H, H-3,4,5), 1.93 (s, 3H, $-\text{CH}_3$), 1.82 (m, 1H, H-6), 1.66 (q, $J = 12.0$ Hz, 1H, H-6); ^{13}C NMR (D_2O + one drop acetone- d_6 , 100 MHz) δ 173.3, 74.2, 72.2, 70.8, 69.9, 47.0, 31.4, 21.8; HRMS m/z 228.0841 $[\text{M}+\text{Na}]^+$ (calcd for $\text{C}_8\text{H}_{15}\text{NO}_5\text{Na}$, 228.0848).

N-((1*S*,2*S*,3*S*,4*S*,5*R*)-2,3,4,5-tetrahydroxycyclohexyl)butyramide (3-4).



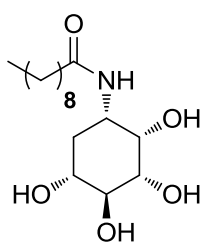
White solid (63%). ^1H NMR (D_2O , 400 MHz) δ 3.89 (s, 1H, H-2), 3.77 (d, $J = 12.8$ Hz, 1H, H-1), 3.41-3.45 (m, 3H, H-3,4,5), 2.13 (t, $J = 7.2$ Hz, 2H, $-\text{OCC}\underline{\text{H}}_2-$), 1.79 (m, 1H, H-6), 1.63 (q, $J = 12.0$ Hz, 1H, H-6), 1.48 (m, 2H, $-\text{CH}_2-$), 0.78 (t, $J = 7.2$ Hz, 3H, $-\text{CH}_3$); ^{13}C NMR (D_2O , 100 MHz) δ 176.4, 74.2, 72.4, 71.0, 70.0, 46.9, 37.6, 31.6, 19.0, 12.8; HRMS m/z 256.1159 $[\text{M}+\text{Na}]^+$ (calcd for $\text{C}_{10}\text{H}_{19}\text{NO}_5\text{Na}$, 256.1161).

N-((1*S*,2*S*,3*S*,4*S*,5*R*)-2,3,4,5-tetrahydroxycyclohexyl)hexanamide (3-5).



White solid (52%). ^1H NMR (D_2O , 400 MHz) δ 3.77 (br s, 1H, H-2), 3.68 (br d, $J = 12.4$ Hz, 1H, H-1), 3.29-3.34 (m, 3H, H-3,4,5), 2.05 (t, $J = 7.2$ Hz, 2H, $-\text{OCCH}_2-$), 1.68 (m, 1H, H-6), 1.53 (q, $J = 12.0$ Hz, 1H, H-6), 1.38 (m, 2H, $-\text{CH}_2-$), 1.08 (br s, 4H, $-(\text{CH}_2)_2-$), 0.66 (t, $J = 6.0$ Hz, 3H, $-\text{CH}_3$); ^{13}C NMR (CD_3OD , 100 MHz) δ 174.2, 74.6, 73.1, 71.2, 70.3, 46.9, 35.5, 32.1, 31.0, 25.2, 22.0, 12.8; HRMS m/z 262.1652 $[\text{M}+\text{H}]^+$ (calcd for $\text{C}_{12}\text{H}_{24}\text{NO}_5$, 262.1654).

***N*-((1*S*,2*S*,3*S*,4*S*,5*R*)-2,3,4,5-tetrahydroxycyclohexyl)decanamide (3-6).**

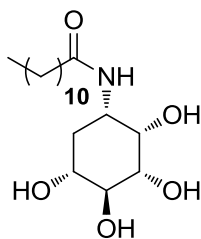


White solid (58%). $[\alpha]_{\text{D}}^{20} = -20.8$ (c 0.23, CH_3OH); ^1H NMR (CD_3OD , 400 MHz) δ 3.77 (br s, 1H, H-2), 3.73 (m, 1H, H-1), 3.41 (dd, $J = 9.6, 9.2$ Hz, 1H, H-4), 3.31 (m, 1H, H-5), 3.23 (m, 1H, H-3), 2.10 (t, $J = 7.6$ Hz, 2H, $-\text{OCCH}_2-$), 1.66-1.73 (m, 2H, H-6), 1.48-1.52 (m, 2H, $-\text{CH}_2-$), 1.20 (br s, 12H, $-(\text{CH}_2)_6-$), 0.80 (t, $J = 6.4$ Hz, 3H, $-\text{CH}_3$); ^{13}C NMR (CD_3OD , 100 MHz) δ 175.7, 76.1, 74.6, 72.6, 71.8, 48.4, 37.0, 33.6, 33.1, 30.6, 30.5, 30.4, 30.3, 27.0, 23.7, 14.4; HRMS m/z 318.2286 $[\text{M}+\text{H}]^+$ (calcd for $\text{C}_{16}\text{H}_{32}\text{NO}_5$, 318.2280).

General procedure for the synthesis of *N*-acyl aminoquercitols 3-7 – 3-12

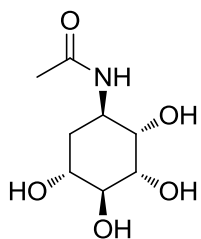
To a stirred solution of aminocyclitol **3-1** or **3-2** (0.14 mmol) in CH_2Cl_2 (1.4 mL) was added DMAP (ca. 1-2 mg) and TEA (1.09 mmol). After the clear solution was obtained, anhydride compounds (0.41 mmol) were added slowly, and the mixture was stirred at room temperature for 3 h. The reaction mixture was extracted with CH_2Cl_2 (3×10 mL), washed with brine, dried over anhydrous Na_2SO_4 , filtered and concentrated under reduced pressure. The crude product was treated with 1.25 M methanolic HCl (0.7 mL) and stirred at room temperature for 4 h. The reaction mixture was evaporated under reduced pressure to give *N*-acyl aminoquercitols.

N-((1*S*,2*S*,3*S*,4*S*,5*R*)-2,3,4,5-tetrahydroxycyclohexyl)dodecanamide (3-7).



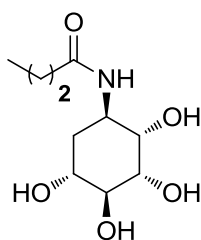
White solid (45%). ^1H NMR (CD_3OD , 400 MHz) δ 3.77 (br s, 1H, H-2), 3.74 (m, 1H, H-1), 3.41 (dd, $J = 9.2, 9.2$ Hz, 1H, H-4), 3.32 (m, 1H, H-5), 3.24 (m, 1H, H-3), 2.11 (t, $J = 7.6$ Hz, 2H, $-\text{OCCH}_2-$), 1.67-1.74 (m, 2H, H-6), 1.49-1.52 (m, 2H, $-\text{CH}_2-$), 1.20 (br s, 16H, $-(\text{CH}_2)_8-$), 0.81 (t, $J = 6.0$ Hz, 3H, $-\text{CH}_3$); ^{13}C NMR (CD_3OD , 100 MHz) δ 175.7, 76.1, 74.6, 72.6, 71.8, 48.4, 37.0, 33.6, 33.1, 30.7, 30.6, 30.5, 30.4, 30.3, 27.0, 23.7, 14.4; HRMS m/z 368.2408 $[\text{M}+\text{Na}]^+$ (calcd for $\text{C}_{18}\text{H}_{35}\text{NO}_5\text{Na}$, 368.2413).

N-((1*R*,2*S*,3*S*,4*S*,5*R*)-2,3,4,5-tetrahydroxycyclohexyl)acetamide (3-8).



Pale yellow oil (quantitative yield). ^1H NMR (D_2O , 400 MHz) δ 3.82 (br s, 1H, H-1), 3.67 (br s, 1H, H-2), 3.48 (br s, 1H, H-5), 3.38 (br s, 2H, H-3,4), 1.74 (s, 3H, $-\text{CH}_3$), 1.64 (m, 2H, H-6); ^{13}C NMR (D_2O , 100 MHz) δ 174.0, 73.8, 71.3, 70.7, 69.2, 48.5, 30.9, 22.0; HRMS m/z 206.1024 $[\text{M}+\text{H}]^+$ (calcd for $\text{C}_8\text{H}_{16}\text{NO}_5$, 206.1028).

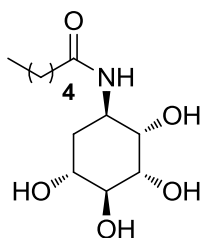
N-((1*R*,2*S*,3*S*,4*S*,5*R*)-2,3,4,5-tetrahydroxycyclohexyl)butyramide (3-9).



Yellow solid (52%). ^1H NMR (D_2O , 400 MHz) δ 3.89 (m, 1H, H-1), 3.72 (br s, 1H, H-1), 3.52 (m, 1H, H-5), 3.43 (m, 2H, H-3,4), 2.02 (t, $J = 7.2$ Hz, 2H, $-\text{OCCH}_2-$), 1.70 (m,

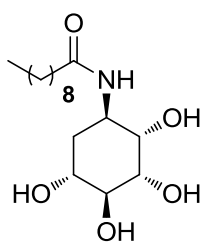
2H, H-6), 1.34-1.43 (m, 2H, -CH₂-), 0.68 (t, $J = 7.6$ Hz, 3H, -CH₃); ¹³C NMR (D₂O, 100 MHz) δ 177.0, 73.7, 71.3, 70.6, 69.2, 48.4, 37.4, 30.8, 19.2, 12.6; HRMS m/z 234.1333 [M+H]⁺ (calcd for C₁₀H₂₀NO₅, 234.1341).

***N*-((1*R*,2*S*,3*S*,4*S*,5*R*)-2,3,4,5-tetrahydroxycyclohexyl)hexanamide (3-10).**



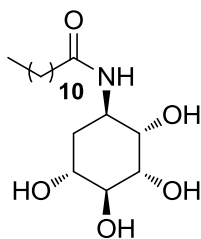
Yellow oil (quantitative yield). ¹H NMR (D₂O, 400 MHz) δ 3.87 (br d, $J = 3.6$ Hz, 1H, H-1), 3.71 (br s, 1H, H-2), 3.51 (m, 1H, H-5), 3.41 (br d, $J = 5.2$ Hz, 2H, H-3,4), 2.03 (t, $J = 7.2$ Hz, 2H, -OCCH₂-), 1.68-1.71 (m, 2H, H-6), 1.33-1.40 (m, 2H, -CH₂-), 1.02-1.12 (m, 4H, -(CH₂)₂-), 0.64 (t, $J = 6.8$ Hz, 3H, -CH₃); ¹³C NMR (D₂O + one drop of acetone-*d*₆, 100 MHz) δ 177.0, 73.6, 71.1, 70.5, 69.0, 48.2, 35.3, 30.7, 30.3, 25.0, 21.5, 13.1; HRMS m/z 262.1650 [M+H]⁺ (calcd for C₁₂H₂₄NO₅, 262.1654).

***N*-((1*R*,2*S*,3*S*,4*S*,5*R*)-2,3,4,5-tetrahydroxycyclohexyl)decanamide (3-11).**



White solid (83%). ¹H NMR (CD₃OD, 400 MHz) δ 4.04 (m, 1H, H-1), 3.71 (m, 1H, H-2), 3.55-3.61 (m, 2H, H-4,5), 3.49 (m, 1H, H-3), 2.11 (t, $J = 7.2$ Hz, 2H, -OCCH₂-), 1.85 (m, 1H, H-6), 1.68 (m, 1H, H-6), 1.50 (br s, 2H, -CH₂-), 1.20 (br s, 12H, -(CH₂)₆-), 0.80 (t, $J = 6.8$ Hz, 3H, -CH₃); ¹³C NMR (CD₃OD, 100 MHz) δ 174.9, 73.5, 72.4, 71.0, 69.6, 47.6, 36.5, 31.7, 31.6, 29.2, 29.1, 29.0, 28.9, 25.7, 22.3, 13.0; HRMS m/z 318.2271 [M+H]⁺ (calcd for C₁₆H₃₂NO₅, 318.2280).

N-((1*R*,2*S*,3*S*,4*S*,5*R*)-2,3,4,5-tetrahydroxycyclohexyl)dodecanamide (**3-12**).



White solid (quantitative yield). ^1H NMR (CD_3OD , 400 MHz) δ 4.03 (m, 1H, H-1), 3.71 (m, 1H, H-2), 3.55-3.61 (m, 2H, H-4,5), 3.49 (m, 1H, H-3), 2.11 (t, $J = 6.8$ Hz, 2H, - OCCH_2 -), 1.83 (m, 1H, H-6), 1.69 (m, 1H, H-6), 1.50 (br s, 2H, - CH_2 -), 1.19 (br s, 16H, - $(\text{CH}_2)_8$ -), 0.80 (t, $J = 6.4$ Hz, 3H, - CH_3); ^{13}C NMR (CD_3OD , 100 MHz) δ 176.4, 74.9, 73.9, 72.5, 71.2, 48.4, 37.0, 33.2, 33.1, 30.7, 30.7, 30.6, 30.5, 30.4, 30.3, 27.1, 23.7, 14.4; HRMS m/z 368.2403 [$\text{M}+\text{Na}$] $^+$ (calcd for $\text{C}_{18}\text{H}_{35}\text{NNaO}_5$, 368.2413).

3.5.3 Synthesis of *N*-alkyl aminoquercitols

3.5.3.1 General procedure for reductive amination

Using AcOH

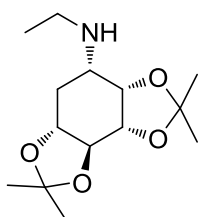
A solution of aminocyclitols **3-1** or **3-2** (0.12 mmol) in methanol (1.1 mL) under an atmosphere of N_2 was treated with sodium cyanoborohydride (0.22 mmol), acetic acid (8 μL) and the corresponding aldehyde (0.11 mmol). After stirring at room temperature for 2 days, the reaction mixture was evaporated to dryness, quenched with water and extracted with EtOAc (3 \times 10 mL). The combined organic layers were washed with brine, dried over anhydrous Na_2SO_4 and concentrated under reduced pressure to afford crude product, which was purified by flash chromatography or Sephadex LH-20 column chromatography.

Using $\text{Ti}(\text{O}^i\text{Pr})_4$

A solution of aminocyclitols **3-1** or **3-2** (0.16 mmol) in methanol (1.6 mL) under an atmosphere of N_2 was treated with corresponding aldehyde (0.19 mmol), titanium isopropoxide (0.20 mmol) and sodium cyanoborohydride (0.40 mmol). After

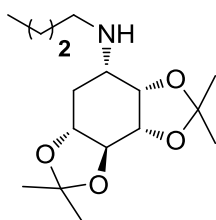
stirring at 0 °C for 1 day, the reaction mixture was evaporated to dryness, quenched with water and extracted with EtOAc (3×10 mL). The combined organic layers were washed with brine, dried over anhydrous Na₂SO₄ and concentrated under reduced pressure to afford crude product, which was purified by flash chromatography or sephadex LH-20 column chromatography.

(1*S*,2*S*,3*S*,4*S*,5*R*)-(2,3:4,5-di-*O*-isopropylidene)-*N*-ethylcyclohexylamine (3-13).

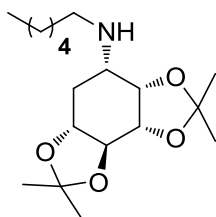


White solid (29%), (5% MeOH-EtOAc for flash column). ¹H NMR (CDCl₃, 400 MHz) δ 4.37 (dd, *J* = 6.0, 4.4 Hz, 1H), 4.08 (dd, *J* = 8.8, 4.8 Hz, 1H), 3.47 (dd, *J* = 10.4, 8.8 Hz, 1H), 3.22 (m, 1H), 3.04 (m, 1H), 2.72 (q, *J* = 7.2 Hz, 2H), 2.33 (m, 1H), 1.50 (m, 1H), 1.47 (s, 3H), 1.36 (s, 3H), 1.34 (s, 3H), 1.30 (s, 3H), 1.10 (t, *J* = 7.2 Hz, 3H); ¹³C NMR (CDCl₃, 100 MHz) δ 111.0, 109.4, 82.4, 76.6, 75.1, 74.4, 54.7, 41.0, 30.5, 28.6, 26.9, 26.9, 26.2, 14.8.

(1*S*,2*S*,3*S*,4*S*,5*R*)-(2,3:4,5-di-*O*-isopropylidene)-*N*-butylcyclohexylamine (3-14).

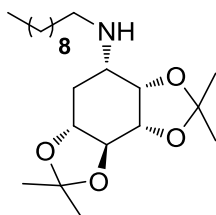


White solid (34%), (100% EtOAc for flash column). ¹H NMR (CDCl₃, 400 MHz) δ 4.36 (dd, *J* = 5.2, 4.4 Hz, 1H), 4.07 (dd, *J* = 8.4, 4.8 Hz, 1H), 3.49 (dd, *J* = 10.4, 8.8 Hz, 1H), 3.23 (m, 1H), 2.97 (m, 1H), 2.62-2.66 (m, 2H), 2.30 (m, 1H), 1.50 (m, 1H), 1.47 (s, 3H), 1.41-1.45 (m, 4H), 1.36 (s, 3H), 1.34 (s, 3H), 1.31 (s, 3H), 0.86 (t, *J* = 7.6 Hz, 3H); ¹³C NMR (CDCl₃, 100 MHz) δ 109.9, 108.4, 81.4, 75.6, 74.3, 73.4, 54.2, 45.8, 31.1, 29.8, 27.6, 25.9, 25.9, 25.2, 19.4, 12.9.

(1*S*,2*S*,3*S*,4*S*,5*R*)-(2,3:4,5-di-*O*-isopropylidene)-*N*-hexylcyclohexylamine (3-15).

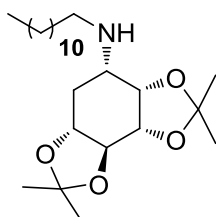
Colorless oil (51%), (100% EtOAc for flash column). ^1H NMR (CDCl_3 , 400 MHz)

δ 4.38 (dd, $J = 5.6, 4.4$ Hz, 1H), 4.08 (dd, $J = 8.4, 4.8$ Hz, 1H), 3.47 (dd, $J = 10.0, 8.4$ Hz, 1H), 3.22 (m, 1H), 3.08 (m, 1H), 2.67 (t, $J = 7.2$ Hz, 2H), 2.33 (m, 1H), 1.54 (m, 1H), 1.46-1.51 (m, 2H), 1.46 (s, 3H), 1.36 (s, 3H), 1.34 (s, 3H), 1.30 (s, 3H), 1.23 (br s, 6H), 0.82 (t, $J = 6.8$ Hz, 3H); ^{13}C NMR (CDCl_3 , 100 MHz) δ 111.0, 109.5, 82.3, 76.5, 74.7, 74.2, 54.5, 46.5, 31.5, 30.1, 29.1, 28.5, 26.9, 26.9, 26.8, 26.2, 22.5, 14.0.

(1*S*,2*S*,3*S*,4*S*,5*R*)-(2,3:4,5-di-*O*-isopropylidene)-*N*-decylcyclohexylamine (3-16).

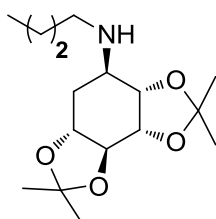
Pale yellow oil (60%), (80% EtOAc-hexane for flash column). ^1H NMR (CDCl_3 ,

400 MHz) δ 4.34 (dd, $J = 4.4, 4.4$ Hz, 1H), 4.06 (dd, $J = 8.4, 4.4$ Hz, 1H), 3.49 (dd, $J = 8.4, 8.4$ Hz, 1H), 3.23 (m, 1H), 2.93 (m, 1H), 2.58-2.61 (m, 2H), 2.28 (m, 1H), 1.46 (s, 3H), 1.42-1.45 (m, 3H), 1.36 (s, 3H), 1.34 (s, 3H), 1.30 (s, 3H), 1.19 (br s, 14H), 0.81 (t, $J = 6.4$ Hz, 3H); ^{13}C NMR (CDCl_3 , 100 MHz) δ 110.8, 109.2, 82.4, 75.6, 75.5, 74.5, 55.2, 47.2, 31.9, 31.0, 30.2, 29.6, 29.6, 29.5, 29.3, 28.6, 27.3, 26.9, 26.9, 26.2, 22.7, 14.1.

(1*S*,2*S*,3*S*,4*S*,5*R*)-(2,3:4,5-di-*O*-isopropylidene)-*N*-dodecylcyclohexylamine (3-17).

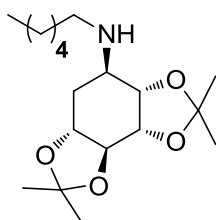
Pale yellow oil (50%), (80% EtOAc-hexane for flash column). ^1H NMR (CDCl_3 , 400 MHz) δ 4.36 (br s, 1H), 4.07 (m, 1H), 3.48 (dd, $J = 8.8, 8.8$ Hz, 1H), 3.23 (m, 1H), 2.98 (m, 1H), 2.63 (t, $J = 7.6$ Hz, 2H), 2.31 (m, 1H), 1.52-1.55 (m, 3H), 1.47 (s, 3H), 1.36 (s, 3H), 1.34 (s, 3H), 1.31 (s, 3H), 1.19 (br s, 18H), 0.81 (t, $J = 6.4$ Hz, 3H); ^{13}C NMR (CDCl_3 , 100 MHz) δ 109.0, 108.4, 81.4, 75.6, 74.3, 73.4, 54.1, 46.1, 30.9, 29.7, 28.9, 28.6, 28.6, 28.6, 28.5, 28.4, 28.3, 27.6, 26.3, 25.9, 25.9, 25.2, 21.7, 13.1.

(1*R*,2*S*,3*S*,4*S*,5*R*)-(2,3:4,5-di-*O*-isopropylidene)-*N*-butylcyclohexylamine (3-18).



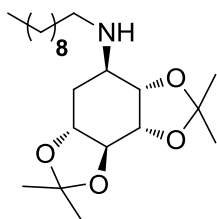
Pale yellow oil (14%), (100% EtOAc for flash column). ^1H NMR (CDCl_3 , 400 MHz) δ 4.24 (dd, $J = 7.6, 6.8$ Hz, 1H), 4.07 (dd, $J = 8.0, 7.2$ Hz, 1H), 3.65-3.68 (m, 2H), 3.02 (dt, $J = 8.0, 7.6$ Hz, 1H), 2.59 (m, 1H), 2.47 (m, 1H), 1.93 (m, 1H), 1.84 (m, 1H), 1.43 (s, 3H), 1.38-1.40 (m, 2H), 1.36 (s, 3H), 1.35 (s, 3H), 1.26-1.32 (m, 2H), 1.28 (s, 3H), 0.85 (t, $J = 7.6$ Hz, 3H); ^{13}C NMR (CDCl_3 , 100 MHz) δ 111.6, 109.9, 80.5, 78.8, 76.2, 72.6, 55.9, 47.3, 32.1, 30.2, 27.8, 27.1, 27.0, 25.2, 20.4, 13.9.

(1*R*,2*S*,3*S*,4*S*,5*R*)-(2,3:4,5-di-*O*-isopropylidene)-*N*-hexylcyclohexylamine (3-19).



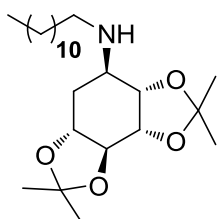
Colorless oil (54%), (80% EtOAc-hexane for flash column). ^1H NMR (CDCl_3 , 400 MHz) δ 4.24 (dd, $J = 6.8, 6.8$ Hz, 1H), 4.07 (dd, $J = 7.2, 7.2$ Hz, 1H), 3.65-3.70 (m, 2H), 3.02 (q, $J = 7.2$ Hz, 1H), 2.59 (m, 1H), 2.46 (m, 1H), 1.81-1.97 (m, 4H), 1.43 (s, 3H), 1.36 (s, 3H), 1.35 (s, 3H), 1.28 (s, 3H), 1.18-1.22 (m, 6H), 0.82 (t, $J = 6.4$ Hz, 3H); ^{13}C NMR (CDCl_3 , 100 MHz) δ 111.6, 109.9, 80.5, 78.7, 76.2, 72.6, 55.8, 47.6, 31.7, 30.2, 29.9, 27.8, 27.2, 27.0, 26.9, 25.2, 22.6, 14.0.

(1*R*,2*S*,3*S*,4*S*,5*R*)-(2,3:4,5-di-*O*-isopropylidene)-*N*-decylcyclohexylamine (3-20).



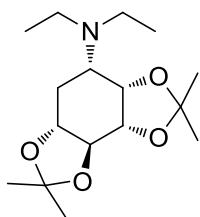
Colorless oil (67%), (80% EtOAc-hexane for flash column). ^1H NMR (CDCl_3 , 400 MHz) δ 4.24 (dd, $J = 8.0, 6.8$ Hz, 1H), 4.07 (dd, $J = 8.0, 6.8$ Hz, 1H), 3.66-3.67 (m, 2H), 3.02 (ddd, $J = 8.0, 7.6, 6.8$ Hz, 1H), 2.58 (m, 1H), 2.47 (m, 1H), 1.94 (br s, 1H), 1.85 (m, 1H), 1.43 (s, 3H), 1.36 (s, 3H), 1.35 (s, 3H), 1.28 (s, 3H), 1.19 (br s, 16H), 0.81 (t, $J = 6.8$ Hz, 3H); ^{13}C NMR (CDCl_3 , 100 MHz) δ 111.6, 109.9, 80.4, 78.7, 76.2, 72.6, 55.8, 47.6, 31.9, 30.2, 29.9, 29.6, 29.5, 29.4, 29.3, 27.8, 27.2, 27.1, 27.0, 25.2, 22.7, 14.1.

(1*R*,2*S*,3*S*,4*S*,5*R*)-(2,3:4,5-di-*O*-isopropylidene)-*N*-dodecylcyclohexylamine (3-21).



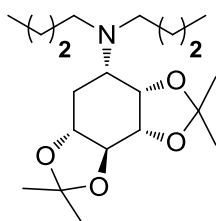
Colorless oil (32%), (80% EtOAc-hexane for flash column). ^1H NMR (CDCl_3 , 400 MHz) δ 4.24 (dd, $J = 8.0, 5.6$ Hz, 1H), 4.08 (dd, $J = 8.0, 7.2$ Hz, 1H), 3.67 (br d, $J = 4.8$ Hz, 2H), 3.01 (ddd, $J = 8.0, 8.0, 7.2$ Hz, 1H), 2.60 (m, 1H), 2.47 (m, 1H), 1.93 (m, 1H), 1.86 (m, 1H), 1.42 (s, 3H), 1.36 (s, 3H), 1.35 (s, 3H), 1.28 (s, 3H), 1.19 (br s, 20H), 0.81 (t, $J = 8.0$ Hz, 3H); ^{13}C NMR (CDCl_3 , 100 MHz) δ 111.6, 109.9, 80.5, 78.7, 76.2, 72.6, 55.8, 47.6, 31.9, 30.2, 29.9, 29.6, 29.6, 29.6, 29.6, 29.5, 29.3, 27.8, 27.2, 27.1, 27.0, 25.2, 22.7, 14.1.

(1*S*,2*S*,3*S*,4*S*,5*R*)-(2,3:4,5-di-*O*-isopropylidene)-*N,N*-diethylcyclohexylamine (3-22).



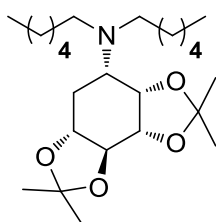
Colorless oil (48%), (100% EtOAc for flash column). ^1H NMR (CDCl_3 , 400 MHz) δ 4.30 (dd, $J = 4.4, 4.4$ Hz, 1H), 4.03 (dd, $J = 8.8, 4.4$ Hz, 1H), 3.47 (dd, $J = 9.6, 8.8$ Hz, 1H), 3.24 (ddd, $J = 11.6, 9.6, 3.2$ Hz, 1H), 2.92 (dt, $J = 12.0, 4.0$ Hz, 1H), 2.69-2.77 (m, 2H), 2.52-2.60 (m, 2H), 2.11 (ddd, $J = 11.6, 4.0, 4.0$ Hz, 1H), 1.74 (m, 1H), 1.47 (s, 3H), 1.37 (s, 3H), 1.35 (s, 3H), 1.29 (s, 3H), 0.98 (t, $J = 6.8$ Hz, 6H); ^{13}C NMR (CDCl_3 , 100 MHz) δ 110.8, 109.7, 82.5, 77.3, 76.7, 75.3, 57.4, 45.1, 28.9, 27.0, 26.9, 26.4, 26.3, 13.5.

(1*S*,2*S*,3*S*,4*S*,5*R*)-(2,3:4,5-di-*O*-isopropylidene)-*N,N*-dibutylcyclohexylamine (3-23).



Yellow oil (51%), (1:4:5 MeOH- CH_2Cl_2 -hexane for sephadex LH-20 column). ^1H NMR (CDCl_3 , 400 MHz) δ 4.27 (br s, 1H), 3.99 (dd, $J = 8.8, 4.8$ Hz, 1H), 3.46 (dd, $J = 10.0, 8.8$ Hz, 1H), 3.22 (m, 1H), 2.89 (br d, $J = 10.8$ Hz, 1H), 2.59-2.66 (m, 2H), 2.41-2.44 (m, 2H), 2.07 (br d, $J = 10.8$ Hz, 1H), 1.74 (ddd, $J = 12.4, 12.4, 11.6$ Hz, 1H), 1.45 (s, 3H), 1.36 (s, 3H), 1.34 (s, 3H), 1.28 (s, 3H), 1.19-1.26 (m, 8H), 0.84 (t, $J = 7.2$ Hz, 6H); ^{13}C NMR (CDCl_3 , 100 MHz) δ 109.8, 108.6, 81.6, 76.6, 75.6, 74.3, 56.7, 50.7, 29.9, 27.9, 25.9, 25.9, 25.1, 24.7, 19.4, 13.1.

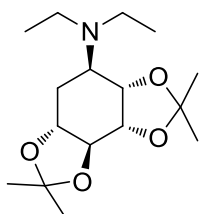
(1*S*,2*S*,3*S*,4*S*,5*R*)-(2,3:4,5-di-*O*-isopropylidene)-*N,N*-dihexylcyclohexylamine (3-24).



Pale yellow oil (38%), (0.5:2.5:7 MeOH- CH_2Cl_2 -hexane for sephadex LH-20 column). ^1H NMR (CDCl_3 , 400 MHz) δ 4.27 (br s, 1H), 4.00 (dd, $J = 8.0, 4.8$ Hz, 1H), 3.46 (dd, $J = 9.2, 9.2$ Hz, 1H), 3.23 (m, 1H), 2.88 (br d, $J = 11.2$ Hz, 1H), 2.57-2.64 (m, 2H), 2.36-2.44 (m, 2H), 2.08 (br d, $J = 11.6$ Hz, 1H), 1.73 (m, 1H), 1.46 (s, 3H), 1.36 (s, 3H), 1.34 (s, 3H), 1.28 (s, 3H), 1.20 (br s, 16H), 0.82 (t, $J = 6.8$ Hz, 6H); ^{13}C NMR (CDCl_3 ,

100 MHz) δ 110.8, 109.6, 82.6, 77.6, 76.6, 75.4, 57.8, 52.1, 31.8, 28.9, 28.7, 27.0, 26.9, 26.9, 26.1, 25.8, 22.7, 14.1.

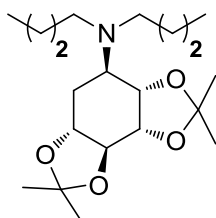
(1*R*,2*S*,3*S*,4*S*,5*R*)-(2,3:4,5-di-*O*-isopropylidene)-*N,N*-diethylcyclohexylamine (3-25).



Colorless oil (45%), (1:7:2 MeOH-CH₂Cl₂-hexane for sephadex LH-20 column).

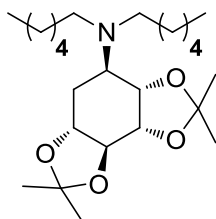
¹H NMR (CDCl₃, 400 MHz) δ 4.29 (dd, J = 10.0, 7.2 Hz, 1H), 4.18 (dd, J = 8.4, 7.2 Hz, 1H), 3.63 (dd, J = 10.4, 8.4 Hz, 1H), 3.54 (dt, J = 10.4, 7.2 Hz, 1H), 3.25 (ddd, J = 10.0, 8.8, 7.2 Hz, 1H), 2.45-2.60 (m, 4H), 1.99 (m, 1H), 1.75 (m, 1H), 1.44 (s, 3H), 1.37 (s, 3H), 1.35 (s, 3H), 1.26 (s, 3H), 1.02 (t, J = 5.6 Hz, 6H); ¹³C NMR (CDCl₃, 100 MHz) δ 112.1, 109.5, 80.4, 76.5, 76.1, 73.5, 57.7, 44.5, 27.4, 27.2, 27.1, 26.2, 24.5, 14.0.

(1*R*,2*S*,3*S*,4*S*,5*R*)-(2,3:4,5-di-*O*-isopropylidene)-*N,N*-dibutylcyclohexylamine (3-26).



White solid (57%), (80% EtOAc-hexane for flash column). ¹H NMR (CDCl₃, 400 MHz) δ 4.27 (dd, J = 9.6, 8.4 Hz, 1H), 4.17 (dd, J = 8.4, 7.2 Hz, 1H), 3.63 (dd, J = 10.8, 7.2 Hz, 1H), 3.54 (dd, J = 10.8, 8.0 Hz, 1H), 3.19 (ddd, J = 9.6, 9.2, 8.4 Hz, 1H), 2.44-2.51 (m, 2H), 2.33-2.40 (m, 2H), 1.94 (m, 1H), 1.74 (m, 1H), 1.43 (s, 3H), 1.36 (s, 3H), 1.35 (s, 3H), 1.26 (s, 3H), 1.18-1.24 (m, 8H), 0.84 (t, J = 7.2 Hz, 6H); ¹³C NMR (CDCl₃, 100 MHz) δ 111.0, 108.4, 79.4, 75.4, 75.1, 72.5, 56.8, 49.9, 30.1, 26.4, 26.2, 26.1, 25.4, 23.7, 19.5, 13.1.

(1*R*,2*S*,3*S*,4*S*,5*R*)-(2,3:4,5-di-*O*-isopropylidene)-*N,N*-dihexylcyclohexylamine (3-27).



Pale yellow oil (91%), (1:4:5 MeOH-CH₂Cl₂-hexane for sephadex LH-20 column). ¹H NMR (CDCl₃, 400 MHz) δ 4.26 (dd, *J* = 10.0, 8.4 Hz, 1H), 4.16 (dd, *J* = 8.4, 7.6 Hz, 1H), 3.63 (dd, *J* = 10.0, 7.6 Hz, 1H), 3.54 (dd, *J* = 10.8, 7.6 Hz, 1H), 3.19 (dd, *J* = 16.0, 10.0 Hz, 1H), 2.42-2.49 (m, 2H), 2.32-2.39 (m, 2H), 1.93 (m, 1H), 1.73 (m, 1H), 1.43 (s, 3H), 1.37 (s, 3H), 1.35 (s, 3H), 1.26 (s, 3H), 1.21-1.24 (br s, 16H), 0.81 (t, *J* = 7.6 Hz, 6H); ¹³C NMR (CDCl₃, 100 MHz) δ 112.0, 109.4, 80.4, 76.5, 76.2, 73.5, 57.9, 56.3, 31.8, 28.9, 27.4, 27.2, 27.1, 27.1, 26.4, 24.6, 22.7, 14.1.

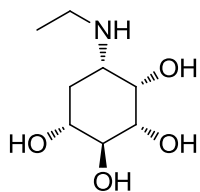
3.5.3.2 General procedure for deprotection

For the synthesis of *N*-alkyl aminoquercitols 3-28 – 3-30, 3-33 – 3-34, and 3-37 – 3-42

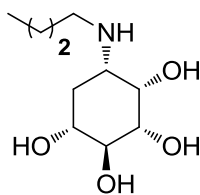
A solution of the protected *N*-alkyl aminoquercitols (0.05 mmol) in 1.25 M methanolic HCl (1 mL) was stirred at room temperature for 4 h. The reaction mixture was evaporated to dryness, redissolved in H₂O, loaded onto Dowex 50W-X8 (H⁺) column and eluted with H₂O followed by 50% NH₃-H₂O. Fractions eluted with 50% NH₃-H₂O were evaporated to give the *N*-alkyl aminoquercitols.

For the synthesis of *N*-alkyl aminoquercitols 3-31 – 3-32 and 3-35 – 3-36

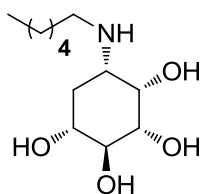
A solution of the protected *N*-alkyl aminoquercitols (0.08 mmol) in 1.25 M methanolic HCl (1 mL) were stirred at room temperature for 4 h. The reaction mixture was evaporated to dryness, redissolved in H₂O and extracted with EtOAc (3×10 mL). The combined aqueous layers were neutralized with 1 M NaHCO₃ and further extracted with EtOAc. The combined organic layers were evaporated under reduced pressure to afford the *N*-alkyl aminoquercitols.

(1*S*,2*S*,3*S*,4*S*,5*R*)-1-ethylamino-cyclohexane-2,3,4,5-tetraol (3-28).

Yellow oil (80%). ^1H NMR (D_2O , 400 MHz) δ 3.96 (br s, 1H, H-2), 3.33-3.35 (m, 2H, H-4,5), 3.25 (m, 1H, H-3), 2.90 (br d, $J = 12.4$ Hz, 1H, H-1), 2.68-2.75 (m, 2H, - HNCH_2 -), 1.88 (m, 1H, H-6), 1.48 (m, 1H, H-6), 0.99 (t, $J = 7.2$ Hz, 3H, $-\text{CH}_3$); ^{13}C NMR (D_2O , 100 MHz) δ 74.1, 72.3, 69.6, 68.5, 53.4, 40.1, 30.5, 11.9; HRMS m/z 192.1239 $[\text{M}+\text{H}]^+$ (calcd for $\text{C}_8\text{H}_{18}\text{NO}_4$, 192.1236).

(1*S*,2*S*,3*S*,4*S*,5*R*)-1-butylamino-cyclohexane-2,3,4,5-tetraol (3-29).

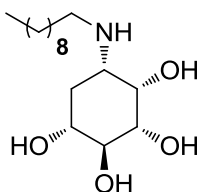
Pale yellow oil (quantitative yield). ^1H NMR (D_2O , 400 MHz) δ 4.04 (br s, 1H, H-2), 3.44-3.46 (m, 2H, H-4,5), 3.36 (m, 1H, H-3), 2.49-2.68 (m, 3H, H-1, - HNCH_2 -), 1.92 (br d, $J = 12.4$ Hz, 1H, H-6), 1.35-1.45 (m, 3H, H-6, $-\text{CH}_2$ -), 1.21-1.28 (m, 2H, $-\text{CH}_2\text{CH}_3$), 0.83 (t, $J = 7.6$ Hz, 3H, $-\text{CH}_3$); ^{13}C NMR (D_2O , 100 MHz) δ 74.5, 72.9, 70.2, 69.6, 53.1, 45.1, 32.1, 30.7, 19.8, 13.2; HRMS m/z 220.1548 $[\text{M}+\text{H}]^+$ (calcd for $\text{C}_{10}\text{H}_{22}\text{NO}_4$, 220.1549).

(1*S*,2*S*,3*S*,4*S*,5*R*)-1-hexylamino-cyclohexane-2,3,4,5-tetraol (3-30).

Pale yellow solid (59%). ^1H NMR (D_2O , 400 MHz) δ 3.94 (br s, 1H, H-2), 3.32-3.34 (m, 2H, H-4,5), 3.24 (m, 1H, H-3), 2.73 (d, $J = 11.6$ Hz, 1H, H-1), 2.50-2.59 (m, 2H, - HNCH_2 -), 1.85 (m, 1H, H-6), 1.34-1.41 (m, 3H, H-6, $-\text{CH}_2$ -), 1.10 (br s, 6H, $-(\text{CH}_2)_3$ -), 0.67

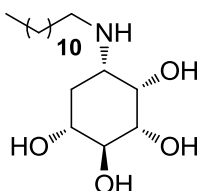
(br s, 3H, -CH₃); ¹³C NMR (D₂O, 100 MHz) δ 74.3, 72.6, 69.9, 69.0, 53.5, 45.4, 31.2, 30.8, 27.5, 26.0, 21.9, 13.3; HRMS m/z 248.1854 [M+H]⁺ (calcd for C₁₂H₂₆NO₄, 248.1862).

(1*S*,2*S*,3*S*,4*S*,5*R*)-1-decylamino-cyclohexane-2,3,4,5-tetraol (3-31).



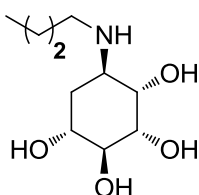
White solid (quantitative yield). ¹H NMR (CD₃OD, 400 MHz) δ 3.91 (br s, 1H, H-2), 3.41 (dd, J = 9.2, 9.2 Hz, 1H, H-4), 3.27 (m, 1H, H-5), 3.16 (m, 1H, H-3), 2.44-2.57 (m, 3H, H-1, -HNCH₂-), 1.81 (m, 1H, H-6), 1.40-1.52 (m, 3H, H-6, -CH₂-), 1.20 (br s, 14H, -(CH₂)₇-), 0.80 (t, J = 6.4 Hz, 3H, -CH₃); ¹³C NMR (CD₃OD, 100 MHz) δ 76.4, 75.1, 72.1, 70.9, 55.6, 47.4, 34.3, 33.1, 30.8, 30.7, 30.7, 30.6, 30.4, 28.5, 23.7, 14.4; HRMS m/z 304.2489 [M+H]⁺ (calcd for C₁₆H₃₄NO₄, 304.2488).

(1*S*,2*S*,3*S*,4*S*,5*R*)-1-dodecylamino-cyclohexane-2,3,4,5-tetraol (3-32).



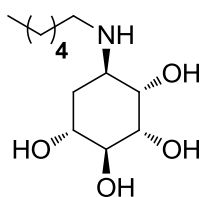
White solid (75%). ¹H NMR (CD₃OD, 400 MHz) δ 3.91 (br s, 1H, H-2), 3.41 (dd, J = 9.2, 9.2 Hz, 1H, H-4), 3.27 (m, 1H, H-5), 3.16 (dd, J = 9.6, 2.4 Hz, 1H, H-3), 2.43-2.58 (m, 3H, H-1, -HNCH₂-), 1.82 (m, 1H, H-6), 1.40-1.49 (m, 3H, H-6, -CH₂-), 1.19 (br s, 18H, -(CH₂)₉-), 0.80 (t, J = 6.0 Hz, 3H, -CH₃); ¹³C NMR (CD₃OD, 100 MHz) δ 76.3, 75.1, 72.1, 70.9, 55.6, 47.4, 34.2, 33.1, 30.8, 30.7, 30.7, 30.7, 30.7, 30.6, 30.5, 28.5, 23.7, 14.4; HRMS m/z 332.2804 [M+H]⁺ (calcd for C₁₈H₃₈NO₄, 332.2801).

(1*R*,2*S*,3*S*,4*S*,5*R*)-1-butylamino-cyclohexane-2,3,4,5-tetraol (3-33).



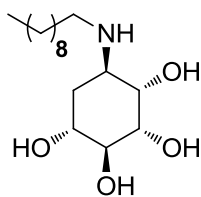
Pale yellow oil (97%). ^1H NMR (D_2O , 400 MHz) δ 3.78 (br s, 1H, H-2), 3.51-3.63 (m, 3H, H-3,4,5), 2.98 (br d, $J = 4.4$ Hz, 1H, H-1), 2.55-2.63 (m, 2H, $-\text{HNCH}_2-$), 1.76 (br s, 2H, H-6), 1.32-1.36 (m, 2H, $-\text{CH}_2-$), 1.13-1.18 (m, 2H, $-\text{CH}_2\text{CH}_3$), 0.72 (t, $J = 7.2$ Hz, 3H, $-\text{CH}_3$); ^{13}C NMR (D_2O , 100 MHz) δ 73.4, 71.8, 70.2, 69.1, 55.4, 46.2, 30.1, 29.7, 19.7, 13.1; HRMS m/z 220.1545 $[\text{M}+\text{H}]^+$ (calcd for $\text{C}_{10}\text{H}_{22}\text{NO}_4$, 220.1549).

(1*R*,2*S*,3*S*,4*S*,5*R*)-1-hexylamino-cyclohexane-2,3,4,5-tetraol (3-34).

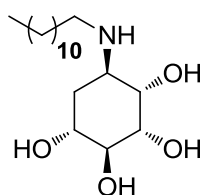


White solid (85%). $[\alpha]_{\text{D}}^{20} = +31.6$ (c 0.31, H_2O); ^1H NMR (D_2O , 400 MHz) δ 3.79 (m, 1H, H-2), 3.52-3.65 (m, 3H, H-3,4,5), 3.01 (br d, $J = 4.8$ Hz, 1H, H-1), 2.57-2.65 (m, 2H, $-\text{HNCH}_2-$), 1.75-1.81 (m, 2H, H-6), 1.37 (br s, 2H, $-\text{CH}_2-$), 1.12 (br s, 6H, $-(\text{CH}_2)_3-$), 0.68 (br t, $J = 6.8$ Hz, 3H, $-\text{CH}_3$); ^{13}C NMR (D_2O , 100 MHz) δ 73.1, 71.7, 70.0, 68.9, 55.3, 46.4, 30.7, 29.9, 27.3, 25.9, 21.9, 13.3; HRMS m/z 248.1858 $[\text{M}+\text{H}]^+$ (calcd for $\text{C}_{12}\text{H}_{26}\text{NO}_4$, 248.1862).

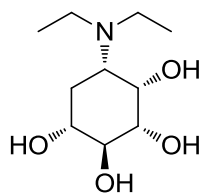
(1*R*,2*S*,3*S*,4*S*,5*R*)-1-decylamino-cyclohexane-2,3,4,5-tetraol (3-35).



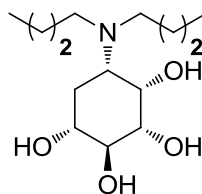
White solid (88%). ^1H NMR (CD_3OD , 400 MHz) δ 3.62-3.72 (m, 4H, H-2,3,4,5), 2.90 (br d, $J = 4.4$ Hz, 1H, H-1), 2.60 (m, 1H, $-\text{HNCH}_2-$), 2.48 (m, 1H, $-\text{HNCH}_2-$), 1.83 (m, 1H, H-6), 1.70 (m, 1H, H-6), 1.41-1.44 (m, 2H, $-\text{CH}_2-$), 1.20 (br s, 14H, $-(\text{CH}_2)_7-$), 0.80 (t, $J = 7.2$ Hz, 3H, $-\text{CH}_3$); ^{13}C NMR (CD_3OD , 100 MHz) δ 74.9, 74.2, 72.6, 71.2, 56.6, 48.4, 33.0, 32.6, 30.7, 30.7, 30.6, 30.5, 30.4, 28.4, 23.7, 14.4; HRMS m/z 304.2476 $[\text{M}+\text{H}]^+$ (calcd for $\text{C}_{16}\text{H}_{34}\text{NO}_4$, 304.2488).

(1*R*,2*S*,3*S*,4*S*,5*R*)-1-dodecylamino-cyclohexane-2,3,4,5-tetraol (3-36).

White solid (52%). ^1H NMR (CD_3OD , 400 MHz) δ 3.60-3.69 (m, 4H, H-2,3,4,5), 2.88 (br d, $J = 3.2$ Hz, 1H, H-1), 2.58 (m, 1H, $-\text{HNCH}_2-$), 2.46 (m, 1H, $-\text{HNCH}_2-$), 1.81 (m, 1H, H-6), 1.69 (m, 1H, H-6), 1.40-1.43 (m, 2H, $-\text{CH}_2-$), 1.19 (br s, 18H, $-(\text{CH}_2)_9-$), 0.80 (t, $J = 6.0$ Hz, 3H, $-\text{CH}_3$); ^{13}C NMR (CD_3OD , 100 MHz) δ 74.9, 74.2, 72.7, 71.2, 56.5, 48.5, 33.1, 32.7, 30.8, 30.7, 30.7, 30.7, 30.6, 30.6, 30.5, 28.5, 23.7, 14.4; HRMS m/z 332.2799 $[\text{M}+\text{H}]^+$ (calcd for $\text{C}_{18}\text{H}_{38}\text{NO}_4$, 332.2801).

(1*S*,2*S*,3*S*,4*S*,5*R*)-1-diethylamino-cyclohexane-2,3,4,5-tetraol (3-37).

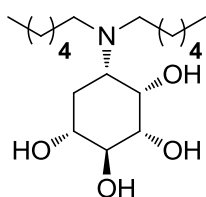
Colorless oil (quantitative yield). ^1H NMR (D_2O , 400 MHz) δ 4.12 (br s, 1H, H-2), 3.38 (br d, $J = 7.2$ Hz, 2H, H-3,5), 3.25 (br d, $J = 7.2$ Hz, 1H, H-4), 3.09 (br d, $J = 12.4$ Hz, 1H, H-1), 2.99 (br d, $J = 6.4$ Hz, 4H, $-\text{HN}(\text{CH}_2)_2-$), 1.98 (br d, $J = 10.0$ Hz, 1H, H-6), 1.68 (m, 1H, H-6), 1.03 (t, $J = 6.4$ Hz, 6H, $-(\text{CH}_3)_2$); ^{13}C NMR (D_2O , 100 MHz) δ 73.9, 72.3, 69.7, 68.2, 57.1, 44.1, 28.6, 8.9; HRMS m/z 220.1550 $[\text{M}+\text{H}]^+$ (calcd for $\text{C}_{10}\text{H}_{22}\text{NO}_4$, 220.1549).

(1*S*,2*S*,3*S*,4*S*,5*R*)-1-dibutylamino-cyclohexane-2,3,4,5-tetraol (3-38).

Pale yellow solid (96%). ^1H NMR (D_2O , 400 MHz) δ 4.13 (br s, 1H, H-2), 3.33-3.38 (m, 2H, H-3,5), 3.23-3.27 (m, 2H, H-1,4), 3.01-3.05 (m, 4H, $-\text{HN}(\text{CH}_2)_2-$), 2.03 (br d, J

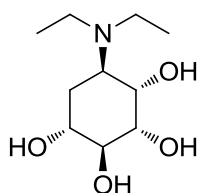
= 12 Hz, 1H, H-6), 1.69 (m, 1H, H-6), 1.44-1.48 (m, 4H, $-(\text{CH}_2)_2-$), 1.15-1.20 (m, 4H, $-(\text{CH}_2)_2\text{CH}_3$), 0.73 (t, $J = 6.8$ Hz, 6H, $-(\text{CH}_3)_2$); ^{13}C NMR (D_2O , 100 MHz) δ 73.4, 71.9, 69.1, 67.4, 58.5, 49.9, 28.2, 24.9, 19.2, 12.6; HRMS m/z 276.2169 $[\text{M}+\text{H}]^+$ (calcd for $\text{C}_{14}\text{H}_{30}\text{NO}_4$, 276.2175).

(1S,2S,3S,4S,5R)-1-dihexylamino-cyclohexane-2,3,4,5-tetraol (3-39).

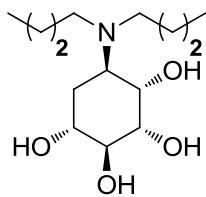


White powder (49%). ^1H NMR (CD_3OD , 400 MHz) δ 4.02 (br s, 1H, H-2), 3.43 (t, $J = 9.2$ Hz, 1H, H-4), 3.30 (m, 1H, H-5), 3.16 (dd, $J = 9.6, 2.0$ Hz, 1H, H-3), 2.74 (br s, 5H, H-1, $-\text{HN}(\text{CH}_2)_2-$), 1.76-1.84 (m, 2H, H-6), 1.43 (br s, 4H, $-(\text{CH}_2)_2-$), 1.23 (br s, 12H, $-(\text{CH}_2)_6-$), 0.82 (t, $J = 6.4$ Hz, 6H, $-(\text{CH}_3)_2$); ^{13}C NMR (CD_3OD , 100 MHz) δ 76.2, 74.9, 72.2, 71.2, 59.3, 52.1, 32.8, 31.0, 28.0, 27.4, 23.7, 14.4; HRMS m/z 332.2796 $[\text{M}+\text{H}]^+$ (calcd for $\text{C}_{18}\text{H}_{38}\text{NO}_4$, 332.2801).

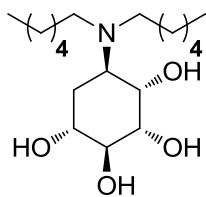
(1R,2S,3S,4S,5R)-1-diethylamino-cyclohexane-2,3,4,5-tetraol (3-40).



Colorless oil (quantitative yield). $[\alpha]_{\text{D}}^{20} = +42.5$ (c 0.25, H_2O); ^1H NMR (D_2O , 400 MHz) δ 3.94 (br s, 1H, H-2), 3.58 (br s, 2H, H-3,5), 3.51 (m, 1H, H-4), 2.87 (br d, $J = 3.6$ Hz, 1H, H-1), 2.50-2.65 (m, 4H, $-\text{HN}(\text{CH}_2)_2-$), 1.79 (m, 1H, H-6), 1.67 (m, 1H, H-6), 0.86 (t, $J = 7.2$ Hz, 6H, $-(\text{CH}_3)_2$); ^{13}C NMR (D_2O , 100 MHz) δ 73.5, 72.1, 69.5, 68.8, 57.3, 43.4, 27.6, 9.6; HRMS m/z 220.1552 $[\text{M}+\text{H}]^+$ (calcd for $\text{C}_{10}\text{H}_{22}\text{NO}_4$, 220.1549).

(1*R*,2*S*,3*S*,4*S*,5*R*)-1-dibutylamino-cyclohexane-2,3,4,5-tetraol (3-41).

Pale yellow oil (50%). ^1H NMR (CD_3OD , 400 MHz) δ 3.86 (br s, 1H, H-2), 3.70-3.77 (m, 3H, H-3,4,5), 3.03 (br s, 1H, H-1), 2.54-2.57 (m, 2H, $-\text{HNCH}_2-$), 2.39-2.42 (m, 2H, $-\text{HNCH}_2-$), 1.72-1.75 (m, 2H, H-6), 1.36-1.40 (m, 4H, $-(\text{CH}_2)_2-$), 1.19-1.28 (m, 4H, $-(\text{CH}_2)_2\text{CH}_3$), 0.85 (t, $J = 6.8$ Hz, 6H, $-(\text{CH}_3)_2$); ^{13}C NMR (CD_3OD , 100 MHz) δ 74.5, 73.2, 72.3, 69.7, 57.3, 51.1, 31.2, 27.9, 21.6, 14.4; HRMS m/z 276.2169 $[\text{M}+\text{H}]^+$ (calcd for $\text{C}_{14}\text{H}_{30}\text{NO}_4$, 276.2175).

(1*R*,2*S*,3*S*,4*S*,5*R*)-1-dihexylamino-cyclohexane-2,3,4,5-tetraol (3-42).

Pale yellow oil (46%). ^1H NMR (D_2O , 400 MHz) δ 3.91-3.97 (m, 3H, H-2,3,5), 3.84 (br s, 1H, H-4), 3.70 (m, 1H, H-1), 3.08-3.16 (m, 2H, $-\text{HNCH}_2-$), 2.89 (br m, 2H, $-\text{HNCH}_2-$), 1.80-1.94 (m, 2H, H-6), 1.51-1.62 (m, 4H, $-(\text{CH}_2)_2-$), 1.13 (br m, 12H, $-(\text{CH}_2)_6-$), 0.68 (t, $J = 6.4$ Hz, 6H, $-(\text{CH}_3)_2$); ^{13}C NMR (D_2O , 100 MHz) δ 73.3, 70.5, 69.2, 65.6, 56.9, 51.2, 30.4, 25.6, 25.1, 24.4, 21.7, 13.2; HRMS m/z 332.2799 $[\text{M}+\text{H}]^+$ (calcd for $\text{C}_{18}\text{H}_{38}\text{NO}_4$, 332.2801).

3.5.4 α -Glucosidase inhibition assay

Evaluation of α -glucosidase inhibition was performed using the methodology described in section 2.5.5.2.

3.5.5 Measurement of kinetic constants

For kinetic analyses of maltase by the active compounds, enzyme and active compounds were incubated with increasing concentrations of maltose (2-20 mM). The type of inhibition was determined by Lineweaver-Burk plot. For calculation of K_i values, slopes from a Lineweaver-Burk plot were replotted vs. $[I]$ which gave the secondary plot.



CHAPTER IV

AMINE-LINKED DIQUERCITOLS AS NEW α -GLUCOSIDASE INHIBITORS

In our previous studies, we have synthesized diverse *N*-substituted aminoquercitol derivatives by installing a variety of alkyl and acyl moieties onto amino group leading to the discovery of more pronounced α -glucosidase inhibitors; some of which are 2-8 times more potent than antidiabetic drug acarbose. With our previous achievement, we next plan to synthesize new aminocyclitols containing two (+)-*proto*-quercitol residues connected through *N*-linked glycosidic bond and evaluate their α -glucosidase inhibition. In fact, the idea of *N*-linked dicyclitols has been introduced by Hudlicky and co-workers since 2002 [45]; however, all synthesized targets (Figure 4.1) showed weak inhibition (IC_{50} 370-2,000 μ M). In this study, we hope that the replacement of the above cyclitols by (+)-*proto*-quercitol would promote inhibitory effect more potent than other *N*-linked dicyclitols previously reported.

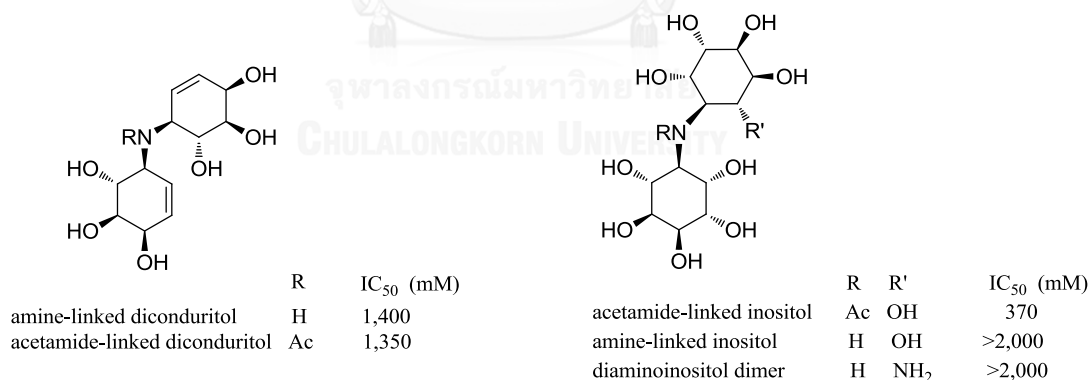
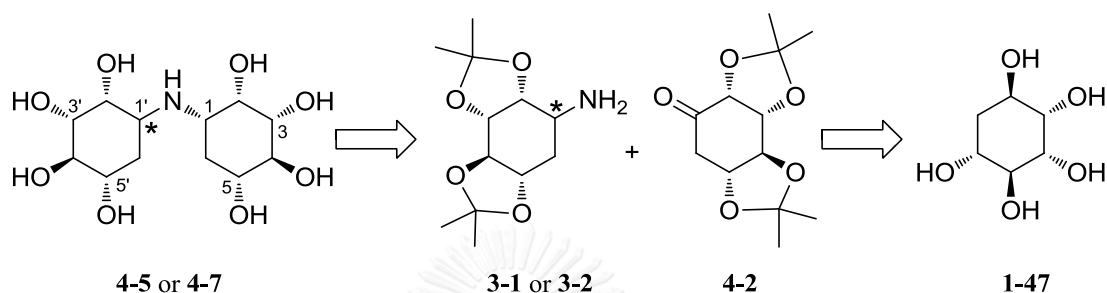


Figure 4.1 Structures of *N*-linked dicyclitols.

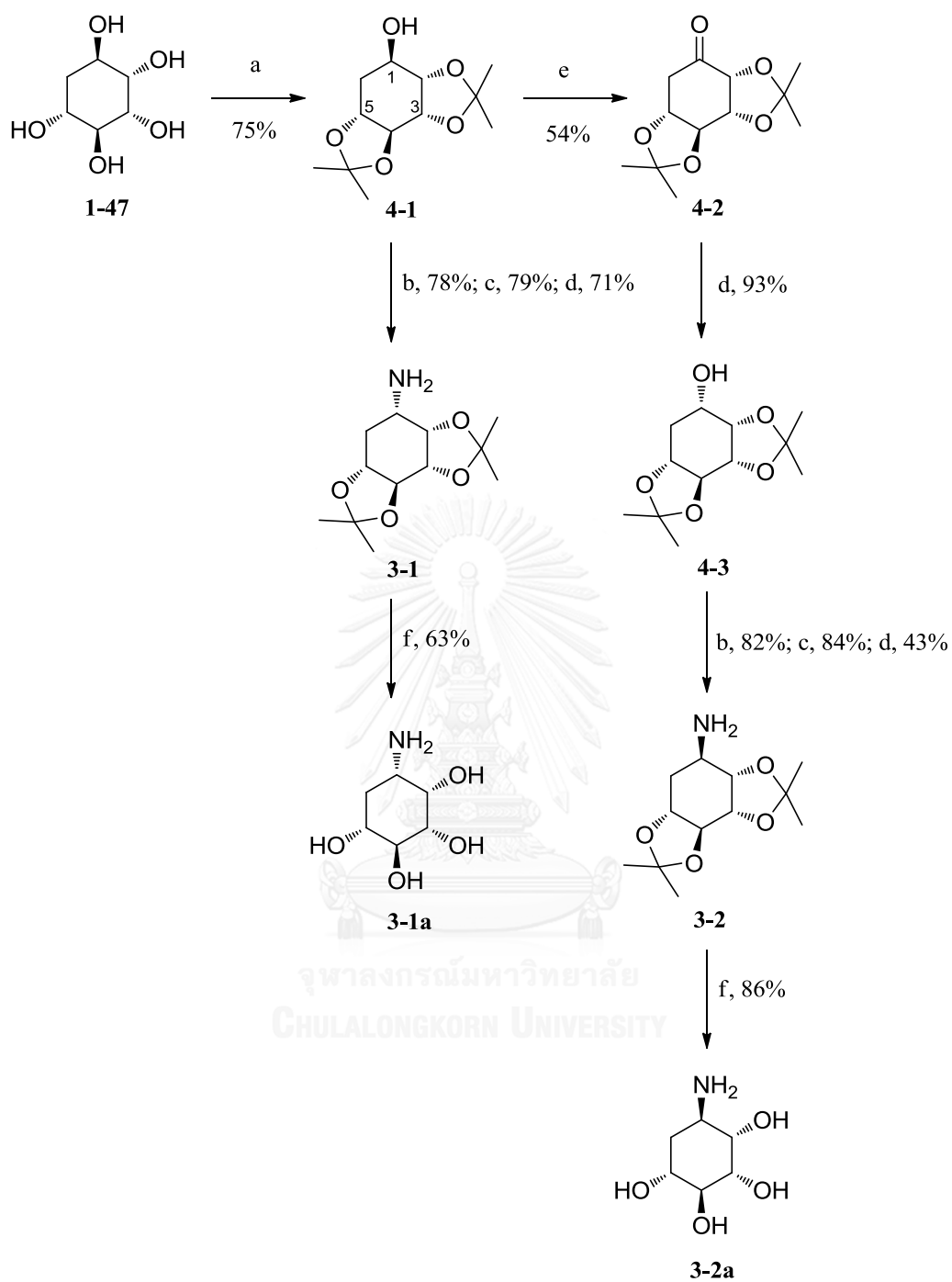
4.1 Synthesis of amine-linked diquercitols

Crucial to the successful synthesis of amine-linked diquercitols (**4-5** or **4-7**) was the use of reductive amination of aminoquercitols **3-1** or **3-2** and ketoquercitol **4-2** (Scheme 4.1), in which high diastereoselectivity was observed in each step.



Scheme 4.1 Synthetic strategy of target amine-linked diquercitols (**4-5** and **4-7**).

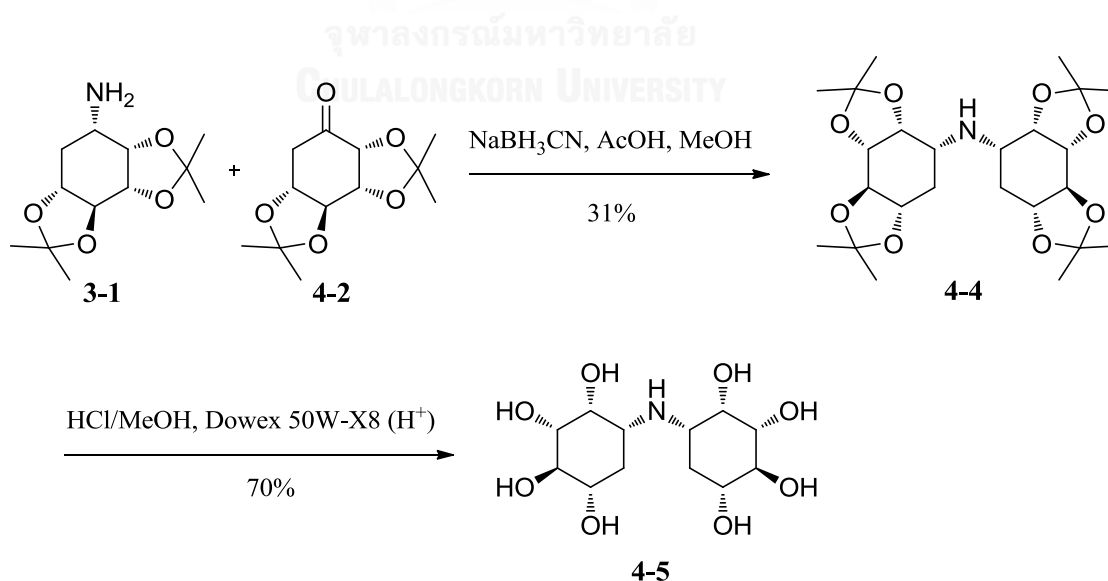
All key coupling intermediates **3-1**, **3-2** and **4-2** were synthesized from (+)-*proto*-quercitol (**1-47**) (Scheme 4.2), using our previous methodology [36]. Initially, hydroxyl groups in **1-47** were protected by reaction with $\text{Me}_2\text{C}(\text{COMe})_2$ in the presence of *p*-TsOH as a catalyst, yielding exclusively bis-acetonide **4-1** in 75% yield. This observation could be rationalized by initial favored formation of *cis*-acetonide at C-2 and C-3 followed by inevitable *trans*-acetonide formation at C-4 and C-5, resulting in the free hydroxyl group at C-1 for further functionalization. The remaining hydroxyl group in **4-1** was converted to a better leaving group (a mesyl moiety), which was further substituted by azide group (NaN_3). The desired aminoquercitol **3-1** was eventually obtained by hydride reduction using LiAlH_4 . Noticeably, transformation of **4-1** to **3-1** proceeded stereospecifically with inversion of configuration.



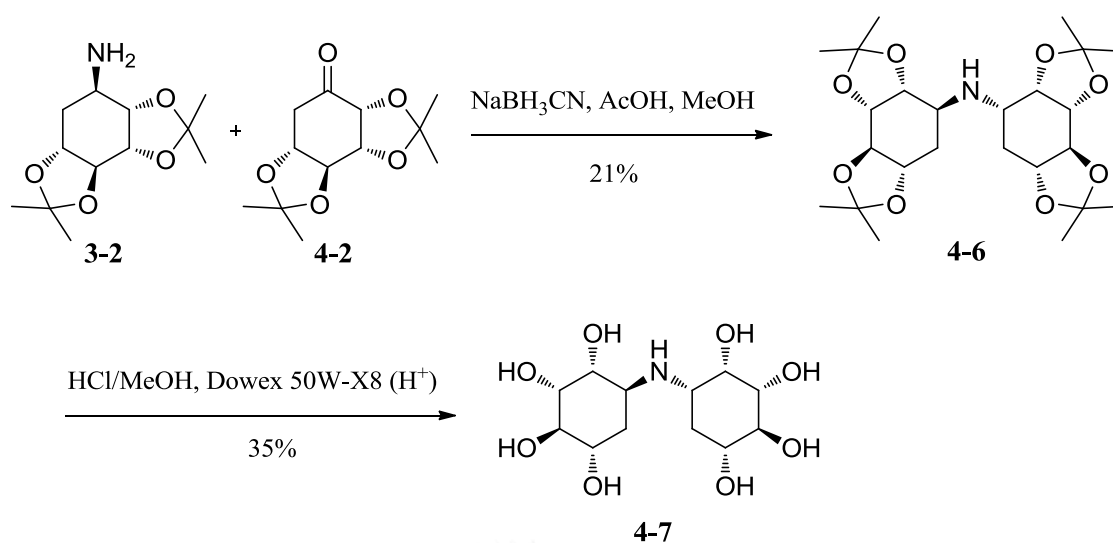
Scheme 4.2 Synthesis of aminoquercitols **3-1a** and **3-2a**. *Reagents and conditions:* (a) $\text{Me}_2\text{C}(\text{OMe})_2$, DMF, *p*-TsOH; (b) MeSO_2Cl , Et_3N , DMAP; (c) NaN_3 , DMF, 15-crown-5-ether, 100 °C; (d) LiAlH_4 ; (e) Ac_2O , DMSO; (f) TFA, THF.

Having aminoquercitol **3-1** in hand, we turned our plan to generate another coupling motif, ketoquercitol **4-2**. Starting from **4-1**, the target ketone **4-2** was synthesized in moderate yield (54%) by Albright-Goldman oxidation [46] using Ac_2O -DMSO. At this stage, we also have an idea to produce another aminoquercitol that is epimeric to **3-1**, which would be coupled to ketone **4-2** to produce a diastereomeric *N*-linked diquercitol. Ketone **4-2** was first reduced by LiAlH_4 , affording the hydroxybisacetone **4-3** with excellent yield (93%) as sole product. The desired aminoquercitol **3-2** was thus generated using the similar conditions applied for **3-1** (Scheme 4.2).

Having aminoquercitols **3-1** and **3-2** together with ketone **4-2** in hand, the required *N*-linked diquercitols were synthesized by reductive amination using NaBH_3CN (Scheme 4.3 and 4.4). Coupling of **3-1** and **4-2** provided the protected amine-linked diquercitol **4-4** which following the global acetonide deprotection under acid condition afforded amine-linked diquercitol **4-5** (Scheme 4.3) while compound **4-7** was generated from **3-2** and **4-2** (Scheme 4.4). Although amine-linked diquercitols **4-5** and **4-7** were obtained as single product from each synthetic route, the configuration of the newly generated chiral center (C-1) remained unclear.



Scheme 4.3 Synthesis of **4-5**.



Scheme 4.4 Synthesis of **4-7**.

The severely overlapped ^1H NMR signals, particularly in the diagnostic region (δ 3.0-4.0 ppm), rendered the determination of configuration impossible. We therefore turned our attempt to inspect ^1H NMR data of the bis-acetonides (**4-4** and **4-6**) of **4-5** and **4-7** because they displayed well-separated spectra. We have demonstrated, in our previous report [36], that ^1H NMR pattern and coupling constants of methylene protons in **3-1** and **3-2** are distinct enough to apply for predicting the configuration of amino-connected chiral carbon as α - or β -oriented. Apparently, bisacetonide **4-4** revealed a single set of methylene protons ($\text{H}_2\text{-6}$ and $\text{H}_2\text{-6}'$) identical to those of **3-1** whereas bisacetonide **4-6** contained two different patterns of **3-1** and **3-2** (Figure 4.2). Therefore, the newly generated chiral C-6s in **4-4** and **4-6** would be α -oriented as shown. Noticeably, the occurrence of α -oriented C-6 and C-6' in **4-4** resulted in its meso compound character, which was consistent with only six carbon signal observed in ^{13}C NMR spectrum.

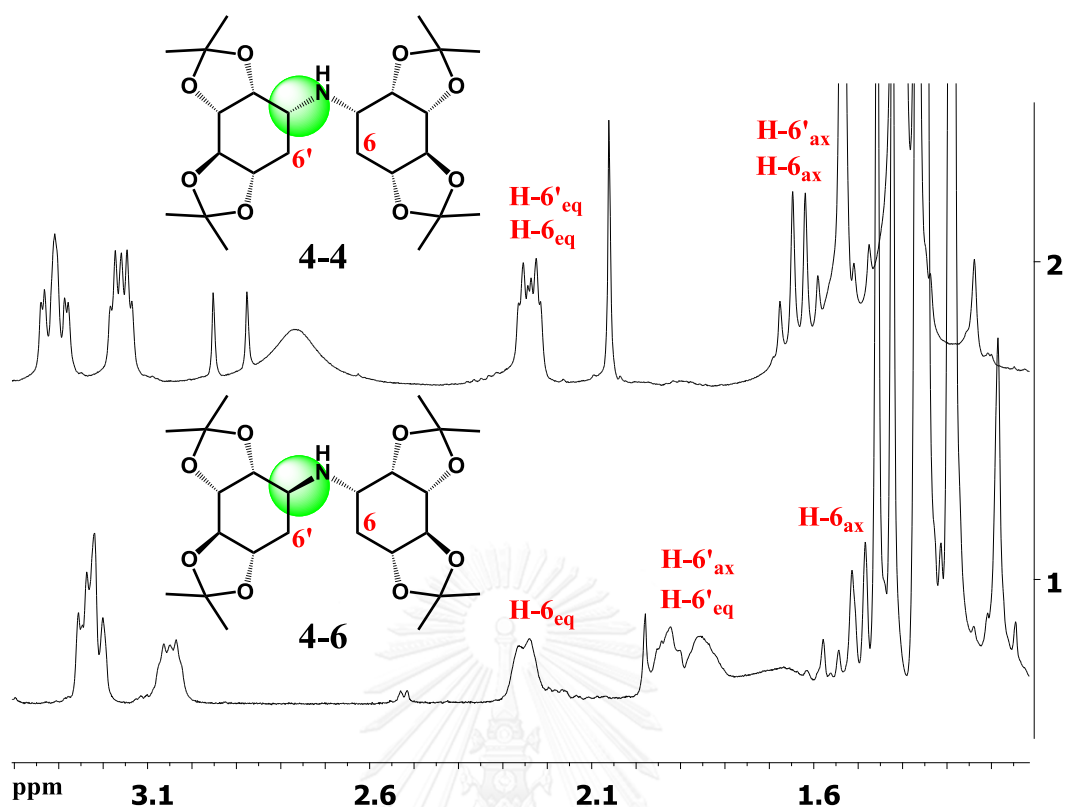
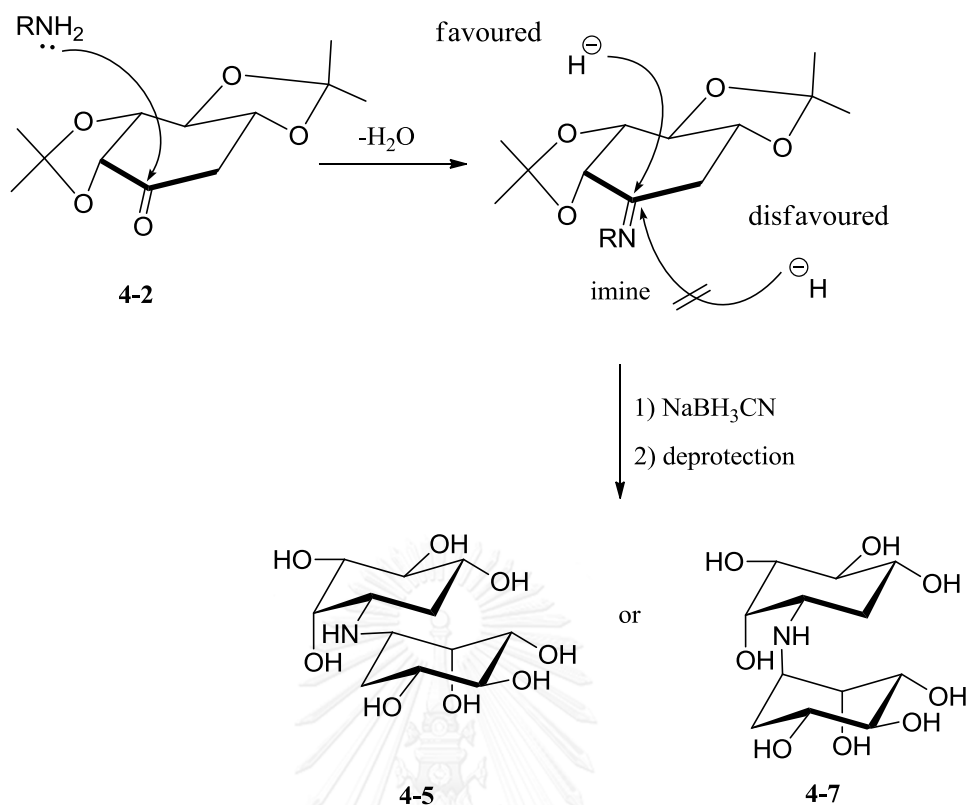


Figure 4.2 Partial ^1H NMR spectra of **4-4** and **4-6** (CDCl_3) focusing on signals of methylene protons ($\text{H}_2\text{-6}$ and $\text{H}_2\text{-6}'$).

Based on the aforementioned data, the proposed mechanism on the formation of amine-linked diquercitols **4-5** and **4-7** would be rationalized in Scheme 4.5. Noticeably, a more steric hindrance on the bottom face of imine, contributed by sterical control of acetonides, allowed α -attack of hydride (NaBH_3CN).



Scheme 4.5 Proposed mechanistic formations of **4-5** and **4-7**.

4.2 α -Glucosidase inhibitory activity

Amine-linked diquercitols **4-5** and **4-7** were evaluated for inhibitory effect toward α -glucosidases (Table 4.1) from two different sources; baker's yeast (type I) and rat intestine (maltase & sucrase, type II). They showed moderate inhibition (32.3-40.1 μ M) against yeast α -glucosidase while 10-time more potent inhibition (3.1-4.0 μ M) toward rat intestine was observed. Although **4-5** and **4-7** are diastereomers different in configuration of C-1', they revealed comparable inhibition against all α -glucosidases tested. Compared to the original aminoquercitols **3-1a** and **3-2a** obtained from acetonide deprotection of **3-1** and **3-2**, the amine-linked diquercitols **4-5** and **4-7** showed slightly improved inhibitory effect against maltase and sucrase. In addition, amine-linked diquercitols **4-5** and **4-7** revealed much more potent inhibition (*ca* 93-500 times) than other related *N*-linked dicyclitols [45] (Figure 4.1). It

is likely that structural motif of quercitol would also critically participate in exerting the inhibitory effect, in addition to the presence of *N*-linked glycosidic bond.

Table 4.1 α -Glucosidase inhibitory effect of synthesized compounds

Compound	IC ₅₀ (μ M)		
	Baker's yeast	Maltase	Sucrase
3-1a	2,890.0	5.8	7.3
3-2a	12.5	4.4	6.8
4-5	32.3	3.1	3.7
4-7	40.1	3.6	4.0
Acarbose	403.9	1.5	2.4

4.3 Conclusion

In conclusion, we reported the first synthesis of diastereomeric amine-linked diquercitols **4-5** and **4-7** through reductive amination of ketone **4-2** and epimeric amines **3-1** and **3-2**. The coupling intermediates were successfully prepared, without the formation of byproducts, from naturally available (+)-*proto*-quercitol (**1-47**). The synthesized amine-linked diquercitols **4-5** and **4-7** showed comparable inhibition against α -glucosidases, while the inhibitory effect toward maltase and sucrase were more enhanced than the original aminoquercitol. Interestingly, they inhibited glucosidase function much more potent than other related *N*-linked dicyclitols, therefore suggesting some pivotal role of the quercitol residues in addition to the presence of nitrogen-linkage.

4.4 Experimental section

4.4.1 General experimental procedures

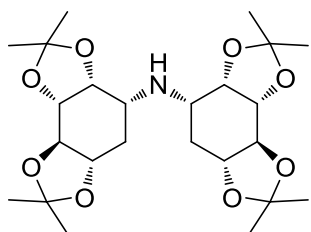
General experiments performed in this Chapter were similar to those described in Chapter 2.

4.4.2 Synthesis of amine-linked diquercitols

4.4.2.1 General procedure for reductive amination

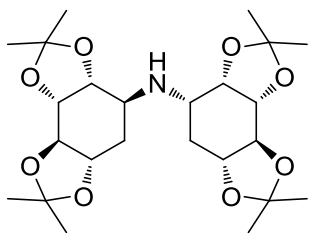
General procedure for reductive amination was performed using the methodology described in section 3.5.3.1.

Protected amine-linked diquercitol (4-4).



Following the general procedure above, reaction of **3-1** (30.0 mg, 0.12 mmol), sodium cyanoborohydride (16.0 mg, 0.25 mmol), protected ketoquercitol **4-2** (30.0 mg, 0.12 mmol), acetic acid (10 μ L) in methanol (1.2 mL) after 24 h yielded compound **4-4** (18.0 mg, 31%) as a colorless oil; ^1H NMR (CDCl_3 , 400 MHz) δ 4.36 (dd, $J = 4.0, 4.0$ Hz, 2H), 4.16 (dd, $J = 8.0, 4.0$ Hz, 2H), 3.62 (t, $J = 8.0$ Hz, 2H), 3.31 (m, 2H), 3.16 (m, 2H), 2.24 (m, 2H), 1.63 (m, 2H), 1.54 (s, 6H), 1.42 (s, 6H), 1.40 (s, 6H), 1.37 (s, 6H); ^{13}C NMR (CDCl_3 , 100 MHz) δ 114.6, 113.2, 85.5, 80.2, 79.7, 77.8, 56.4, 34.6, 32.1, 30.5, 29.8.

Protected amine-linked diquercitol (4-6).



Following the general procedure above, reaction of **3-2** (26.9 mg, 0.11 mmol), sodium cyanoborohydride (14.0 mg, 0.22 mmol), protected ketoquercitol **4-2** (27.0 mg, 0.11 mmol), acetic acid (9 μ L) in methanol (1.2 mL) after 24 h yielded compound **4-6** (11.1 mg, 21%) as a colorless oil; ^1H NMR (CDCl_3 , 400 MHz) δ 4.25-4.31 (m, 2H), 4.03-4.08 (m, 2H), 3.68-3.71 (m, 2H), 3.46 (t, J = 10.0 Hz, 1H), 3.20-3.25 (m, 2H), 3.04 (m, 1H), 2.24 (m, 1H), 1.92 (m, 1H), 1.84 (m, 1H), 1.48 (m, 1H), 1.46 (s, 3H), 1.42 (s, 3H), 1.36 (br s, 12H), 1.29 (s, 3H), 1.28 (s, 3H); ^{13}C NMR (CDCl_3 , 100 MHz) δ 111.9, 111.0, 110.4, 109.4, 82.4, 80.3, 76.6, 76.2, 74.3, 72.3, 51.9, 31.8, 28.6, 27.9, 27.2, 27.0, 26.9, 26.4, 25.4.

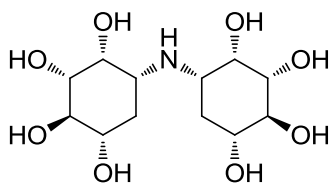
4.4.2.2 General procedure for deprotection of compounds 4-4 and

4-6

General procedure for deprotection was performed using the methodology described in section 3.5.3.2.

(1*R*,2*S*,3*S*,4*S*,5*S*)-5-((1'*R*,2'*R*,3'*R*,4'*R*,5'*S*)-2,3,4,5-

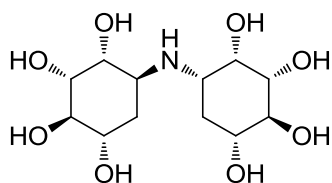
tetrahydroxycyclohexylamino)cyclohexane-1',2',3',4'-tetraol (**4-5**) or amine-linked diquercitol **4-5**.



White solid (70%). ^1H NMR (D_2O , 400 MHz) δ 3.95 (br s, 1H), 3.34-3.37 (m, 2H), 3.26 (m, 1H), 3.15 (br d, J = 9.6 Hz, 1H), 1.88 (br d, J = 12.0 Hz, 1H), 1.58 (q, J = 11.2

Hz, 1H); ^{13}C NMR (D_2O , 100 MHz) δ 73.7, 71.9, 69.2, 67.8, 50.8, 30.2; HRMS m/z 310.1499 $[\text{M}+\text{H}]^+$ (calcd for $\text{C}_{12}\text{H}_{24}\text{NO}_8$, 310.1502).

(1*R*,2*S*,3*S*,4*S*,5*S*)-5-((1'*S*,2'*R*,3'*R*,4'*R*,5'*S*)-2,3,4,5-tetrahydroxycyclohexylamino)cyclohexane-1',2',3',4'-tetraol (4-7) or amine-linked diquercitol 4-7.



Pale yellow oil (35%). ^1H NMR (D_2O , 400 MHz) δ 3.88 (br s, 1H), 3.63-3.66 (m, 3H), 3.51 (m, 1H), 3.25-3.34 (m, 3H), 2.99 (br s, 1H), 2.76 (br d, $J = 8.0$ Hz, 1H), 1.67-1.80 (m, 3H), 1.39 (m, 1H); ^{13}C NMR (D_2O , 100 MHz) δ 74.4, 73.7, 72.8, 71.8, 71.5, 70.2, 69.5, 69.2, 52.3, 51.3, 32.6, 30.8; HRMS m/z 332.1321 $[\text{M}+\text{Na}]^+$ (calcd for $\text{C}_{12}\text{H}_{23}\text{NNaO}_8$, 332.1321).

4.4.3 α -Glucosidase inhibition assay

Evaluation of α -glucosidase inhibition was performed using the methodology described in section 2.5.5.2.

CHAPTER V

NEW α -GLUCOSIDASE INHIBITORS FROM NATURALLY AVAILABLE

(+)-*proto*-QUERCITOL: SYNTHESIS, KINETIC AND COMPUTATIONAL PREDICTION

In previous work, we found that α -glucosidase inhibition of aminoquercitols could be improved by installing appropriate hydrophobic or hydrophilic moieties. In this chapter, we extended our study toward the effect of π -electron on glucosidase inhibition by installing aryl residues to nitrogen atom. Moreover, we also investigated the effect of particular hydrophilic moiety, generally called hydroxyalkyl, on glucosidase inhibition. Thus, (2-hydroxy-1-hydroxymethyl)ethyl, the *N*-substituted group in voglibose, was employed for this purpose. We also discussed the mechanism underlying α -glucosidase inhibitory effect of the most potent inhibitor. In addition, the binding mode and the key structural factors affecting activity between a series of *N*-substituted aminoquercitol derivatives and the enzyme were also elaborated using molecular docking and 3D-QSAR.

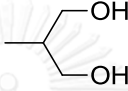
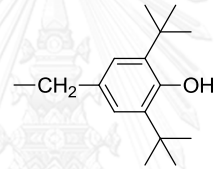
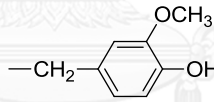
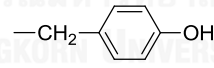
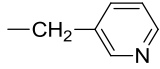
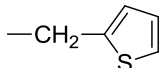
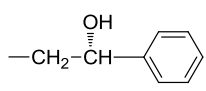
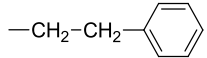
5.1 Synthesis of *N*-substituted aminoquercitols and voglibose-like compounds

A series of *N*-aryl and *N*-hydroxyalkyl aminoquercitols were prepared by reductive amination of bisacetonides (**3-1** and **3-2**) and aldehydes under the conditions previously described. *N*-aryl aminoquercitols (**5-2** – **5-8**, **5-10** – **5-12**, Table 5.1) were generated using aromatic aldehyde and *N*-hydroxyalkyl aminoquercitols (**5-1** and **5-9**) were synthesized using 1,3-dihydroxyacetone dimer.

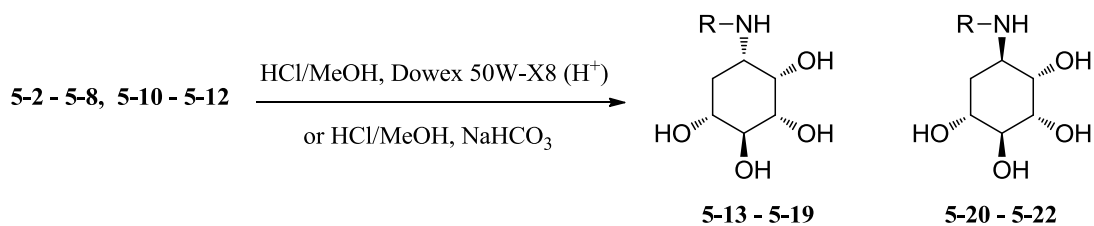
Next, deprotection of the protected *N*-substituted aminoquercitols were easily achieved in a single step under acidic condition to afford the target *N*-substituted analogues **5-13** – **5-22** in fair to good yields (Scheme 5.1). In addition, the *N*-bromobenzyl derivative **5-24** was prepared via alkylation reaction using *p*-bromobenzyl bromide as alkylating agent in the presence of TEA and DMF as a solvent to obtain compound **5-23** in 72% yield. Finally, cleavage of bis-acetonide protecting groups of compound **5-23** gave the target product (**5-24**) in fair yields (Scheme 5.2).



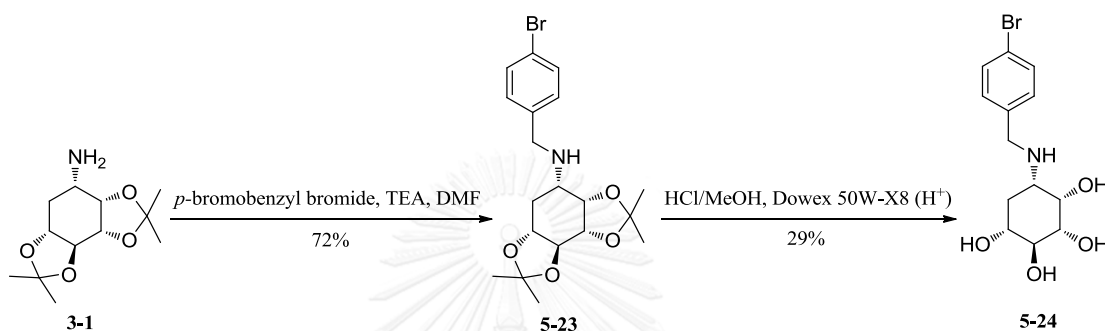
Table 5.1 Reaction conditions and yields for reductive amination

3-1, 3-2		Aldehydes	R-NH	
		NaBH ₃ CN, AcOH, MeOH	5S	5R
			5-5 - 5-8	5-10 - 5-12
Compound number		R	Isolated yield (%)	
5S	5R		5S	5R
5-1	5-9		62 ^a	89 ^a
5-2	5-10		70	60
5-3	5-11		80	75
5-4	5-12		86	62
5-5	- ^c		86 ^b	- ^c
5-6	-		34	-
5-7	-		69	-
5-8	-		47	-

^a Yield in two steps. ^b Using Ti(O^{*i*}Pr)₄ as catalyst. ^c Not synthesized.



Scheme 5.1 Synthesis of *N*-substituted aminoquercitols.



Scheme 5.2 Synthesis of **5-24**.

The relative stereochemistry of compound **5-7** was addressed based on chemical transformation and NMR analysis. Compound **5-7** was converted to the corresponding oxazolidinone **5-25** by reaction with 1,1-carbonyldiimidazole in dry CH_2Cl_2 and TEA (Figure 5.1a). The NOESY data showed a correlation between H-7' and H-8' including H-8' and H-6 (Figure 5.1b), indicating 7'*S* configuration.

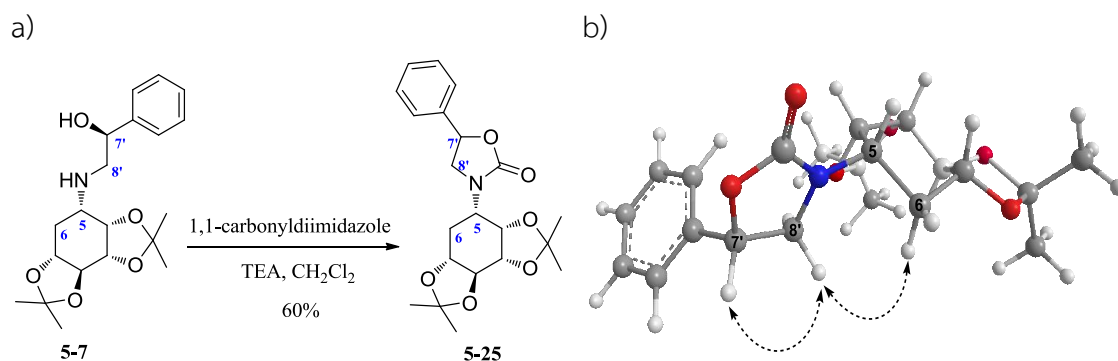


Figure 5.1 (a) Preparation of oxazolidinone derivative **5-25**; (b) Selected NOESY correlations of **5-25**.

5.2 α -Glucosidase inhibitory activity and kinetic analysis

All of the target compounds were tested in α -glucosidase enzymatic assay as described in our previously reported method [25] using enzymes from two different sources; baker's yeast (type I) and rat intestine (type II), and the results are illustrated in Table 5.2. Focusing initially on the inhibitory activity of α -glucosidase from baker's yeast, the introduction of hydrophilic groups on nitrogen position of aminoquercitol such as a series of voglibose-like compounds (**5-1** and **5-9**) showed no inhibition against this enzyme. In contrast, hydrophobic groups of aryl and heteroaryl side chain displayed moderate inhibition. Among them, the *N*-substitution compounds with 3,5-di-*tert*-butyl-4-hydroxybenzyl group (**5-13** and **5-20**) were the most potent type I α -glucosidase inhibitors with IC_{50} values of 89.1 and 80.5 μ M, respectively, which were five-fold more potent than antidiabetic drug acarbose. From these results above, we supposed that the aromatic ring which possesses alkyl groups as substituents may play an important role in the type I α -glucosidase inhibition.

Table 5.2 α -Glucosidase inhibitory effect of *N*-substituted aminoquercitols

Compound	IC ₅₀ (μ M)		
	Baker's yeast	Maltase ^a	Sucrase ^a
5-1	NI ^b	0.9	1.7
5-9	NI	0.53	2.5
5-13	89.1	5.8	81
5-14	94.4	7.6	120
5-15	110.6	9.8	570
5-16	3145	NI	NI
5-17	1350	140	NI
5-18	3010	NI	NI
5-19	NI	NI	NI
5-20	80.5	5.56	79.5
5-21	92.7	6.14	90.2
5-22	103.8	7.61	117
5-24	2110	350	NI
Acarbose[®]	480	1.5	2.3
Voglibose[®]	4300	0.25	0.094

^a α -Glucosidase was obtained from rat small intestine. ^b No inhibition (inhibitory effect < 30% at 10 mg/mL for baker's yeast and at 1 mg/mL for maltase and sucrase).

For rat intestinal α -glucosidase, *N*-substituted aminoquercitols inhibited maltase more selectively than sucrase, varying from low (IC₅₀ 140-350 μ M) to high (IC₅₀ 0.53-9.80 μ M) potency. Of all synthesized compounds, voglibose-like compound **5-9** showed the highest inhibition against rat intestinal maltase with an IC₅₀ value of 0.53 μ M which had potency similar to the most effective antidiabetic drug, voglibose (IC₅₀ 0.25 μ M). Also, the 5*S*-voglibose-like congener **5-1** possessed good inhibition on this enzyme with an IC₅₀ value of 0.90 μ M. In addition, the inhibitory activity of the hydrophobic compounds particularly with the substituted aromatic side chain were

similar in potency to acarbose with IC_{50} values in the range of 5.56-9.80 μM whereas compound **5-24** was much less potent than acarbose. Among them, **5-20** showed high inhibition with an IC_{50} value of 5.56 μM . In contrast, changing the side chain of *N*-substituted aminoquercitols to be either unsubstituted aromatic or heteroaryl groups (**5-16** – **5-19**) tends to reduce maltase inhibition markedly. Moreover, we found that the configuration at C-5 of the synthesized compounds had no effect on the inhibitory activity of both enzymes (type I and type II α -glucosidase).

To obtain further information on the type of inhibition exerted by the most potent inhibitor **5-9** on rat intestinal α -glucosidase, the kinetic analysis was studied using Lineweaver-Burk plots and the results are shown in Figure 5.2. The inhibitory mode of **5-9** was found to be of the competitive type (both maltase and sucrase) since K_m values increased with compound **5-9** concentration, while V_{max} value remained unchanged. This result suggests that compound **5-9** occupies the active site of this enzyme, much in the same manner as the antidiabetic drug voglibose. The slopes of Lineweaver-Burk plots *versus* compound **5-9** concentrations (Figure 5.2, inset) produced the inhibition constants (K_i) of 0.29 μM for maltase and 2.57 μM for sucrase (Table 5.3). The higher K_i value of **5-9** toward sucrase over that of voglibose reflects the weaker binding affinity between sucrase and inhibitor **5-9**. However, the remarkable result was observed on maltase. The K_i value of **5-9** was similar to, or slightly higher than that of the antidiabetic drug voglibose. The low K_i value of **5-9** on maltase indicated its strong binding affinity.

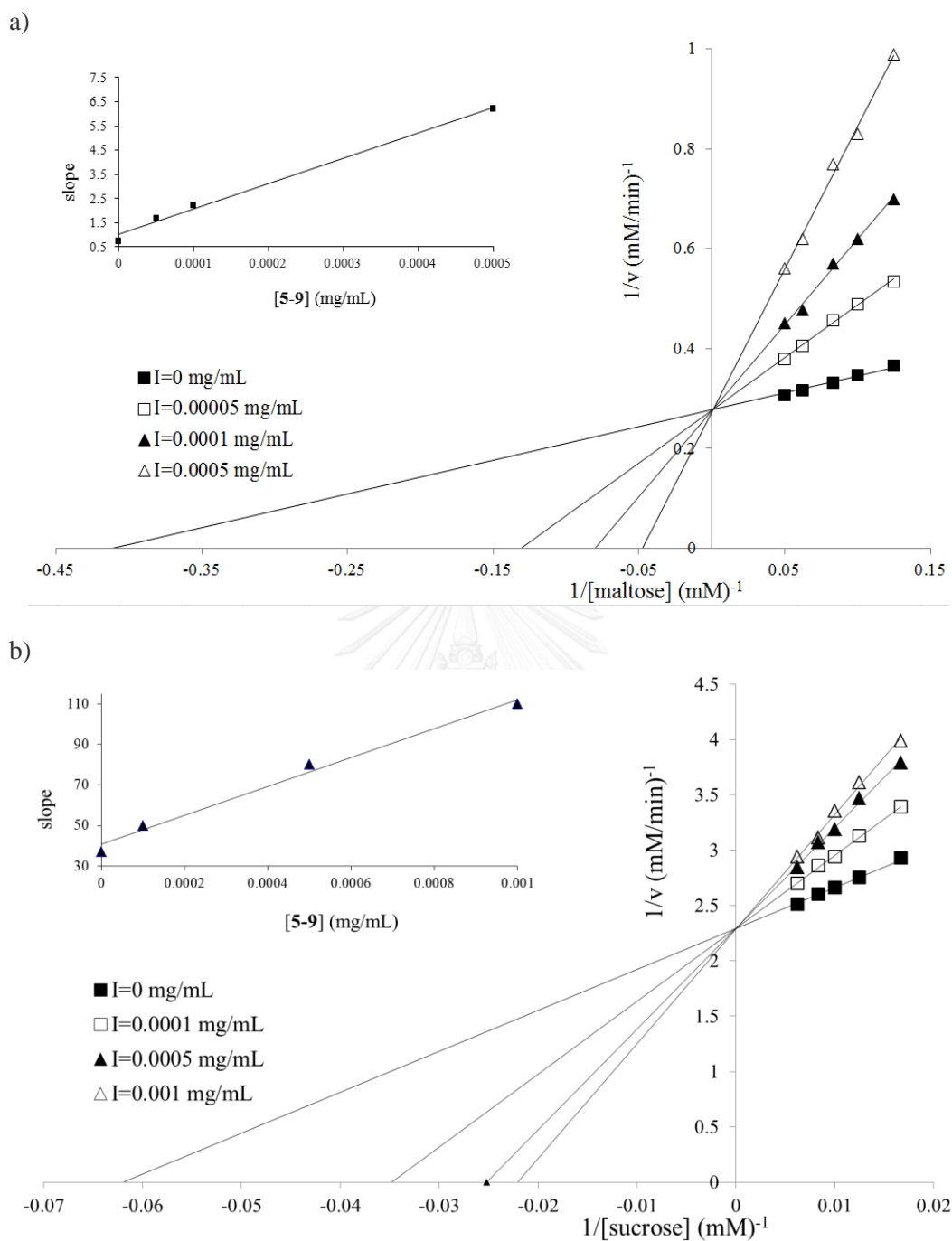


Figure 5.2 Lineweaver-Burk plots for inhibitory activity of **5-9** against rat intestinal: (a) maltase; (b) sucrose. Inset: secondary replots of slope vs. $[I]$ from a primary Lineweaver-Burk plot for the determination of K_i .

Table 5.3 IC₅₀ and K_i values of 5-9

Compound	IC ₅₀ (μM)		K _i (μM)		Type of Inhibition
	Maltase	Sucrase	Maltase	Sucrase	
5-9	0.53	2.5	0.29	2.57	Competition
Voglibose [®]	0.25	0.094	0.12 ^a	0.07 ^a	Competition

^a From another paper [47].

5.3 Molecular docking of synthesized compounds with rat intestinal maltase

In order to envisage the detailed binding modes of the *N*-substituted aminoquercitols with rat intestinal maltase, a molecular docking study was further performed using the open-source program AutoDock Vina [48]. As the first step, the docking reliability was tested using the miglitol (MIG) ligand docked to the active site of the human N-terminal catalytic subunit of maltase-glucoamylase (hu-ntMGAM) receptor. The binding mode obtained from the docking result was compared with the previous report [49] and we found that the result was able to reproduce the crystallographic binding pose. Next, a three-dimensional model of N-terminal subunit of rat maltase-glucoamylase (rat-ntMGAM) was constructed using the crystal structure of hu-ntMGAM complexed with miglitol as template and the results are shown in Figure 5.3a.

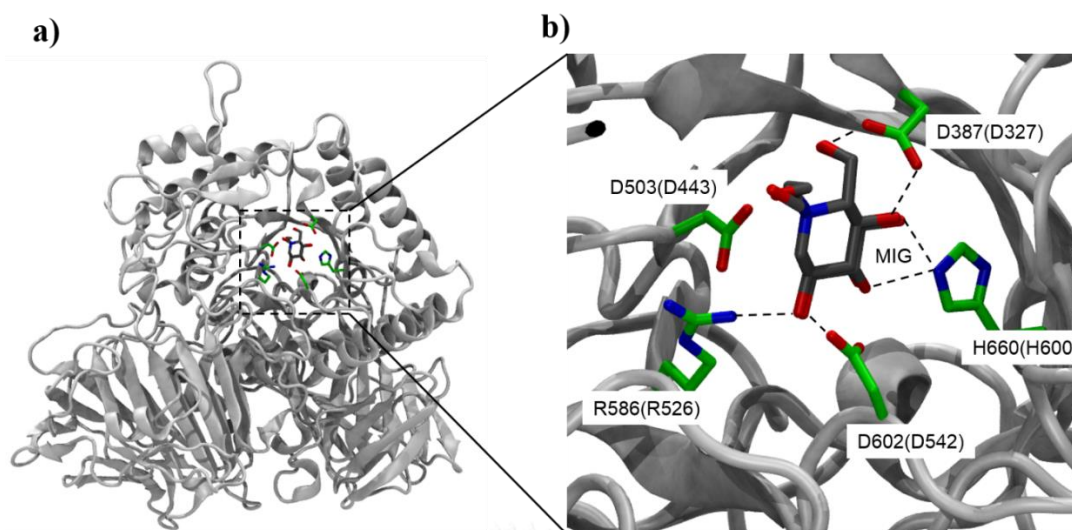


Figure 5.3 (a) Homology model of the rat intestinal N-terminal domain of maltase-glucoamylase (rat-ntMGAM) and (b) Structural superimposition between the crystal and docked miglitol (RMSD = 0.48 Å). The figure also shows the conserved residues important for the binding of the inhibitor in the active site of rat-ntMGAM and hu-ntMGAM (number in parentheses). The dashed lines illustrate atom pairs within hydrogen bond distances.

From the Ramachandran plot, the main-chain conformation for 98.8% amino acid residues, except gly and proline, were within the allowed or most favoured regions and the overall Procheck G-factor was 0.04. The Qmean4 and Z-score of the homology model of rat-ntMGAM was 0.705 and -0.86, respectively. Both the G-factor and Qmean scores were above the threshold, suggesting the good quality of the model. A further validation of the homology model by docking MIG into the binding site showed that the ligand binding pose was highly similar to the one in the X-ray structure of hu-ntMGAM (Figure 5.3b), especially a significant conservation in the binding site. This includes the key conserved residues: D387, D503, D542, R586 and H660, which have been shown to make important hydrogen bonds with the inhibitor [49].

All synthesized compounds that have been geometrically optimized were successfully docked into the rat-ntMGAM active site. Figure 5.4a shows the close view of the active site with the best predicted orientation of all ligands, obtained from the

molecular docking, almost superposition with each other. The interactions between rat maltase and a group of active compounds **5-9** and **5-20 – 5-22** are illustrated in Figure 5.4b-c. The most potent **5-9** made hydrogen bonding interactions with D387, D503, D602, H660, and R586 (Figure 5.4b). According to the flexible docking (allowing receptor flexibility) for **5-20 – 5-22**, the side chain of residue D602 can rotate from the native conformation (yellow stick representation) to the docked conformation (green stick representation) to form hydrogen bond with hydroxyl group at aromatic aryl chain (Figure 5.4c). In addition, the hydroxyl groups of the quercitol moiety were within hydrogen bonding distance (3.3 Å) to D387, D503, and H660 (Figure 5.4c). The alkyl chain moiety on aromatic ring of **5-20** would be stabilized by hydrophobic contact with residue W466 (Figure 5.4c).



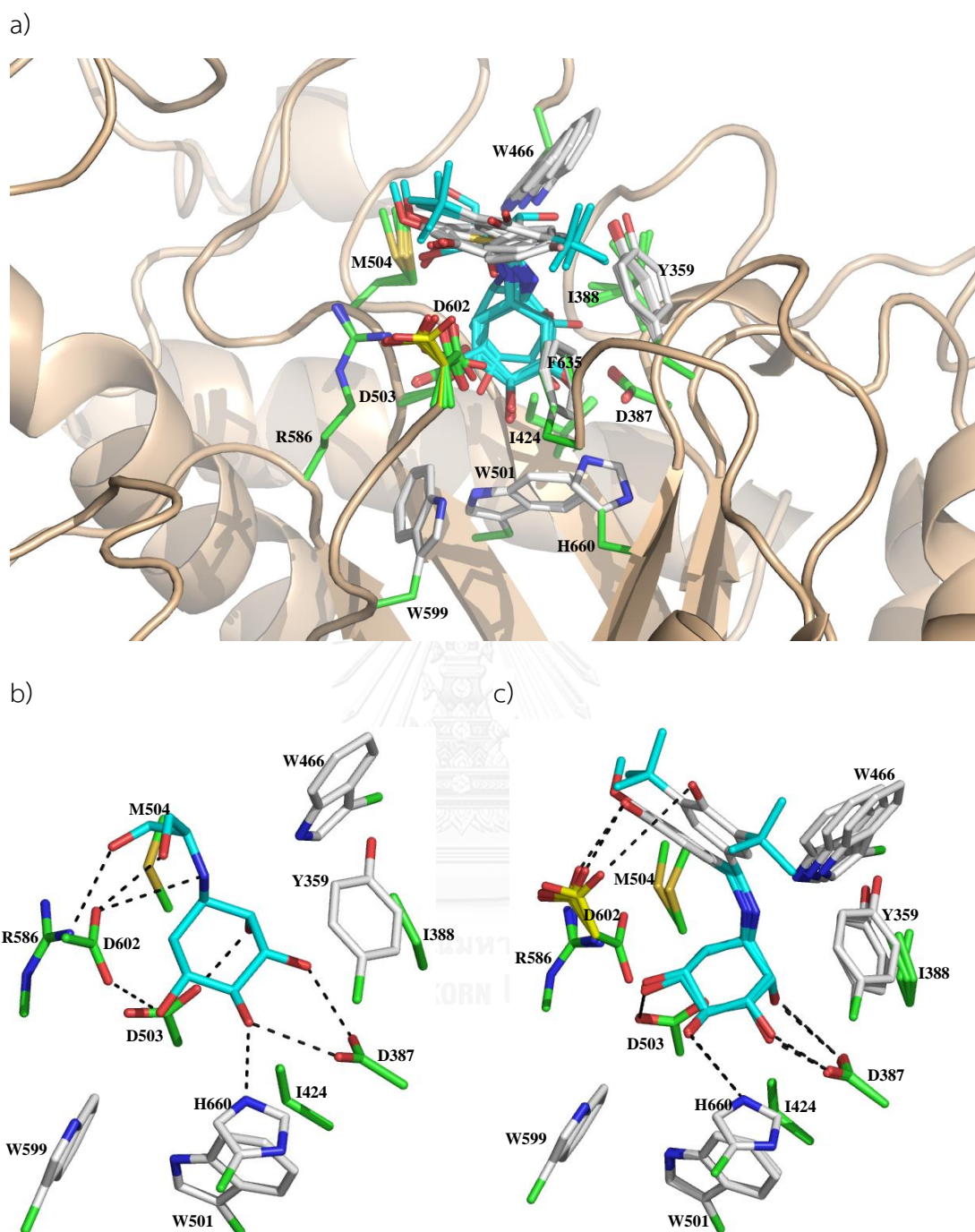
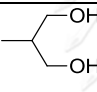
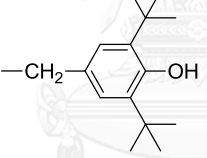
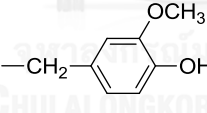
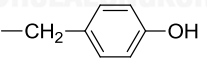
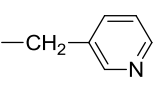
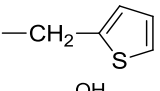
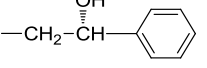
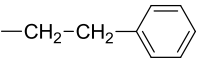
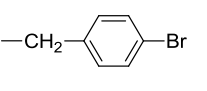


Figure 5.4 (a) The superimposed lowest energy conformations of all ligands (5-1, 5-9, 5-13 – 5-22, and 5-24) obtained by docking at active site of the modeled rat intestinal maltase. Interactions of amino acid residues with (b) 5-9 and (c) the superimposition of 5-20, 5-21, and 5-22. The surrounding conserved residues and ligand molecules are in stick representation. Hydrogen bonds are depicted by dashed lines.

The Vina docking scores for the active inhibitors (**5-1**, **5-9**, **5-13** – **5-15**, and **5-20** – **5-22**) were approximately with values in the range of -8.3 to -9.9 kcal/mol while the Vina docking scores for the weak inhibitors (**5-16** – **5-19** and **5-24**) were approximately with values in the range of -7.2 to -7.9 kcal/mol (Table 5.4). These results were consistent with the experimental results (IC_{50}) showing that a group of voglibose-like compounds (**5-1** and **5-9**) have the highest inhibitory activity against rat maltase.

Table 5.4 IC_{50} , and Vina docking scores of synthesized compounds with rat maltase

Compound number		R	IC_{50} (μM) ^a		Vina Docking Scores ^b (kcal/mol)	
5S	5R		5S	5R	5S	5R
5-1	5-9		0.9	0.53	-9.7	-9.9
5-13	5-20		5.8	5.56	-9.1	-9.4
5-14	5-21		7.6	6.14	-8.6	-8.8
5-15	5-22		9.8	7.61	-8.3	-8.4
5-16	- ^c		NI	- ^c	-7.6	- ^c
5-17	-		140	-	-7.2	-
5-18	-		NI	-	-7.6	-
5-19	-		NI	-	-7.6	-
5-24	-		350	-	-7.9	-
MIG [®]	-	-	0.59 ^d		-10.1	

^a From rat intestinal maltase. ^b Calculated using AutoDock Vina from homology rat intestinal maltase. ^c Not synthesized. ^d From another paper [42].

5.4 3D-QSAR analysis

To further investigate the structural and chemical features contributing to the biological activity of series of *N*-substituted aminoquercitols with their 3D conformation, a 3D-QSAR study was carried out. Due to limited data on the active compounds in this study, we also took our previous data (from Chapter III, [50]) for performing a 3D-QSAR analysis. The PLS statistic parameters of CoMFA and CoMSIA models were summarized in Table 5.5. For CoMFA model, the q^2 and r^2 was 0.662 and 0.928, while for CoMSIA model was 0.666 and 0.886. The statistic results indicated good predictive ability of CoMFA and CoMSIA models. The optimal numbers of components used to generate CoMFA and CoMSIA models are 4 and 3, respectively, which were reasonable according to the number of compounds used to derive the models. The standard errors of estimate of CoMFA and CoMSIA models were also reasonably low (0.127 and 0.154, respectively). Fisher test results were 48.189 and 41.627 for CoMFA and CoMSIA models, respectively. As shown in Table 5.5, for CoMFA model, the steric term contributed 64.2% to the interacting energy, indicated the SAR of *N*-substituted aminoquercitols were more influenced by steric effect than by electrostatic effect (35.8%). The predominant field contributions from CoMSIA were electrostatic (28.1%) and hydrophobic (26.3%), indicating the importance of the electrostatic and hydrophobic of the substituent for the activity. The other contributions, steric (25.1%), hydrogen bond donor (15.6%), and hydrogen bond acceptor (4.9%), showed minor effects. The predicted inhibition versus their experimental data of training and test set compounds are depicted graphically in Figure 5.5 for CoMFA and CoMSIA models, respectively. The actual and predicted activity of the test set was shown in Table 5.6.

Table 5.5 Statistical results of CoMFA and CoMSIA models

Models	Descriptors	Statistical parameters					
		q^{2a}	r^{2b}	N^c	SEE ^d	F^e	Field contribution (%)
CoMFA	S^f/E^g	0.662	0.928	4	0.127	48.189	64.2/35.8
CoMSIA	$S/E/H^h/D^i/A^j$	0.666	0.886	3	0.154	41.627	25.1/28.1/26.3/15.6/4.9

^a Cross-validated correlation coefficient. ^b Non-cross-validated correlation coefficient.

^c Optimal number of components. ^d Standard error of estimate. ^e F-test. ^f Steric field.

^g Electrostatic field. ^h Hydrophobic field. ⁱ Donor. ^j Acceptor.

To view the field effect on the target property, CoMFA and CoMSIA contour maps were generated. The contour maps can identify the important regions where any change in the steric, electrostatic, hydrophobic, hydrogen bond donor, and hydrogen bond acceptor fields may affect the biological activity. 3D-QSAR contour maps of both CoMFA and CoMSIA models are illustrated in Figure 5.6.

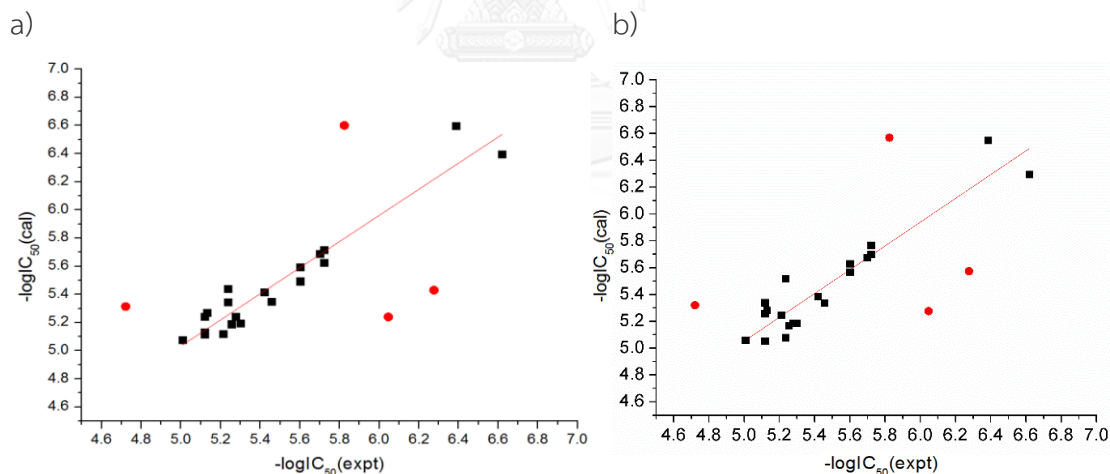


Figure 5.5 Plots between the experimental and predicted biological activities of training (filled square) and test set (filled circle): (a) CoMFA plot and (b) CoMSIA plot.

From both 3D-QSAR models, the predicted pIC_{50} of the four test compounds differ from the experimental data by about 0.6-0.9. This implies that the accuracy of prediction is within one order of magnitude of the observed IC_{50} data.

Table 5.6 Experimental and predicted activities of the test set

Cpd	Actual pIC ₅₀	CoMFA		CoMSIA	
		Predicted pIC ₅₀	Residual	Predicted pIC ₅₀	Residual
5-1	6.0	5.1	0.9	5.2	0.8
5-9	6.3	5.4	0.9	5.5	0.8
3-9^a	4.7	5.3	0.6	5.3	0.6
3-36^a	5.8	6.6	0.8	6.5	0.7
		Avg	0.8	Avg	0.7

^a From our previous report [50].

In this study, we focused on the effects of alkyl side chain at nitrogen atom of aminoquercitols to rat maltase inhibitory activity. One of the active compounds in the series (compound **5-22**) is shown superimposed with the CoMFA and CoMSIA contour maps. In the case of CoMFA, the green contour shows favorable steric interaction and the yellow contour shows the region where the steric group is not favored. The red contours show favorable electronegative regions, and the blue contours show the region where the electropositive region is favored. Large yellow contour region near the *N*-aryl side chain shows that substituents at nitrogen atom have unfavorable steric interactions (Figure 5.6a). This is consistent with the reported experimental results. For example, *N,N*-dihexyl aminoquercitol (IC₅₀ 32 μM) has inhibitory activity lower than *N*-hexyl aminoquercitol (IC₅₀ 2.5 μM) [50]. On the other hand, the green contours are present below the plane of aromatic side chain. This shows that there would be a favorable steric interaction if bulky substitutions were introduced in that region. For example, **5-13** and **5-20**, having bulky group, show inhibitory activity higher than **5-15** and **5-22**. There are the red contours close to the hydroxyl group of the cyclitol moiety suggesting the preference for electronegative groups at those locations. The small blue contour was located around the *N*-position (Figure 5.6b) indicating that electropositive group is predicted to increase activity in

that area. This is consistent with the observation that H-bond interaction from cyclitol moiety plays an important role [34, 49].

For CoMSIA contour maps, steric and electrostatic are similar to those of CoMFA as shown by the yellow contour at the *N*-aryl side chain and the red contour near the cyclitol moiety (Figure 5.6c-d). The additional hydrophobic, hydrogen bond donor, and hydrogen bond acceptor contours of CoMSIA are displayed in Figure 5.6e-g, respectively. The hydrophobic fields (yellow, hydrophobic group favored; white, hydrophobic disfavored) and the hydrogen bond donor (cyan, favored; purple, disfavored) and hydrogen bond acceptor (magenta, favored; red, disfavored) fields indicate areas around the molecules where changes increased or decreased activity.

In Figure 5.6e, hydrophobicity is favored at out-of-plane of aromatic side chain (yellow contour), while the white contour was located around the *N*-aryl side chain emphasizing the favoring effect of a hydrophilic substituent. This explains the lower activity of compounds **5-16** – **5-19** ($IC_{50} > 100 \mu M$) compared to that of compounds **5-1**, **5-9** (have propane diol, hydrophilic group). For hydrogen bond donor contour maps (Figure 5.6f), cyan contour under the –NH group favors activity, while small purple contour located on the –NH group indicated that this position requires the hydrogen bond acceptor substituent. The magenta contour in the region of cyclitol moiety and the *N*-aryl side chain favor activity (Figure 5.6g).

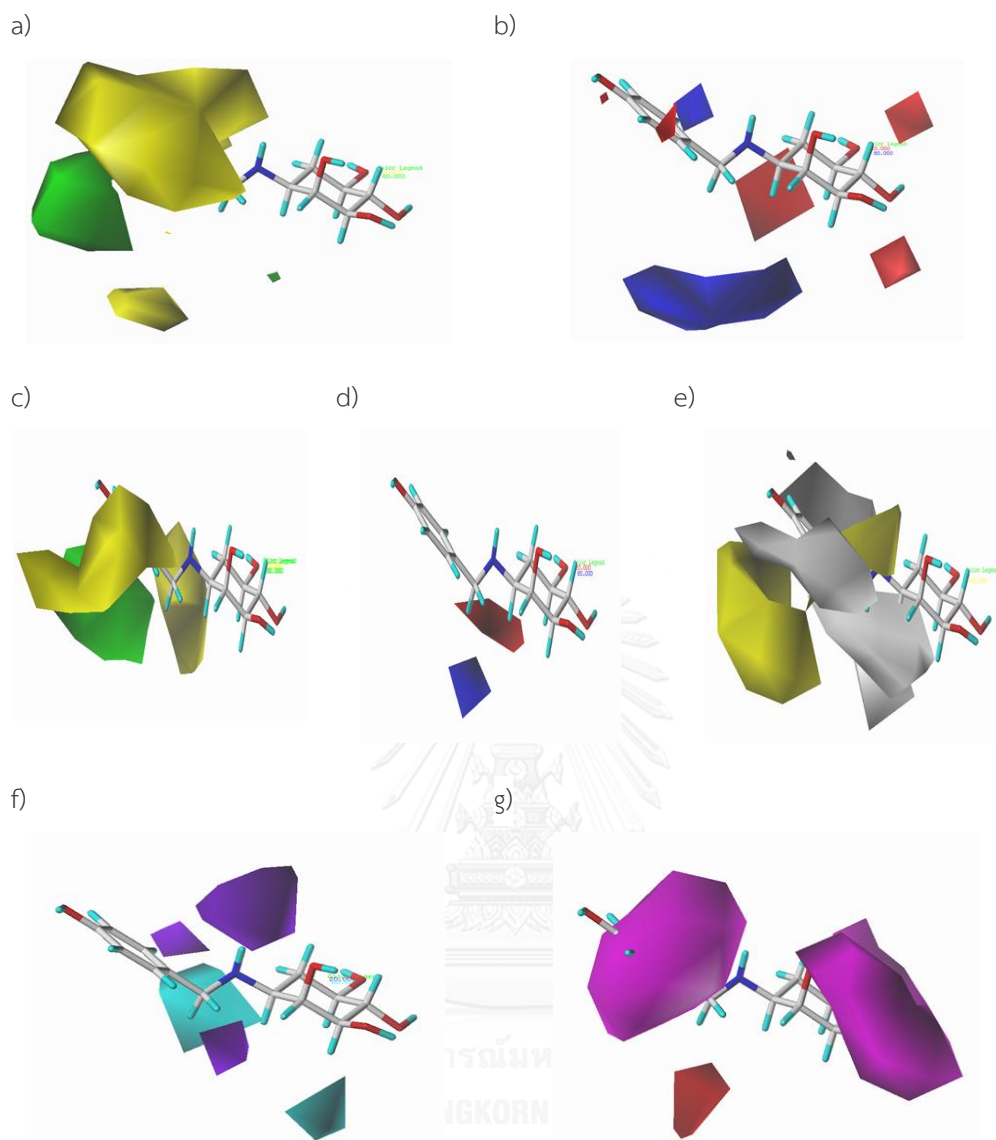


Figure 5.6 The stdev^* coeff. contour maps. (a) and (b) represent CoMFA steric and electrostatic, respectively. (c) to (g) represent CoMSIA steric, electrostatic, hydrophobic, hydrogen bond donor, and hydrogen bond acceptor, respectively. Steric field is represented by green and yellow contour maps. Electrostatic field is represented by blue and red contour maps. Hydrophobic field is represented by yellow and white contour maps. Hydrogen bond donor field is represented by cyan and purple contour maps. Hydrogen bond acceptor field is represented by magenta and red contour maps. All the contours represented the default 80% and 20% level contributions for favorable and unfavorable regions, respectively.

5.5 Conclusion

In summary, we first synthesized a series of *N*-substituted aminoquercitols having hydrophobic aryl and hydrophilic moieties from naturally available (+)-*proto*-quercitol. Evaluation of their α -glucosidase inhibition revealed that they selectively inhibited rat intestinal maltase rather than yeast glucosidase. Among the synthesized compounds, **5-1** and **5-9**, carrying propane diol hydrophilic group, showed potent inhibitory activity against rat intestinal maltase with IC_{50} values of 0.90 and 0.53 μ M, respectively. Interestingly, voglibose-like compound **5-9** was the most effective inhibitor that not only displayed more prominent inhibition than the antidiabetic drug acarbose (IC_{50} 1.5 μ M) but also showed the similar inhibition to the antidiabetic drug voglibose (IC_{50} 0.25 μ M). In addition, mechanism underlying the inhibitory effect of **5-9** against maltase and sucrase were proved to be competitive inhibition. The molecular docking and 3D-QSAR were performed for a series of *N*-substituted aminoquercitols to study the molecular interaction, binding mode, and the structural features contributing to the biological activity of this series in the active site of the modeled rat intestinal maltase. A molecular docking result suggested that the hydrogen bond interaction, from hydroxyl groups at aminoquercitol moiety and *N*-alkyl side chain with the key residues in the rat maltase active site, play an important role in molecular interactions. In addition, the $-NH$ group might also establish the hydrogen bond interaction within the active site of enzyme. However, no π - π interactions were recognized between aromatic rings of *N*-aryl side chain and aromatic rings of key residues in the active site of rat intestinal maltase in this binding model. 3D-QSAR study emphasized structural features around *N*-substituted part of aminoquercitol derivatives as the α -glucosidase inhibitory activity. The resulting contour maps from the 3D-QSAR models provide a good insight into the molecular features relevant to the biological activity for this series, suggesting that the less steric and hydrophilic groups at *N*-position of aminoquercitol could increase activity. Therefore, voglibose-like compounds **5-1** and **5-9** could represent a new class of promising compounds that have the potential for treating diabetes mellitus.

5.6 Experimental section

5.6.1 General experimental procedures

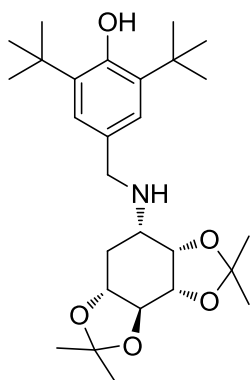
General experiments performed in this Chapter were similar to those described in Chapter 2.

5.6.2 Synthesis of *N*-substituted aminoquercitols

5.6.2.1 General procedure for reductive amination

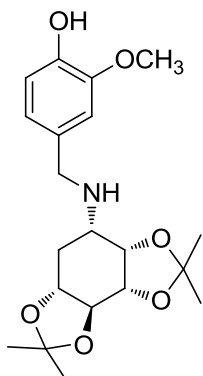
General procedure for reductive amination was performed using the methodology described in section 3.5.3.1.

Protected-*N*-(3,5-di-*tert*-butyl-4-hydroxybenzyl)-*epi*-aminoquercitol (**5-2**).



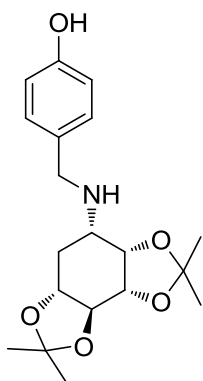
Following the general procedure above, reaction of **3-1** (65.4 mg, 0.27 mmol), sodium cyanoborohydride (34.0 mg, 0.54 mmol), 3,5-di-*tert*-butyl-4-hydroxybenzaldehyde (131.0 mg, 0.54 mmol), acetic acid (21 μ L) in methanol (1.5 mL) after 24 h yielded compound **5-2** (86.6 mg, 70%) as a colorless oil; ^1H NMR (CDCl_3 , 400 MHz) δ 7.07 (s, 2H), 5.09 (s, 1H), 4.39 (dd, J = 8.0, 4.0 Hz, 1H), 4.06 (m, 1H), 3.74 (br d, J = 4.0 Hz, 2H), 3.50 (dd, J = 10.0, 8.0 Hz, 1H), 3.21 (m, 1H), 2.97 (m, 1H), 2.32 (m, 1H), 1.53 (m, 1H), 1.47 (s, 3H), 1.37 (br s, 21H), 1.33 (s, 3H), 1.32 (s, 3H); ^{13}C NMR (CDCl_3 , 100 MHz) δ 152.9, 136.0, 130.4, 124.7, 110.8, 109.2, 82.5, 76.7, 75.3, 74.5, 54.1, 51.1, 34.3, 31.2, 30.3, 28.6, 26.9, 26.2.

Protected-*N*-(4-hydroxy-3-methoxybenzyl)-*epi*-aminoquercitol (**5-3**).



Following the general procedure above, reaction of **3-1** (52.0 mg, 0.21 mmol), sodium cyanoborohydride (27.0 mg, 0.43 mmol), 4-hydroxy-3-methoxybenzaldehyde (33.0 mg, 0.21 mmol), acetic acid (17 μ L) in methanol (2 mL) after 2 days yielded compound **5-3** (65.0 mg, 80%) as a colorless oil; ^1H NMR (CDCl_3 , 400 MHz) δ 6.90 (br s, 1H), 6.81 (d, $J = 8.0$ Hz, 1H), 6.77 (d, $J = 8.0$ Hz, 1H), 4.39 (t, $J = 8.0$ Hz, 1H), 4.09 (dd, $J = 8.0, 4.0$ Hz, 1H), 3.84 (s, 3H), 3.81 (s, 2H), 3.53 (m, 1H), 3.23 (m, 1H), 2.99 (m, 1H), 2.36 (m, 1H), 1.57 (m, 1H), 1.52 (s, 3H), 1.41 (s, 3H), 1.37 (s, 3H), 1.36 (s, 3H); ^{13}C NMR (CDCl_3 , 100 MHz) δ 146.8, 144.9, 131.5, 121.0, 114.3, 110.9, 110.8, 109.3, 82.5, 76.6, 75.5, 74.4, 55.9, 53.7, 50.7, 31.0, 28.6, 26.9, 26.2.

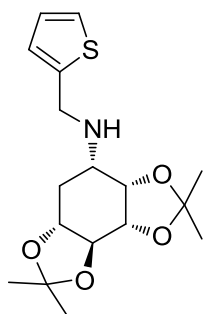
Protected-*N*-(4-hydroxybenzyl)-*epi*-aminoquercitol (**5-4**).



Following the general procedure above, reaction of **3-1** (41.9 mg, 0.17 mmol), sodium cyanoborohydride (22.0 mg, 0.34 mmol), 4-hydroxybenzaldehyde (21.0 mg, 0.17 mmol), acetic acid (14 μ L) in methanol (1.7 mL) after 2 days yielded compound **5-4** (51.5 mg, 86%) as a white solid; ^1H NMR (CDCl_3 , 400 MHz) δ 7.05 (d, $J = 8.0$ Hz,

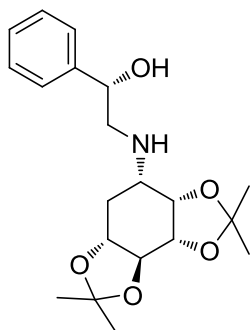
2H), 6.58 (d, $J = 8.0$ Hz, 2H), 4.37 (t, $J = 4.0$ Hz, 1H), 4.05 (dd, $J = 8.0, 4.0$ Hz, 1H), 3.75 (br s, 2H), 3.47 (t, $J = 8.0$ Hz, 1H), 3.18 (t, $J = 8.0$ Hz, 1H), 3.03 (m, 1H), 2.36 (m, 1H), 1.54 (m, 1H), 1.45 (s, 3H), 1.35 (s, 3H), 1.32 (s, 3H), 1.27 (s, 3H); ^{13}C NMR (CDCl_3 , 100 MHz) δ 155.1, 128.8, 128.3, 114.8, 110.1, 108.5, 81.4, 75.5, 74.0, 73.2, 52.7, 49.1, 29.4, 27.6, 25.9, 25.9, 25.2.

Protected-*N*-thenyl-*epi*-aminoquercitol (5-6).



Following the general procedure above, reaction of **3-1** (46.4 mg, 0.19 mmol), sodium cyanoborohydride (24.0 mg, 0.38 mmol), 2-thiophenecarboxaldehyde (36 μL , 0.38 mmol), acetic acid (15 μL) in methanol (2 mL) after 2 days yielded compound **5-6** (21.5 mg, 34%) as a colorless oil; ^1H NMR (CDCl_3 , 400 MHz) δ 7.16 (dd, $J = 3.2, 3.2$ Hz, 1H), 6.88-6.89 (m, 2H), 4.31 (dd, $J = 6.0, 4.4$ Hz, 1H), 4.04 (br s, 3H), 3.48 (dd, $J = 10.4, 8.8$ Hz, 1H), 3.17 (m, 1H), 2.98 (m, 1H), 2.28 (m, 1H), 1.52 (m, 1H), 1.47 (s, 3H), 1.36 (s, 3H), 1.31 (br s, 6H); ^{13}C NMR (CDCl_3 , 100 MHz) δ 143.8, 126.7, 125.0, 124.7, 110.9, 109.3, 82.4, 76.6, 75.4, 74.4, 53.5, 45.5, 30.8, 28.6, 26.9, 26.2.

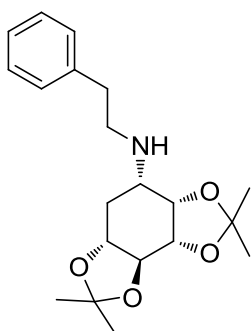
Protected-*N*-[(*S*)-hydroxyphenethyl]-*epi* aminoquercitol (5-7).



Following the general procedure above, reaction of **3-1** (27.0 mg, 0.11 mmol), sodium cyanoborohydride (14.0 mg, 0.22 mmol), phenylglyoxal monohydrate (28.0

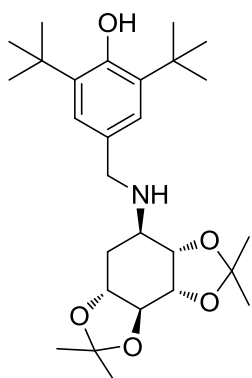
mg, 0.21 mmol), acetic acid (10 μ L) in methanol (1.5 mL) after 2 days yielded compound **102** (27.6 mg, 69%) as a colorless oil; ^1H NMR (CDCl_3 , 400 MHz) δ 7.22-7.30 (m, 5H), 4.64 (br d, $J = 12.0$ Hz, 1H), 4.34 (dd, $J = 4.0, 4.0$ Hz, 1H), 4.08 (dd, $J = 8.0, 4.0$ Hz, 1H), 3.48 (t, $J = 8.0$ Hz, 1H), 3.21 (m, 1H), 2.94-2.99 (m, 2H), 2.65 (dd, $J = 12.0, 8.0$ Hz, 1H), 2.24 (m, 1H), 1.50 (m, 1H), 1.45 (s, 3H), 1.36 (s, 3H), 1.34 (s, 3H), 1.30 (s, 3H); ^{13}C NMR (CDCl_3 , 100 MHz) δ 142.1, 128.4, 127.6, 125.8, 111.0, 109.4, 82.4, 76.4, 75.4, 74.3, 72.1, 55.3, 54.7, 31.3, 28.6, 26.9, 26.2.

Protected-*N*-phenethyl-*epi*-aminoquercitol (**5-8**).



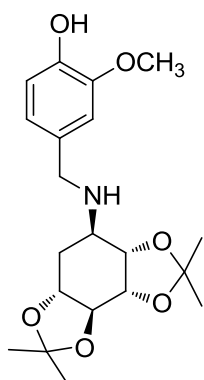
Following the general procedure above, reaction of **3-1** (35.4 mg, 0.14 mmol), sodium cyanoborohydride (18.0 mg, 0.29 mmol), phenylacetaldehyde (17 μ L, 0.14 mmol), acetic acid (12 μ L) in methanol (1.4 mL) after 2 days yielded compound **5-8** (23.8 mg, 47%) as a colorless oil; ^1H NMR (CDCl_3 , 400 MHz) δ 7.14-7.25 (m, 5H), 4.34 (dd, $J = 5.2, 4.4$ Hz, 1H), 4.06 (dd, $J = 8.4, 5.2$ Hz, 1H), 3.46 (dd, $J = 9.2, 8.8$ Hz, 1H), 3.21 (m, 1H), 3.00 (m, 1H), 2.88-2.91 (m, 2H), 2.76-2.79 (m, 2H), 2.27 (m, 1H), 1.48 (m, 1H), 1.42 (s, 3H), 1.35 (s, 3H), 1.33 (s, 3H), 1.28 (s, 3H); ^{13}C NMR (CDCl_3 , 100 MHz) δ 138.6, 127.6, 127.5, 125.3, 109.9, 108.3, 81.4, 75.6, 74.1, 73.4, 54.1, 47.3, 35.3, 29.9, 27.5, 25.9, 25.1.

Protected-*N*-(3,5-di-*tert*-butyl-4-hydroxybenzyl)-*proto*-aminoquercitol (**5-10**).



Following the general procedure above, reaction of **3-2** (29.0 mg, 0.12 mmol), sodium cyanoborohydride (15.0 mg, 0.24 mmol), 3,5-di-*tert*-butyl-4-hydroxybenzaldehyde (58.0 mg, 0.24 mmol), acetic acid (10 μ L) in methanol (1.5 mL) after 2 days yielded compound **5-10** (32.3 mg, 60%) as a colorless oil; ^1H NMR (CDCl_3 , 400 MHz) δ 7.07 (br s, 2H), 4.30 (t, $J = 8.0$ Hz, 1H), 4.19 (t, $J = 8.0$ Hz, 1H), 3.59-3.82 (m, 4H), 3.14 (q, $J = 8.0$ Hz, 1H), 2.00 (t, $J = 4.0$ Hz, 2H), 1.43 (br s, 27H), 1.33 (s, 3H); ^{13}C NMR (CDCl_3 , 100 MHz) δ 152.9, 135.9, 130.1, 124.8, 111.5, 109.9, 80.6, 78.7, 76.3, 72.6, 54.9, 51.8, 34.3, 30.3, 30.0, 27.8, 27.1, 27.0, 25.3.

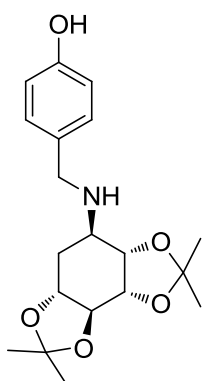
Protected-*N*-(4-hydroxy-3-methoxybenzyl)-*proto*-aminoquercitol (**5-11**).



Following the general procedure above, reaction of **3-2** (23.8 mg, 0.10 mmol), sodium cyanoborohydride (13.0 mg, 0.19 mmol), 4-hydroxy-3-methoxybenzaldehyde (15.0 mg, 0.10 mmol), acetic acid (8 μ L) in methanol (1.5 mL) after 2 days yielded compound **5-11** (27.8 mg, 75%) as a colorless oil; ^1H NMR (CDCl_3 , 400 MHz) δ 6.78 (d, $J = 8.0$ Hz, 1H), 6.76 (s, 1H), 6.71 (d, $J = 8.0$ Hz, 1H), 4.24 (t, $J = 8.0$ Hz, 1H), 4.11 (t, $J =$

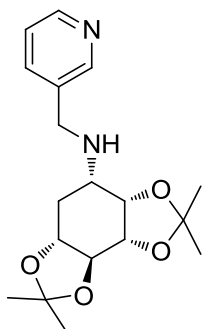
8.0 Hz, 1H), 3.80 (s, 3H), 3.56-3.77 (m, 4H), 3.05 (q, $J = 8.0$ Hz, 1H), 1.87-1.95 (m, 2H), 1.38 (s, 3H), 1.35 (s, 6H), 1.26 (s, 3H); ^{13}C NMR (CDCl_3 , 100 MHz) δ 146.7, 144.9, 131.5, 120.9, 114.4, 111.7, 110.7, 110.0, 80.5, 78.8, 76.3, 72.6, 55.9, 54.9, 51.4, 30.1, 27.8, 27.1, 27.0, 25.2.

Protected-*N*-(4-hydroxybenzyl)-*proto*-aminoquercitol (5-12).



Following the general procedure above, reaction of **3-2** (23.7 mg, 0.10 mmol), sodium cyanoborohydride (12.0 mg, 0.19 mmol), 4-hydroxybenzaldehyde (12.0 mg, 0.10 mmol), acetic acid (8 μL) in methanol (1.2 mL) after 2 days yielded compound **5-12** (21.0 mg, 62%) as a colorless oil; ^1H NMR (CDCl_3 , 400 MHz) δ 7.05 (d, $J = 8.0$ Hz, 2H), 6.63 (d, $J = 8.0$ Hz, 2H), 4.24 (t, $J = 8.0$ Hz, 1H), 4.14 (t, $J = 8.0$ Hz, 1H), 3.54-3.77 (m, 4H), 3.03 (q, $J = 8.0$ Hz, 1H), 1.89-1.98 (m, 2H), 1.38 (s, 3H), 1.36 (s, 3H), 1.35 (s, 3H), 1.25 (s, 3H); ^{13}C NMR (CDCl_3 , 100 MHz) δ 155.5, 130.6, 129.5, 115.6, 111.9, 110.2, 80.3, 78.5, 76.2, 72.5, 54.9, 50.8, 29.7, 27.7, 27.1, 27.0, 25.2.

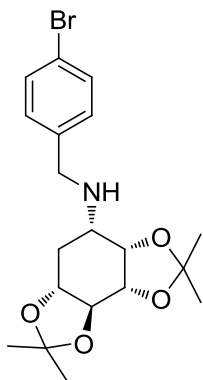
Protected-*N*-(3-pyridylmethyl)-*epi*-aminoquercitol (5-5).



Following the general procedure from Chapter III in 3.5.3.1 using $\text{Ti}(\text{O}^i\text{Pr})_4$ as catalyst, reaction of **3-1** (37.5 mg, 0.15 mmol), sodium cyanoborohydride (29.0 mg,

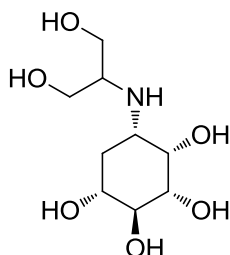
0.46 mmol), 3-pyridinecarboxaldehyde (29 μL , 0.31 mmol), titanium isopropoxide (91 μL , 0.31 mmol) in methanol (1.5 mL) after 2 days yielded compound **5-5** (43.9 mg, 86%) as a yellow oil; ^1H NMR (CDCl_3 , 400 MHz) δ 8.54 (s, 1H), 8.48 (d, $J = 4.0$ Hz, 1H), 7.71 (d, $J = 8.0$ Hz, 1H), 7.25 (m, 1H), 4.37 (t, $J = 4.0$ Hz, 1H), 4.09 (dd, $J = 8.0, 4.0$ Hz, 1H), 3.88 (br s, 2H), 3.53 (t, $J = 8.0$ Hz, 1H), 3.22 (m, 1H), 2.95 (m, 1H), 2.33 (m, 1H), 1.56 (m, 1H), 1.50 (s, 3H), 1.39 (s, 3H), 1.36 (s, 3H), 1.35 (s, 3H); ^{13}C NMR (CDCl_3 , 100 MHz) δ 149.5, 148.5, 136.0, 135.2, 123.5, 111.0, 109.3, 82.3, 76.5, 75.3, 74.3, 54.1, 48.2, 30.9, 28.6, 26.9, 26.2.

Protected-*N*-(4-bromobenzyl)-*epi*-aminoquercitol (**5-23**).



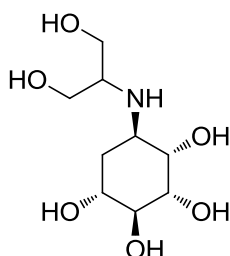
A solution of **3-1** (26.2 mg, 0.11 mmol) in DMF (1 mL) under an atmosphere of N_2 was treated with TEA (23 μL , 0.16 mmol) and *p*-bromobenzyl bromide (40 mg, 0.16 mmol). After stirring at room temperature for 5 h, the reaction mixture was quenched with water and extracted with EtOAc (3 \times 10 mL). The combined organic layers were washed with brine, dried over anhydrous Na_2SO_4 and concentrated under reduced pressure to afford crude product, which was purified by flash chromatography using 50% EtOAc-hexane as a mobile phase to give compound **5-23** (31.7 mg, 72%) as a colorless oil; ^1H NMR (CDCl_3 , 400 MHz) δ 7.38 (d, $J = 8.0$ Hz, 2H), 7.18 (d, $J = 8.0$ Hz, 2H), 4.31 (t, $J = 4.0$ Hz, 1H), 4.04 (dd, $J = 8.0, 4.0$ Hz, 1H), 3.78 (br s, 2H), 3.49 (t, $J = 8.0$ Hz, 1H), 3.16 (m, 1H), 2.90 (m, 1H), 2.28 (br s, 1H), 1.51 (m, 1H), 1.46 (s, 3H), 1.35 (s, 3H), 1.32 (s, 3H), 1.31 (s, 3H); ^{13}C NMR (CDCl_3 , 100 MHz) δ 138.8, 131.6, 129.9, 120.9, 111.0, 109.3, 82.4, 76.6, 75.4, 74.4, 54.0, 50.2, 30.9, 28.6, 26.9, 26.2.

N-[2-hydroxy-1-(hydroxymethyl)ethyl]-*epi* aminoquercitol (**5-1**).



A solution of **3-1** (36.8 mg, 0.15 mmol) in methanol (1.5 mL) under an atmosphere of N₂ was treated with sodium cyanoborohydride (29 mg, 0.45 mmol), acetic acid (12 μL) and 1,3-dihydroxyacetonedimer (82 mg, 0.45 mmol). After stirring at room temperature for 2 days, the reaction mixture was evaporated to dryness, further added with 1.25 M methanolic HCl (1 mL) and stirred at room temperature for 4 h. The reaction mixture was filtered to remove the white precipitate and the filtrate was evaporated to dryness. The crude product was redissolved with H₂O, loaded onto Dowex 50W-X8 (H⁺) column which was eluted with H₂O and 50% NH₃-H₂O. Fractions eluted with 50% NH₃-H₂O were evaporated to give compound **5-1** (22.1 mg, 62%) as a yellow oil; ¹H NMR (D₂O, 400 MHz) δ 3.93 (br s, 1H), 3.24-3.57 (m, 7H), 2.93-3.00 (m, 2H), 1.86 (br d, *J* = 10.8 Hz, 1H), 1.45 (br d, *J* = 10.8 Hz, 1H); ¹³C NMR (D₂O, 100 MHz) δ 74.2, 72.5, 69.8, 69.1, 60.3, 59.8, 56.9, 51.4, 31.6; HRMS *m/z* 238.1292 [M+H]⁺ (calcd for C₉H₂₀NO₆, 238.1291).

N-[2-hydroxy-1-(hydroxymethyl)ethyl]-*proto*-aminoquercitol (**5-9**).



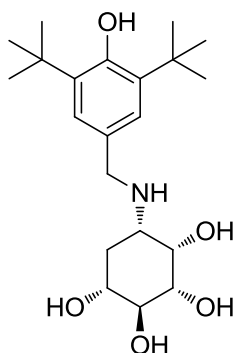
Following the procedure for the synthesis of **5-1**, reaction of **3-2** (30.9 mg, 0.13 mmol), sodium cyanoborohydride (24 mg, 0.38 mmol), acetic acid (10 μL), 1,3-dihydroxyacetonedimer (69 mg, 0.38 mmol) in methanol (1.3 mL) after that yielded compound **5-9** (26.9 mg, 89%) as a yellow oil; ¹H NMR (D₂O, 400 MHz) δ 3.74 (br s, 1H), 3.33-3.55 (m, 7H), 2.91 (br s, 1H), 2.66 (br s, 1H), 1.65-1.71 (m, 2H); ¹³C NMR (D₂O,

100 MHz) δ 72.7, 70.0, 69.6, 67.4, 59.4, 59.2, 56.4, 52.3, 29.6; HRMS m/z 238.1284 $[M+H]^+$ (calcd for $C_9H_{20}NO_6$, 238.1291).

5.6.2.2 General procedure for deprotection of all synthesized compounds

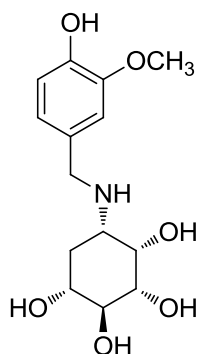
General procedure for deprotection was performed using the methodology described in section 3.5.3.2.

N-(3,5-di-*tert*-butyl-4-hydroxybenzyl)-*epi*-aminoquercitol (5-13).



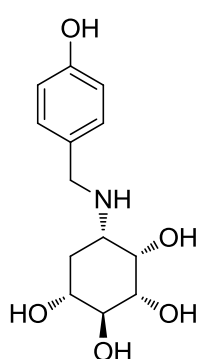
Yellow oil (74%). 1H NMR (CD_3OD , 400 MHz) δ 7.05 (br s, 2H), 4.00 (s, 1H), 3.66 (d, J = 12.0 Hz, 1H), 3.56 (d, J = 12.0 Hz, 1H), 3.43 (dd, J = 8.0, 8.0 Hz, 1H), 3.26 (m, 1H), 3.15 (dd, J = 12.0, 4.0 Hz, 1H), 2.59 (br d, J = 12.0 Hz, 1H), 1.86 (m, 1H), 1.56 (m, 1H), 1.32 (br s, 18H); ^{13}C NMR (CD_3OD , 100 MHz) δ 154.6, 139.4, 130.8, 126.3, 76.4, 75.1, 72.0, 70.8, 55.0, 51.5, 35.6, 34.1, 30.8, 30.8; HRMS m/z 382.2582 $[M+H]^+$ (calcd for $C_{21}H_{36}NO_5$, 382.2593).

N-(4-hydroxy-3-methoxybenzyl)-*epi*-aminoquercitol (5-14).



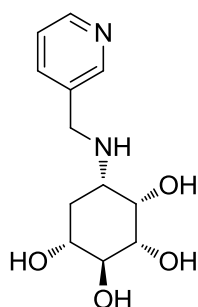
Pale yellow oil (63%). ^1H NMR (CD_3OD , 400 MHz) δ 7.03 (br s, 1H), 6.85 (d, J = 8.0 Hz, 1H), 6.79 (d, J = 8.0 Hz, 1H), 4.14 (br s, 1H), 3.97 (m, 1H), 3.90 (m, 1H), 3.86 (s, 3H), 3.55 (t, J = 10.0 Hz, 1H), 3.38 (m, 1H), 3.29 (m, 1H), 2.97 (br d, J = 12.0 Hz, 1H), 2.01 (m, 1H), 1.78 (m, 1H); ^{13}C NMR (CD_3OD , 100 MHz) δ 149.3, 148.0, 127.6, 123.4, 116.5, 114.0, 76.0, 74.5, 71.5, 69.9, 56.6, 55.3, 50.4, 32.6; HRMS m/z 300.1440 $[\text{M}+\text{H}]^+$ (calcd for $\text{C}_{14}\text{H}_{22}\text{NO}_6$, 300.1447).

***N*-(4-hydroxybenzyl)-*epi*-aminoquercitol (5-15).**



White solid (75%). ^1H NMR (D_2O , 400 MHz) δ 7.01 (d, J = 8.0 Hz, 2H), 6.61 (d, J = 8.0 Hz, 2H), 3.93 (br s, 1H), 3.61-3.71 (m, 2H), 3.13-3.32 (m, 3H), 2.77 (br d, J = 12.0 Hz, 1H), 1.80 (br s, 1H), 1.43 (m, 1H); ^{13}C NMR (D_2O , 100 MHz) δ 156.6, 130.9, 126.3, 116.0, 74.2, 72.5, 69.7, 68.7, 52.9, 48.5, 30.9; HRMS m/z 270.1339 $[\text{M}+\text{H}]^+$ (calcd for $\text{C}_{13}\text{H}_{20}\text{NO}_5$, 270.1341).

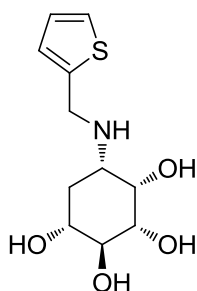
***N*-(3-pyridylmethyl)-*epi*-aminoquercitol (5-16).**



Pale yellow oil (85%). ^1H NMR (CD_3OD , 400 MHz) δ 8.64 (br s, 1H), 8.55 (d, J = 4.0 Hz, 1H), 8.02 (d, J = 8.0 Hz, 1H), 7.51 (dd, J = 8.0, 4.0 Hz, 1H), 4.11-4.23 (m, 3H), 3.57 (t, J = 8.0 Hz, 1H), 3.47 (m, 1H), 3.37 (m, 1H), 3.18 (br d, J = 12.0 Hz, 1H), 2.10 (m,

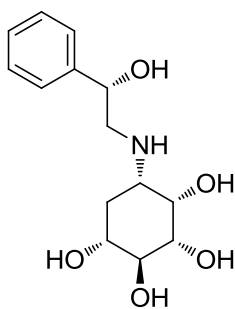
1H), 1.84 (m, 1H); ^{13}C NMR (CD_3OD , 100 MHz) δ 149.6, 148.8, 138.3, 130.8, 124.2, 74.3, 72.7, 69.7, 68.2, 54.6, 46.2, 30.7; HRMS m/z 255.1339 $[\text{M}+\text{H}]^+$ (calcd for $\text{C}_{12}\text{H}_{19}\text{N}_2\text{O}_4$, 255.1345).

***N*-thenyl-*epi*-aminoquercitol (5-17).**

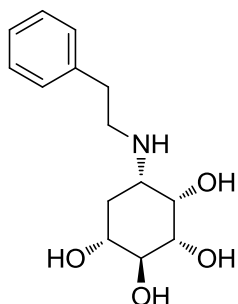


White solid (29%). ^1H NMR (CD_3OD , 400 MHz) δ 7.20 (br s, 1H), 6.86-6.91 (m, 2H), 3.88-3.97 (m, 3H), 3.42 (dd, $J = 9.2, 9.2$ Hz, 1H), 3.25 (m, 1H), 3.12 (br d, $J = 9.6$ Hz, 1H), 2.58 (br d, $J = 12.0$ Hz, 1H), 1.83 (br d, $J = 9.6$ Hz, 1H), 1.53 (q, $J = 12.0$ Hz, 1H); ^{13}C NMR (CD_3OD , 100 MHz) δ 143.8, 127.8, 126.9, 125.8, 76.3, 75.0, 72.0, 71.0, 54.6, 45.5, 34.2; HRMS m/z 260.0951 $[\text{M}+\text{H}]^+$ (calcd for $\text{C}_{11}\text{H}_{18}\text{NO}_4\text{S}$, 260.0957).

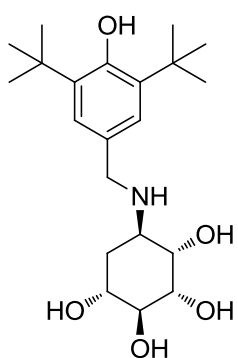
***N*-[(*S*)-hydroxyphenethyl]-*epi*-aminoquercitol (5-18).**



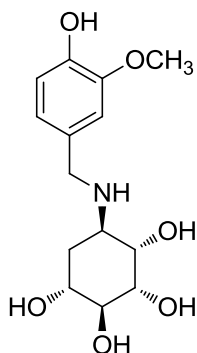
Yellow oil (72%). ^1H NMR (D_2O , 400 MHz) δ 7.25-7.32 (m, 5H), 4.89 (dd, $J = 12.0, 4.0$ Hz, 1H), 4.08 (br d, $J = 12.0$ Hz, 1H), 3.11-3.44 (m, 6H), 2.03 (m, 1H), 1.71 (m, 1H); ^{13}C NMR (D_2O , 100 MHz) δ 139.6, 129.1, 129.1, 126.1, 73.8, 71.9, 69.1, 67.6, 67.4, 54.8, 50.9, 29.4; HRMS m/z 284.1497 $[\text{M}+\text{H}]^+$ (calcd for $\text{C}_{14}\text{H}_{22}\text{NO}_5$, 284.1498).

N-phenethyl-*epi*-aminoquercitol (5-19).

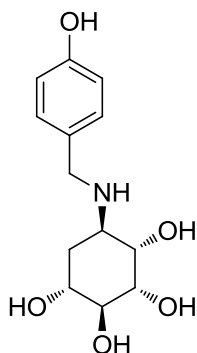
Colorless oil (72%). ^1H NMR (CD_3OD , 400 MHz) δ 7.12-7.23 (m, 5H), 3.97 (br s, 1H), 3.43 (dd, $J = 9.2, 9.2$ Hz, 1H), 3.31 (m, 1H), 3.19 (m, 1H), 2.78-2.99 (m, 5H), 1.89 (m, 1H), 1.61 (q, $J = 12.0$ Hz, 1H); ^{13}C NMR (CD_3OD , 100 MHz) δ 139.6, 129.8, 129.7, 127.8, 76.0, 74.5, 71.5, 70.1, 56.0, 48.3, 35.3, 32.7; HRMS m/z 268.1543 $[\text{M}+\text{H}]^+$ (calcd for $\text{C}_{14}\text{H}_{22}\text{NO}_4$, 268.1549).

N-(3,5-di-*tert*-butyl-4-hydroxybenzyl)-*proto*-aminoquercitol (5-20).

Yellow oil (67%); ^1H NMR (CD_3OD , 400 MHz) δ 7.13 (s, 2H), 3.62-3.82 (m, 6H), 3.04 (br d, $J = 4.0$ Hz, 1H), 1.95 (m, 1H), 1.84 (m, 1H), 1.42 (br s, 18H); ^{13}C NMR (CD_3OD , 100 MHz) δ 154.5, 139.3, 131.4, 126.1, 75.1, 74.3, 72.8, 71.3, 56.0, 52.7, 35.5, 32.7, 30.8; HRMS m/z 382.2584 $[\text{M}+\text{H}]^+$ (calcd for $\text{C}_{21}\text{H}_{36}\text{NO}_5$, 382.2593).

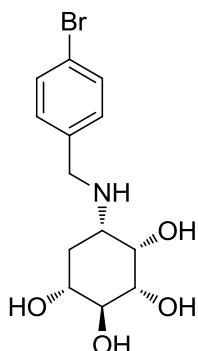
N-(4-hydroxy-3-methoxybenzyl)-*proto*-aminoquercitol (5-21).

Yellow oil (78%). ^1H NMR (D_2O , 400 MHz) δ 6.86 (s, 1H), 6.72 (s, 2H), 3.56-3.87 (m, 9H), 3.13 (br d, $J = 4.0$ Hz, 1H), 1.79-1.84 (m, 2H); ^{13}C NMR (D_2O , 100 MHz) δ 147.7, 145.2, 127.0, 122.6, 115.7, 113.5, 72.7, 72.0, 69.5, 69.0, 56.1, 54.1, 49.4, 29.7; HRMS m/z 300.1456 $[\text{M}+\text{H}]^+$ (calcd for $\text{C}_{14}\text{H}_{22}\text{NO}_6$, 300.1447).

N-(4-hydroxybenzyl)-*proto*-aminoquercitol (5-22).

Pale yellow oil (quantitative yield). ^1H NMR (D_2O , 400 MHz) δ 7.21 (d, $J = 8.0$ Hz, 2H), 6.82 (d, $J = 8.0$ Hz, 2H), 3.62-3.89 (m, 6H), 3.10 (m, 1H), 1.87 (t, $J = 8.0$ Hz, 2H); ^{13}C NMR (D_2O , 100 MHz) δ 155.7, 130.8, 130.8, 115.8, 73.3, 71.8, 70.0, 69.1, 54.3, 49.3, 30.1; HRMS m/z 270.1341 $[\text{M}+\text{H}]^+$ (calcd for $\text{C}_{13}\text{H}_{20}\text{NO}_5$, 270.1341).

N-(4-bromobenzyl)-*epi*-aminoquercitol (5-24).



White solid (29%). ^1H NMR (D_2O + 2 drops MeOD, 400 MHz) δ 7.36 (d, J = 8.0 Hz, 2H), 7.09 (d, J = 8.0 Hz, 2H), 3.94 (br s, 1H), 3.63-3.74 (m, 2H), 3.21-3.34 (m, 2H), 3.15 (m, 1H), 2.70 (br d, J = 11.6 Hz, 1H), 1.81 (m, 1H), 1.42 (q, J = 12.0 Hz, 1H); ^{13}C NMR (D_2O + 2 drops MeOD, 100 MHz) δ 135.3, 131.8, 130.8, 121.5, 74.2, 72.5, 69.8, 68.9, 53.1, 48.5, 31.3; HRMS m/z 332.0498, 334.0479 $[\text{M}+\text{H}]^+$ (calcd for $\text{C}_{13}\text{H}_{19}^{79}\text{BrNO}_4$, 332.0497 and $\text{C}_{13}\text{H}_{19}^{81}\text{BrNO}_4$, 334.0477).

5.6.3 α -Glucosidase inhibition assay

Evaluation of α -glucosidase inhibition was performed using the methodology described in section 2.5.5.2.

5.6.4 Measurement of kinetic constant

Kinetic analysis was performed using the methodology described in section 3.5.5.

5.6.5 Homology modeling and validation

The template used for homology modeling is human intestinal N-terminal domain of maltase-glucoamylase (hu-ntMGAM) complexed with miglitol (PDB: 3L4W). The *Rattus norvegicus* rat intestinal maltase amino acid sequence (Acc. no. XP_008761090) was retrieved from the NCBI web server after performing BLAST search against the sequence of the template. The best match for the selected sequence of rat intestinal maltase shows 82% sequence identity with the template sequence. The three-dimensional homology model of rat intestinal maltase is constructed from 68 to 928 amino acid residues by Swiss-Model Workspace server.

The final protein model was obtained by energy minimization using the NAMD program [51]. The quality of the rat homology model was validated using PROCHECK and QMEAN [52].

5.6.6 Molecular docking

To investigate the binding mode of *N*-substituted aminoquercitols with the surrounding residues of rat intestinal maltase, the flexible docking was performed using AutoDock Vina [48]. 3D structures of all synthesized compounds (ligands) were built and optimized at the semiempirical AM1 level using Gauss View 3.09 [53]. AutoDockTools [54] was used to add polar hydrogens and compute partial atomic charges for protein and ligands using Gasteiger charges. For ligands, all open-chain bonds were treated as active torsional bonds. The center of the 28 x 28 x 28 Å grid box was estimated from the miglitol position present in the crystal structure. The exhaustiveness parameter was set to 64. For each compound, the docked poses that adopt an orientation similar to that of the experimental X-ray structure were chosen as a representative bound conformation. The docking results generated were analyzed using PyMOL (The PyMOL Molecular Graphics System, Version 1.5.0.4 Schrödinger, LLC) and VMD [55].

5.6.7 3D-QSAR Models

All the synthesized *N*-substituted aminoquercitols including *N*-acyl and *N*-alkyl aminoquercitols (from Chapter III) and their maltase inhibitory activity were used to construct CoMFA and CoMSIA models using the program SYBYL (Tripos International, Missouri, USA). The training set of 20 *N*-substituted aminoquercitols was selected on the basis of structural diversity and wide range of activities and the test set contains 4 compounds (from Chapter III). Model building of the compounds was already described in the previous section (molecular docking). Atomic charges of the compounds were assigned according to Gasteiger-Huckel method. Structural alignment of the compounds was performed using the SYBYL automatic alignment feature. For CoMFA, steric and electrostatic fields of the compounds were automatically computed using the standard CoMFA method with default parameters.

Analogously, the calculated CoMSIA fields are associated with five descriptors including steric, electrostatic, hydrophobic, hydrogen bond donor, and hydrogen bond acceptor. The partial least squares (PLS) analysis was carried out using the “leave-one-out” cross-validation protocol to choose the optimum number of components (ONC) that does not exceed one-third of the number of the training compounds but yields the highest cross-validated correlation coefficient (q^2). Subsequently, non-cross-validation analysis was performed with the same ONC to calculate the conventional correlation coefficient (r^2), standard error of estimation (SEE), and F values.



CHAPTER VI

DIASTEREOSELECTIVE TOTAL SYNTHESIS OF CJ-16,264 ANALOGUES

6.1 Introduction

Antibiotics provide the main basis for the treatment of microbial (bacterial and fungal) infections [56]. The introduction of sulfonamide antibiotics in the 1930s and penicillin in the 1940s revolutionized the medical field by substantially decreasing the number of deaths due to bacterial infections [57]. Unfortunately, efforts to develop new antibiotics have significantly decreased during the past two decades. In addition, overuse of the known antibiotics has led to the emergence and dissemination of multi-drug resistant (MDR) strains of several groups of microorganisms [58]. For example, the methicillin-resistant strains of *Staphylococcus aureus* (MRSA) have created serious problems in the hospitals since they affect patients with already weakened immune systems who often succumb to secondary nosocomial infections [59]. Currently, this problem has become more critical by the emerging enterococci strains that are resistant to vancomycin, a powerful antibiotic that is effective against MRSA and is considered as the “last-resort” in antibiotic treatment. Accordingly, there is a need for new, safe and effective antibiotics against MDR clinical strains [59].

Natural products have played an important role in the development of antibiotic drugs. Most of antibiotic drugs have derived from natural products or natural product leads [60]. Recently, pyrrolizidinones; CJ-16,264, UCS1025A, and UCS1025B, have attracted considerable attention from the synthetic community for the synthetic and biological studies because of their remarkable biological properties, particularly antibiotic, coupled with their highly complex structure [61, 62].

6.1.1 Isolation and biological activity of pyrrolizidinones

CJ-16,264 (**6-1**), a pyrrolizidinone antibiotic isolated from the fermentation broth of an unidentified fungus CL39457 by Sugie et al. in 2001 [59], was shown to inhibit the growth of Gram-positive multi-drug resistant bacteria (MIC 0.39-12.5 µg/mL)

and some Gram-negative strains. In addition, CJ-16,264 has also showed cytotoxicity against HeLa cells with an IC_{50} value of 8.0 $\mu\text{g}/\text{mL}$. As discussed in the previous study, the results suggested that the presence of the γ -lactone seemed to be critical to its antibacterial activities. CJ-16,264 has a tricyclic skeleton composed of a pyrrolizidinone moiety fused with a γ -lactone, which was connected to a decalin moiety by a ketone (Figure 6.1).

UCS1025A and UCS1025B (Figure 6.1), isolated from the fungus *Acremonium* sp. KY4917, were first described and tested for biological activities in 2000 then later assigned relative and absolute stereochemistries in 2002 [63]. UCS1025A and UCS1025B, whose intriguing structures and interesting biological activities have led to considerable synthetic efforts towards their total synthesis [61, 64], are structurally closely related to CJ-16,264. UCS1025A and UCS1025B were found to contain virtually the same γ -hydroxypyrrolizidinone moiety as found in CJ-16,264, though adjoined to less highly methylated *trans*-decalin (instead of adjoined to *cis*-decalin as in CJ-16,264). UCS1025A was discovered to have antibacterial activity against Gram-positive bacteria *Staphylococcus aureus*, *Bacillus subtilis* and *Enterococcus hirae*, and Gram-negative bacterium *Proteus vulgaris* with a MIC from 1.3 – 5.2 $\mu\text{g}/\text{mL}$. UCS1025B was discovered to have much lower antibacterial activity against Gram-positive bacteria *Staphylococcus aureus*, *Bacillus subtilis* and *Enterococcus hirae*, and Gram-negative bacterium *Proteus vulgaris* with MIC values ranging from 42–83 $\mu\text{g}/\text{mL}$. UCS1025A was shown to have weak antiproliferative activity against human tumor cell lines with IC_{50} values of cell lines ACHN, A4321, MCF-7 and T24 ranging from 21–58 μM , whereas UCS1025B exhibited no antiproliferative activity against these cell lines up to 100 μM . UCS1025A was also shown to be a novel telomerase inhibitor with an IC_{50} value of 1.3 μM in a TRAP assay [65].

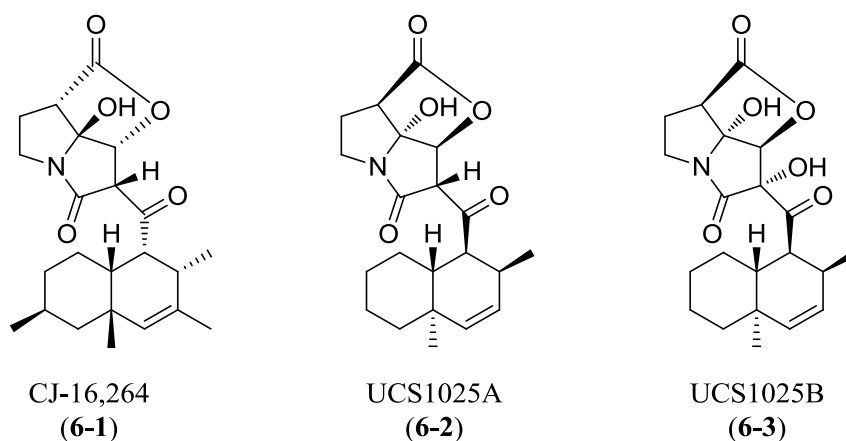


Figure 6.1 Structures of pyrrolizidinone antibiotics CJ-16,264, UCS1025A, and UCS1025B.

6.1.2 Synthetic strategies towards pyrrolizidinones

The beautiful and complex molecular architecture and remarkable biological activities of a group of pyrrolizidinones such as CJ-16,264 and UCS1025A make them very attractive targets for total synthesis. As a result, there have been several synthetic studies and many total syntheses of UCS1025A [61, 64].

The first reported total synthesis of UCS1025A [61], achieved by the Danishefsky group, involved a novel BEt_3 mediated Reformatsky-type cross coupling reaction of aldehyde **6-5** and iodolactam **6-6**, and a subsequent deprotection and oxidation sequence to furnish UCS1025A (Figure 6.2). While *trans*-decalin aldehyde **6-5** has previously been prepared [66], both the racemic, as well as the enantiopure **6-6** were both prepared in several steps with excellent yield from commercially available material. This synthetic method employed a highly efficient and novel late stage coupling that allowed efficient conversion of aldehyde **6-5** into **6-2** in short order from previously synthesized material.

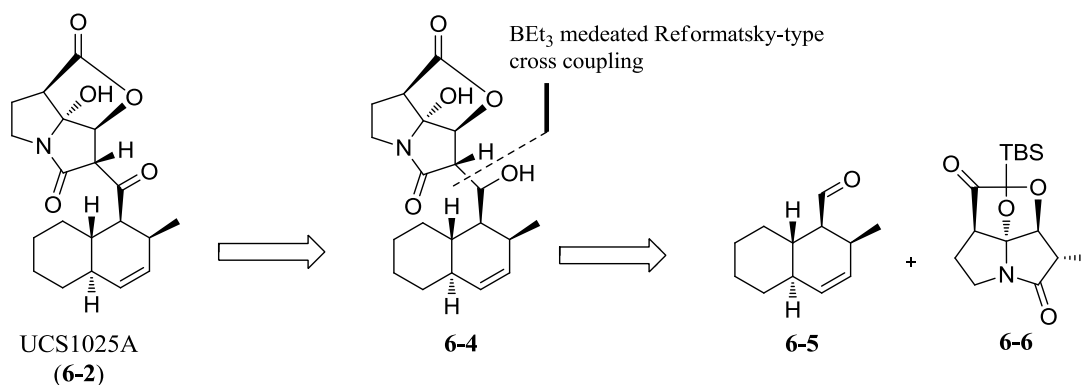


Figure 6.2 Reformatsky-type approach to **6-2** by Danishefsky.

The total synthesis of **6-2** by the Hoyer group [67] employed a biomimetic strategy (Figure 6.3). This synthetic strategy sought to explore whether enzymatic catalysis of a triene (\pm)-**6-7** would be necessary for this system to undergo an intramolecular Diels–Alder (IMDA) reaction, or if this reaction could occur in the laboratory under biologically relevant conditions. Their synthesis was highlighted by a remarkable and fast ($t_{1/2} = 10$ min at room temperature) biomimetic IMDA reaction of triene (\pm)-**6-7** to yield (\pm)-**6-2**, as well as tetraepi-(\pm)-**6-2**, in a 1:1 ratio. While this synthesis did demonstrate that this IMDA would indeed take place extremely quickly, the chiral heterocyclic fragment of (\pm)-**6-7** did not impart diastereocontrol in the IMDA, resulting in the formation of the natural product UCS1025A (**6-2**) and tetraepi-(\pm)-**6-2** in a 1:1 ratio.

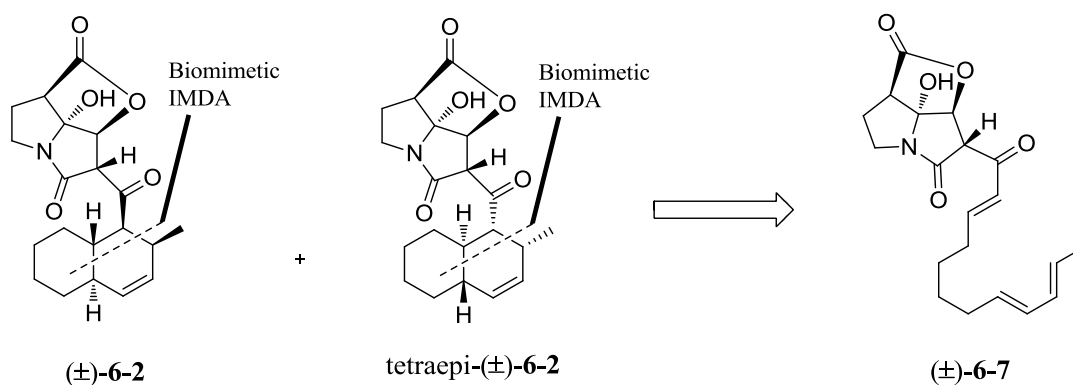


Figure 6.3 Hoyer's approach to (\pm)-**6-2**.

From these synthetic reports above, they endeavored to access a class of pyrrolizidinones in different synthetic strategies. The Danishefsky synthesis introduces an interesting, highly efficient and reliable boron mediate Reformatsky-type coupling in the synthesis of UCS1025A. The final step coupling of iodolactam with a decalin aldehyde enables a convenient disconnection for the synthesis of UCS1025A and congeners such as other pyrrolizilactones. Biomimetic approach was designed by Hoye. They demonstrated the spontaneity of an IMDA reaction to form UCS1025A, as well as another *trans*-decalin analogue. It has not been shown if this remarkably fast IMDA could be used to design a *cis*-decalin such as those found in CJ-16,264.

Most importantly, no total synthesis has been reported for CJ-16,264. Therefore, we are interested in the study of the total synthesis of CJ-16,264. Herein, we report a strategy that allows access to several diastereomers of CJ-16,264 from commercially available citronellal.

With the absolute configuration of CJ-16,264 unknown, these compounds' enantiomers may also be the true structure. Thus, the true structure of CJ-16,264 may well be any of the structures in Figure 6.4.

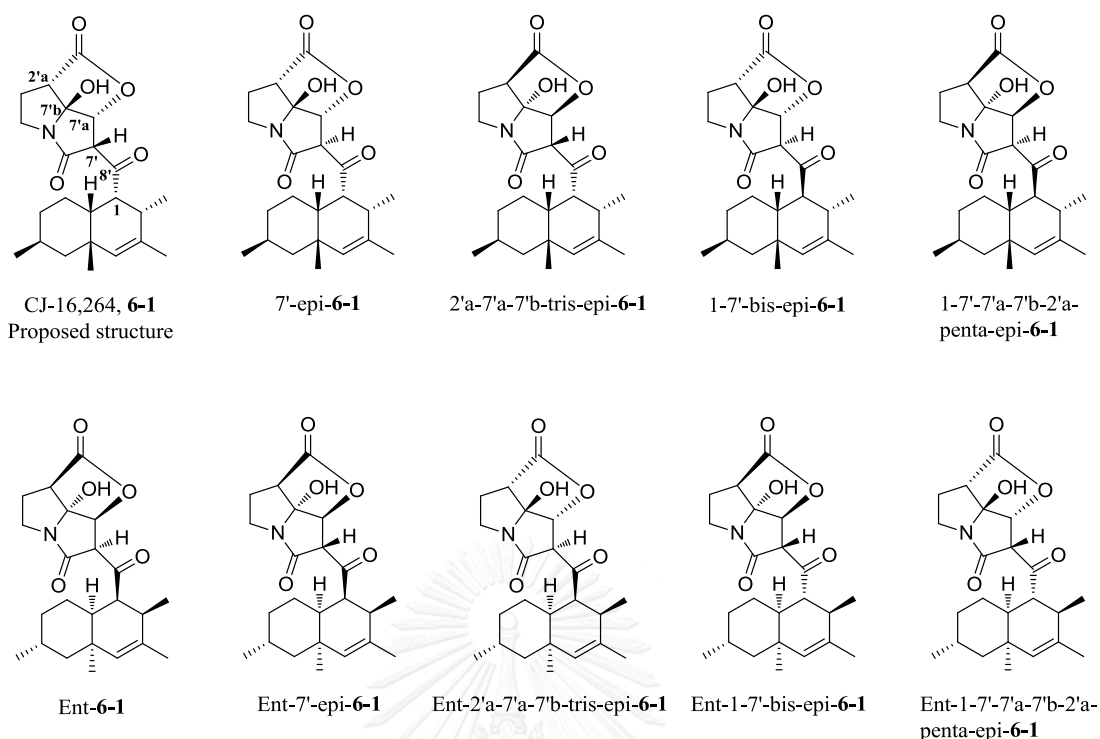
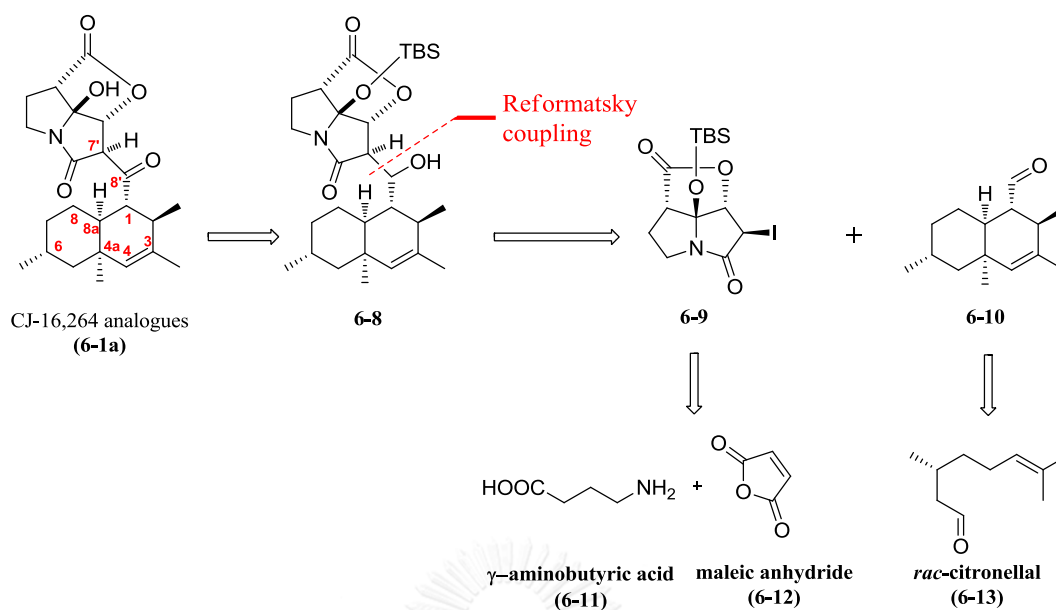


Figure 6.4 Possible true structures of CJ-16,264.

6.2 Total synthesis of CJ-16,264 analogues

6.2.1 Retrosynthesis of CJ-16,264 diastereomers (6-1a)

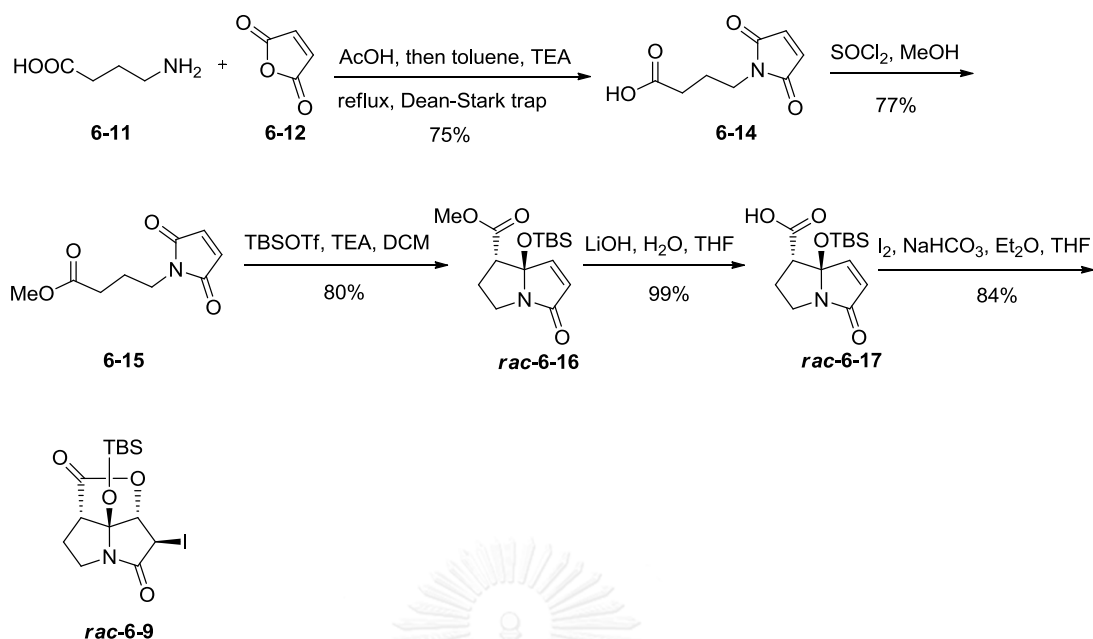
Scheme 6.1 illustrates the basis of our synthetic plan. The substantial challenges associated with a total synthesis of **6-1a** focus on constructing the C7'-C8' σ -bond via a diastereoselective Reformatsky coupling. We envisioned that CJ-16,264 diastereomers could be constructed via oxidation of alcohol precursor **6-8**. A Reformatsky coupling would produce compound **6-8** from racemic tricyclic iodolactone (**6-9**) and racemic decalin motif **6-10** by a diastereoselective reaction. Tricyclic iodolactone **6-9** could arise from cyclization and iodolactonization of γ -aminobutyric acid (**6-11**) and maleic anhydride (**6-12**). Decalin aldehyde **6-10** could be obtained from commercially available *rac*-citronellal (**6-13**).



Scheme 6.1 Synthetic strategy of target CJ-16,264 analogues (6-1a).

6.2.2 Synthesis of racemic tricyclic iodolactone (6-9)

An obvious disconnection would entail a cyclization of compound **6-15** (Scheme 6.2) [61]. Therefore, maleimido ester **6-15**, which is readily available from γ -aminobutyric acid (**6-11**) and maleic anhydride (**6-12**), was subjected to soft enolization conditions, furnishing the bicyclic pyrrolizidine ester **6-16** in good yield as a single diastereomer [61]. Basic hydrolysis to acid **6-17** followed by iodolactonization then provided the target tricyclic iodolactone **6-9** in high yield as a racemic mixture (Scheme 6.2). Although racemic **6-9** is readily separable using chiral HPLC, we preferred to focus on a diastereoselective Reformatsky reaction to gain access to various diastereomers of natural product. Thus, we took iodolactone **6-9** in racemic form to perform the reaction in the next step without separation.

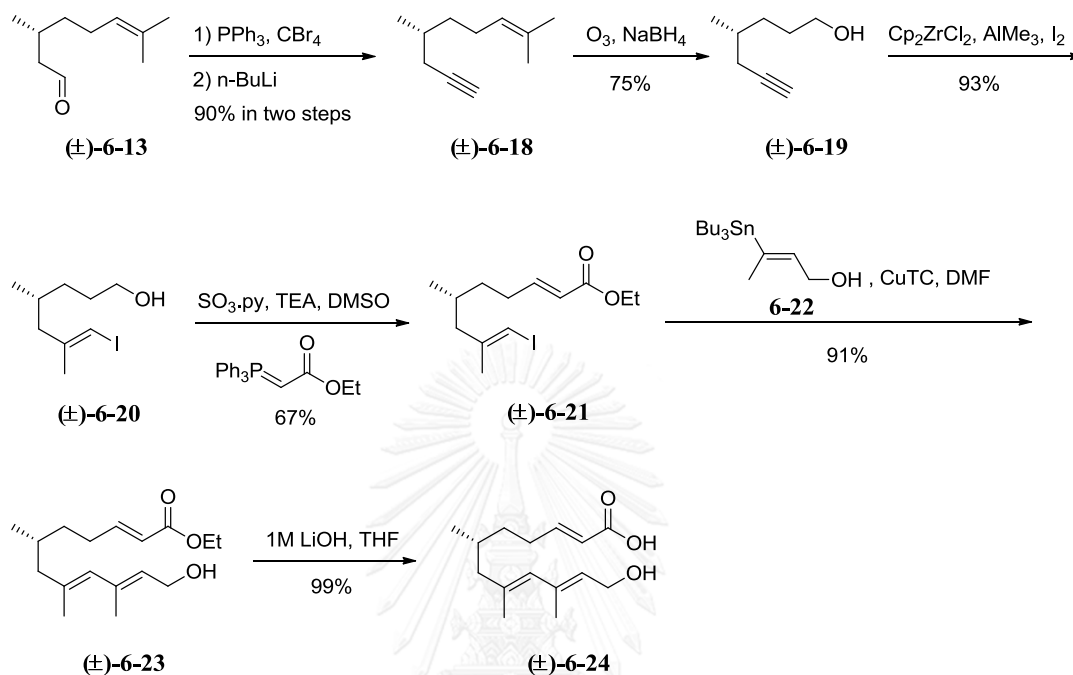


Scheme 6.2 Synthesis of racemic tricyclic iodolactone (6-9).

6.2.3 Synthesis of the key intermediate seco-acid (\pm)-6-24

The synthesis of the seco-acid (\pm)-6-24 was fairly straightforward and completed as described in Scheme 6.3. Commercially available *rac*-citronellal (6-13) was converted to the corresponding alkyne (\pm)-6-18 via the Corey-Fuchs reaction. Chemoselective ozonolysis of (\pm)-6-18, carefully monitored by TLC, followed by reductive work-up with NaBH_4 , provided the corresponding alcohol (\pm)-6-19. Next, carboalumination-iodination of the terminal alkyne (\pm)-6-19 using Cp_2ZrCl_2 as catalyst furnished iodide (\pm)-6-20 in excellent yield. It is known [68] that to undergo initial carboalumination, analogous alkyne with methyl group in the β -position, would be set at rt for 24 h, followed by iodination at lower temperature. A one-pot synthesis of (\pm)-6-21 was carried out via Parikh-Doering oxidation of (\pm)-6-20 with sulfur trioxide pyridine complex, TEA and DMSO, carefully monitored by TLC, followed by Horner-Wadsworth-Emmons (HWE) Wittig reaction with ethyl (triphenylphosphoranylidene)acetate, affording the desired product in good yield. Stille cross-coupling reaction of vinyl iodide (\pm)-6-21 with vinylstannane 6-22 mediated by copper (I) thiophene-2-carboxylate (CuTC) provided the target product

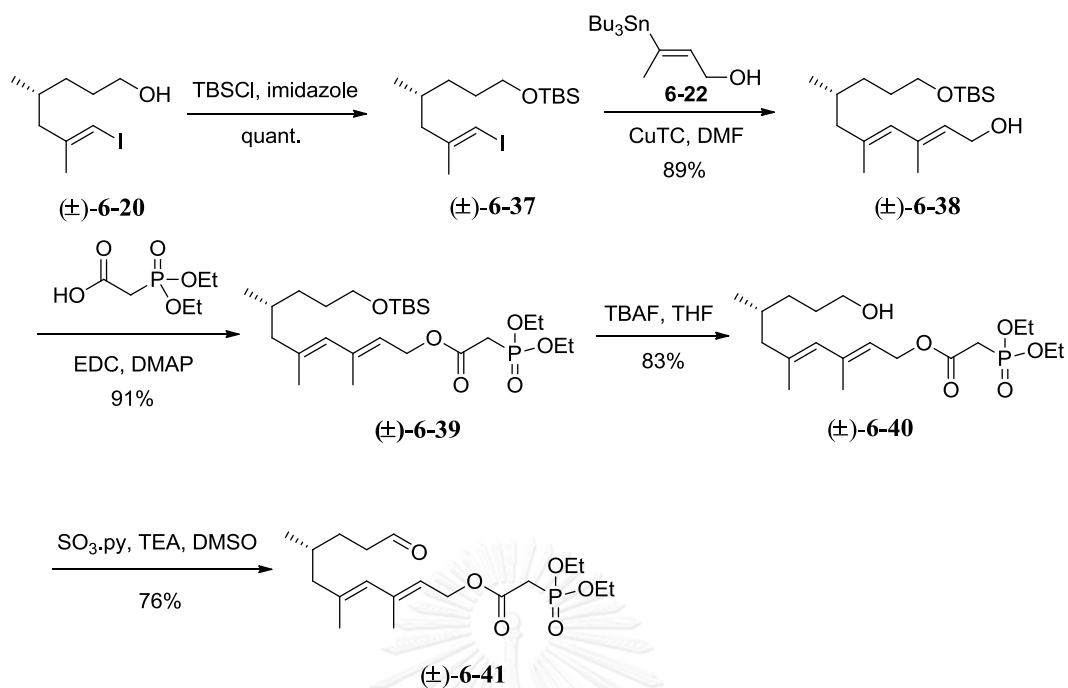
(\pm)-**6-23** in excellent yield. Ester (\pm)-**6-23** was further subjected to hydrolysis under basic condition to form the corresponding seco-acid (\pm)-**6-24** in excellent yield.



Scheme 6.3 Synthesis of seco-acid (\pm)-**6-24**.

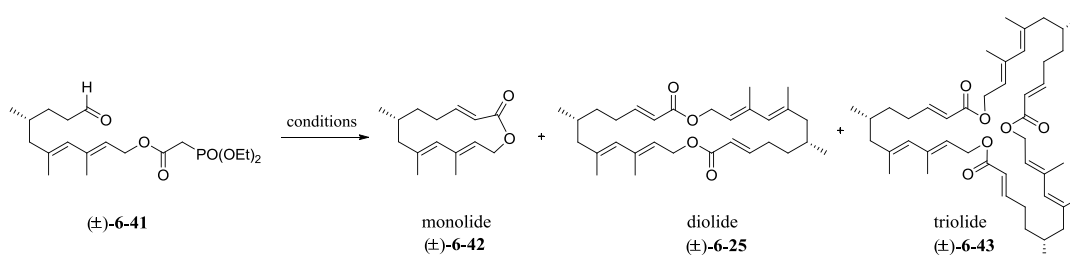
6.2.4 Macrocyclization optimization

To optimize the macrocyclization, we designed to obtain monolide (\pm)-**6-42** by intramolecular Horner-Wadsworth-Emmons (HWE) cyclization (Table 6.1) and macrolactonization approach (Table 6.2). For the HWE cyclization study, initially, the phosphonate aldehyde (\pm)-**6-41** was synthesized from alcohol (\pm)-**6-20** (Scheme 6.4). The primary hydroxyl group in alcohol (\pm)-**6-20** was protected as a silyl group to give (\pm)-**6-37** in quantitative yield. Stille cross-coupling reaction of (\pm)-**6-37** with vinylstannane **6-22** afforded the target product (\pm)-**6-38** in good yield. Ester (\pm)-**6-39** was prepared from diethylphosphonoacetic acid and alcohol (\pm)-**6-38** in the presence of EDC and DMAP to give the target ester in excellent yield. The TBS group of (\pm)-**6-39** was removed by TBAF, and following the Parikh-Doering oxidation, the target phosphonate aldehyde (\pm)-**6-41** was obtained in good yield.



Scheme 6.4 Preparation of phosphonate aldehyde $(\pm)\text{-6-41}$.

For our first endeavor to gain access to the monolide $(\pm)\text{-6-42}$, the intramolecular olefinations by HWE-reaction of $(\pm)\text{-6-41}$ was studied (Table 6.1). Subjecting $(\pm)\text{-6-41}$ to the standard Masamune-Roush protocols [69] (entries 1 and 2) did not result in the formation of monolide $(\pm)\text{-6-42}$, and mostly diolide $(\pm)\text{-6-25}$ were isolated. Unfortunately, the combination of zinc(II) trifluoromethanesulfonate, TMEDA, and triethylamine [70] (entry 3), in the hope that it would be converted to monolide $(\pm)\text{-6-42}$, was unsuccessful. More than 50% of $(\pm)\text{-6-41}$ was recovered along with diolide $(\pm)\text{-6-25}$ in low yield (19% yield).

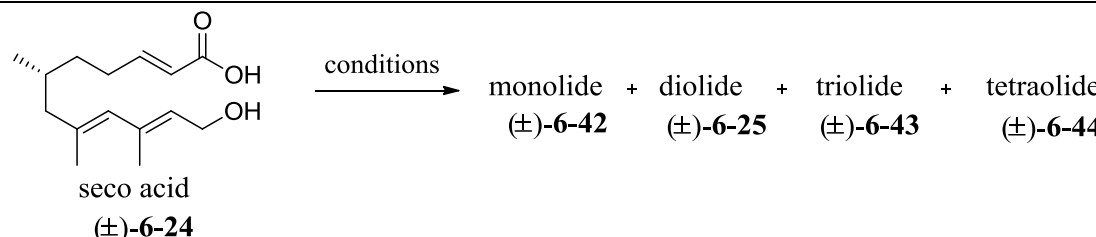
Table 6.1 Study of HWE cyclization of **(±)-6-41**

entry	conditions	%yield ^a		
		(±)-6-42	(±)-6-25	(±)-6-43
1	LiCl, DBU, MeCN, rt, 48 h	0	18	7
2	LiCl, DIPEA, MeCN, rt, 24 h	0	18	5
3	Zn(OTf) ₂ , TMEDA, Et ₃ N, THF, rt, 24 h	0	19	0

^a Isolated yield; TMEDA = tetramethylethylenediamine.

Next, we attempted the macrolactonization of seco acid **(±)-6-24**, as illustrated in Table 6.2. The macrolactonization of **(±)-6-24** under Shiina conditions (entry 1) provided trace amount of triolide **(±)-6-43** (8% yield) and tetraolide **(±)-6-44** (2% yield) and mostly resulted in diolide **(±)-6-25**, but the yield was low (20% yield). We next tried the macrolactonization under Yamamoto conditions. However, the reaction did not afford the desired monolide **(±)-6-42** and furnished diolide **(±)-6-25** in 18% yield (entry 2). Similarly, the macrolactonization under Mukaiyama conditions did not provide the desired monolide **(±)-6-42** (entry 3).

Table 6.2 Study of macrolactonization of seco acid (**(±)**-6-24

					
entry	conditions	%yield ^a			
		((±) -6-42	((±) -6-25	((±) -6-43	((±) -6-44
1	MNBA, DIPEA, DMAP, DCM, rt, 6 h	0	20	8	2
2	MNBA, Sc(OTf) ₃ , MeCN/THF (10/1), rt, 24 h	0	18	4	ND ^b
3	PyCl/I, lutidine, MeCN, rt, 24 h	0	7	ND	ND

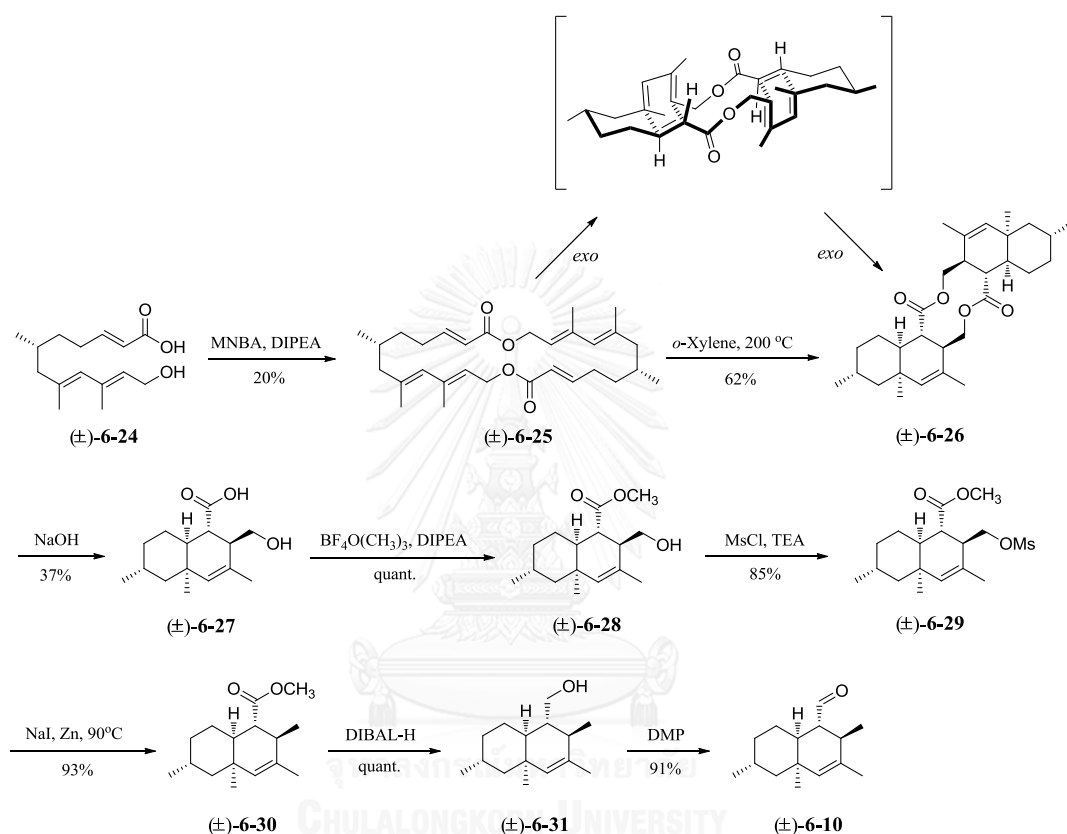
^a Isolated yield; ^b Not detected; MNBA = 2-methyl-6-nitrobenzoic anhydride.

From the attempted optimization for macrocyclization (Table 6.1 and Table 6.2), diolide (**(±)**-6-25) was obtained as a major component in low yields. We hypothesized that the nature of structures of starting materials (**(±)**-6-24 and (**(±)**-6-41) in the presence of the (*E, E*)-diene moiety may not be suitable for the intramolecular cyclization to construct 13-membered macrolactone of (**(±)**-6-42. In addition, these synthetic methods may promote the rate of intermolecular pathway, leading to the formation of the diolide in very low yields. Therefore, we selected the macrolactonization of seco-acid (**(±)**-6-24) under Shiina conditions (Table 6.2, entry 1) to construct the diolide (**(±)**-6-25) for the synthesis of decalin moiety (**(±)**-6-10).

6.2.5 Synthesis of decalin aldehyde (**(±)**-6-10

With the diolide (**(±)**-6-25) in hand, we further studied the intramolecular Diels-Alder (IMDA) cycloaddition as shown in Scheme 6.5. (**(±)**-6-25) underwent cycloaddition at 200 °C for 9 h to form decalin (**(±)**-6-26) in good yield and good diastereoselectivity (the minor diastereomer unassigned). This result indicated that the substrate control influenced the IMDA of (**(±)**-6-25) to favor the *exo* cycloaddition. Hydrolysis of diester (**(±)**-6-26) using NaOH provided the desired decalin (**(±)**-6-27) in

fair yield. Treatment of the carboxylic acid functionality of (\pm)-**6-27** with Meerwein's trimethyl oxonium salt and DIPEA under methylation conditions afforded methylester (\pm)-**6-28** in quantitative yield. Mesylation of alcohol (\pm)-**6-28** with methanesulfonyl chloride followed by substitution with sodium iodide-zinc dust at 90 °C provided the desired (\pm)-**6-30** in excellent yield.



Scheme 6.5 Synthesis of decalin aldehyde (\pm)-**6-10**.

The ester (\pm)-**6-30** showed NOESY correlation between H-8a and Me-C4a leading to the *cis*-fused decalin system (Figure 6.5). In addition, no NOESY correlation between H-1 and H-8a but showed correlation between H-2 and H-8a indicating that ester group on C1 and Me group on C2 was *trans* relative orientation. Next, the DIBAL-H reduction of methylester (\pm)-**6-30** gave alcohol (\pm)-**6-31** in excellent yield. The decalin aldehyde (\pm)-**6-10** was prepared via Dess-Martin periodinane oxidation of alcohol (\pm)-**6-31**.

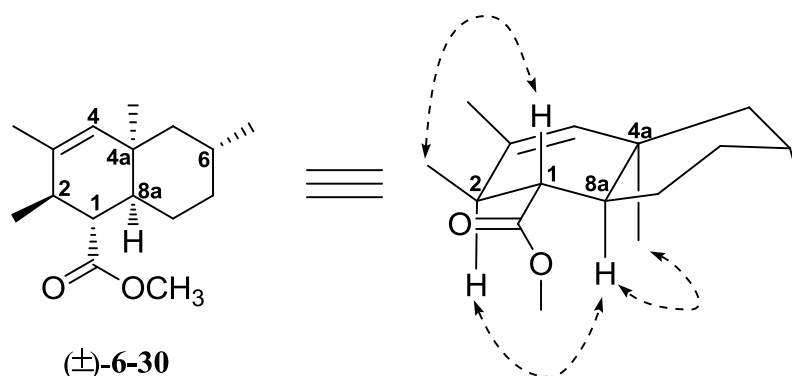
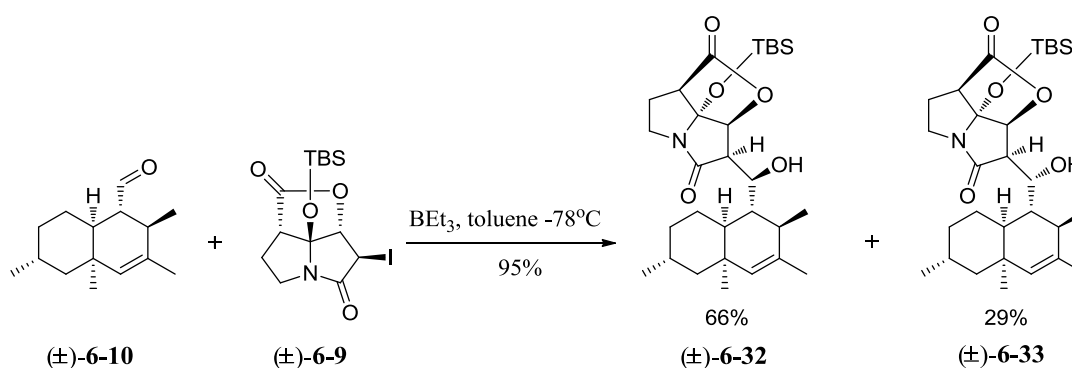


Figure 6.5 Selected NOESY correlations of **(±)-6-30**. For clarity, certain H atoms are omitted.

6.2.6 Studies toward completion of the synthesis of CJ-16,264 analogues

The synthesis of alcohols **(±)-6-32** and **(±)-6-33** would be achieved by direct coupling of iodolactone **(±)-6-9** and aldehyde **(±)-6-10** via Reformatsky reaction (Scheme 6.6). Treatment of **(±)-6-9** and **(±)-6-10** with triethylborane in toluene at -78°C led to a good stereoselective aldol coupling affording only two diastereomers (from 16 possible stereoisomers, Figure 6.6) **(±)-6-32** and **(±)-6-33** in an overall 95% yield in a 2:1 ratio. The relative stereochemistries of **(±)-6-32** and **(±)-6-33** were confirmed by X-ray crystallography of TASF deprotected **(±)-6-34** and **(±)-6-35** (Scheme 6.7 and 6.8).



Scheme 6.6 BEt_3 mediated Reformatsky-type coupling of **(±)-6-9** and **(±)-6-10**.

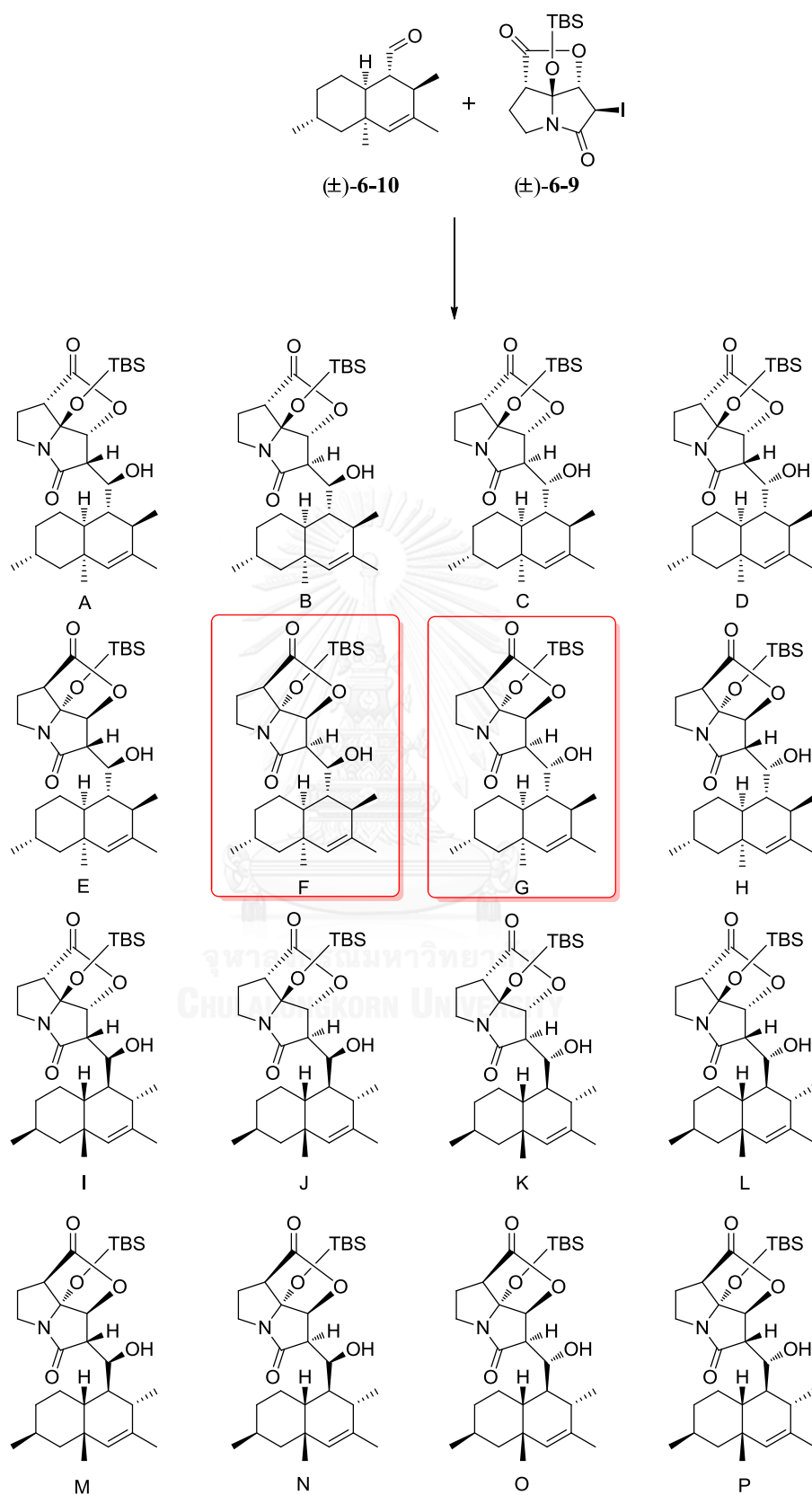
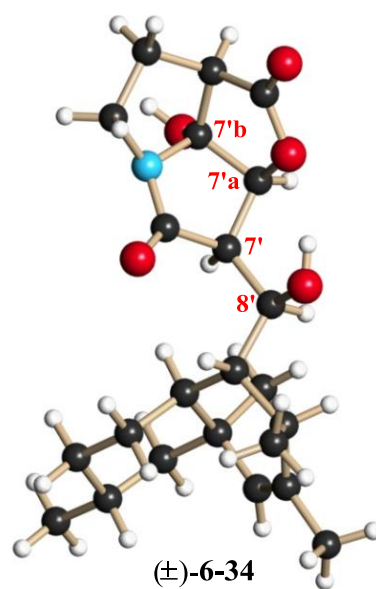
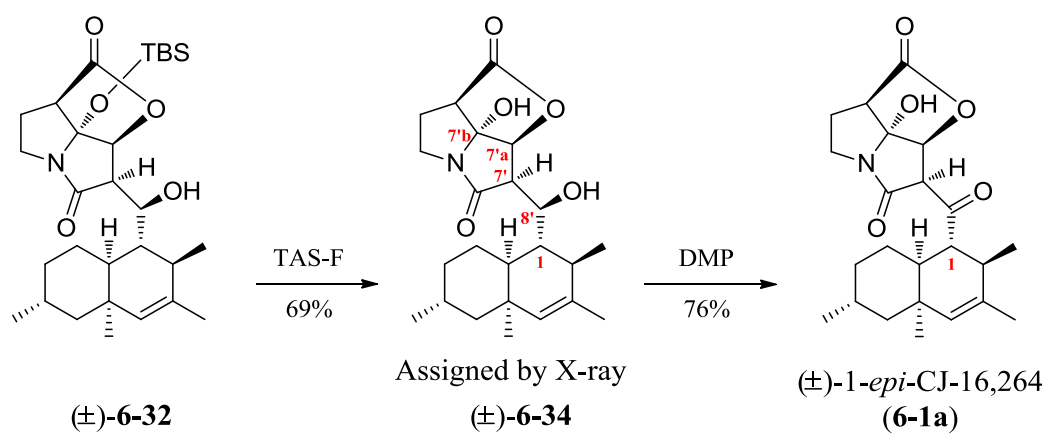
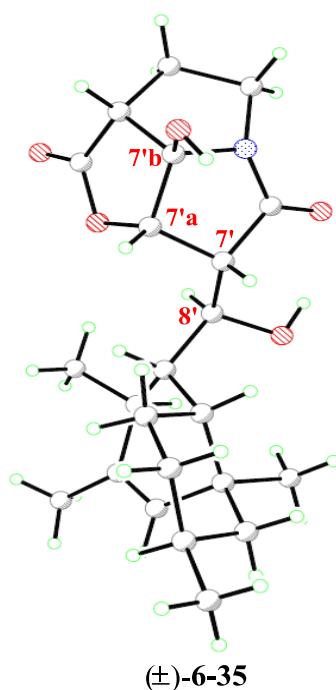
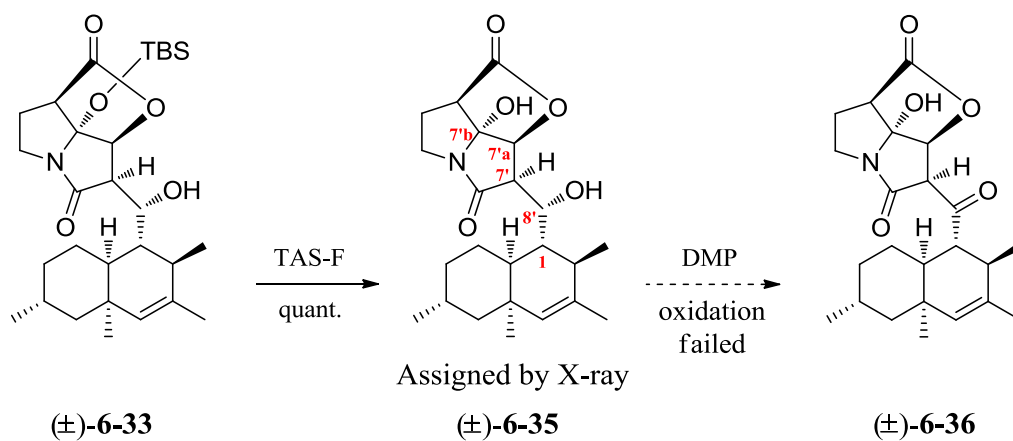


Figure 6.6 Possible structures of products from Reformatsky reaction.



Scheme 6.7 Completion for the synthesis of **6-1a**.



Scheme 6.8 Preparation of (\pm) -6-36 from (\pm) -6-33.

To complete the synthesis, the simple and effective strategies were used to access **6-1a** in only two steps from adduct (\pm) -6-32 (Scheme 6.7). TBS deprotection using tris(dimethylamino)sulfonium difluorotrimethylsilicate (TAS-F) followed by Dess-Martin periodinane oxidation provided the full CJ-16,264 skeleton in good yield.

Unfortunately, similar treatment of the minor coupling product (\pm) -6-33 with the same synthetic sequence in Scheme 6.7 led to decomposition upon DMP

oxidation (Scheme 6.8). Therefore, studies towards completing this synthesis are currently underway in our laboratory (Theodorakis group).

6.3 Conclusion

In summary, we have described an efficient approach to construct pyrrolizidinone, the core skeleton of antibiotic CJ-16,264. The key strategy involved an *exo*-selective IMDA reaction of macrolactone system and boron mediated Reformatsky-type coupling. The results of this synthetic route provided the first access to the highly methylated *cis*-decalin scaffold in CJ-16,264. Therefore, this synthetic work would be an alternative way for the development of new medicines.

6.4 Experimental section

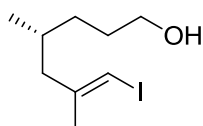
6.4.1 General experimental procedures

All reactions were carried out under an argon atmosphere with dry solvents under anhydrous conditions, unless otherwise noted. Dry tetrahydrofuran (THF), toluene, benzene, diethyl ether (Et₂O), *N,N*-dimethylformamide (DMF), and methylene chloride (CH₂Cl₂) were obtained by passing commercially available pre-dried, oxygen-free formulations through activated alumina columns. Yields refer to chromatographically and spectroscopically (¹H NMR) homogeneous materials, unless otherwise stated. Reagents were purchased at the highest commercial quality and used without further purification, unless otherwise stated. Reactions were monitored by thin-layer chromatography (TLC) carried out on 0.25 mm E. Merck silica gel plates (60F-254) using UV light as visualizing agent and an ethanolic solution of phosphomolybdic acid and cerium sulfate, and heat as developing agents. E. Merck silica gel (60, particle size 0.040 – 0.063 mm) was used for flash column chromatography. Preparative thin-layer chromatography (PTLC) separations were carried out on 0.25 or 0.50 mm E. Merck silica gel plates (60F-254). NMR spectra were recorded on Bruker DRX-400, DRX-500 or DRX-600 instruments and calibrated using residual undeuterated solvent (CDCl₃; δ_{H} = 7.26 ppm, δ_{C} = 77.0 ppm) as an internal reference. The following abbreviations were used to designate multiplicities: s = singlet, d = doublet, t = triplet, q = quartet, p = pentet, sext = sextet, m = multiplet,

br = broad. High-resolution mass spectra (HRMS) were recorded on an Agilent ESI-TOF (time of flight) mass spectrometer using MALDI (matrix-assisted laser desorption ionization) or ESI (electrospray ionization).

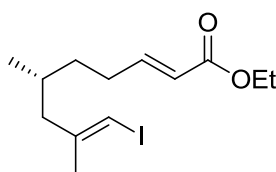
6.4.2 Total synthesis of CJ-16,264 analogues

Compound 6-20



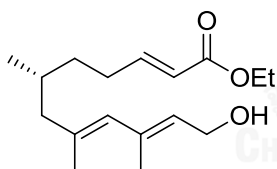
AlMe_3 (32 mL, 2.0 M in hexane, 63.4 mmol) was added under an atmosphere of Ar to a solution of Cp_2ZrCl_2 (4.6 g, 15.85 mmol) in dry 1,2-dichloroethane (70 mL) at 0°C and the mixture was allowed to warm to room temperature. 10 min later compound **6-19** (2 g, 15.85 mmol) was added as a solution in 10 mL of dry 1,2-dichloroethane and the reaction mixture was stirred for 24 h at room temperature. Then it was cooled to -78°C , I_2 (16 g, 63.4 mmol) was added as a solution in dry THF (75 mL) and the reaction was kept at -78°C for 30 min and further was warmed to 0°C for 1 h. The mixture was quenched by slowly adding H_2O , was extracted with EtOAc, was washed with brine, dried over anhydrous Na_2SO_4 , filtered and concentrated under reduced pressure. The crude product was purified by flash chromatography (10% ethyl acetate in hexane) to give compound **6-20** (3.9 g, 93%) as a yellow oil; ^1H NMR (400 MHz, CDCl_3) δ : 5.81 (s, 1H), 3.58 (t, 2H, $J = 6.4$ Hz), 2.81 (dd, 1H, $J = 13.2, 6.4$ Hz), 1.98 (dd, 1H, $J = 13.2, 8.4$ Hz), 1.77 (s, 3H), 1.65-1.48 (m, 3H), 1.31 (m, 1H), 1.12 (m, 1H), 0.81 (d, 3H, $J = 6.8$ Hz, H-8, $-\text{CH}_3$); ^{13}C NMR (100 MHz, CDCl_3) δ : 147.0, 75.5, 63.1, 47.5, 32.6, 30.9, 30.2, 23.8, 19.3.

Compound 6-21



To a solution of compound **6-20** (5 g, 18.65 mmol) in dichloromethane (70 mL) was added DMSO (23 mL) and TEA (10 mL, 74.60 mmol). After the reaction mixture was cooled to 0°C, SO₃.pyridine complex (6 g, 37.29 mmol) was added, and the mixture was stirred at room temperature until completion by TLC analysis (ca. 3 h). The reaction mixture was added ethyl(triphenylphosphoranylidene)acetate (13 g, 37.29 mmol) and was stirred at rt for 1 h. The mixture was quenched with sat. NH₄Cl, extracted with DCM, washed with brine, dried over anhydrous Na₂SO₄, filtered and concentrated under reduced pressure. The crude product was purified by flash chromatography (10% ethyl acetate in hexane) to give compound **6-21** (4 g, 67%) as a pale yellow oil; ¹H NMR (400 MHz, CDCl₃) δ: 6.94 (m, 1H), 5.85 (s, 1H), 5.81 (d, 1H, *J* = 15.6 Hz), 4.18 (q, 2H, *J* = 7.2 Hz), 2.22-2.15 (m, 3H), 2.01 (dd, 1H, *J* = 13.6, 8.4 Hz), 1.79 (s, 3H, H-13), 1.66-1.59 (m, 2H), 1.44 (m, 1H), 1.27 (t, 3H, *J* = 7.2 Hz), 0.84 (d, 3H, *J* = 6.8 Hz, H-12); ¹³C NMR (100 MHz, CDCl₃) δ: 166.8, 149.1, 146.8, 121.5, 75.7, 60.3, 47.5, 34.9, 30.6, 29.8, 23.8, 19.2, 14.4; HRMS *m/z* 359.0479 [M+Na]⁺ (calcd for C₁₃H₄₄IO₂Na, 359.0478).

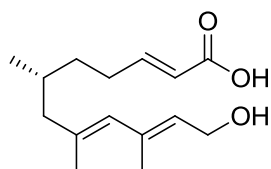
Compound 6-23



To a solution of compound **6-21** (1 g, 2.97 mmol) and stannane (3.2 g, 8.92 mmol) in 1.4 mL anhydrous DMF at 0 °C was added CuTC (3.4 g, 17.85 mmol) under Ar. The reaction mixture was stirred at 0 °C for 3 h. The mixture was quenched with 20% NH₄OH, extracted with Et₂O, washed with brine, dried over anhydrous Na₂SO₄, filtered and concentrated under reduced pressure. The crude product was purified by flash chromatography (10% ethyl acetate in hexane) to give compound **6-23** (757 mg, 91%) as a pale yellow oil; ¹H NMR (400 MHz, CDCl₃) δ: 6.91 (m, 1H), 5.77 (d, 1H, *J* = 16.0 Hz), 5.56 (s, 1H), 5.42 (t, 1H, *J* = 6.8 Hz), 4.18 (d, 2H, *J* = 6.8 Hz), 4.13 (q, 2H, *J* = 7.2 Hz), 2.25-2.10 (m, 3H), 1.99 (dd, 1H, *J* = 13.2, 6.4 Hz), 1.78 (dd, 1H, *J* = 13.2, 8.0 Hz), 1.71 (s, 3H), 1.69 (s, 3H), 1.61 (m, 1H), 1.44 (m, 1H), 1.23 (t, 3H, *J* = 7.2 Hz), 0.80 (d, 3H, *J* = 6.8 Hz); ¹³C NMR (100 MHz, CDCl₃) δ : 166.8, 149.6, 135.9, 135.8, 129.7, 127.4,

121.2, 60.2, 59.4, 48.5, 34.9, 30.5, 29.8, 19.3, 17.8, 17.3, 14.3; HRMS m/z 303.1932 $[M+Na]^+$ (calcd for $C_{17}H_{28}O_3Na$, 303.1931).

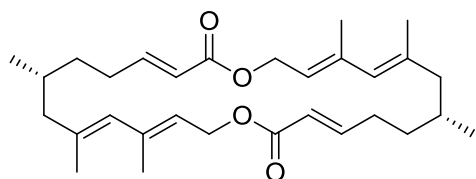
Compound 6-24



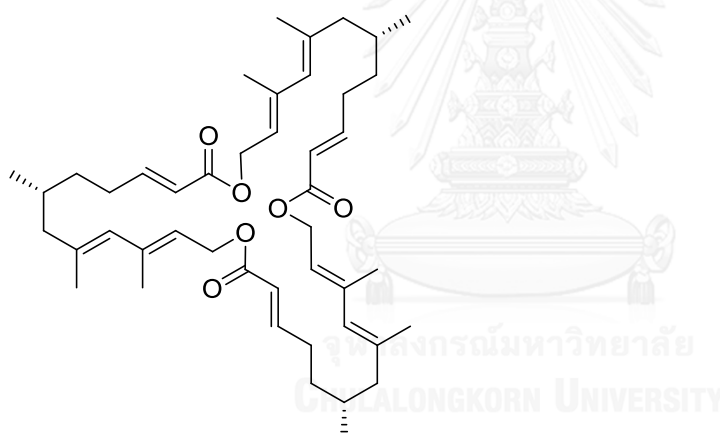
To a solution of compound **6-23** (2 g, 7.13 mmol) in 14 mL THF was added 14 mL of 1 M LiOH. The reaction mixture was stirred at 60 °C for 24 h. The mixture was acidified with 10% HCl, extracted with EtOAc, washed with brine, dried over anhydrous Na_2SO_4 , filtered and concentrated under reduced pressure. The crude product was purified by flash chromatography (50% ethyl acetate in hexane) to give compound **6-24** (1.4 g, 76%) as a colorless oil; 1H NMR (400 MHz, $CDCl_3$) δ : 7.04 (m, 1H), 5.80 (d, 1H, $J = 16.0$ Hz), 5.58 (s, 1H), 5.44 (t, 1H, $J = 6.8$ Hz), 4.22 (d, 2H, $J = 6.8$ Hz), 2.30-2.15 (m, 2H), 2.01 (dd, 1H, $J = 13.2, 6.0$ Hz), 1.80 (dd, 1H, $J = 13.2, 8.0$ Hz), 1.73 (s, 3H), 1.71 (s, 3H), 1.63 (m, 1H), 1.46 (m, 1H), 1.24 (m, 1H), 0.83 (d, 3H, $J = 6.4$ Hz); ^{13}C NMR (100 MHz, $CDCl_3$) δ : 171.6, 152.2, 136.3, 135.9, 129.8, 127.0, 120.8, 59.4, 48.6, 34.8, 30.5, 30.0, 19.3, 17.9, 17.4; HRMS m/z 275.1619 $[M+Na]^+$ (calcd for $C_{15}H_{24}O_3Na$, 275.1618).

Diolide and triolide

To a solution of compound **6-24** (250 mg, 0.99 mmol) in DCM (100 mL) was added DIPEA (0.3 mL, 1.98 mmol), MNBA (512 mg, 1.49 mmol) and DMAP (catalytic amount) under Ar. The reaction mixture was stirred at rt for 6 h. The mixture was quenched with H_2O , extracted with DCM, washed with brine, dried over anhydrous Na_2SO_4 , filtered and concentrated under reduced pressure. The crude product was purified by flash chromatography (20% ether in hexane) to give 73 mg (20%) of diolide **6-25**, 20 mg (8%) of triolide (**6-43**).

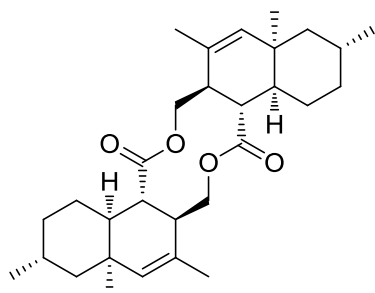
For (*E*)-diolide 6-25

^1H NMR (400 MHz, CDCl_3) δ : 6.94 (m, 1H), 5.81 (d, 1H, $J = 15.6$ Hz), 5.59 (s, 1H), 5.38 (t, 1H, $J = 6.8$ Hz), 4.76-4.67 (m, 2H), 2.28 (m, 1H), 2.12-1.99 (m, 2H), 1.85 (m, 1H), 1.78 (s, 3H), 1.68 (s, 3H), 1.64 (m, 1H), 1.49 (m, 1H), 1.08 (m, 1H), 0.89 (d, 3H, $J = 6.4$ Hz); ^{13}C NMR (100 MHz, CDCl_3) δ : 166.6, 149.4, 138.4, 136.4, 129.6, 122.3, 121.4, 61.1, 48.9, 33.1, 30.1, 29.7, 20.2, 17.9, 17.5; HRMS m/z 491.3131 $[\text{M}+\text{Na}]^+$ (calcd for $\text{C}_{30}\text{H}_{44}\text{O}_4\text{Na}$, 491.3132).

For (*E*)-triolide (6-43):

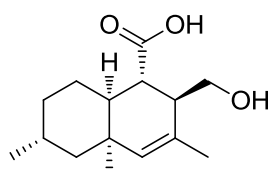
^1H NMR (500 MHz, CDCl_3) δ : 6.95 (m, 1H), 5.83 (d, 1H, $J = 15.5$ Hz), 5.61 (s, 1H), 5.41 (t, 1H, $J = 7.0$ Hz), 4.72 (d, 2H, $J = 7.0$ Hz), 2.28 (m, 1H), 2.16 (m, 1H), 1.94-1.88 (m, 3H), 1.79 (s, 3H, $-\text{CH}_3$), 1.72 (s, 3H, $-\text{CH}_3$), 1.66 (m, 1H), 1.50 (m, 1H), 0.86 (d, 3H, $J = 6.5$ Hz, $-\text{CH}_3$). ^{13}C NMR (125 MHz, CDCl_3) δ : 166.8, 149.7, 138.5, 136.6, 129.6, 122.3, 121.4, 61.3, 48.8, 34.3, 30.3, 29.9, 19.8, 18.1, 17.7; HRMS m/z 725.4753 $[\text{M}+\text{Na}]^+$ (calcd for $\text{C}_{45}\text{H}_{66}\text{O}_6\text{Na}$, 725.4752).

Compound 6-26



A solution of diolide **6-25** (92 mg, 0.20 mmol) in 7 mL of *o*-xylene was degassed for 30 min. The reaction mixture was stirred at 200°C for 9 h. The mixture was concentrated under reduced pressure and purified by flash chromatography (10% ether in hexane) to give IMDA adduct **6-26** (58 mg, 62%) as a white solid; ^1H NMR (400 MHz, CDCl_3) δ : 5.23 (s, 2H), 4.72 (t, 1H, $J = 11.2$ Hz), 4.58 (dd, 1H, $J = 10.4$, 4.4 Hz), 4.10-4.03 (m, 2H), 3.05 (br s, 1H), 2.88 (t, 1H, $J = 10.4$ Hz), 2.55 (t, 2H, $J = 11.2$ Hz), 1.82-1.70 (m, 10H), 1.66 (s, 3H), 1.65 (s, 3H), 1.55-1.49 (m, 2H), 1.18-1.14 (m, 4H), 1.11 (s, 3H), 1.06 (s, 3H), 1.02 (d, 3H, $J = 7.6$ Hz), 1.00 (d, 3H, $J = 7.2$ Hz); ^{13}C NMR (100 MHz, CDCl_3) δ : 176.7, 176.1, 137.7, 136.7, 126.6, 125.8, 66.9, 65.9, 47.6, 47.0, 43.4, 42.0, 41.1, 41.0, 40.8, 40.6, 35.0, 34.6, 29.2, 29.0, 27.1, 26.8, 25.9, 21.8, 21.6, 21.2, 21.0, 20.4; HRMS m/z 491.3134 $[\text{M}+\text{Na}]^+$ (calcd for $\text{C}_{30}\text{H}_{44}\text{O}_4\text{Na}$, 491.3132).

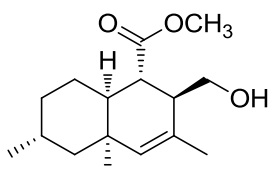
Compound 6-27



To a solution of compound **6-26** (63 mg, 0.13 mmol) in 3.4 mL THF was added NaOH (470 mg, 11.8 mmol), 2.2 mL MeOH, and 1.1 mL H_2O . The reaction mixture was stirred at 100 °C for 3 h. The mixture was acidified with 10% HCl, extracted with EtOAc, washed with brine, dried over anhydrous Na_2SO_4 , filtered and concentrated under reduced pressure. The crude product was purified by flash chromatography (50% ethyl acetate in hexane) to give compound **6-27** (25 mg, 37%) as a white solid; ^1H NMR (400 MHz, CDCl_3) δ : 5.23 (s, 1H), 3.90 (dd, 1H, $J = 10.8$, 4.0

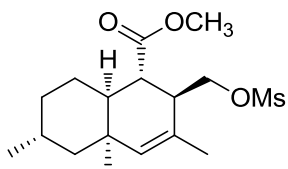
Hz), 3.61 (t, 1H, $J = 9.2$ Hz), 2.86 (br s, 1H), 2.72 (t, 1H, $J = 3.6$ Hz), 2.11 (d, 1H, $J = 10.8$ Hz), 1.74 (s, 3H), 1.62 (m, 1H), 1.54 (m, 1H), 1.46-1.39 (m, 3H), 0.99-0.90 (m, 2H), 0.90 (s, 3H), 0.86 (d, 3H, $J = 6.4$ Hz); ^{13}C NMR (100 MHz, CDCl_3) δ : 182.1, 134.1, 129.3, 64.6, 48.4, 46.0, 41.9, 40.3, 36.2, 33.9, 29.9, 29.4, 28.8, 22.4, 21.9; HRMS m/z 251.1654 $[\text{M}-\text{H}]^-$ (calcd for $\text{C}_{15}\text{H}_{23}\text{O}_3$, 251.1653).

Compound 6-28



To a solution of compound **6-27** (34 mg, 0.14 mmol) in DCM (1.5 mL) was added Meerweins salt (22 mg, 0.15 mmol) and DIPEA (0.05 mL, 1.5 mmol). The reaction mixture was stirred at rt for 5 min. The mixture was concentrated under reduced pressure and purified by flash chromatography (20% EtOAc in hexane) to give **6-28** (40 mg, quant.) as a colorless oil; ^1H NMR (400 MHz, CDCl_3) δ : 5.21 (s, 1H), 3.83 (dd, 1H, $J = 10.8, 4.0$ Hz), 3.70 (s, 3H), 3.61 (dd, 1H, $J = 10.8, 7.6$ Hz), 2.90 (br s, 1H), 2.70 (t, 1H, $J = 4.0$ Hz), 2.04 (m, 1H), 1.74 (s, 3H), 1.64 (m, 1H), 1.56-1.40 (m, 4H), 0.99-0.92 (m, 2H), 0.86 (d, 3H, $J = 6.8$ Hz), 0.85 (s, 3H); ^{13}C NMR (100 MHz, CDCl_3) δ : 176.4, 132.9, 128.3, 63.4, 50.9, 46.9, 44.8, 40.9, 39.7, 34.9, 32.3, 28.7, 28.1, 27.5, 21.2, 20.7; HRMS m/z 289.1776 $[\text{M}+\text{Na}]^+$ (calcd for $\text{C}_{16}\text{H}_{26}\text{O}_3\text{Na}$, 289.1774).

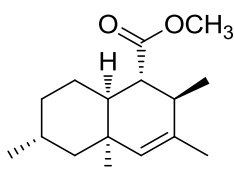
Compound 6-29



To a solution of **6-28** (75 mg, 0.28 mmol) in 3 mL DCM at 0 °C was added TEA (0.1 mL, 0.84 mmol) and MsCl (0.05 mL, 0.56 mmol) under Ar. The reaction mixture was stirred at 0 °C for 3 h. The mixture was quenched with sat. NH_4Cl , extracted with DCM, washed with brine, dried over anhydrous Na_2SO_4 , filtered and concentrated under reduced pressure. The crude product was purified by flash chromatography (20% ethyl acetate in hexane) to give **6-29** (82 mg, 85%) as a colorless oil; ^1H NMR

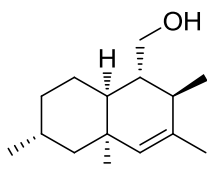
(400 MHz, CDCl₃) δ : 5.26 (s, 1H), 4.34-4.25 (m, 2H), 3.71 (s, 3H), 3.18 (br s, 1H), 3.01 (s, 3H), 2.55 (br s, 1H), 2.08 (br d, 1H, $J = 11.2$ Hz), 1.77 (s, 3H), 1.62 (br d, 1H, $J = 11.6$ Hz), 1.53-1.36 (m, 4H), 0.96-0.91 (m, 2H), 0.84 (d, 3H, $J = 6.4$ Hz), 0.81 (s, 3H); ¹³C NMR (100 MHz, CDCl₃) δ : 176.4, 134.7, 127.9, 71.1, 52.3, 48.8, 46.3, 42.1, 37.6, 37.3, 36.2, 34.2, 30.2, 29.1, 28.9, 22.4, 22.6; HRMS m/z 367.1552 [M+Na]⁺ (calcd for C₁₇H₂₈O₅Na, 367.1550).

Compound 6-30



To a solution of **6-29** (124 mg, 0.36 mmol) in 3.6 mL DME was added NaI (540 mg, 3.60 mmol) and activated Zn dust (470 mg, 7.20 mmol). The reaction mixture was stirred at 90 °C for 24 h. The mixture was concentrated under reduced pressure and purified by flash chromatography (hexane) to give **6-30** (84 mg, 93%) as a colorless oil; ¹H NMR (400 MHz, CDCl₃) δ : 5.07 (s, 1H), 3.68 (s, 3H), 2.75 (m, 1H), 2.27 (t, 1H, $J = 4.8$ Hz), 1.97 (m, 1H), 1.69 (s, 3H), 1.66-1.35 (m, 5H), 1.07 (d, 3H, $J = 7.2$ Hz), 0.99-0.94 (m, 2H), 0.88 (d, 3H, $J = 6.8$ Hz), 0.86 (s, 3H); ¹³C NMR (100 MHz, CDCl₃) δ : 177.4, 133.1, 131.4, 51.8, 51.5, 47.6, 42.6, 36.0, 32.8, 29.6, 28.7, 28.5, 22.3, 21.9, 20.5; HRMS m/z 251.2006 [M+H]⁺ (calcd for C₁₆H₂₇O₂, 251.2006).

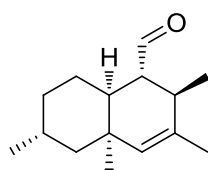
Compound 6-31



To a solution of **6-30** (86 mg, 0.34 mmol) in 1 mL DCM at 0 °C was added DIBAL-H (1.4 mL, 1.37 mmol). The reaction mixture was stirred at 0 °C for 5 min. The mixture was quenched with 20% NaOH, extracted with DCM, washed with brine, dried over anhydrous Na₂SO₄, filtered and concentrated under reduced pressure. The crude product was purified by flash chromatography (20% ethyl acetate in hexane) to give **6-31** (66 mg, 87%) as a colorless oil; ¹H NMR (400 MHz, CDCl₃) δ : 5.11 (s, 1H),

3.71-3.60 (m, 2H), 1.82 (m, 1H), 1.72 (m, 1H), 1.68 (s, 3H), 1.54 (m, 1H), 1.44-1.34 (m, 6H), 1.13 (d, 3H, $J = 7.2$ Hz), 0.90 (s, 3H), 0.87 (m, 1H), 0.82 (d, 3H, $J = 6.8$ Hz); ^{13}C NMR (100 MHz, CDCl_3) δ : 134.3, 131.1, 68.8, 51.7, 50.4, 41.9, 36.3, 35.1, 34.2, 32.9, 31.1, 28.9, 22.6, 22.1, 21.7; HRMS m/z 205.1950 $[\text{M}-\text{H}_2\text{O}+\text{H}]^+$ (calcd for $\text{C}_{15}\text{H}_{25}$, 205.1951).

Compound 6-10

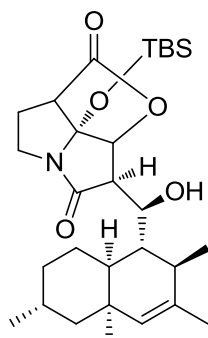


To a solution of **6-31** (9.90 mg, 0.04 mmol) in 1.2 mL DCM was added Dess-Martin periodinane (DMP) (38 mg, 0.08 mmol). The reaction mixture was stirred at rt for 30 min. The mixture was quenched with sat. sodium thiosulfate and sat. sodium bicarbonate (1:1), extracted with DCM, washed with brine, dried over anhydrous Na_2SO_4 , filtered and concentrated under reduced pressure. The crude product was purified by flash chromatography (5% ethyl acetate in hexane) to give **6-10** (8.90 mg, 91%) as a colorless oil; ^1H NMR (400 MHz, CDCl_3) δ : 9.75 (s, 1H), 5.04 (s, 1H), 2.81 (m, 1H), 2.00-1.97 (m, 2H), 1.71 (s, 3H), 1.66-1.38 (m, 5H), 1.13 (d, 3H, $J = 7.6$ Hz), 0.94-0.88 (m, 2H), 0.85 (d, 3H, $J = 6.4$ Hz), 0.72 (s, 3H); ^{13}C NMR (100 MHz, CDCl_3) δ : 205.1, 133.7, 130.1, 60.8, 49.6, 41.6, 36.4, 35.3, 31.8, 31.3, 29.2, 28.7, 22.6, 22.1, 21.5; HRMS m/z 221.1907 $[\text{M}+\text{H}]^+$ (calcd for $\text{C}_{15}\text{H}_{25}\text{O}$, 221.1905).

Compounds 6-32 and 6-33

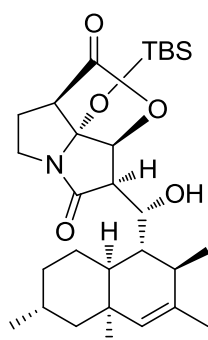
A solution of **6-10** (5.4 mg, 0.03 mmol) and iodo-lactam (29 mg, 0.07 mmol) in toluene (0.2 mL) at -78 °C was treated with BEt_3 (1 M in hexane, 0.1 mL, 0.07 mmol). The reaction mixture was stirred at -78 °C for 3 h. The mixture was quenched with H_2O , extracted with EtOAc, washed with brine, dried over anhydrous Na_2SO_4 , filtered and concentrated under reduced pressure. The crude product was purified by flash chromatography (10% ethyl acetate in hexane) to give 8.5 mg (66%, colorless oil) of **6-32** and 3.7 mg (29%, white powder) of **6-33**.

For 6-32



^1H NMR (500 MHz, C_6D_6) δ : 5.20 (s, 1H), 4.81 (br d, 1H, $J = 0.9$ Hz), 4.41 (d, 1H, $J = 3.8$ Hz), 4.38 (dt, 1H, $J = 8.5, 3.0$ Hz), 3.40 (m, 1H), 3.21 (dd, 1H, $J = 8.7, 3.8$ Hz), 2.81 (br d, 1H, $J = 7.5$ Hz), 2.64 (m, 1H), 2.35 (d, 1H, $J = 8.3$ Hz), 2.03 (m, 1H), 1.78 (s, 3H), 1.71-1.49 (m, 9H), 1.32 (s, 3H), 1.24 (d, 3H, $J = 7.5$ Hz), 0.96 (m, 1H), 0.90 (d, 3H, $J = 7.0$ Hz), 0.79 (br s, 9H), -0.12 (s, 3H), -0.22 (s, 3H); ^{13}C NMR (125 MHz, C_6D_6) δ : 177.1, 173.7, 134.6, 131.5, 100.4, 82.6, 73.0, 51.6, 51.3, 50.9, 49.2, 45.9, 42.5, 36.3, 35.4, 33.7, 30.7, 29.9, 29.4, 28.7, 25.4, 23.2, 22.8, 22.7, 17.8, -3.6, -4.0; HRMS m/z 540.3122 $[\text{M}+\text{Na}]^+$ (calcd for $\text{C}_{29}\text{H}_{47}\text{NO}_5\text{SiNa}$, 540.3121).

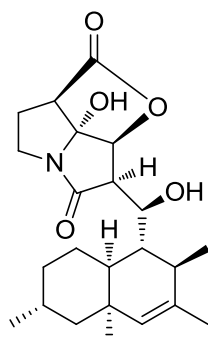
For 6-33



^1H NMR (500 MHz, C_6D_6) δ : 5.40 (s, 1H), 4.87 (s, 1H), 4.40 (d, 1H, $J = 10.0$ Hz), 4.29 (d, 1H, $J = 3.5$ Hz), 3.42 (dt, 1H, $J = 10.5, 7.5$ Hz), 3.26 (dd, 1H, $J = 10.0, 3.5$ Hz), 2.65 (m, 1H), 2.57 (br t, 1H, $J = 7.0$ Hz), 2.33 (d, 1H, $J = 8.5$ Hz), 2.05 (ddd, 1H, $J = 14.0, 9.0, 3.0$ Hz), 1.87 (dd, 1H, $J = 12.5, 4.0$ Hz), 1.77 (s, 3H), 1.73 (m, 1H), 1.67-1.61 (m, 2H), 1.53-1.45 (m, 2H), 1.36 (s, 3H), 1.32-1.28 (m, 2H), 1.15 (d, 3H, $J = 7.0$ Hz), 1.09 (m, 1H), 1.22 (m, 1H), 0.94 (d, 3H, $J = 6.5$ Hz), 0.79 (br s, 9H), -0.12 (s, 3H), -0.22 (s, 3H); ^{13}C NMR (125 MHz, C_6D_6) δ : 177.8, 173.7, 136.3, 132.6, 100.4, 82.1, 68.9, 53.3, 51.4, 49.7, 49.1,

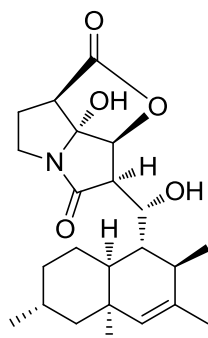
42.2, 40.5, 37.2, 36.9, 36.0, 32.3, 30.3, 29.3, 28.6, 25.3, 22.9, 21.8, 19.3, 17.8, -3.7, -4.0; HRMS m/z 540.3119 $[M+Na]^+$ (calcd for $C_{29}H_{47}NO_5SiNa$, 540.3121).

Compound 6-34



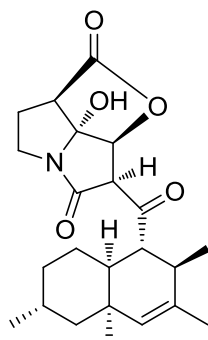
To a solution of **6-32** (10.3 mg, 0.02 mmol) in 0.8 mL THF at 0 °C was added TASF (11.0 mg, 0.04 mmol). The reaction mixture was stirred at 0 °C for 10 min. The mixture was quenched with H_2O , extracted with EtOAc, washed with brine, dried over anhydrous Na_2SO_4 , filtered and concentrated under reduced pressure. The crude product was purified by flash chromatography (50% ethyl acetate in hexane) to give **6-34** (5.5 mg, 69%) as a white powder; 1H NMR (500 MHz, acetone- d_6) δ : 6.29 (br s, 1H), 5.07 (d, 1H, $J = 3.5$ Hz), 5.05 (br s, 1H), 4.54 (d, 1H, $J = 2.5$ Hz), 4.04 (m, 1H), 3.76 (m, 1H), 3.36 (dd, 1H, $J = 8.0, 4.0$ Hz), 3.33-3.28 (m, 2H), 2.69 (m, 1H), 2.54 (m, 1H), 2.42 (m, 1H), 1.69 (s, 3H), 1.65 (br s, 1H), 1.58-1.53 (m, 2H), 1.48-1.40 (m, 3H), 1.35-1.28 (m, 3H), 1.18 (d, 3H, $J = 7.5$ Hz), 1.08 (s, 3H), 0.88 (m, 1H), 0.82 (d, 3H, $J = 6.5$ Hz); ^{13}C NMR (125 MHz, acetone- d_6) δ : 176.7, 175.9, 135.6, 131.1, 100.2, 83.0, 73.4, 52.1, 51.6, 51.5, 49.1, 46.0, 42.2, 36.7, 36.1, 33.9, 30.6, 29.9, 29.6, 29.4, 23.4, 22.9, 22.7; HRMS m/z 426.2254 $[M+Na]^+$ (calcd for $C_{23}H_{33}NO_5Na$, 426.2256).

Compound 6-35



To a solution of **6-33** (5.4 mg, 0.01 mmol) in 0.4 mL THF at 0 °C was added TASF (6.0 mg, 0.02 mmol). The reaction mixture was stirred at 0 °C for 30 min. The mixture was quenched with H₂O, extracted with EtOAc, washed with brine, dried over anhydrous Na₂SO₄, filtered and concentrated under reduced pressure. The crude product was purified by flash chromatography (50% ethyl acetate in hexane) to give **6-35** (4.2 mg, quant. yield) as a white powder; ¹H NMR (500 MHz, Acetone-d₆) δ: 6.34 (br s, 1H), 5.26 (s, 1H), 4.96 (d, 1H, *J* = 4.0 Hz), 4.66 (t, 1H, *J* = 1.5 Hz), 4.07 (m, 1H), 3.77 (ddd, 1H, *J* = 11.5, 9.5, 6.5 Hz), 3.39 (dd, 1H, *J* = 10.0, 4.0 Hz), 3.34-3.28 (m, 2H), 2.71 (m, 1H), 2.44 (dddd, 1H, *J* = 13.5, 9.5, 4.5, 2.0 Hz), 2.29 (m, 1H), 1.76 (dd, 1H, *J* = 12.5, 5.0 Hz), 1.72 (s, 3H), 1.56-1.52 (m, 2H), 1.39-1.32 (m, 4H), 1.15 (m, 1H), 1.09 (d, 3H, *J* = 7.0 Hz), 0.98 (s, 3H), 0.87 (m, 1H), 0.83 (d, 3H, *J* = 6.5 Hz); ¹³C NMR (125 MHz, Acetone-d₆) δ: 177.8, 175.9, 136.3, 132.7, 100.3, 82.7, 69.9, 66.2, 53.6, 53.5, 51.9, 50.1, 49.0, 42.1, 40.3, 37.1, 36.6, 36.4, 32.8, 30.6, 23.0, 21.9, 19.8; HRMS *m/z* 426.2257 [M+Na]⁺ (calcd for C₂₃H₃₃NO₅Na, 426.2256).

CJ-16,264 diastereomer (6-1a)



To a solution of **6-34** (2.9 mg, 0.007 mmol) in 0.5 mL DCM was added Dess-Martin periodinane (DMP) (4.0 mg, 0.009 mmol). The reaction mixture was stirred at rt for 30 min. The mixture was quenched with sat. sodium thiosulfate and sat. sodium bicarbonate (1:1), extracted with DCM, washed with brine, dried over anhydrous Na₂SO₄, filtered and concentrated under reduced pressure. The crude product was purified by flash chromatography (30% ethyl acetate in hexane) to give **6-1a** (2.2 mg, 76%) as a white solid; ¹H NMR (500 MHz, C₆D₆) δ: 5.03 (s, 1H), 4.99 (s, 1H), 4.09 (s, 1H), 3.98 (s, 1H), 3.46 (ddd, 1H, *J* = 12.5, 11.0, 5.0 Hz), 2.93 (br t, 1H, *J* = 3.5 Hz), 2.70 (ddd, 1H, *J* = 12.0, 10.5, 4.5 Hz), 2.65 (dd, 1H, *J* = 9.5, 1.5 Hz), 2.51 (br d, 1H, *J* = 11.0 Hz), 2.07 (br t, 1H, *J* = 3.5 Hz), 2.02 (dddd, 1H, *J* = 13.5, 9.5, 4.5, 2.0 Hz), 1.86 (m, 1H), 1.62 (s, 3H), 1.56 (br d, 1H, *J* = 13.0 Hz), 1.38-1.26 (m, 4H), 1.04-0.96 (m, 2H), 0.88 (d, 3H, *J* = 7.0 Hz), 0.88 (s, 3H), 0.83 (d, 3H, *J* = 6.5 Hz); ¹³C NMR (125 MHz, C₆D₆) δ: 209.9, 174.0, 167.7, 133.1, 131.4, 100.9, 81.1, 63.7, 63.6, 48.9, 47.5, 41.8, 38.9, 37.1, 34.3, 31.9, 29.7, 29.6, 29.1, 28.9, 22.4, 21.7, 21.1; HRMS *m/z* 424.2099 [M+Na]⁺ (calcd for C₂₃H₃₁NO₅Na, 424.2100).

CHAPTER VII

CONCLUSION

In this research, we reported the first synthesis of α -glucosidase inhibitors; conduritol and its analogues and *N*-substituted aminoquercitols from naturally available (+)-*proto*-quercitol. With the proper configuration of (+)-*proto*-quercitol, conduritol F and inositols were synthesized in short synthesis steps with an excellent overall yield. A key step involved dehydration of protected (+)-*proto*-quercitol (**2-1**) after addition of Tf_2O in pyridine, therefore taking a total of three steps to produce optically pure (+)-conduritol F in excellent yield. Furthermore, our method also provides rapid access to the corresponding dihydroxy analogues, (+)-*chiro*- and (+)-*epi*-inositols. A potent inhibition of conduritol F, selectively against type I α -glucosidase, over related compounds as well as antidiabetic drug acarbose suggested that its half-chair conformation is critical for exerting inhibition.

Moreover, (+)-*proto*-quercitol not only perfectly set up the potent type I α -glucosidase inhibitor, conduritol F, but also provided an aminoquercitol framework in high enantiomeric purity without any congeners. This methodology allowed us to further investigate and discover new α -glucosidase inhibitors. Thus, we next synthesized a series of *N*-substituted aminocyclitols. *N*-acyl and *N*-alkyl aminoquercitols having different chain lengths, were first prepared for the study of SAR. Evaluation of their α -glucosidase inhibition revealed that they selectively inhibited rat intestinal maltase (type II glucosidase) rather than yeast glucosidase (type I glucosidase). Of the compounds examined, *N*-alkyl aminoquercitols (**3-34** and **3-35**) having medium chains (C_6 and C_{10}) showed highly potent inhibition at sub-micromolar level (IC_{50} 0.24 and 0.41 μM), whereas antidiabetic drug acarbose was 3–6 times less active (IC_{50} 1.5 μM). Our findings also provided an insight into the importance of the hydrophobicity of medium alkyl chains ($\leq \text{C}_{10}$) in exerting inhibitory activity, possibly due to being a more preferred structure to fit into the binding site of enzyme.

New diastereomeric amine-linked diquercitols **4-5** and **4-7** were prepared to study the improvement of α -glucosidase inhibition, with direct comparison to other related *N*-linked dicyclitols. The synthesized *N*-linked diquercitols **4-5** and **4-7** showed comparable inhibition against α -glucosidases, while the inhibitory effect toward maltase and sucrase were more enhanced than the original aminoquercitol. Interestingly, they inhibited glucosidase function much more potent than other related *N*-linked dicyclitols, therefore suggesting some pivotal roles of quercitol residue in addition to the presence of nitrogen-linkage.

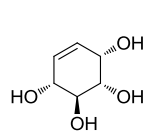
Aryl and hydroxyalkyl groups were required to complete the study of SAR analysis of *N*-substituted aminoquercitols. Among the *N*-aryl aminoquercitols for rat intestinal maltase, **5-20** was the most potent inhibitor. Of all synthesized compounds, **5-9** (IC_{50} 0.53 μ M) was the most effective inhibitor that not only displayed more prominent inhibition than the antidiabetic drug acarbose (IC_{50} 1.5 μ M) but also showed the similar inhibition to the most antidiabetic drug voglibose (IC_{50} 0.25 μ M).

The kinetic studies on the mechanism of α -glucosidase inhibition by particularly active compounds suggested competitive inhibition. More importantly, the most potent *N*-hydroxyalkyl **5-9** revealed stronger binding to maltase than acarbose while equipotent to voglibose. In addition, to further study on the molecular interactions and the binding mode of *N*-substituted aminoquercitols, the molar docking and 3D-QSAR were performed. A molecular docking result suggested that the hydrogen bond interaction from hydroxyl groups at aminoquercitol moiety and *N*-alkyl side chain with the key residues in the rat maltase active site, play an important role in molecular interactions. However, no π - π interactions were recognized between aromatic rings of *N*-aryl series and aromatic rings of key residues in the active site of rat intestinal maltase in this binding model. 3D-QSAR suggested that the less steric and hydrophilic groups at *N*-position of aminoquercitol could increase activity. All experimental results suggested that **5-9** could represent a new class of promising compounds that have the potential for diabetes therapy.

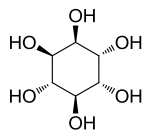
An efficient total synthesis of (\pm)-1-*epi*-CJ-16,264 from commercially available citronellal was also described. The ability to successfully synthesize the requisite methylated *cis*-decalin scaffold found in these molecules was demonstrated *via* an *exo*-selective IMDA reaction of a sterically constrained macrolactone system. The results of this synthetic strategy provided the first access to the highly methylated *cis*-decalin scaffold of CJ-16,264. Therefore, this synthetic work would be an alternative way for the development of new medicines.



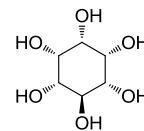
Structures of all synthesized compounds in this research



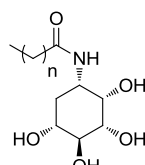
(+)-conduritol F (2-4)



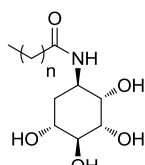
(+)-chiro-inositol (2-6a)



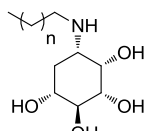
(+)-epi-inositol (2-6b)



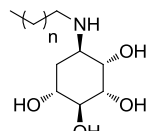
3-3 - 3-7



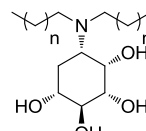
3-8 - 3-12



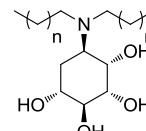
3-28 - 3-32



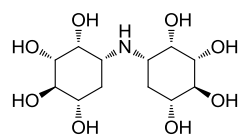
3-33 - 3-36



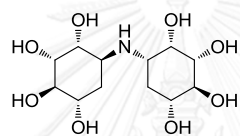
3-37 - 3-39



3-40 - 3-42

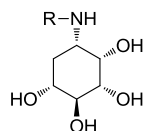


amine-linked diquercitol 4-5

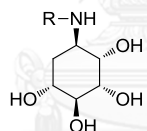


amine-linked diquercitol 4-7

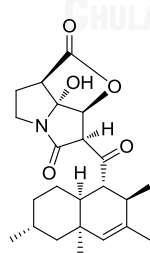
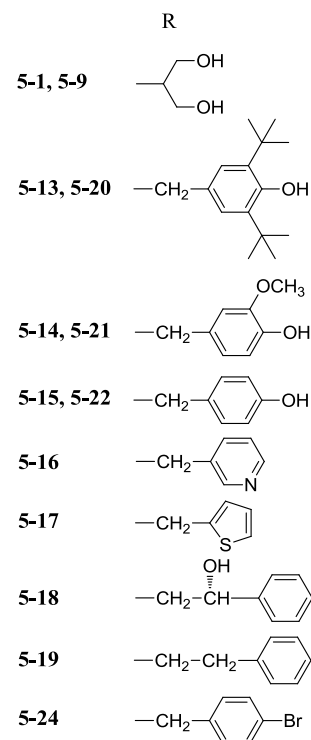
3-3, 3-8, 3-28, 3-37, 3-40 (n=0)
 3-4, 3-9, 3-29, 3-33, 3-38, 3-41 (n=2)
 3-5, 3-10, 3-30, 3-34, 3-39, 3-42 (n=4)
 3-6, 3-11, 3-31, 3-35 (n=8)
 3-7, 3-12, 3-32, 3-36 (n=10)



5-1, 5-13 - 5-19, 5-24



5-9, 5-20 - 5-22

(±)-1-epi-CJ-16,264
(6-1a)

REFERENCES

- [1] Skyler, J.S. Diabetes mellitus: Pathogenesis and treatment strategies. Journal of Medicinal Chemistry 47(17) (2004): 4113-4117.
- [2] Sharma, D.K., Pandey, J., Tamrakar, A.K., and Mukherjee, D. Synthesis of heteroaryl/aryl kojic acid conjugates as stimulators of glucose uptake by GLUT4 translocation. European Journal of Medicinal Chemistry 85(0) (2014): 727-736.
- [3] Chaudhuri, A. and Dandona, P. Effects of insulin and other antihyperglycaemic agents on lipid profiles of patients with diabetes. Diabetes, Obesity and Metabolism 13(10) (2011): 869-879.
- [4] Tuomi, T. Type 1 and type 2 diabetes: What do they have in common? Diabetes 54(SUPPL. 2) (2005): S40-S45.
- [5] Costanian, C., Bennett, K., Hwalla, N., Assaad, S., and Sibai, A.M. Prevalence, correlates and management of type 2 diabetes mellitus in Lebanon: Findings from a national population-based study. Diabetes Research and Clinical Practice 105(3): 408-415.
- [6] Wild, S., Roglic, G., Green, A., Sicree, R., and King, H. Global prevalence of diabetes: Estimates for the year 2000 and projections for 2030. Diabetes Care 27(5) (2004): 1047-1053.
- [7] Fava, S. Role of postprandial hyperglycemia in cardiovascular disease. Expert Review of Cardiovascular Therapy 6(6) (2008): 859-872.
- [8] Krentz, A.J. and Bailey, C.J. Oral antidiabetic agents: Current role in type 2 diabetes mellitus. Drugs 65(3) (2005): 385-411.
- [9] McCarter, J.D. and Stephen Withers, G. Mechanisms of enzymatic glycoside hydrolysis. Current Opinion in Structural Biology 4(6) (1994): 885-892.
- [10] Zechel, D.L. and Withers, S.G. Glycosidase mechanisms: Anatomy of a finely tuned catalyst. Accounts of Chemical Research 33(1) (1999): 11-18.

- [11] Borges de Melo, E., da Silveira Gomes, A., and Carvalho, I. α - and β -Glucosidase inhibitors: Chemical structure and biological activity. Tetrahedron 62(44) (2006): 10277-10302.
- [12] Trapero, A. and Llebaria, A. A prospect for pyrrolidine iminosugars as antidiabetic α -glucosidase inhibitors. Journal of Medicinal Chemistry 55(23) (2012): 10345-10346.
- [13] Moorthy, N.S.H.N., Ramos, M.J., and Fernandes, P.A. Studies on α -glucosidase inhibitors development: Magic molecules for the treatment of carbohydrate mediated diseases. Mini-Reviews in Medicinal Chemistry 12(8) (2012): 713-720.
- [14] Yoon, S.-H. and Robyt, J.F. Addition of maltodextrins to the nonreducing-end of acarbose by reaction of acarbose with cyclomaltohexaose and cyclomaltohextrin glucanyltransferase. Carbohydrate Research 337(6) (2002): 509-516.
- [15] Asano, N. Glycosidase inhibitors: Update and perspectives on practical use. Glycobiology 13(10) (2003): 93R-104R.
- [16] Gravier-Pelletier, C., Maton, W., Dintinger, T., Tellier, C., and Le Merrer, Y. Synthesis and glycosidase inhibitory activity of aminocyclitols with a C6- or a C7-ring. Tetrahedron 59(44) (2003): 8705-8720.
- [17] El Blidi, L., Ahbala, M., Bolte, J., and Lemaire, M. Straightforward chemoenzymatic synthesis of new aminocyclitols, analogues of valioline and their evaluation as glycosidase inhibitors. Tetrahedron: Asymmetry 17(18) (2006): 2684-2688.
- [18] Gupta, P., Pal, A.P.J., Reddy, Y.S., and Vankar, Y.D. Synthesis of aminocyclitols and trihydroxylated indolizidinone from a D-mannitol-derived common building block. European Journal of Organic Chemistry (6) (2011): 1166-1175.
- [19] Delgado, A. Recent advances in the chemistry of aminocyclitols. European Journal of Organic Chemistry (23) (2008): 3893-3906.
- [20] Duchek, J., Adams, D.R., and Hudlicky, T. Chemoenzymatic synthesis of inositols, conduritols, and cyclitol analogues. Chemical Reviews 111(7) (2011): 4223-4258.

- [21] Nair, J.J., Rárová, L., Strnad, M., Bastida, J., and van Staden, J. Apoptosis-inducing effects of distichamine and narciprimine, rare alkaloids of the plant family Amaryllidaceae. Bioorganic and Medicinal Chemistry Letters 22(19) (2012): 6195-6199.
- [22] Cantekin, S., Baran, A., Çalışkan, R., and Balci, M. Synthesis of bromo-condurotol-B and bromo-condurotol-C as glycosidase inhibitors. Carbohydrate Research 344(4) (2009): 426-431.
- [23] Liao, H., Shelor, C.P., Chen, Y., Sabaa-Srur, A.U.O., Smith, R.E., and Dasgupta, P.K. Anion composition of Açai extracts. Journal of Agricultural and Food Chemistry 61(25) (2013): 5928-5935.
- [24] Gültekin, M.S., Çelik, M., and Balci, M. Cyclitols: Condurotols and related compounds. Current Organic Chemistry 8(13) (2004): 1159-1186.
- [25] Worawalai, W., Rattanangkool, E., Vanitcha, A., Phuwapraisirisan, P., and Wacharasindhu, S. Concise synthesis of (+)-condurotol F and inositol analogues from naturally available (+)-*proto*-quercitol and their glucosidase inhibitory activity. Bioorganic and Medicinal Chemistry Letters 22(4) (2012): 1538-1540.
- [26] Kılbaş, B. and Balci, M. Recent advances in inositol chemistry: Synthesis and applications. Tetrahedron 67(13) (2011): 2355-2389.
- [27] Mahmud, T. The C7N aminocyclitol family of natural products. Natural Product Reports 20(1) (2003): 137-166.
- [28] Shing, T.K.M. and Wan, L.H. Enantiospecific syntheses of valioline and its (1*R*), (2*R*), (1*R*, 2*R*) diastereomers from (-)-quinic acid. Angewandte Chemie (International Edition in English) 34(15) (1995): 1643-1645.
- [29] Mondal, S., Prathap, A., and Sureshan, K.M. Vinylogy in orthoester hydrolysis: Total syntheses of cyclophellitol, valienamine, gabosine K, valienone, gabosine G, 1-*epi*-streptol, streptol, and uvamalol A. Journal of Organic Chemistry 78(15) (2013): 7690-7700.
- [30] Shih, T.L., Lin, Y.L., and Kuo, W.S. Highly stereoselective and stereospecific syntheses of a variety of quercitols from D-(-)-quinic acid. Tetrahedron 61(7) (2005): 1919-1924.

- [31] Ogawa, S., Asada, M., Ooki, Y., Mori, M., Itoh, M., and Korenaga, T. Design and synthesis of glycosidase inhibitor 5-amino-1,2,3,4-cyclohexanetetrol derivatives from (-)-*vibo*-quercitol. Bioorganic and Medicinal Chemistry 13(13) (2005): 4306-4314.
- [32] Gravier-Pelletier, C., Maton, W., and Le Merrer, Y. New azadisaccharide analogs as potential antidiabetics. Tetrahedron Letters 43(46) (2002): 8285-8288.
- [33] Łysek, R., et al. Search for α -glucosidase inhibitors: New *N*-substituted valienamine and conduramine F-1 derivatives. Bioorganic and Medicinal Chemistry 14(18) (2006): 6255-6282.
- [34] Bian, X., Fan, X., Ke, C., Luan, Y., Zhao, G., and Zeng, A. Synthesis and α -glucosidase inhibitory activity evaluation of *N*-substituted aminomethyl- β -D-glucopyranosides. Bioorganic and Medicinal Chemistry 21(17) (2013): 5442-5450.
- [35] Chen, X., Fan, Y., Zheng, Y., and Shen, Y. Properties and production of valienamine and its related analogues. Chemical Reviews 103(5) (2003): 1955-1978.
- [36] Wacharasindhu, S., Worawalai, W., Rungprom, W., and Phuwapraisirisan, P. (+)-*proto*-Quercitol, a natural versatile chiral building block for the synthesis of the α -glucosidase inhibitors, 5-amino-1,2,3,4-cyclohexanetetrols. Tetrahedron Letters 50(19) (2009): 2189-2192.
- [37] Cerè, V., Mantovani, G., Peri, F., Pollicino, S., and Ricci, A. A general procedure to enantiopure conduritols: Sulfur-mediated synthesis of (+)-conduritol B and (-)-conduritol F derivatives and of (-)-conduritol E and F. Tetrahedron 56(9) (2000): 1225-1231.
- [38] Heo, J.-N., Holson, E.B., and Roush, W.R. Common-intermediate strategy for synthesis of conduritols and inositols via β -hydroxy cyclohexenylsilanes. Organic Letters 5(10) (2003): 1697-1700.
- [39] Wikul, A., Damsud, T., Kataoka, K., and Phuwapraisirisan, P. (+)-Pinoresinol is a putative hypoglycemic agent in defatted sesame (*Sesamum indicum*) seeds though inhibiting α -glucosidase. Bioorganic and Medicinal Chemistry Letters 22(16) (2012): 5215-5217.

- [40] Takahashi, H., Kittaka, H., and Ikegami, S. Novel synthesis of enantiomerically pure natural inositols and their diastereoisomers. Journal of Organic Chemistry 66(8) (2001): 2705-2716.
- [41] Abdel-Magid, A.F., Carson, K.G., Harris, B.D., Maryanoff, C.A., and Shah, R.D. Reductive amination of aldehydes and ketones with sodium triacetoxyborohydride. Studies on direct and indirect reductive amination procedures. The Journal of Organic Chemistry 61(11) (1996): 3849-3862.
- [42] Natori, Y., et al. The synthesis and biological evaluation of 1-C-alkyl-L-arabinoiminofuranoses, a novel class of α -glucosidase inhibitors. Bioorganic and Medicinal Chemistry Letters 21(2) (2011): 738-741.
- [43] Oki, T., Matsui, T., and Osajima, Y. Inhibitory effect of α -glucosidase inhibitors varies according to its origin. Journal of Agricultural and Food Chemistry 47(2) (1999): 550-553.
- [44] Kimura, A., et al. Two potent competitive inhibitors discriminating α -glucosidase family I from family II. Carbohydrate Research 339(6) (2004): 1035-1040.
- [45] Paul, B.J., Willis, J., Martinot, T.A., Ghiviriga, I., Abboud, K.A., and Hudlicky, T. Synthesis, structure, and biological evaluation of novel *N*- and *O*-Linked diinositols. Journal of the American Chemical Society 124(35) (2002): 10416-10426.
- [46] Tadanier, J., Martin, J.R., Goldstein, A.W., and Hirner, E.A. Diastereomeric 10,11-epoxyerythromycins B and the preparation of 10-*epi*-erythromycin B. The Journal of Organic Chemistry 43(12) (1978): 2351-2356.
- [47] Yoshikawa, M., Morikawa, T., Matsuda, H., Tanabe, G., and Muraoka, O. Absolute stereostructure of potent α -glucosidase inhibitor, salacinol, with unique thiosugar sulfonium sulfate inner salt structure from *Salacia reticulata*. Bioorganic and Medicinal Chemistry 10(5) (2002): 1547-1554.
- [48] Trott, O. and Olson, A.J. Software news and update AutoDock Vina: Improving the speed and accuracy of docking with a new scoring function, efficient optimization, and multithreading. Journal of Computational Chemistry 31(2) (2010): 455-461.

- [49] Sim, L., et al. New glucosidase inhibitors from an ayurvedic herbal treatment for type 2 diabetes: Structures and inhibition of human intestinal maltase-glucoamylase with compounds from *Salacia reticulata*. Biochemistry 49(3) (2009): 443-451.
- [50] Worawalai, W., Wacharasindhu, S., and Phuwapraisirisan, P. Synthesis of new *N*-substituted aminoquercitols from naturally available (+)-*proto*-quercitol and their α -glucosidase inhibitory activity. MedChemComm 3(11) (2012): 1466-1470.
- [51] Arnold, K., Bordoli, L., Kopp, J., and Schwede, T. The SWISS-MODEL workspace: A web-based environment for protein structure homology modelling. Bioinformatics 22(2) (2006): 195-201.
- [52] Gasteiger, J. and Marsili, M. Iterative partial equalization of orbital electronegativity—a rapid access to atomic charges. Tetrahedron 36(22) (1980): 3219-3228.
- [53] Rinnan, Å., Christensen, N.J., and Engelsen, S.B. How the energy evaluation method used in the geometry optimization step affect the quality of the subsequent QSAR/QSPR models. Journal of Computer-Aided Molecular Design 24(1) (2010): 17-22.
- [54] Bikadi, Z. and Hazai, E. Application of the PM6 semi-empirical method to modeling proteins enhances docking accuracy of AutoDock. Journal of Cheminformatics 1(1) (2009).
- [55] Humphrey, W., Dalke, A., and Schulten, K. VMD: Visual molecular dynamics. Journal of Molecular Graphics 14(1) (1996): 33-38.
- [56] Butler, M.S., Blaskovich, M.A., and Cooper, M.A. Antibiotics in the clinical pipeline in 2013. Journal of Antibiotics 66(10) (2013): 571-591.
- [57] Butler, M.S. and Buss, A.D. Natural products—The future scaffolds for novel antibiotics? Biochemical Pharmacology 71(7) (2006): 919-929.
- [58] Khan, R., et al. Antimicrobial activity of five herbal extracts against Multi Drug Resistant (MDR) strains of bacteria and fungus of clinical origin. Molecules 14(2) (2009): 586-597.

- [59] Sugie, Y., et al. New pyrrolizidinone antibiotics CJ-16,264 and CJ-16,367. Journal of Antibiotics 54(11) (2001): 917-925.
- [60] Butler, M.S. Natural products to drugs: Natural product derived compounds in clinical trials. Natural Product Reports 22(2) (2005): 162-195.
- [61] Lambert, T.H. and Danishefsky, S.J. Total synthesis of UCS1025A. Journal of the American Chemical Society 128(2) (2005): 426-427.
- [62] Uchida, K., et al. Stereocontrolled total synthesis of (+)-UCS1025A. Angewandte Chemie International Edition 51(51) (2012): 12850-12853.
- [63] Agatsuma, T., et al. UCS1025A and B, New antitumor antibiotics from the fungus *Acremonium* species. Organic Letters 4(25) (2002): 4387-4390.
- [64] de Figueiredo, R.M., Fröhlich, R., and Christmann, M. Efficient synthesis and resolution of pyrrolizidines. Angewandte Chemie International Edition 46(16) (2007): 2883-2886.
- [65] Nakai, R., et al. Telomerase inhibitors identified by a forward chemical genetics approach using a yeast strain with shortened telomere length. Chemistry and Biology 13(2) (2006): 183-190.
- [66] Wilson, R.M., Jen, W.S., and MacMillan, D.W.C. Enantioselective organocatalytic intramolecular Diels–Alder reactions. The asymmetric synthesis of solanapyrone D. Journal of the American Chemical Society 127(33) (2005): 11616-11617.
- [67] Hoyer, T.R. and Dvornikovs, V. Comparative Diels–Alder reactivities within a family of valence bond isomers: A biomimetic total synthesis of (±)-UCS1025A. Journal of the American Chemical Society 128(8) (2006): 2550-2551.
- [68] Negishi, E.-i., Kondakov, D.Y., Choueiry, D., Kasai, K., and Takahashi, T. Multiple mechanistic pathways for zirconium-catalyzed carboalumination of alkynes. Requirements for cyclic carbometalation processes involving C–H activation. Journal of the American Chemical Society 118(40) (1996): 9577-9588.
- [69] Hayashi, N., Suzuki, T., Usui, K., and Nakada, M. Alternative synthetic approach for (+)-phomopsidin via the highly stereoselective TADA reaction. Tetrahedron 65(4) (2009): 888-895.

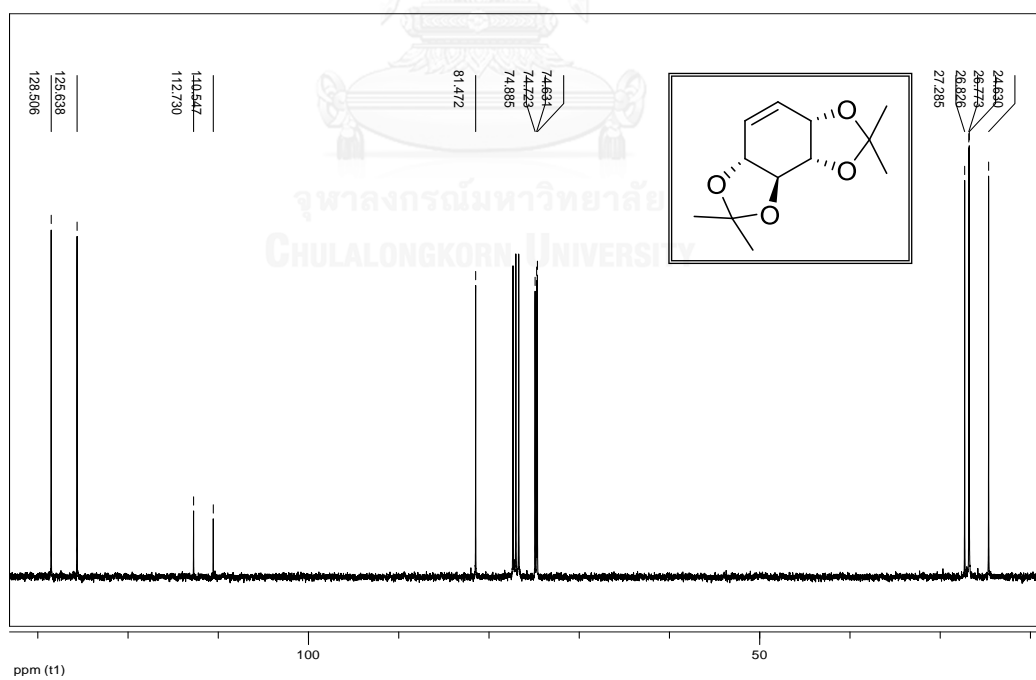
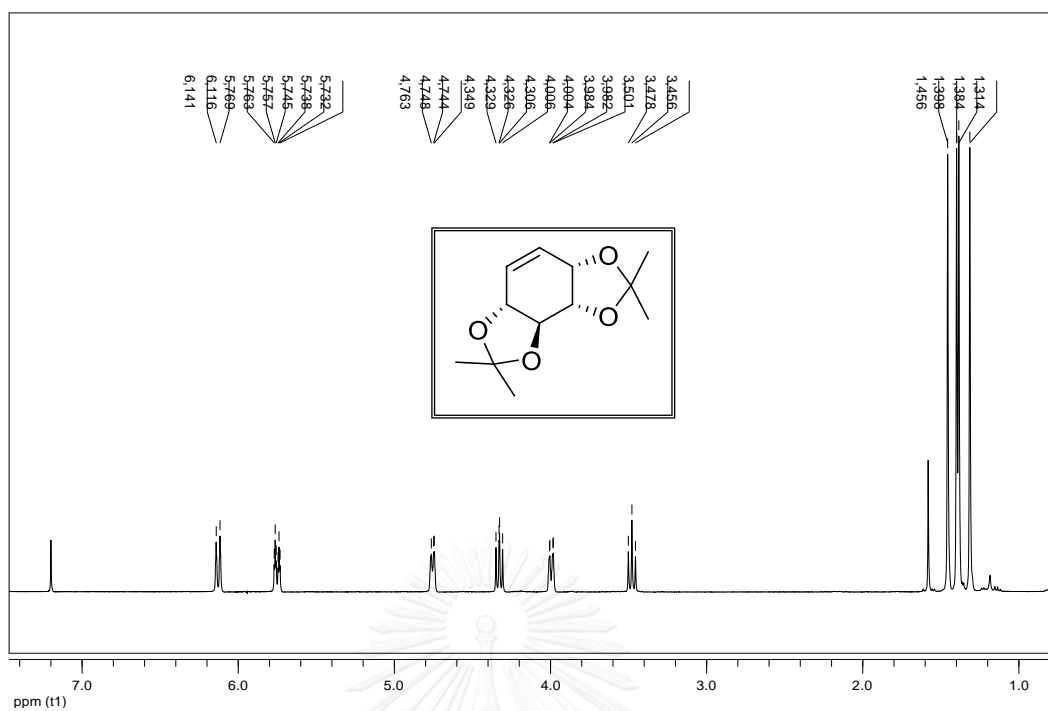
- [70] Larsen, B.J., Sun, Z., and Nagorny, P. Synthesis of eukaryotic translation elongation inhibitor lactimidomycin via Zn(II)-Mediated Horner–Wadsworth–Emmons Macrocyclization. Organic Letters 15(12) (2013): 2998-3001.





APPENDIX

จุฬาลงกรณ์มหาวิทยาลัย
CHULALONGKORN UNIVERSITY



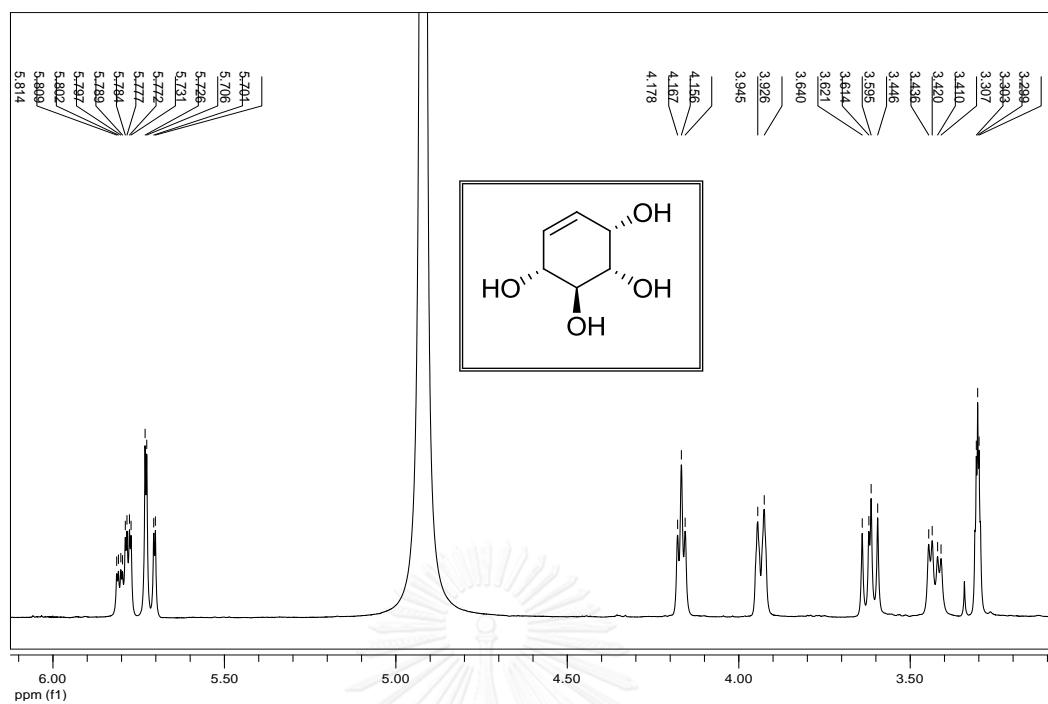


Figure 3. ^1H NMR spectrum of 2-4 (CD_3OD)

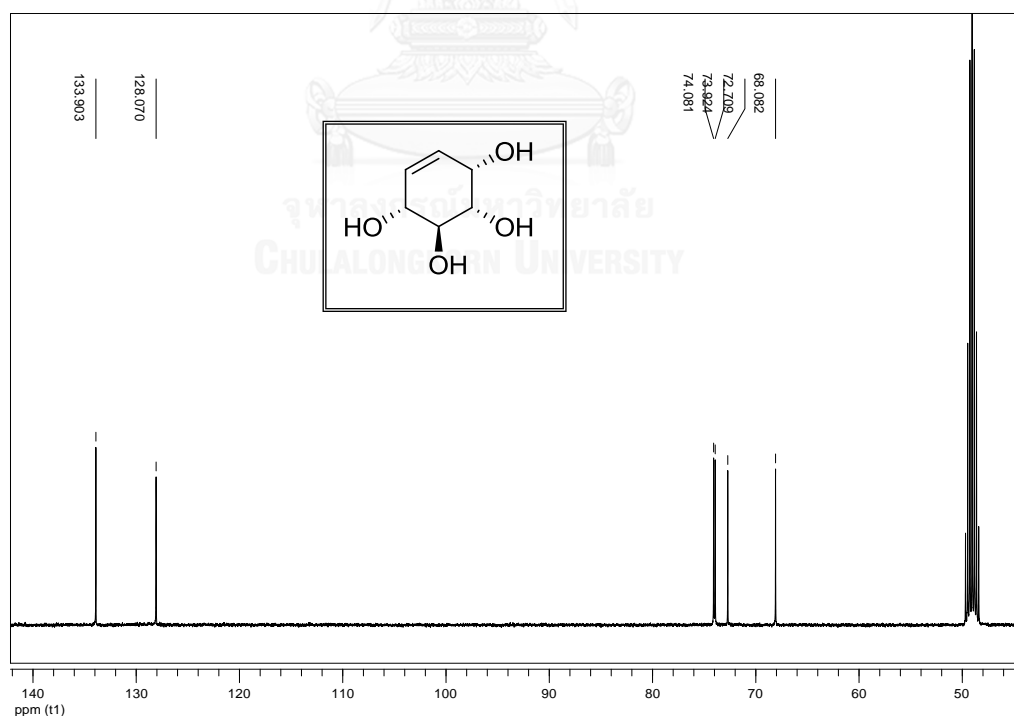


Figure 4. ^{13}C NMR spectrum of 2-4 (CD_3OD)

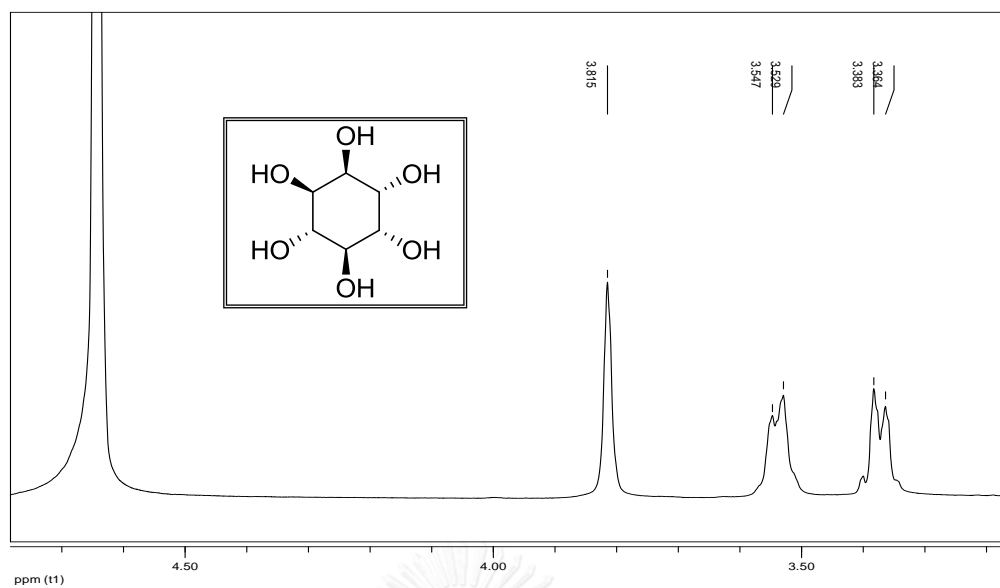


Figure 5. ^1H NMR spectrum of 2-6a (D_2O)

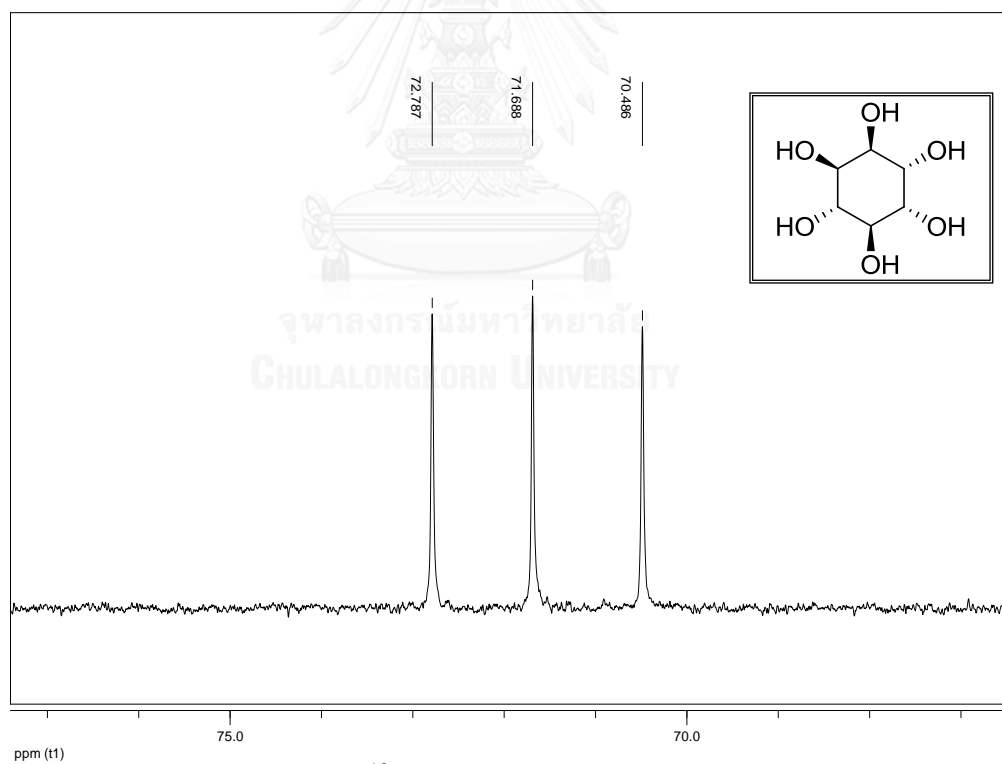


Figure 6. ^{13}C NMR spectrum of 2-6a (D_2O)

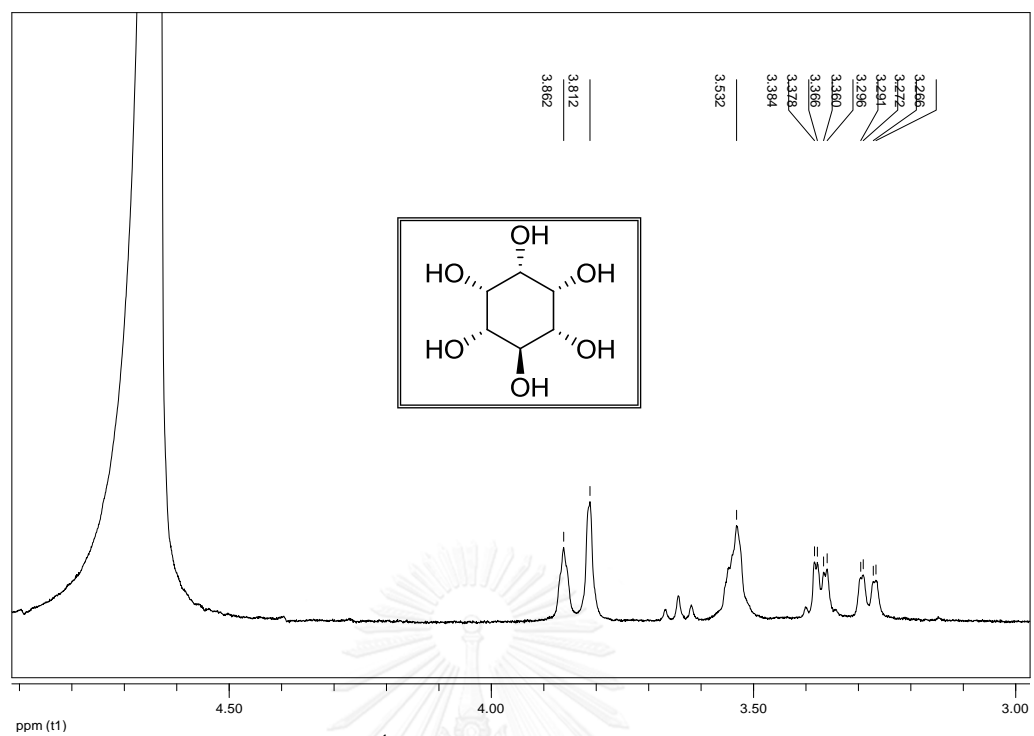


Figure 7. ^1H NMR spectrum of 2-6b (D_2O)

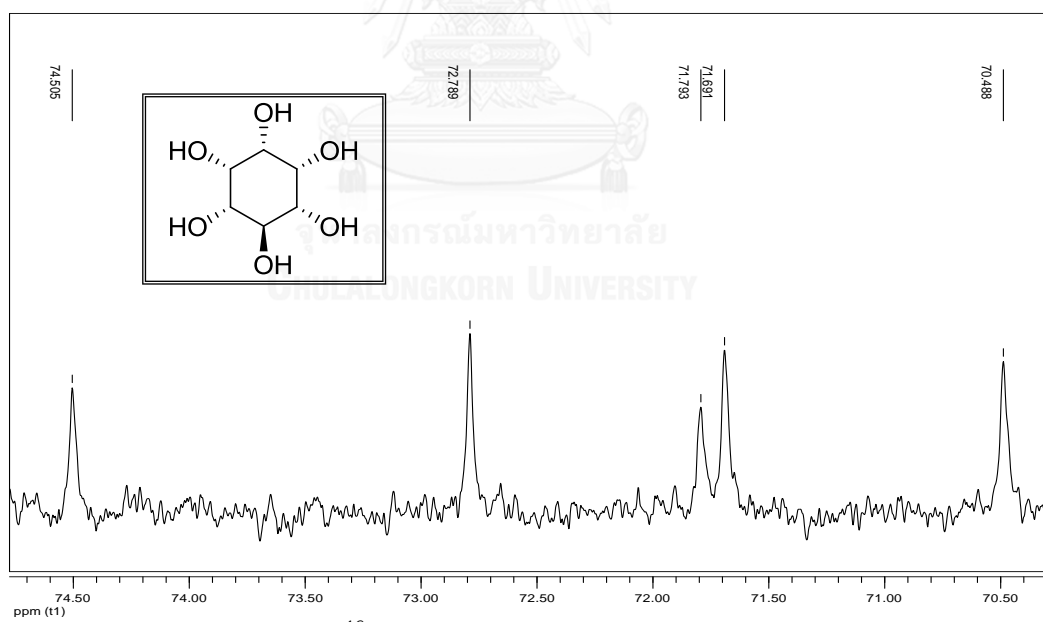


Figure 8. ^{13}C NMR spectrum of 2-6b (expanded)

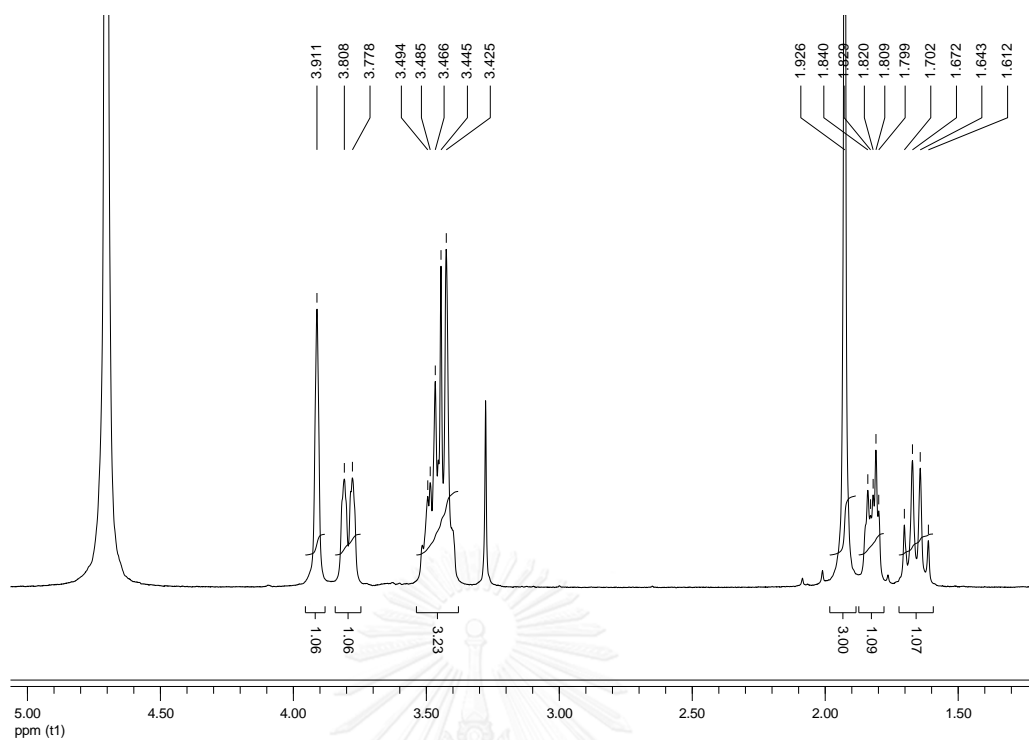


Figure 9. ^1H NMR spectrum of 3-3 (D_2O)

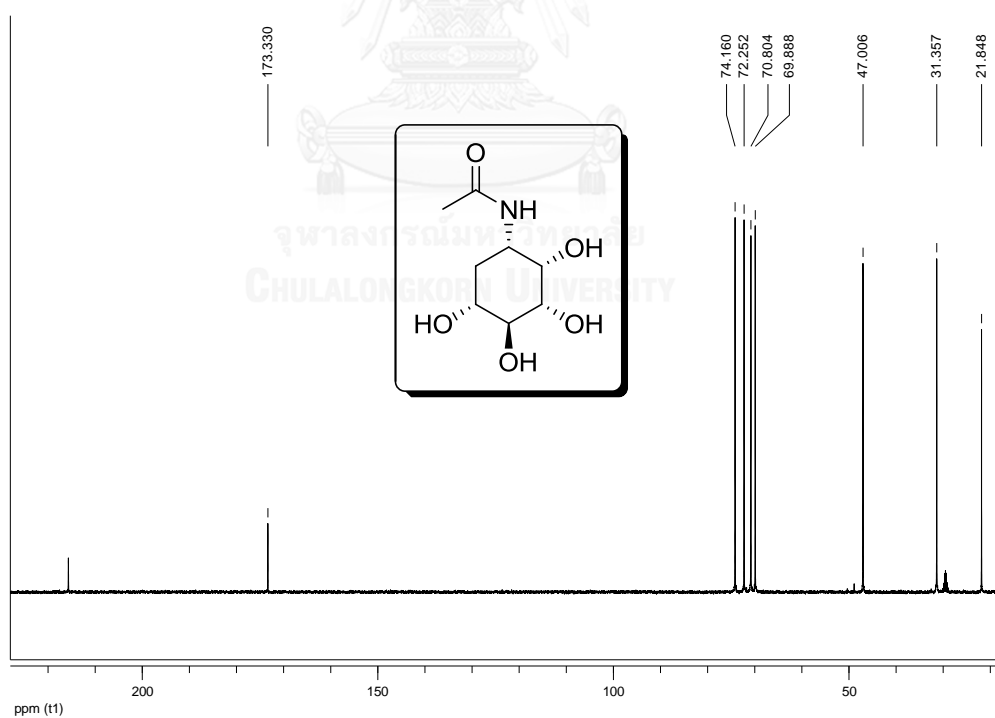


Figure 10. ^{13}C NMR spectrum of 3-3 ($\text{D}_2\text{O}+\text{acetone-}d_6$)

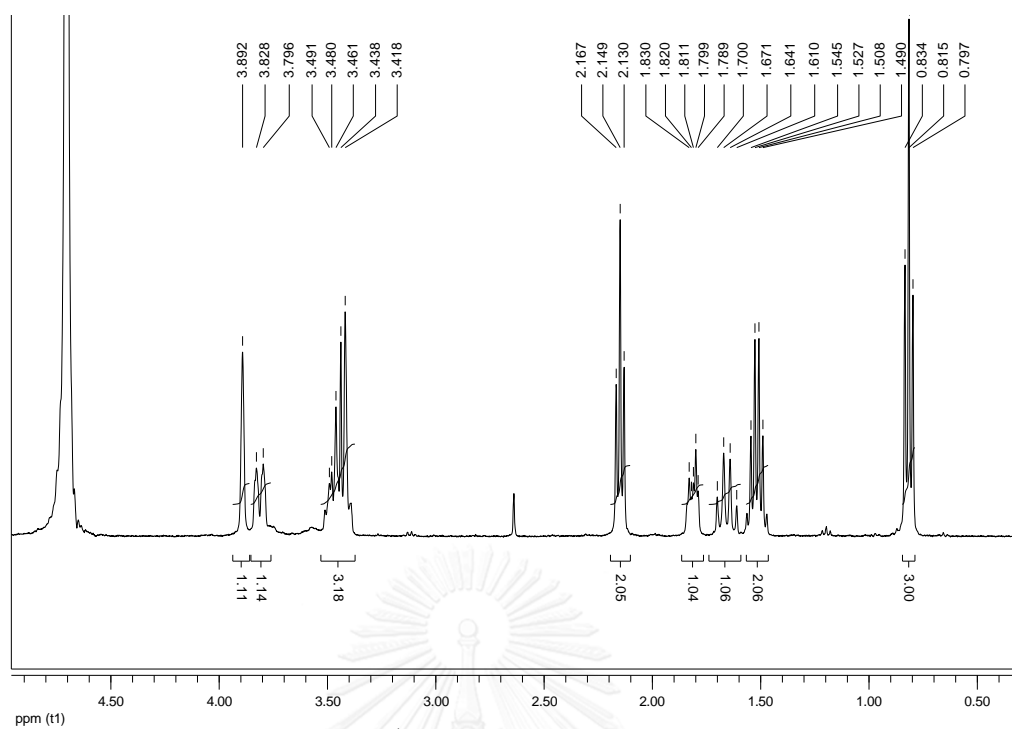


Figure 11. ^1H NMR spectrum of **3-4** (D_2O)

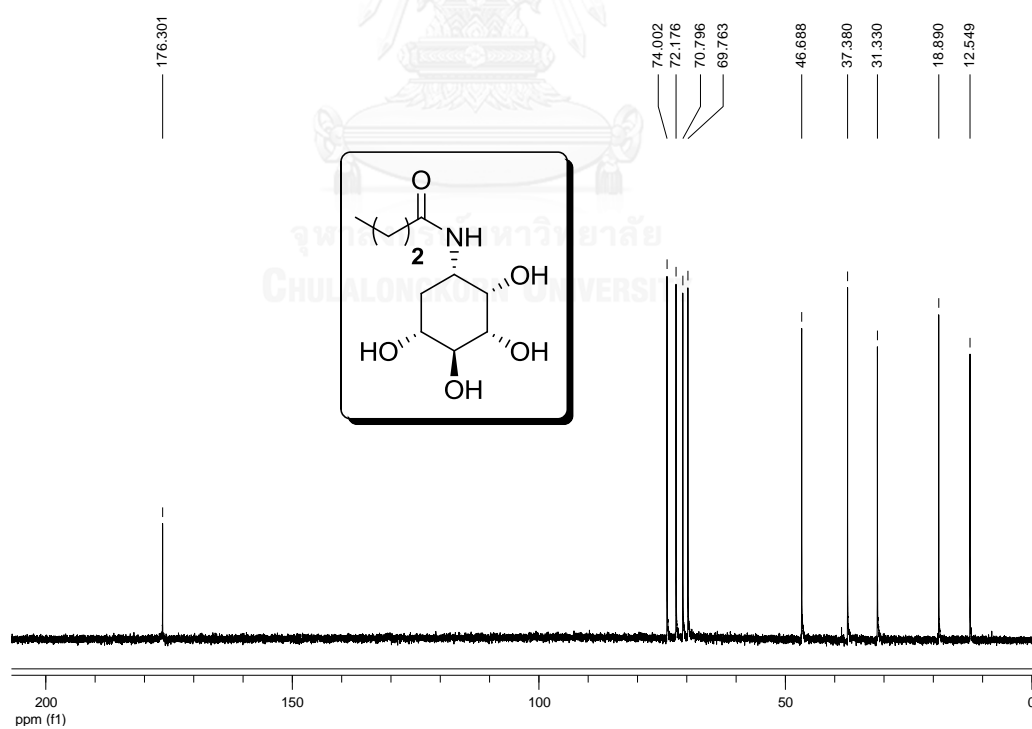


Figure 12. ^{13}C NMR spectrum of **3-4** (D_2O)

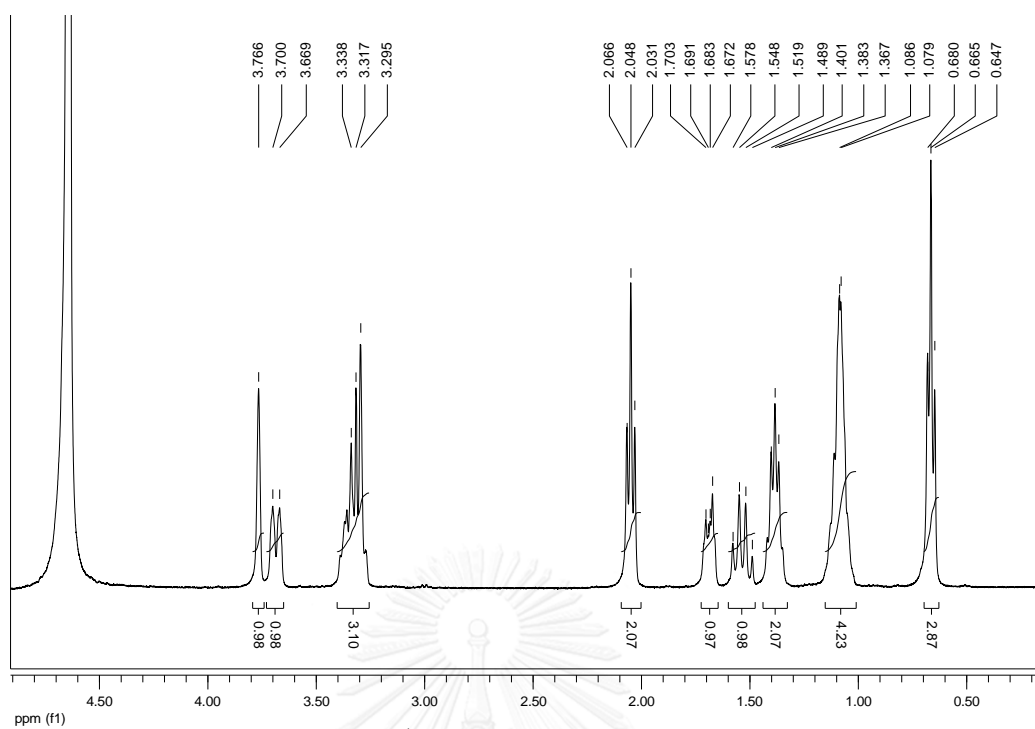


Figure 13. ^1H NMR spectrum of 3-5 (D_2O)

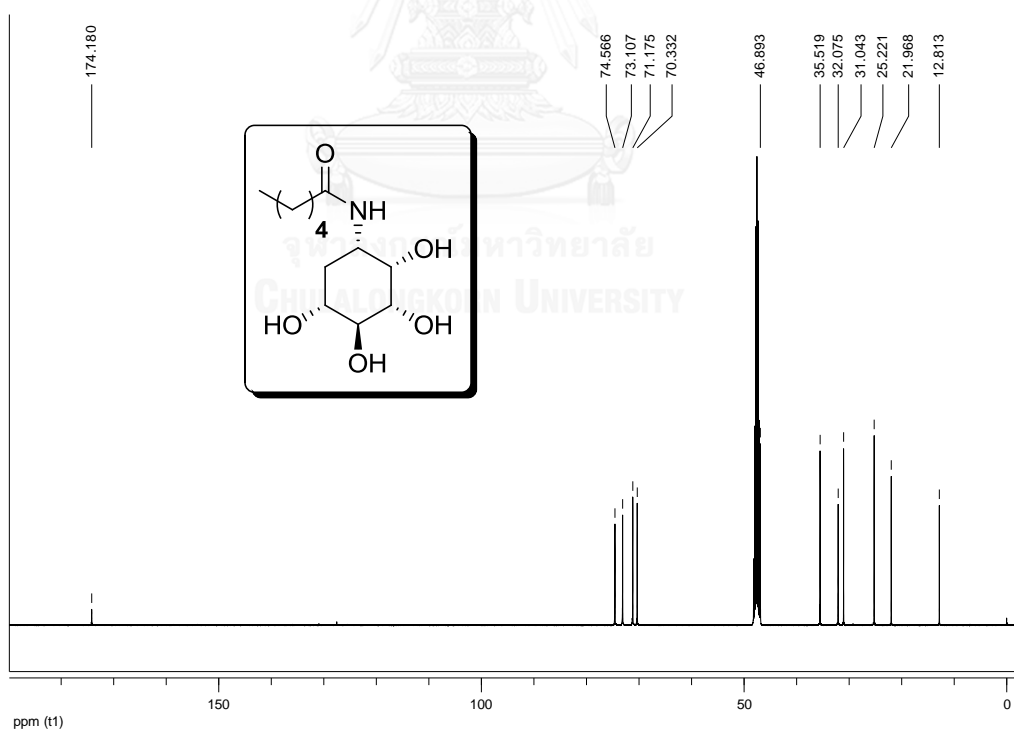


Figure 14. ^{13}C NMR spectrum of 3-5 (CD_3OD)

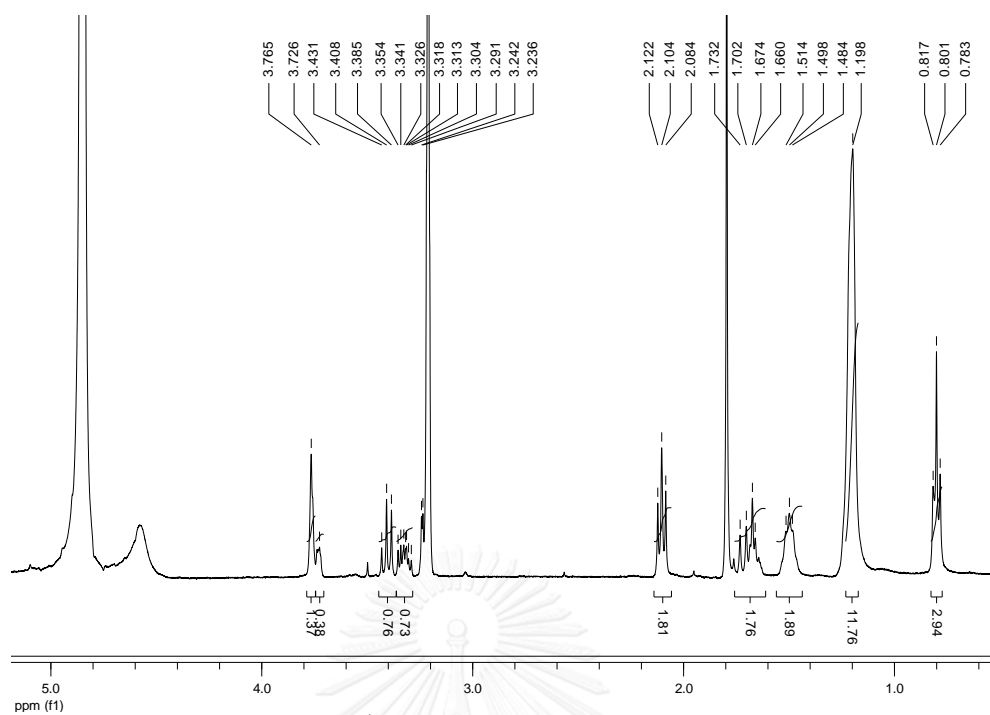


Figure 15. ^1H NMR spectrum of **3-6** (CD_3OD)

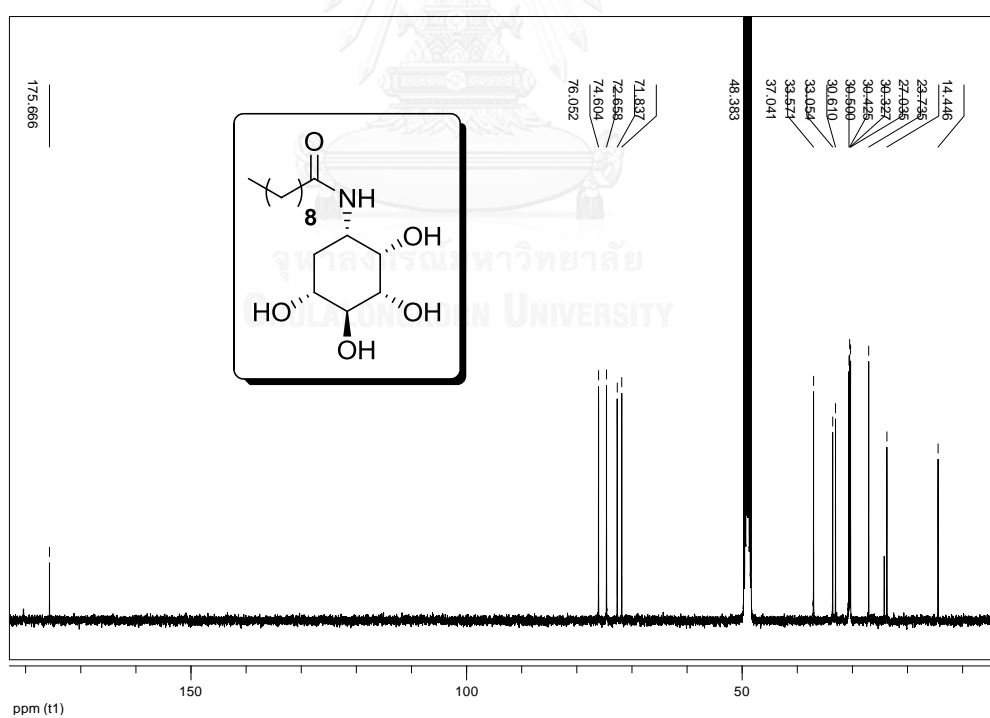


Figure 16. ^{13}C NMR spectrum of **3-6** (CD_3OD)

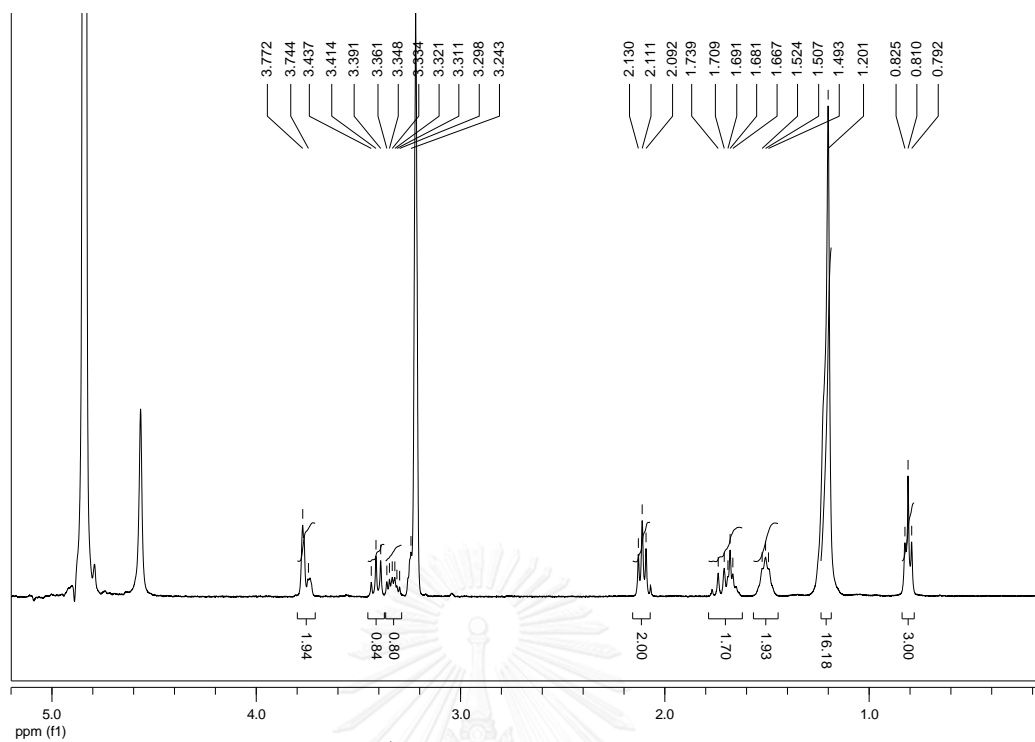


Figure 17. ^1H NMR spectrum of **3-7** (CD_3OD)

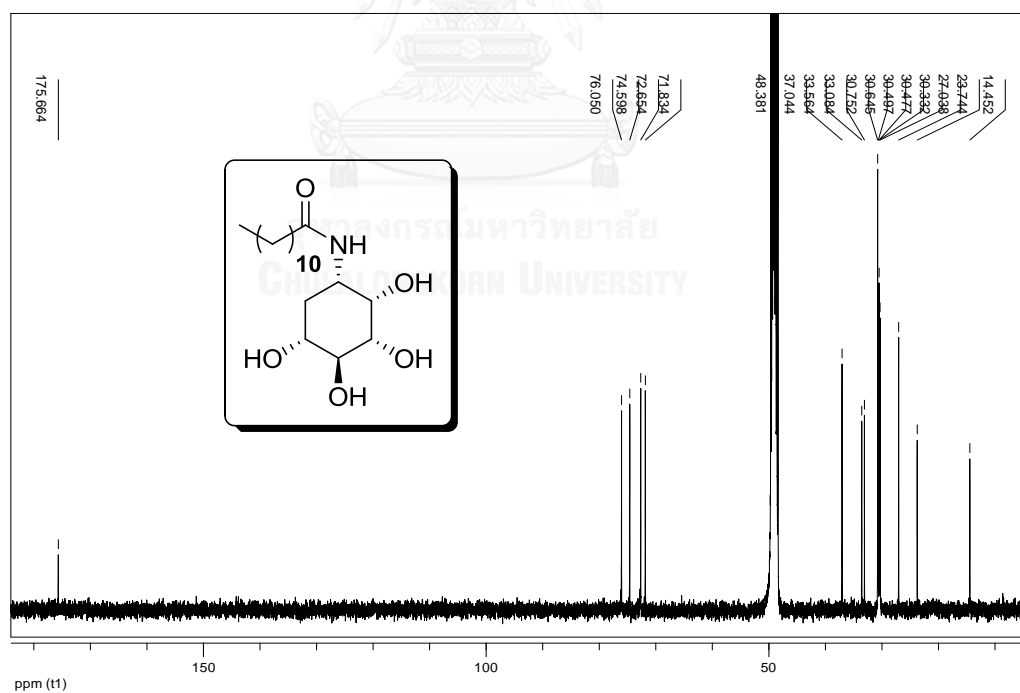


Figure 18. ^{13}C NMR spectrum of **3-7** (CD_3OD)

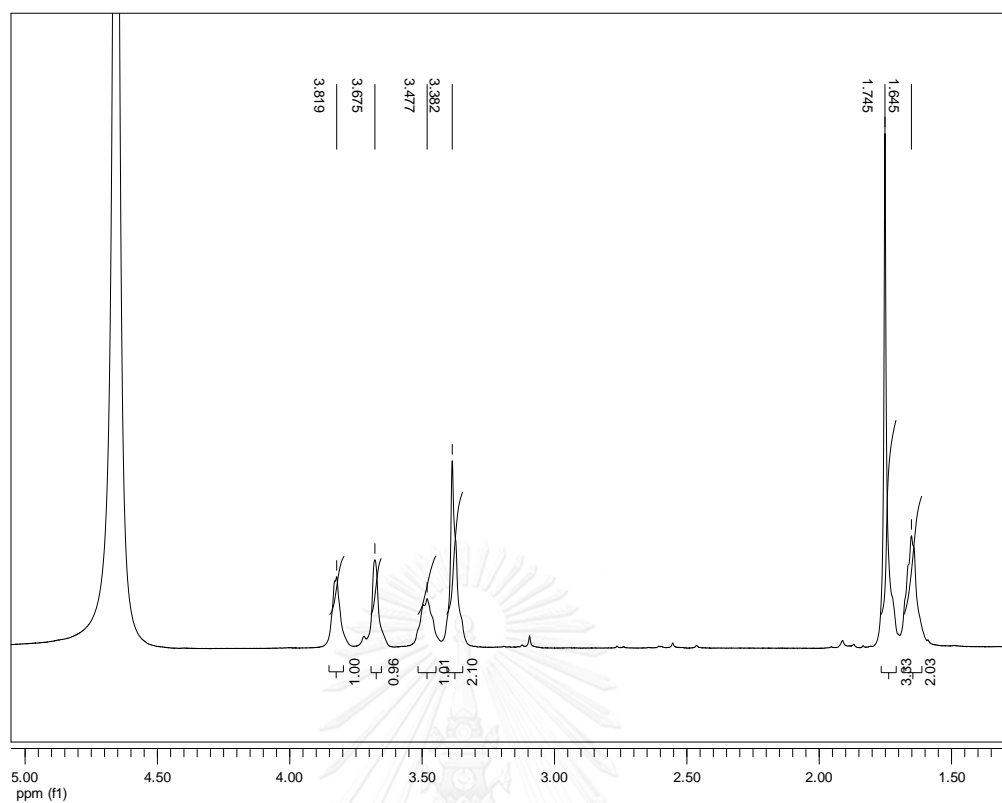


Figure 19. ^1H NMR spectrum of **3-8** (D_2O)

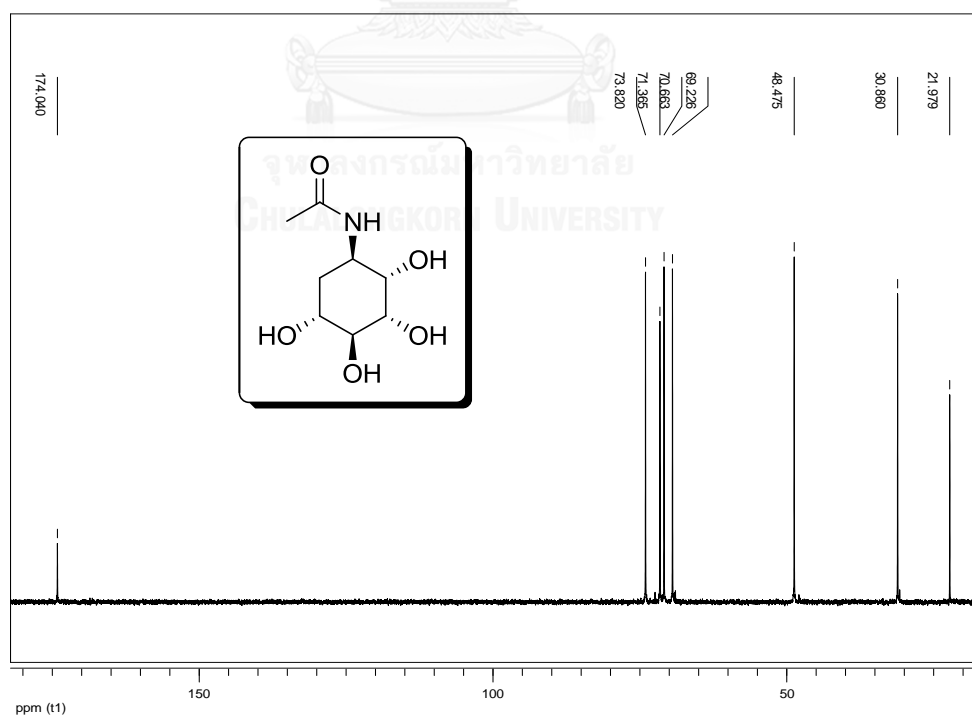


Figure 20. ^{13}C NMR spectrum of **3-8** (D_2O)

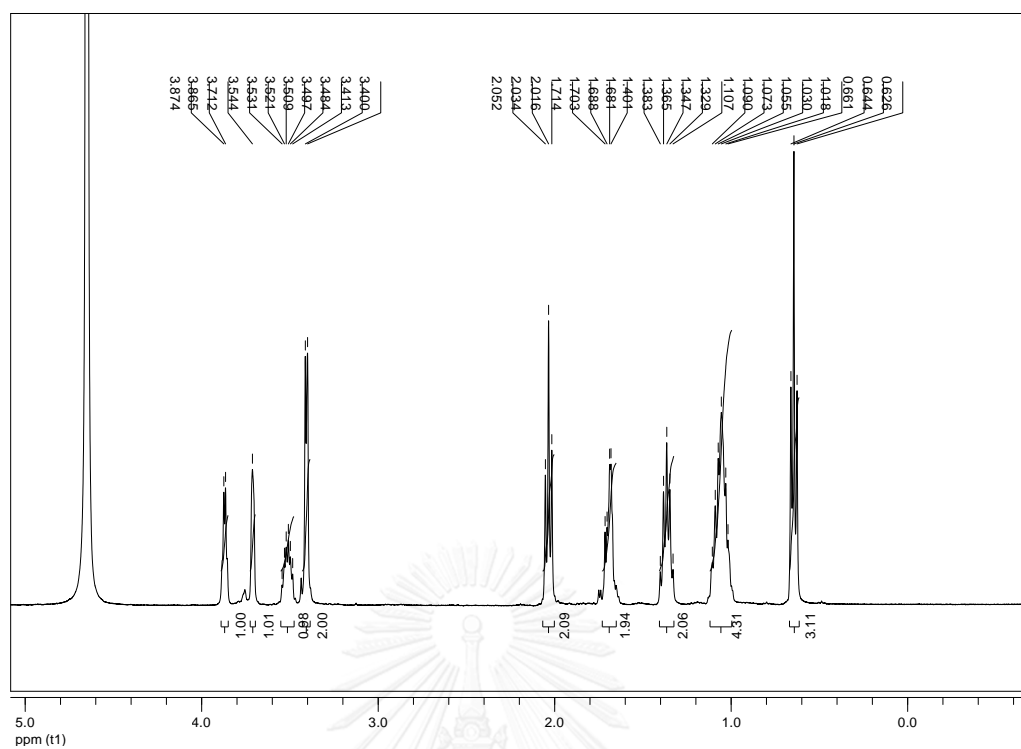


Figure 23. ^1H NMR spectrum of 3-10 (D_2O)

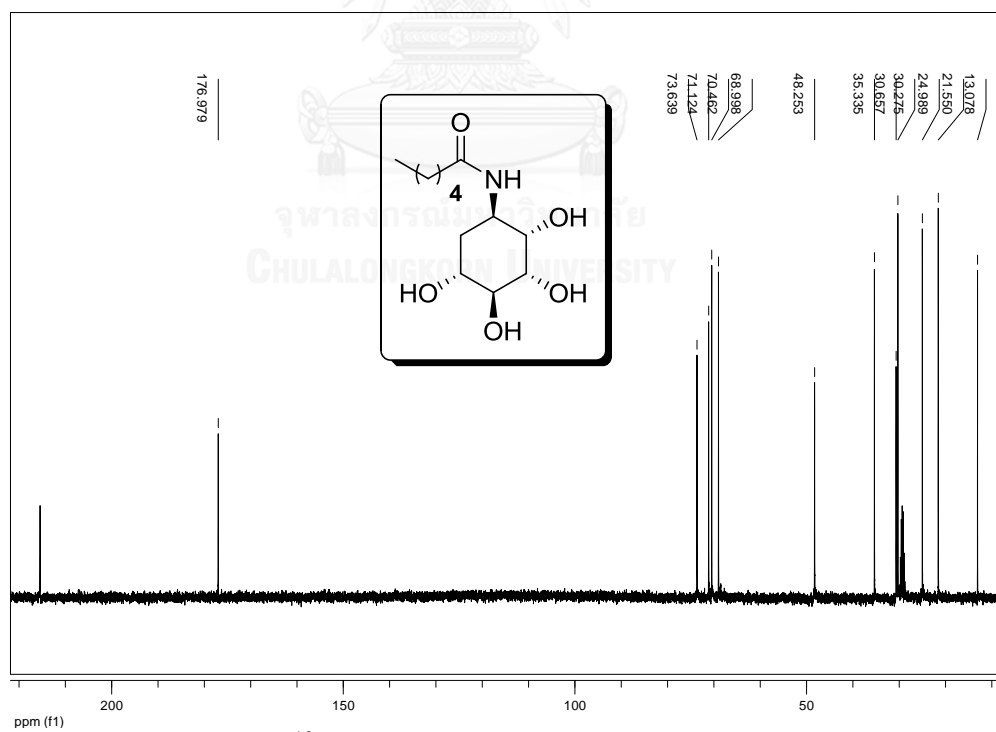


Figure 24. ^{13}C NMR spectrum of 3-10 ($\text{D}_2\text{O}+\text{acetone-}d_6$)

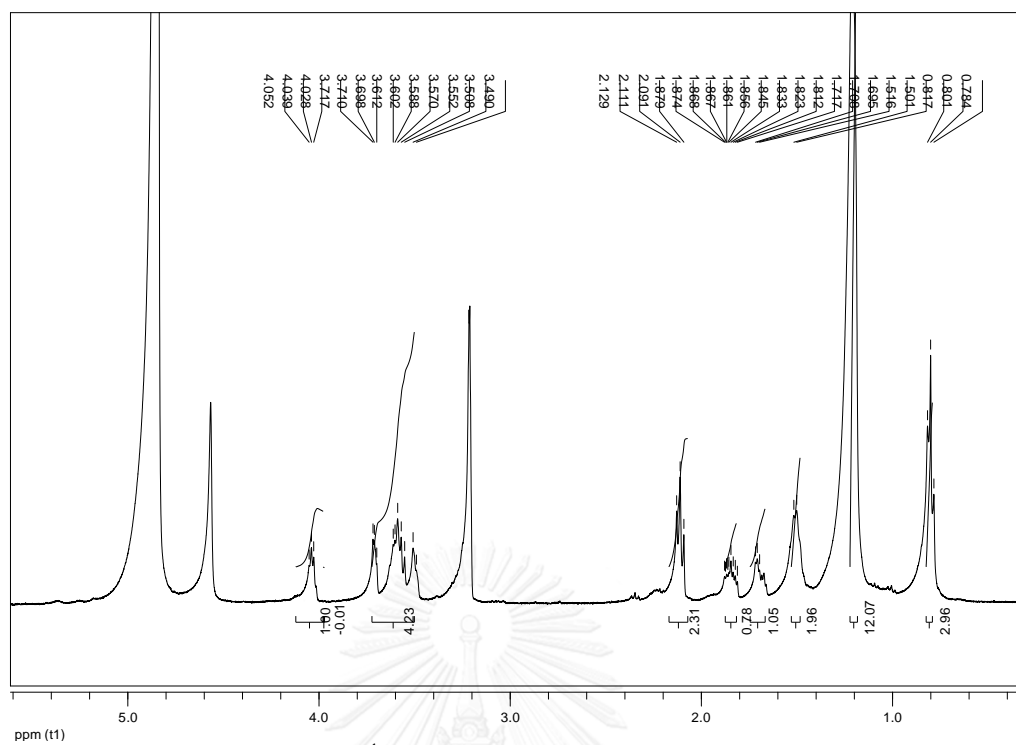


Figure 25. ^1H NMR spectrum of **3-11** (CD_3OD)

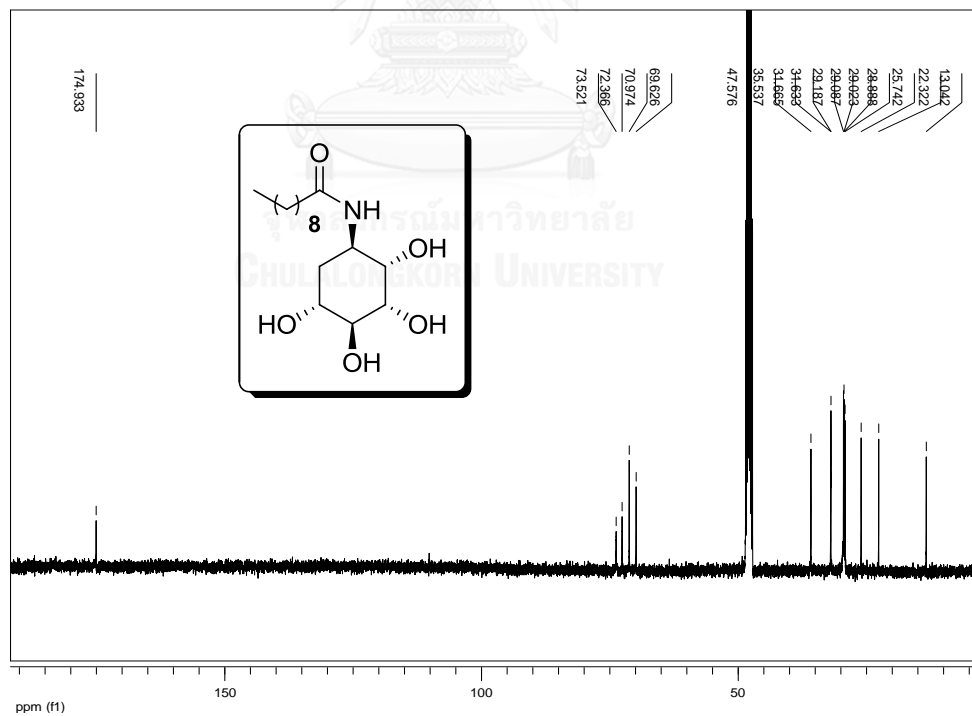


Figure 26. ^{13}C NMR spectrum of **3-11** (CD_3OD)

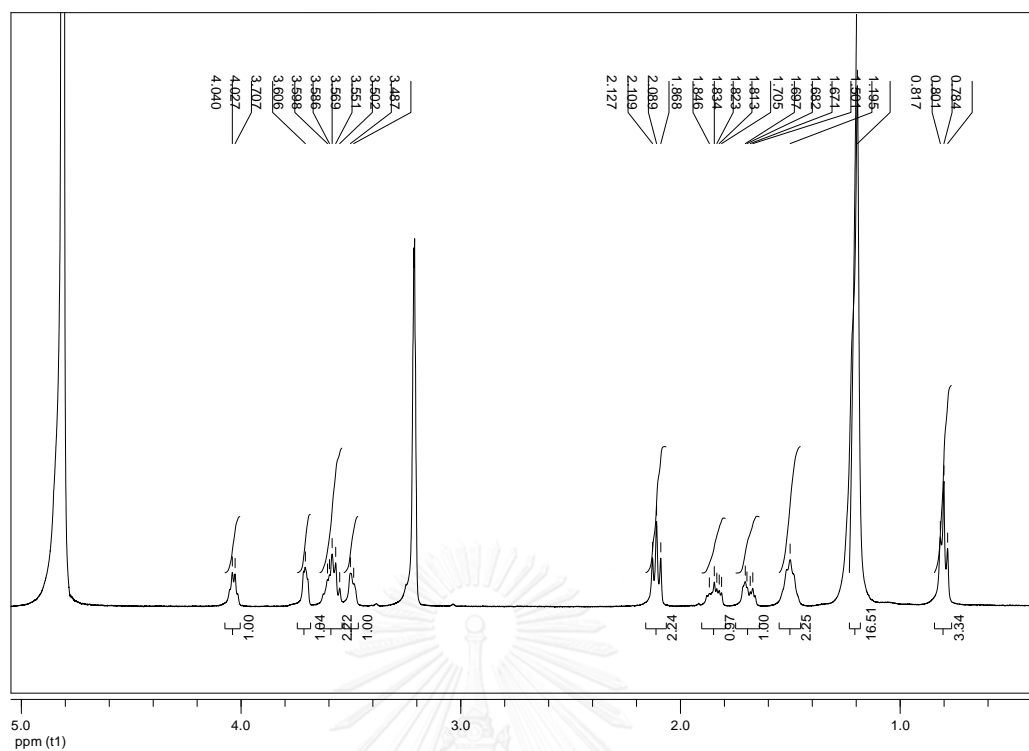


Figure 27. ^1H NMR spectrum of 3-12 (CD_3OD)

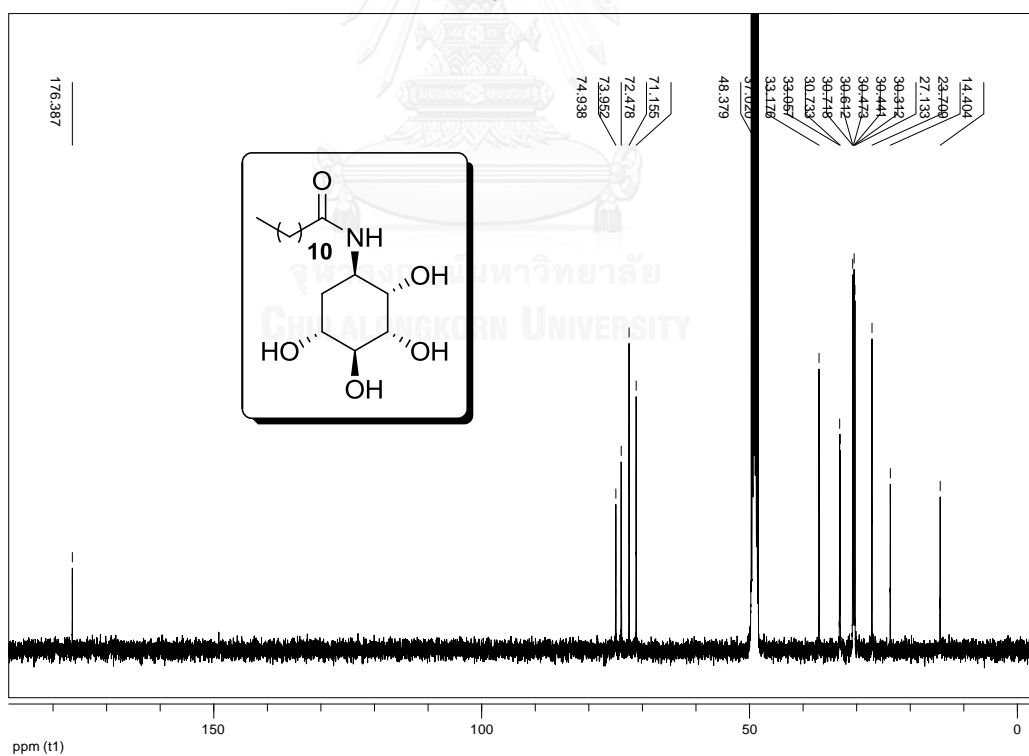


Figure 28. ^{13}C NMR spectrum of 3-12 (CD_3OD)

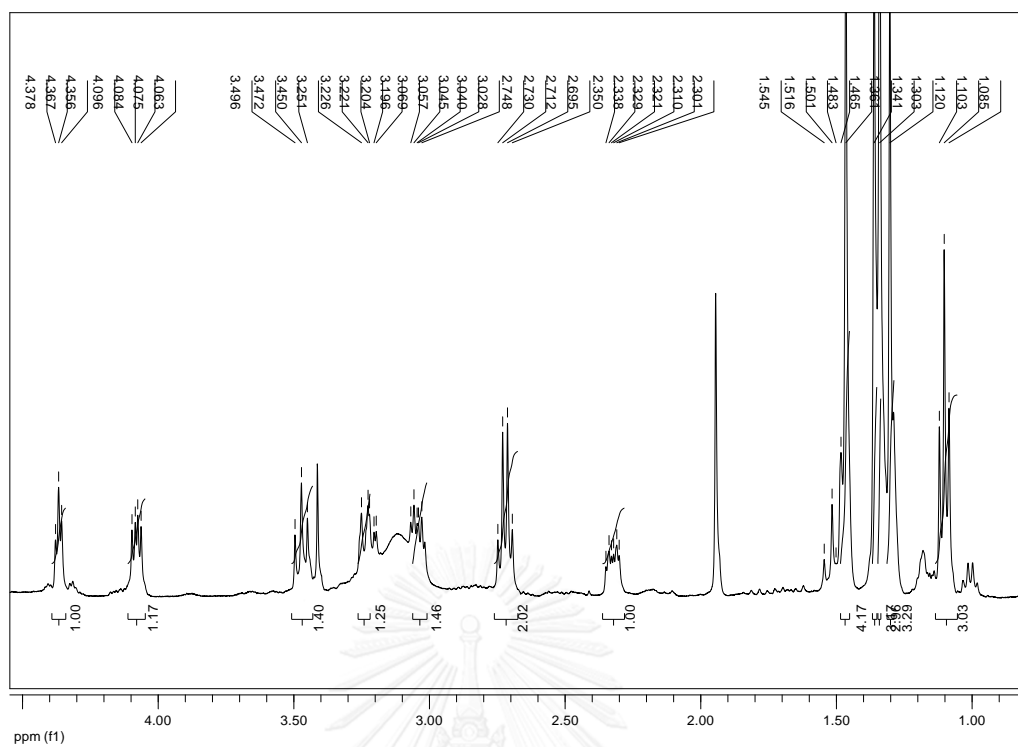


Figure 29. ^1H NMR spectrum of **3-13** (CDCl_3)

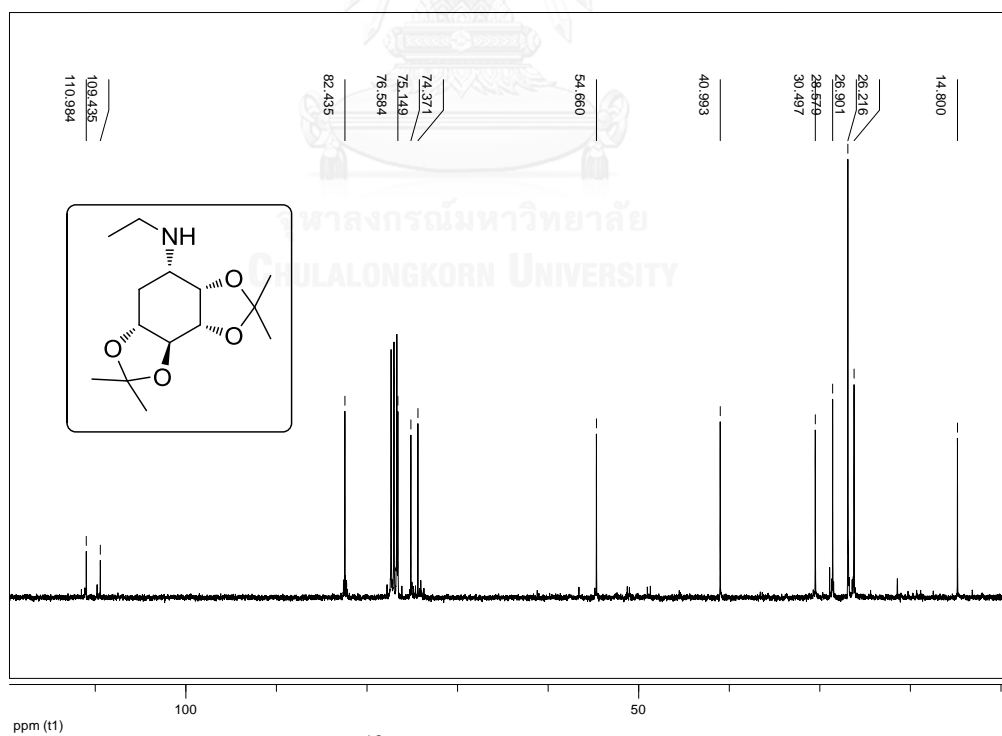


Figure 30. ^{13}C NMR spectrum of **3-13** (CDCl_3)

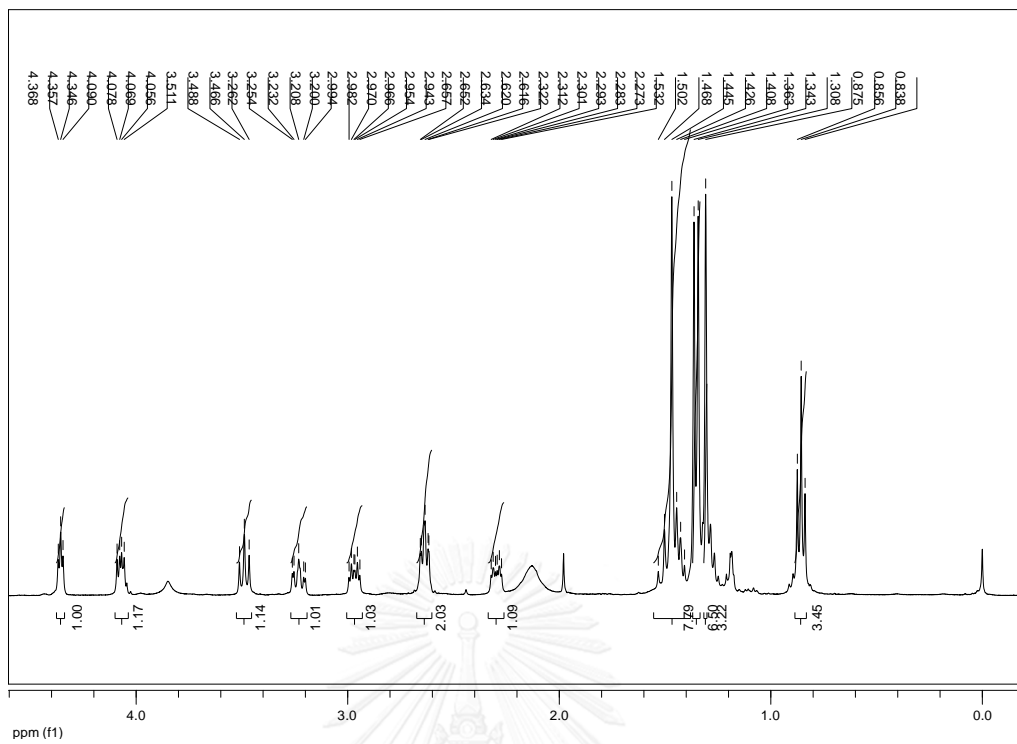


Figure 31. ¹H NMR spectrum of 3-14 (CDCl₃)

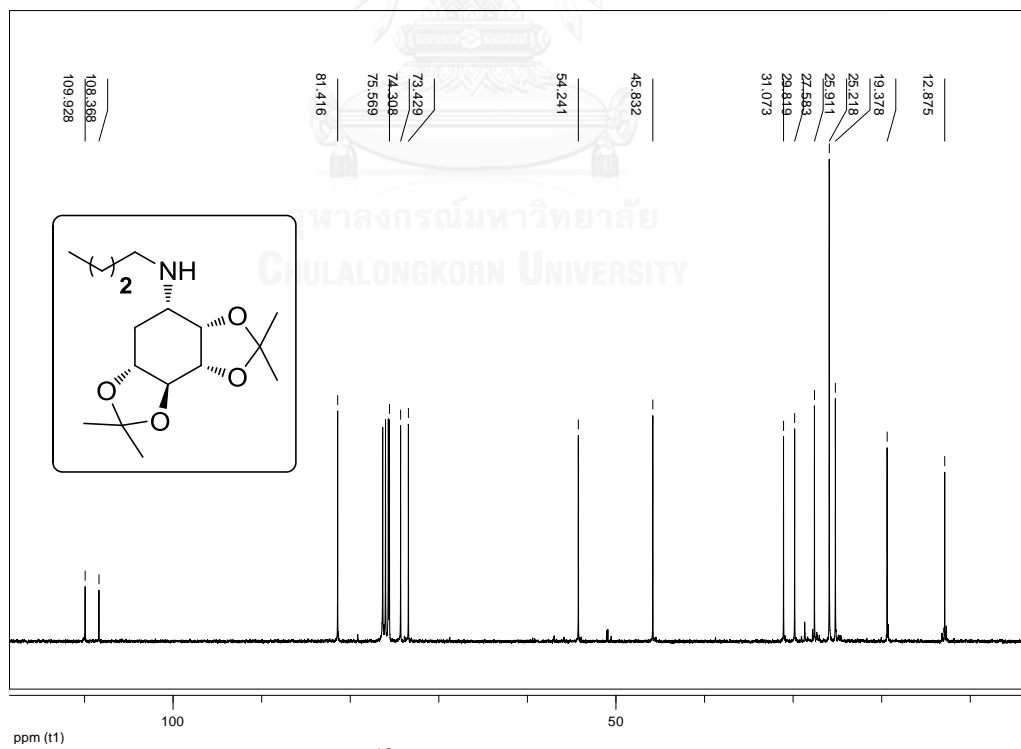


Figure 32. ¹³C NMR spectrum of 3-14 (CDCl₃)

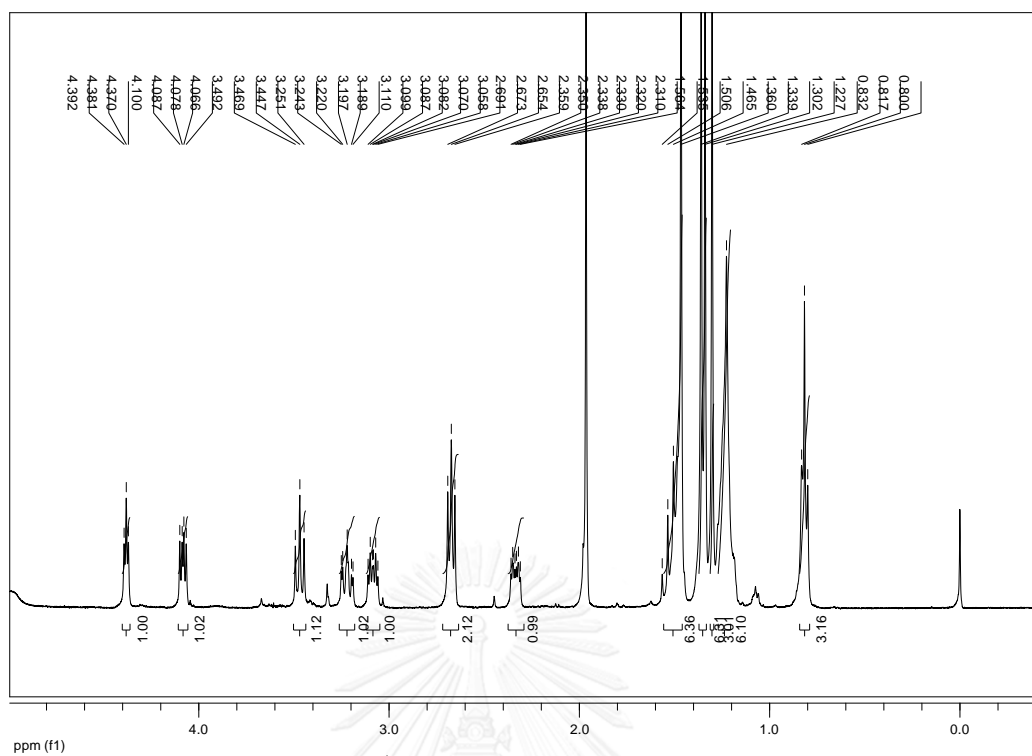


Figure 33. ^1H NMR spectrum of **3-15** (CDCl_3)

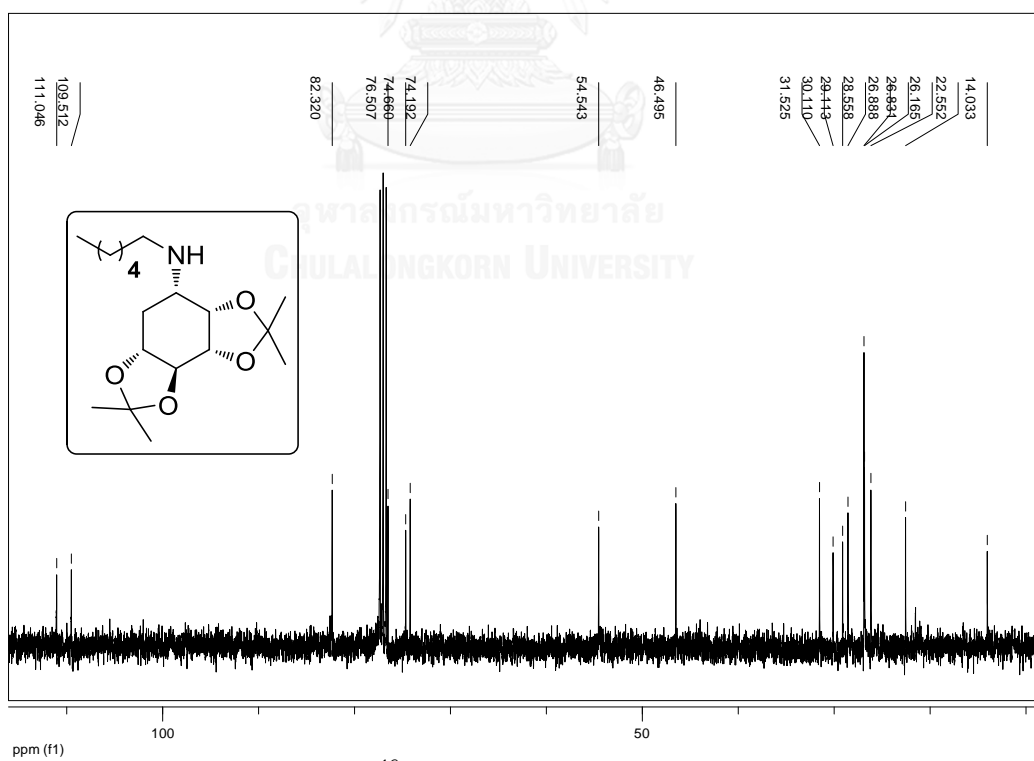
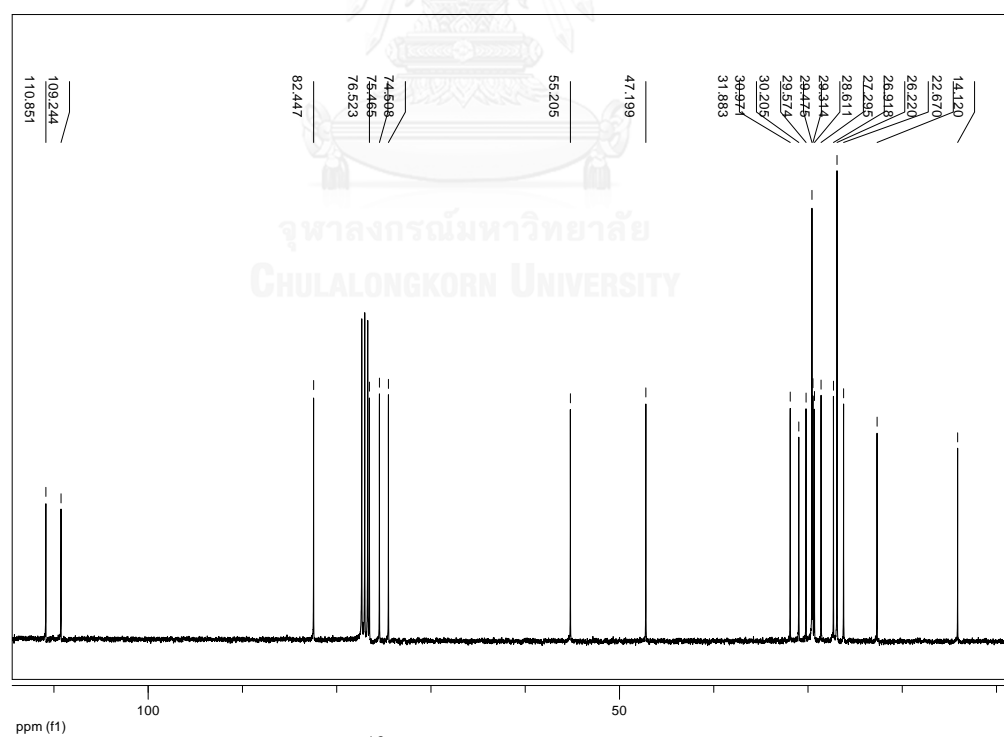
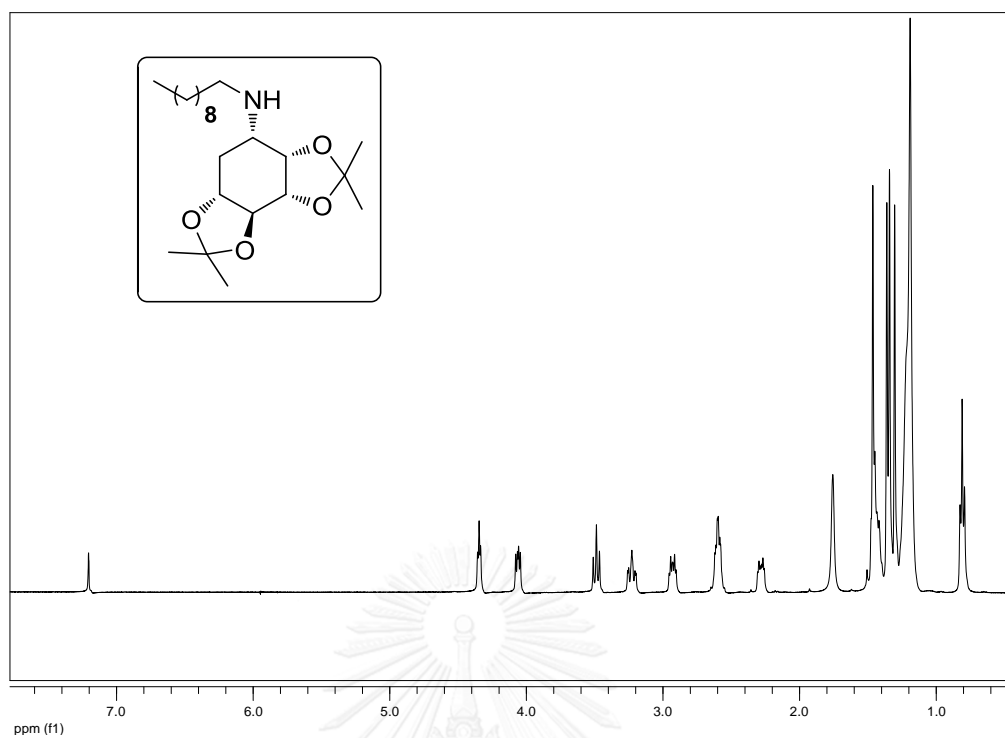
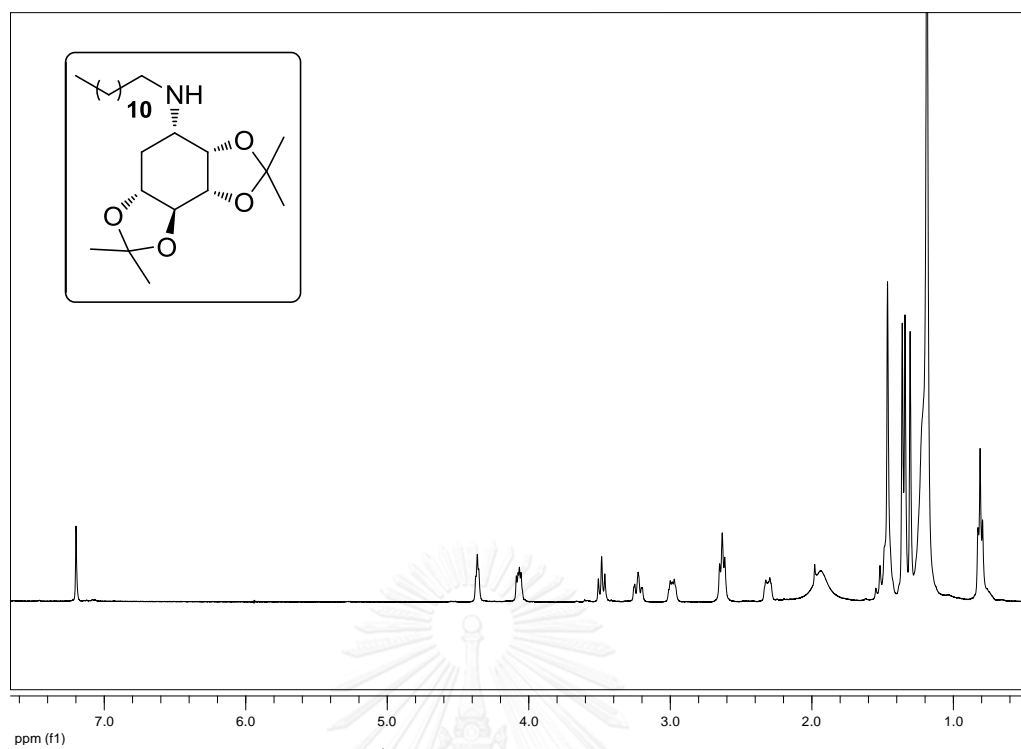
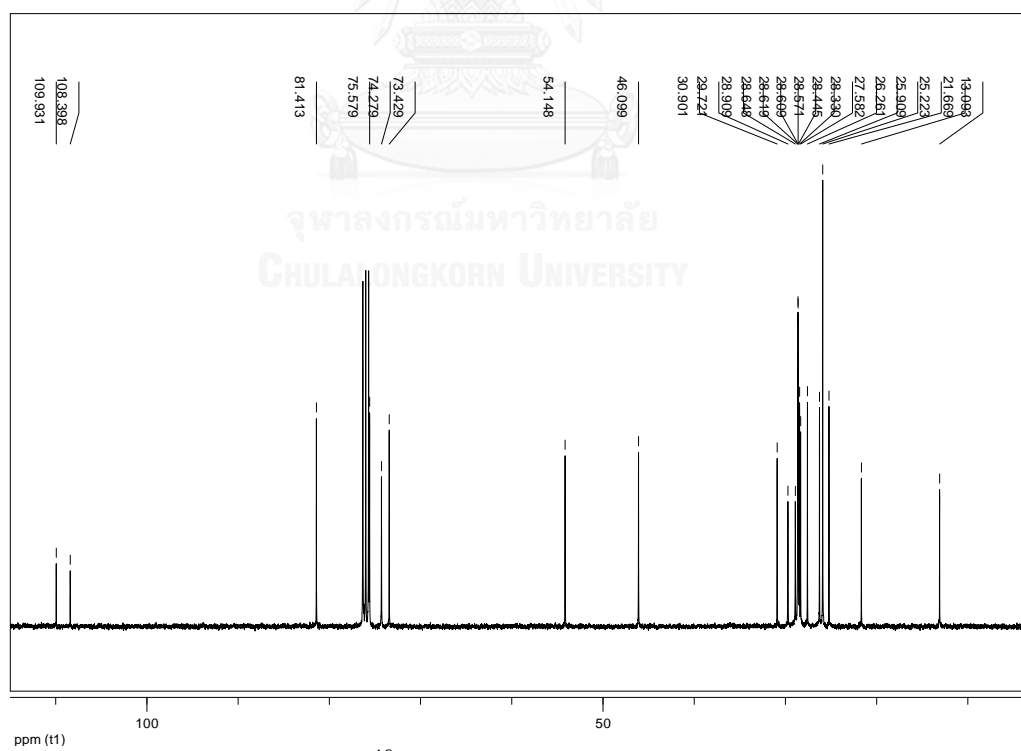


Figure 34. ^{13}C NMR spectrum of **3-15** (CDCl_3)



Figure 37. ^1H NMR spectrum of 3-17 (CDCl_3)Figure 38. ^{13}C NMR spectrum of 3-17 (CDCl_3)

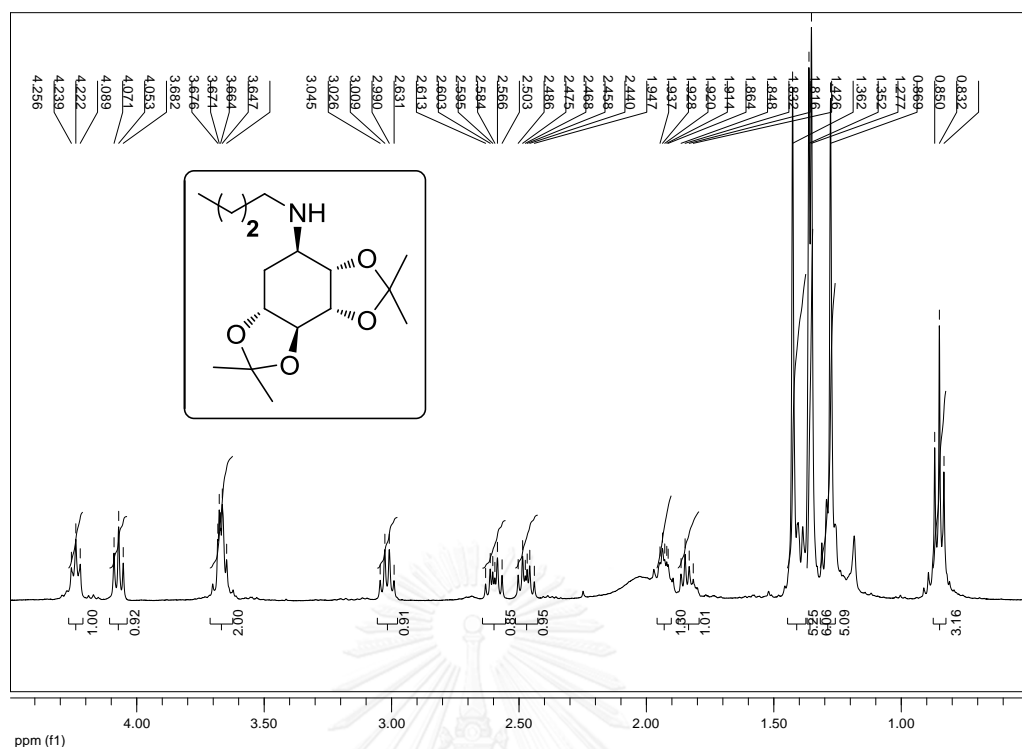


Figure 39. $^1\text{H NMR}$ spectrum of 3-18 (CDCl_3)

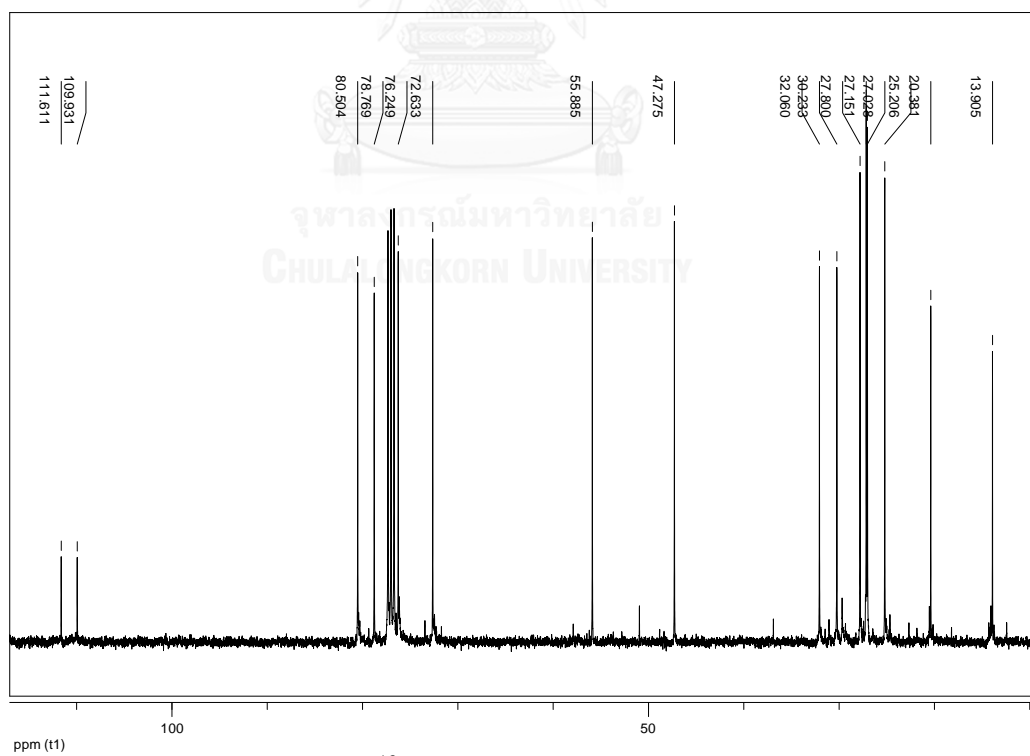
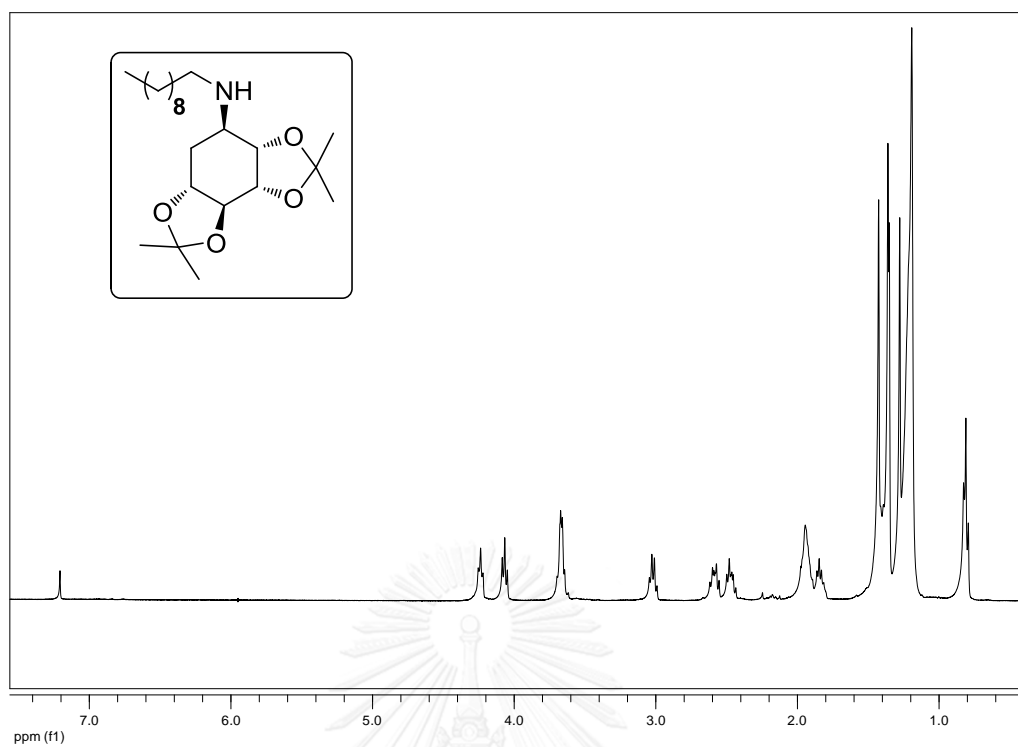
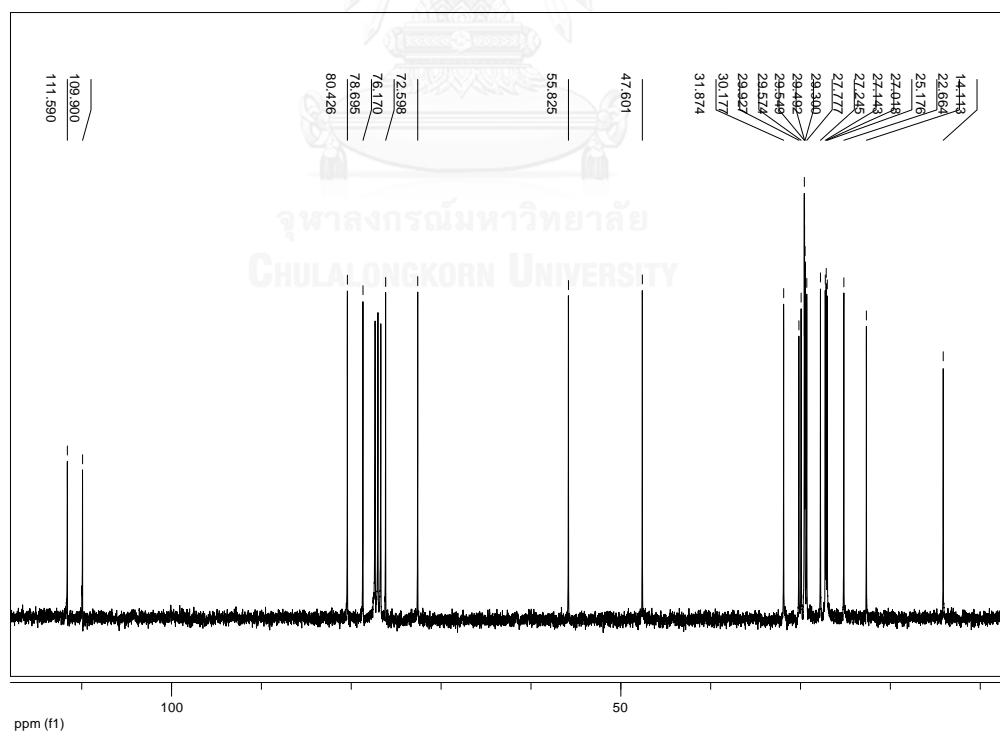
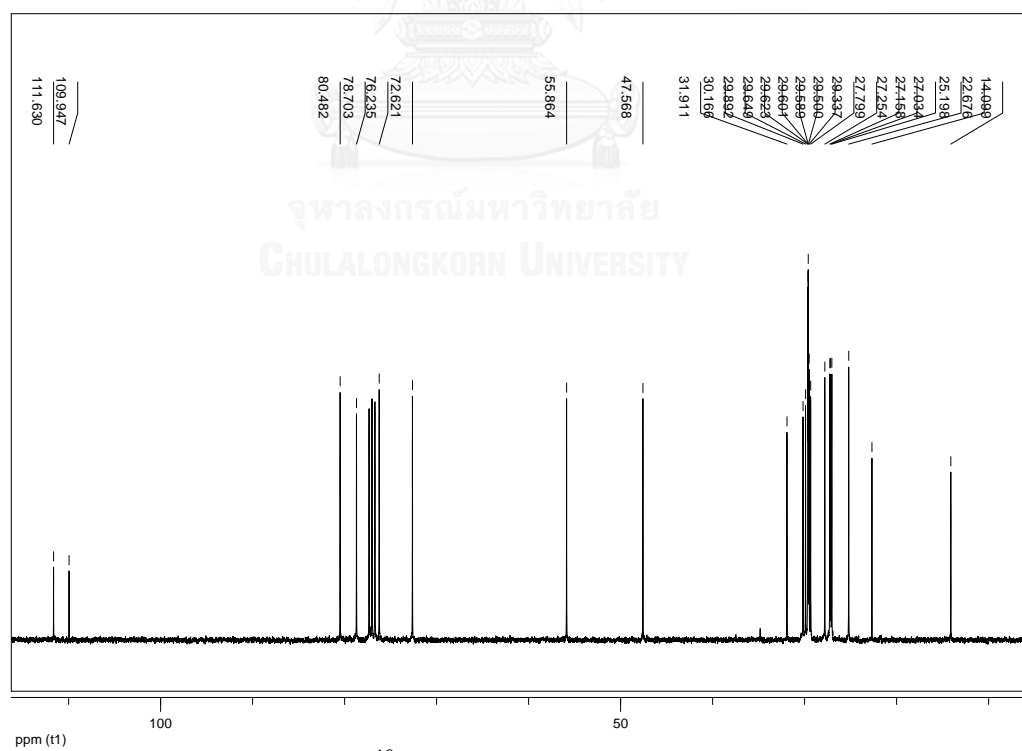
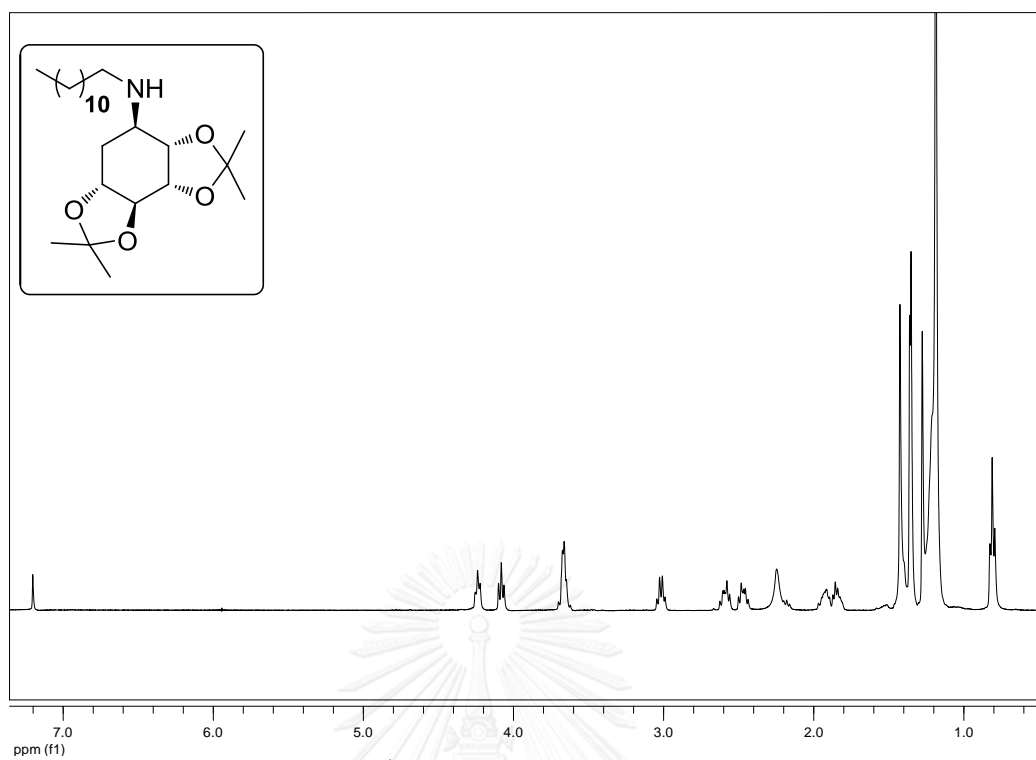


Figure 40. $^{13}\text{C NMR}$ spectrum of 3-18 (CDCl_3)

Figure 43. ^1H NMR spectrum of 3-20 (CDCl_3)Figure 44. ^{13}C NMR spectrum of 3-20 (CDCl_3)



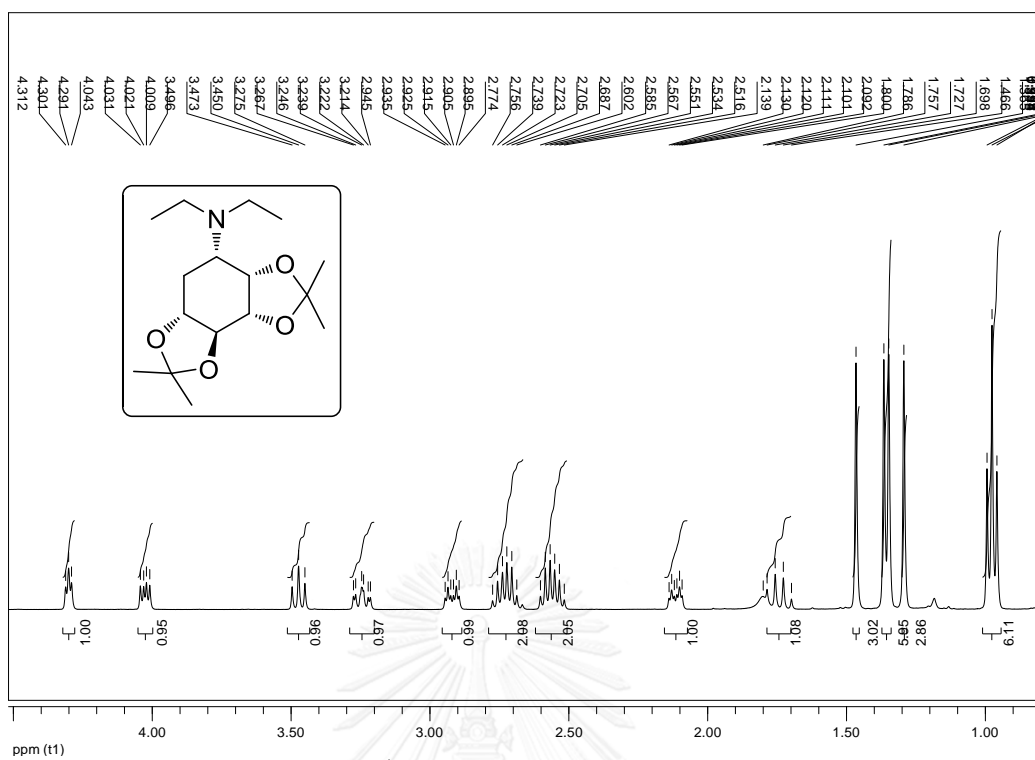


Figure 47. ^1H NMR spectrum of 3-22 (CDCl_3)

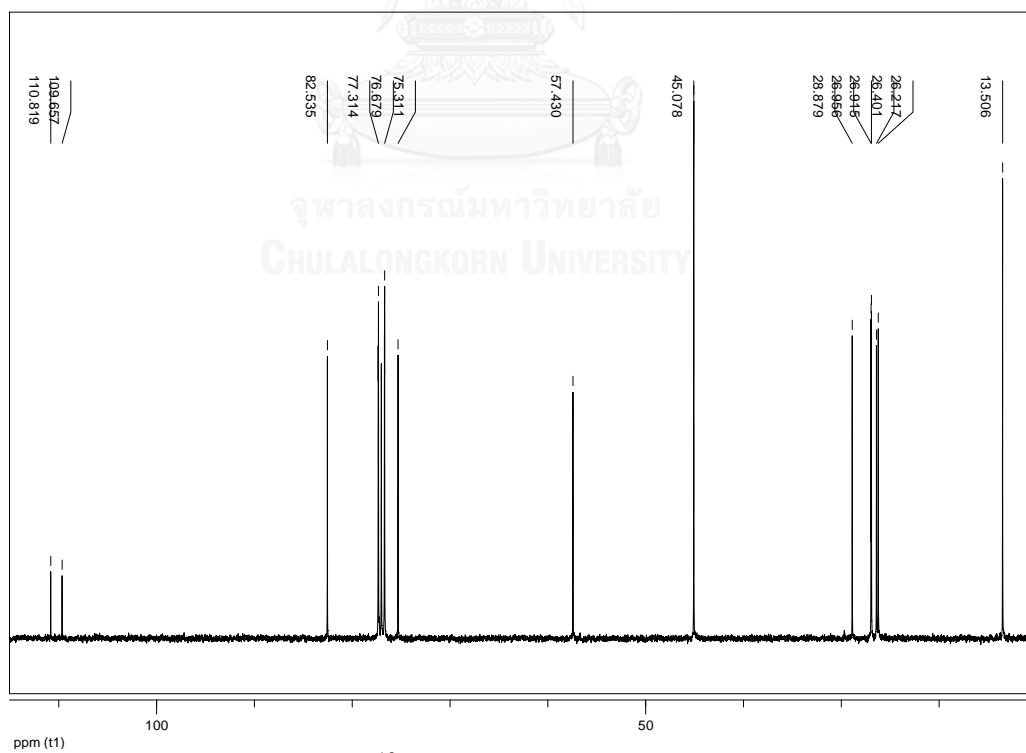


Figure 48. ^{13}C NMR spectrum of 3-22 (CDCl_3)

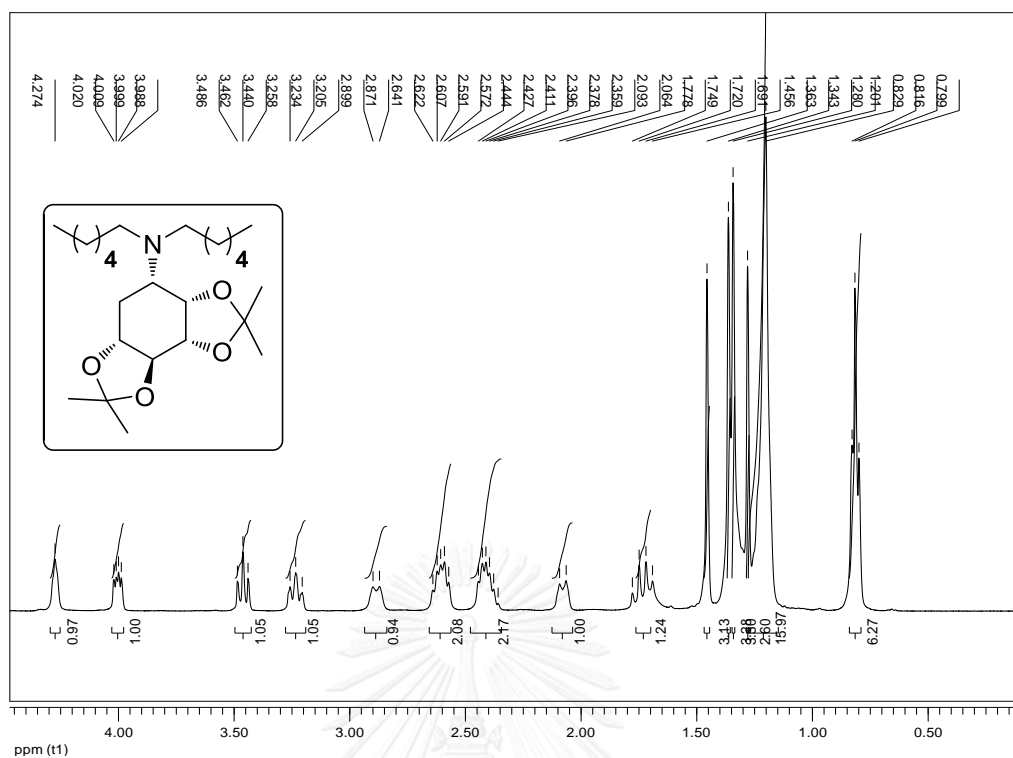


Figure 51. ^1H NMR spectrum of **3-24** (CDCl_3)

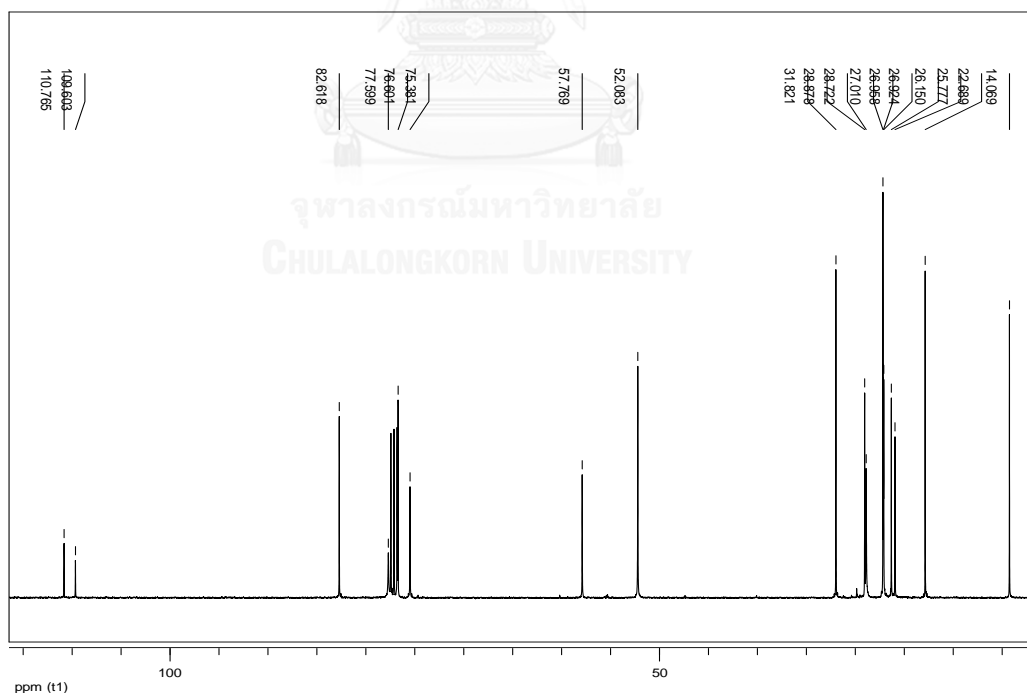
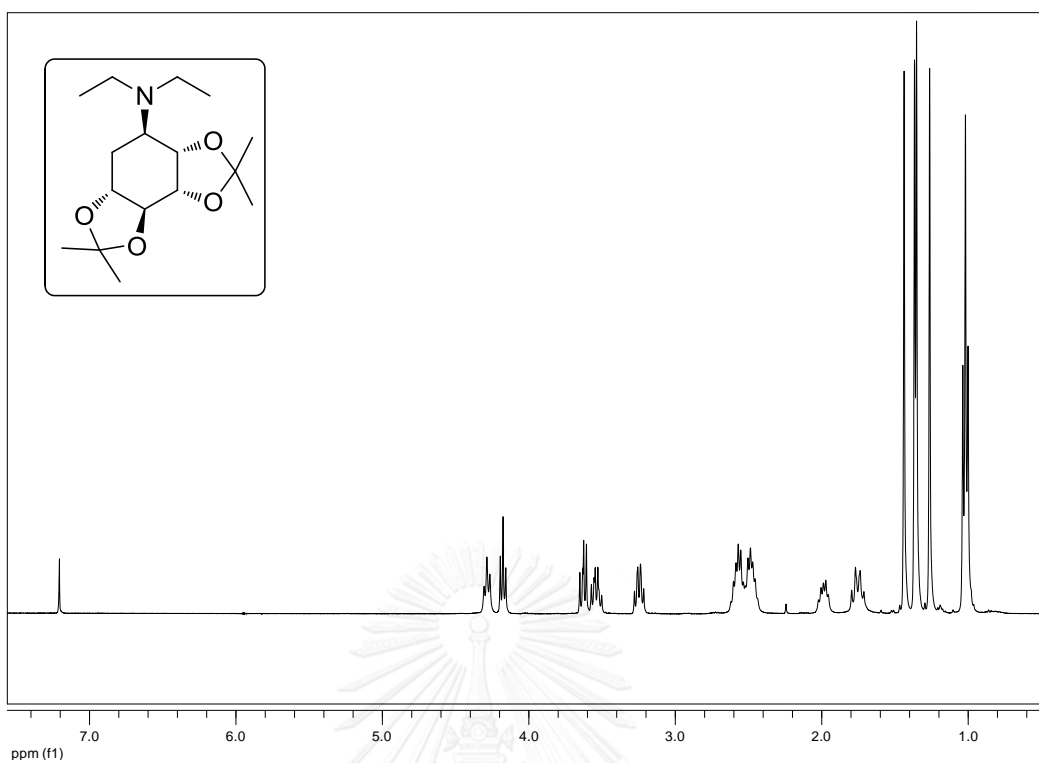
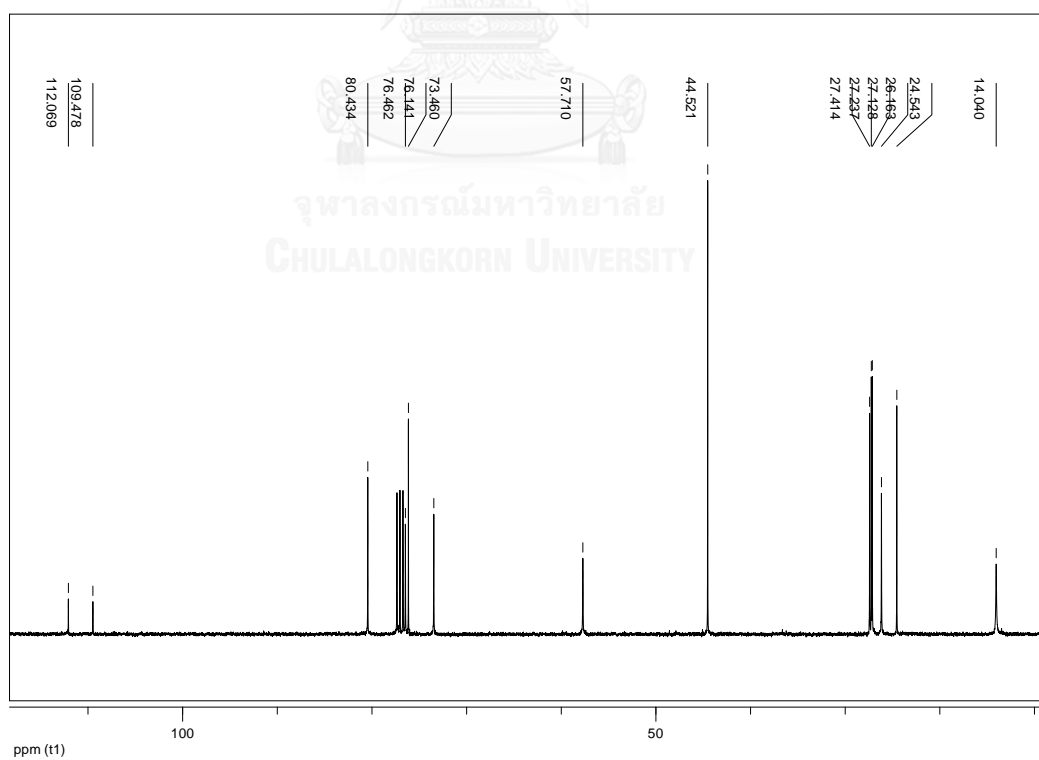
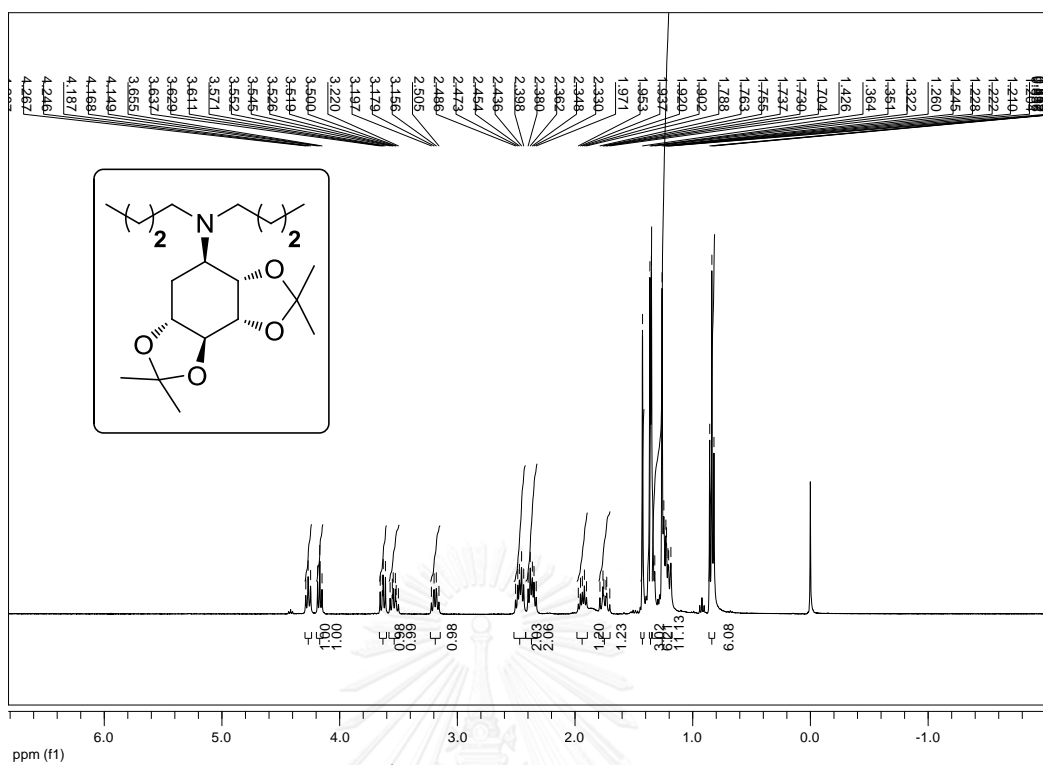
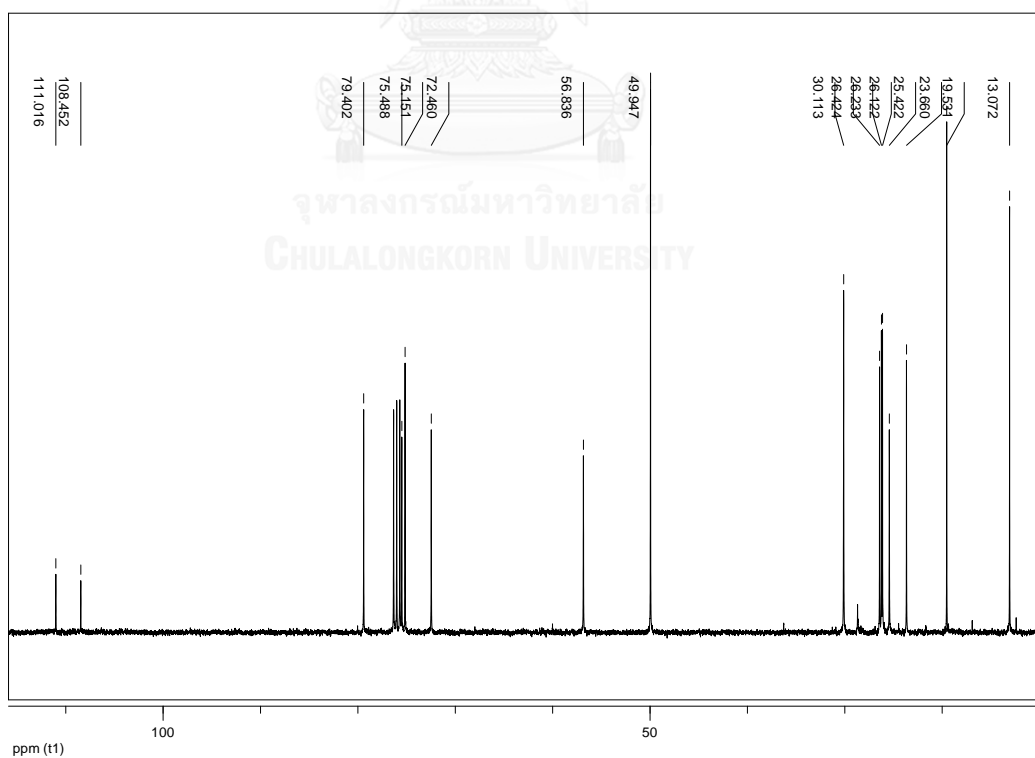


Figure 52. ^{13}C NMR spectrum of **3-24** (CDCl_3)

Figure 53. ^1H NMR spectrum of 3-25 (CDCl_3)Figure 54. ^{13}C NMR spectrum of 3-25 (CDCl_3)

Figure 55. ^1H NMR spectrum of 3-26 (CDCl_3)Figure 56. ^{13}C NMR spectrum of 3-26 (CDCl_3)

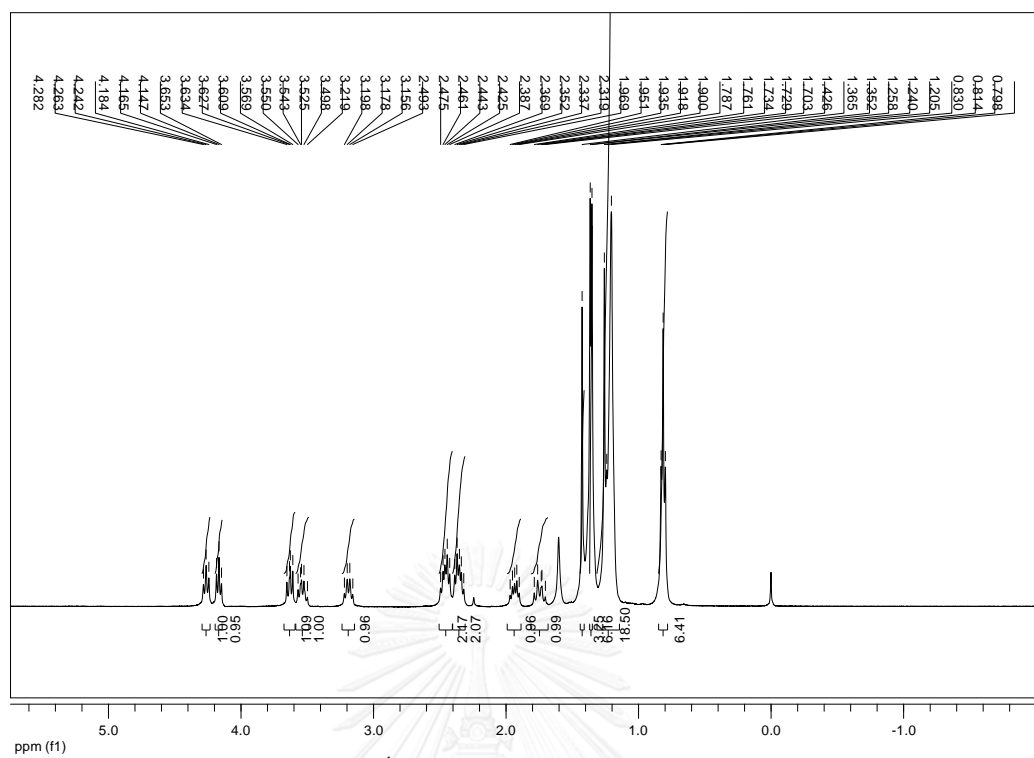


Figure 57. ¹H NMR spectrum of 3-27 (CDCl₃)

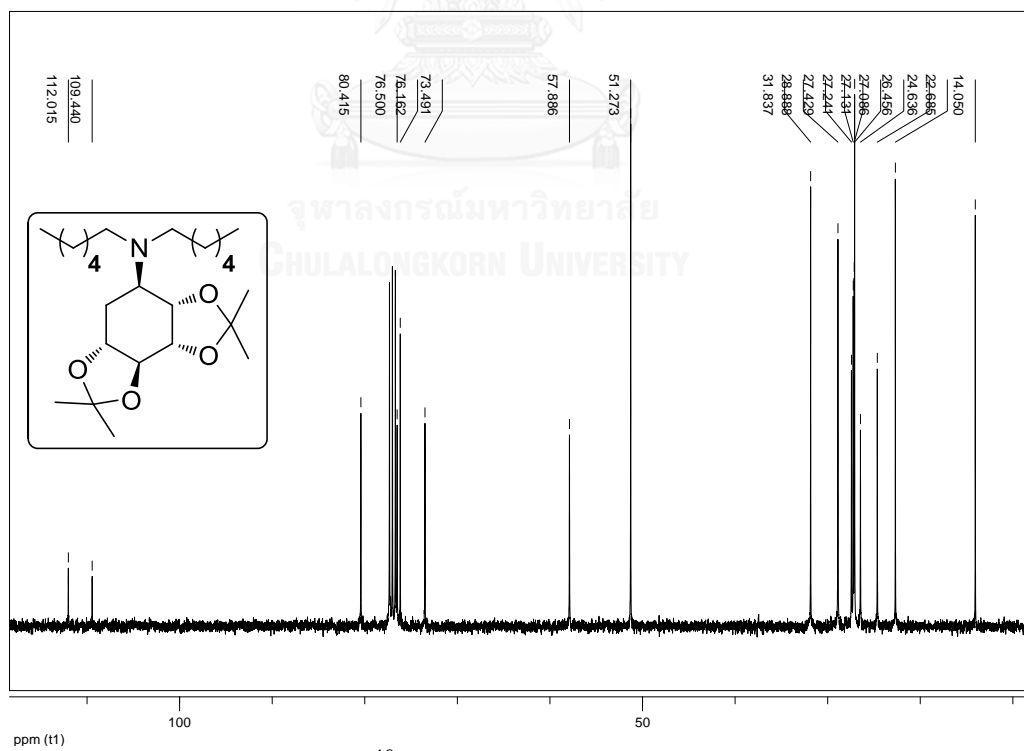


Figure 58. ¹³C NMR spectrum of 3-27 (CDCl₃)

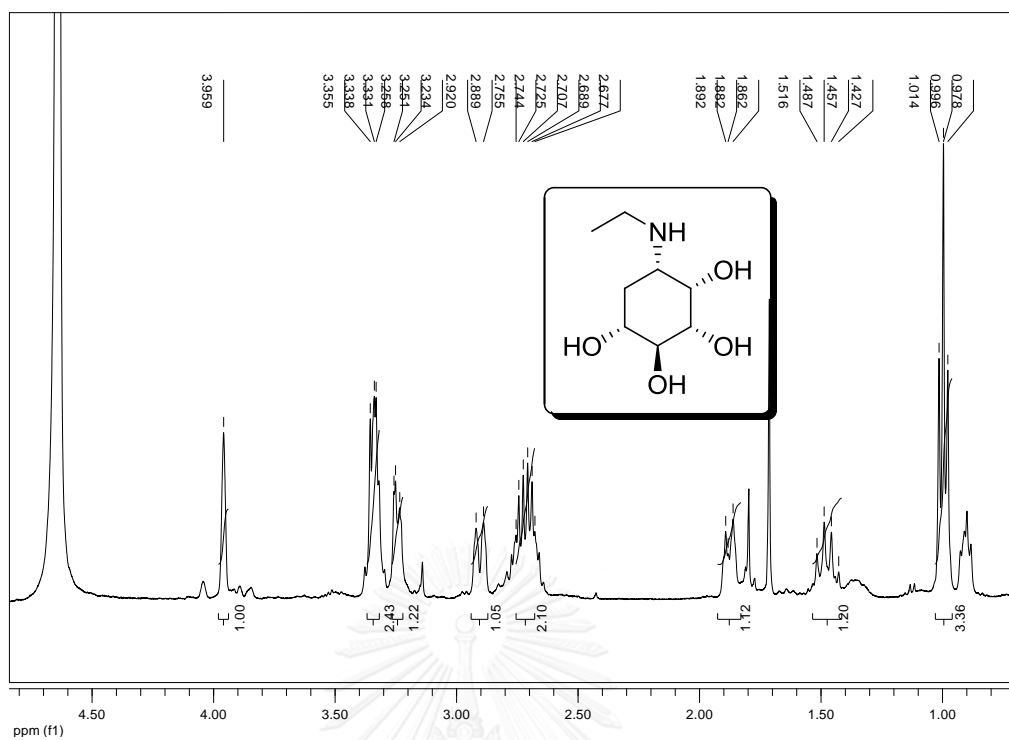


Figure 59. ^1H NMR spectrum of 3-28 (D_2O)

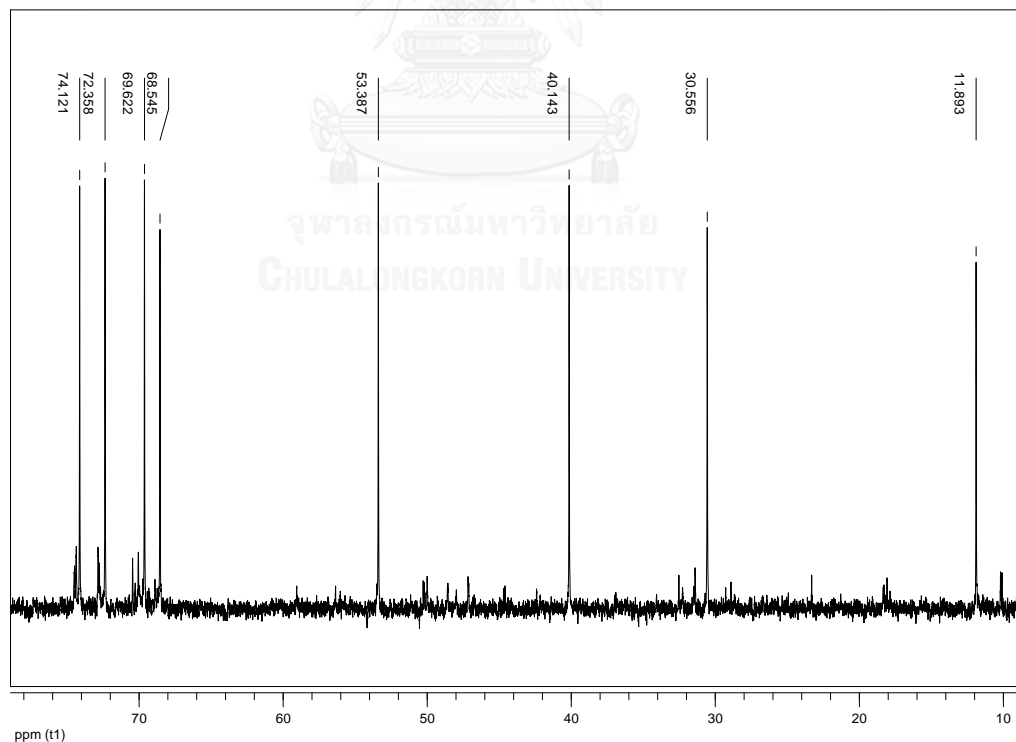


Figure 60. ^{13}C NMR spectrum of 3-28 (D_2O)

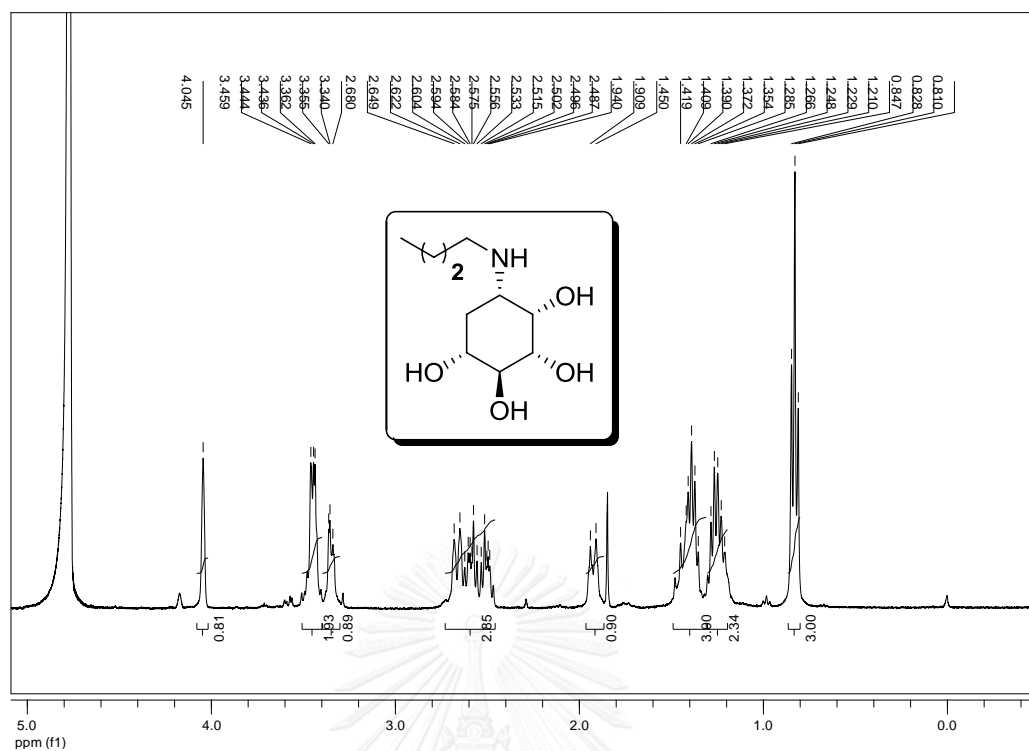


Figure 61. ^1H NMR spectrum of 3-29 (D_2O)

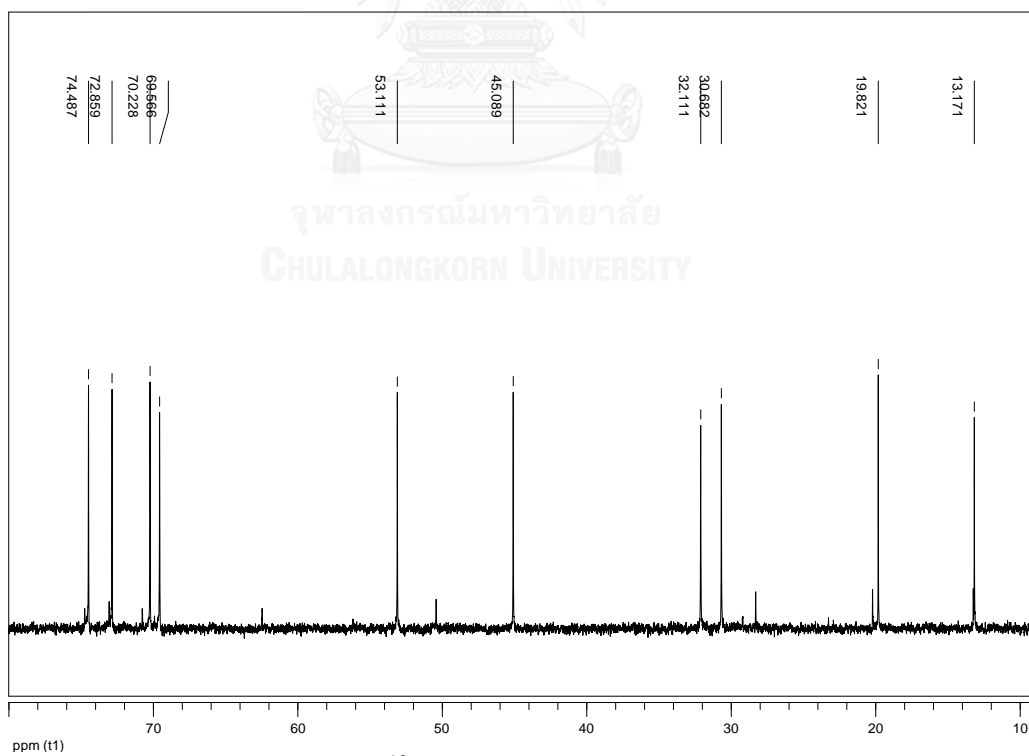
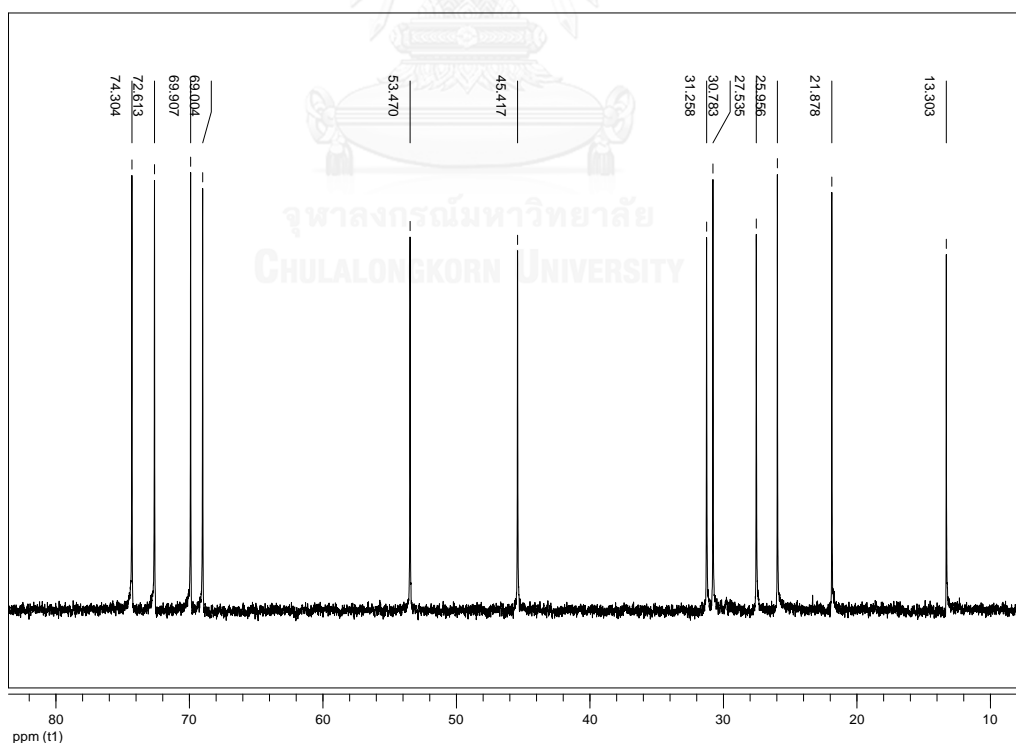
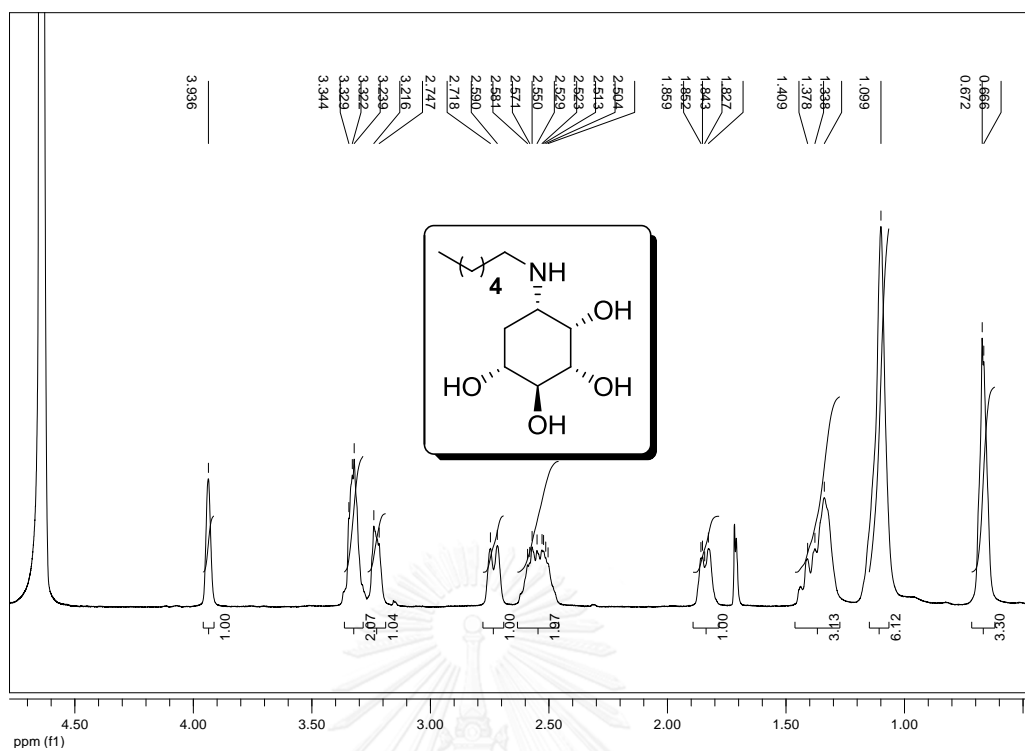


Figure 62. ^{13}C NMR spectrum of 3-29 (D_2O)



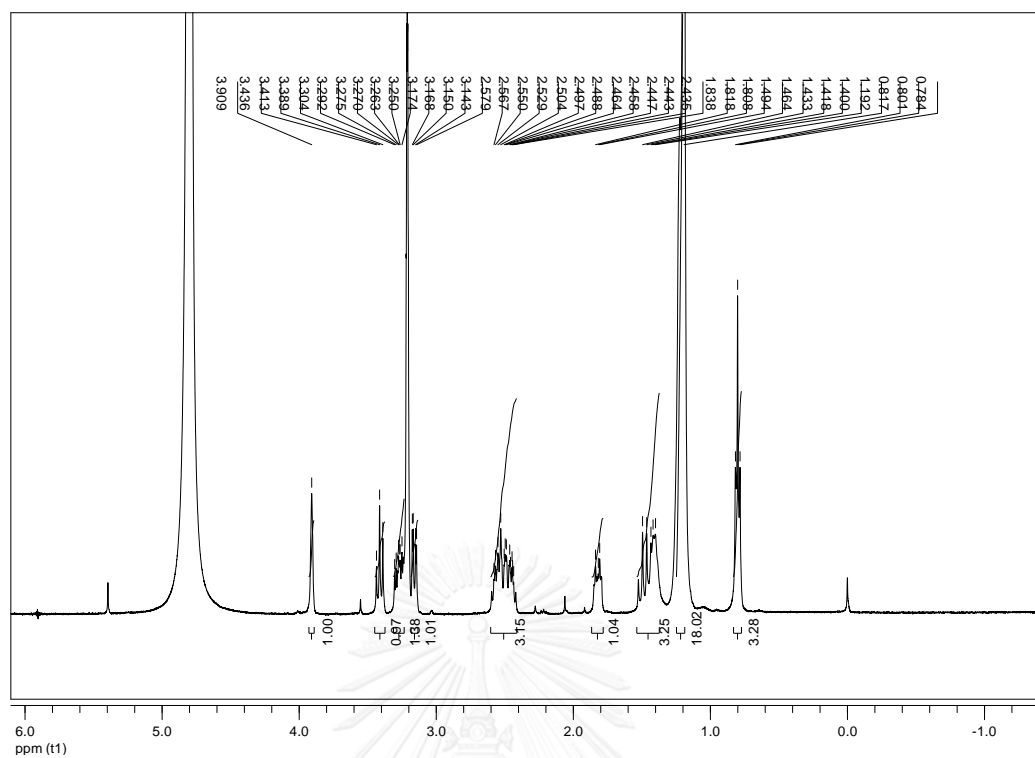


Figure 67. ¹H NMR spectrum of 3-32 (CD₃OD)

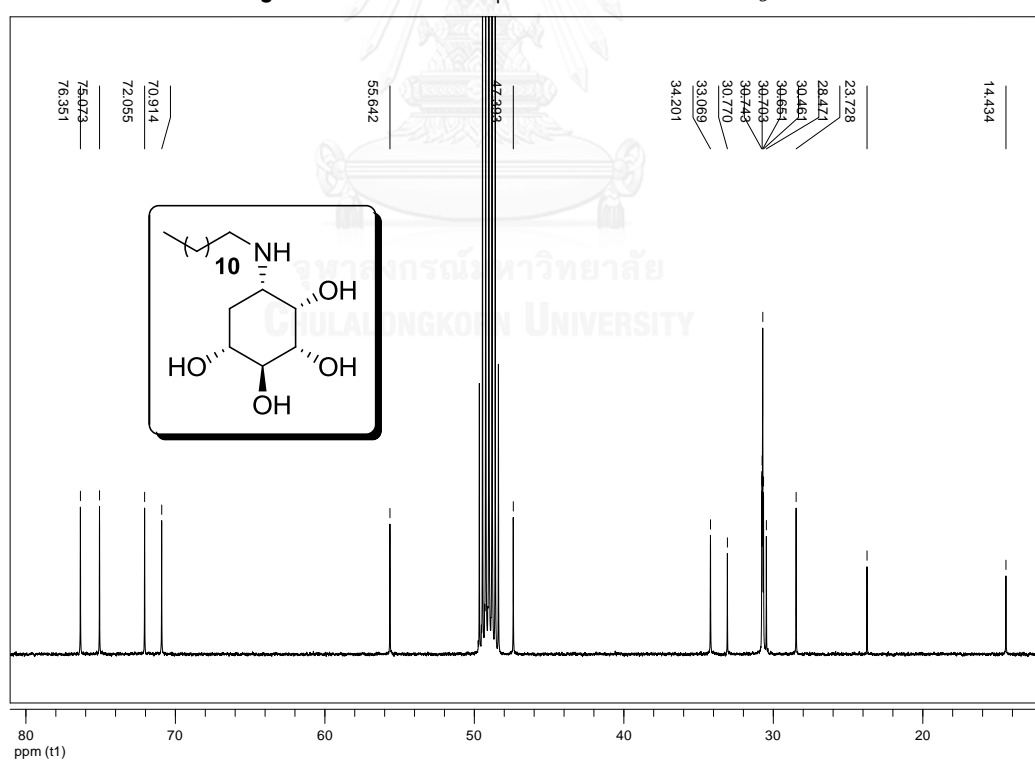
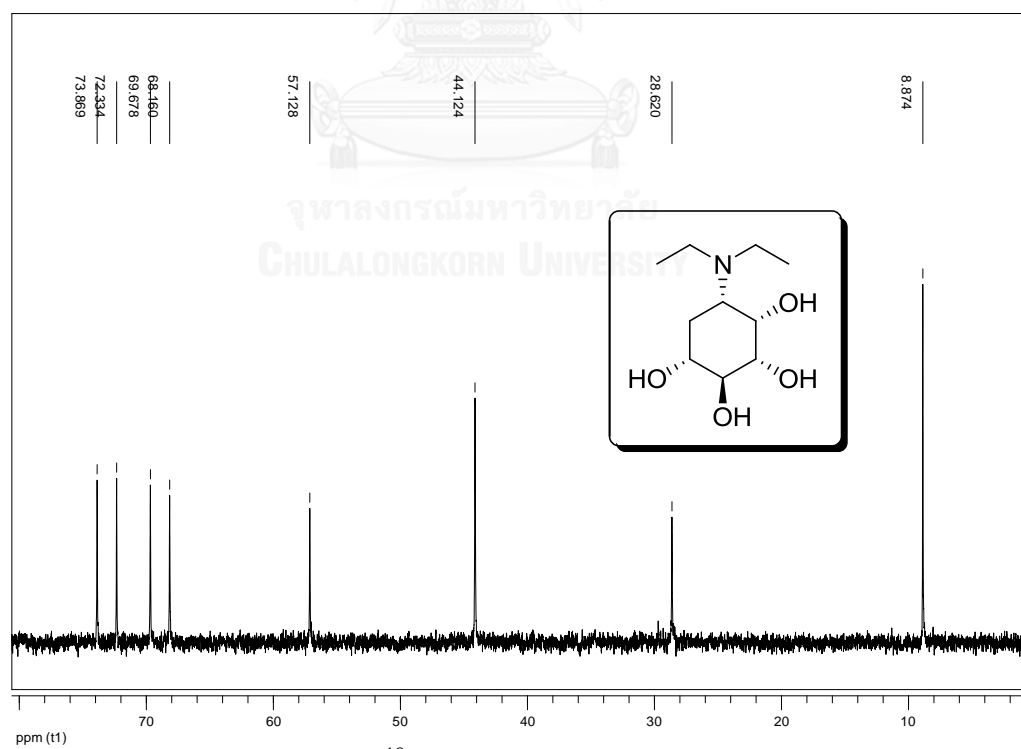
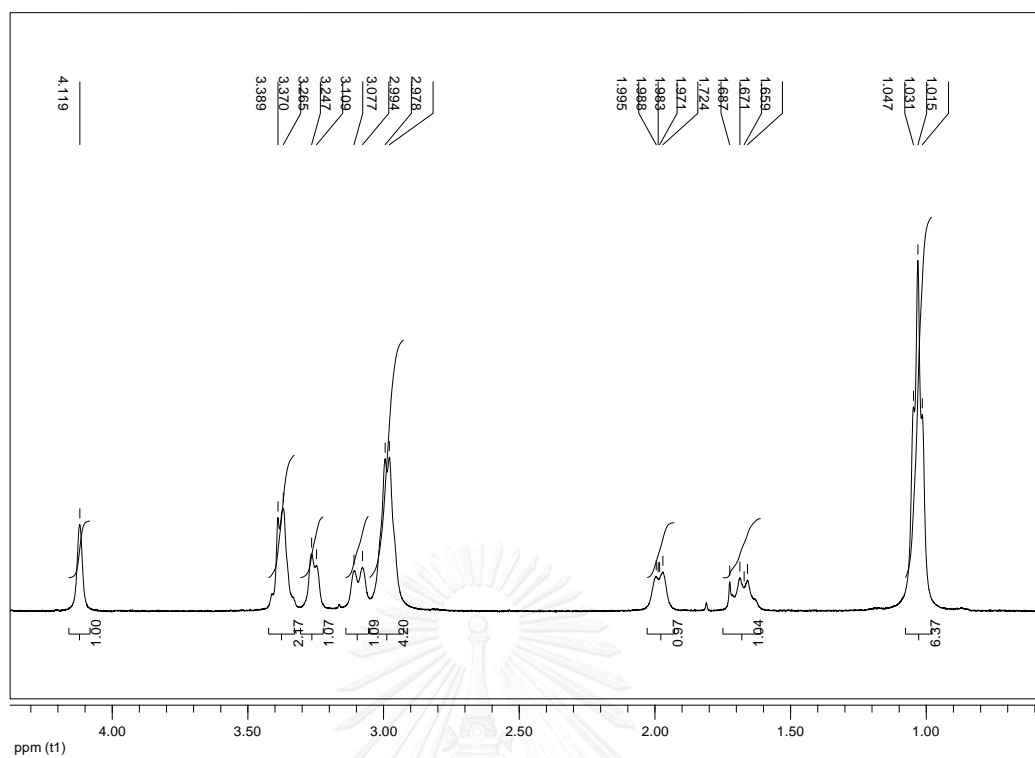


Figure 68. ¹³C NMR spectrum of 3-32 (CD₃OD)



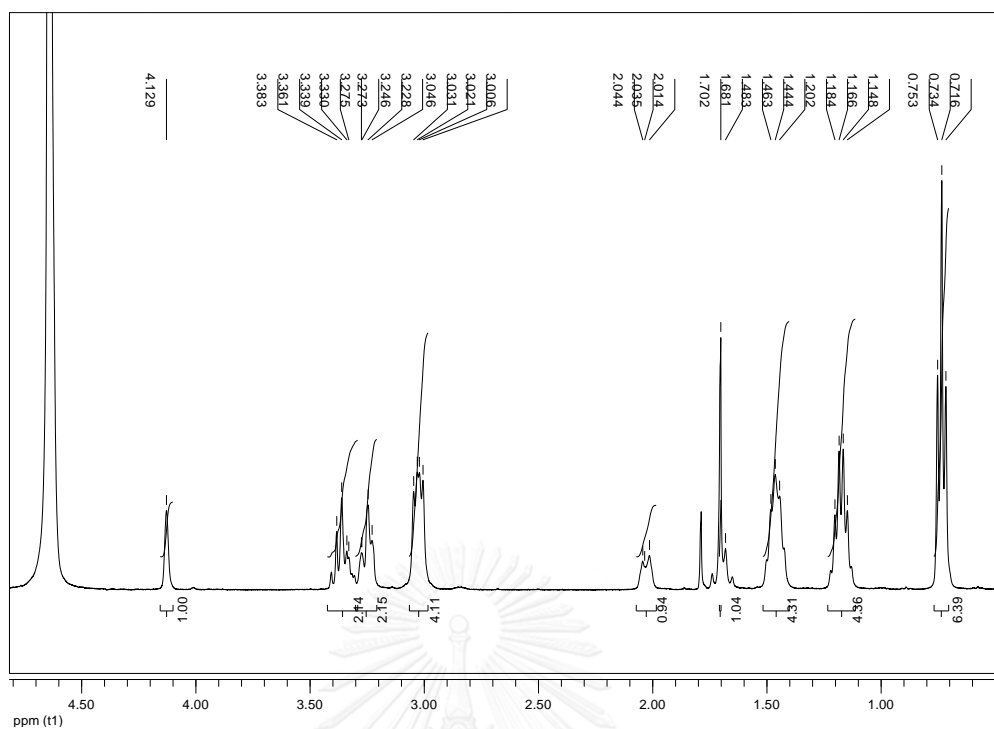


Figure 71. ^1H NMR spectrum of 3-38 (D_2O)

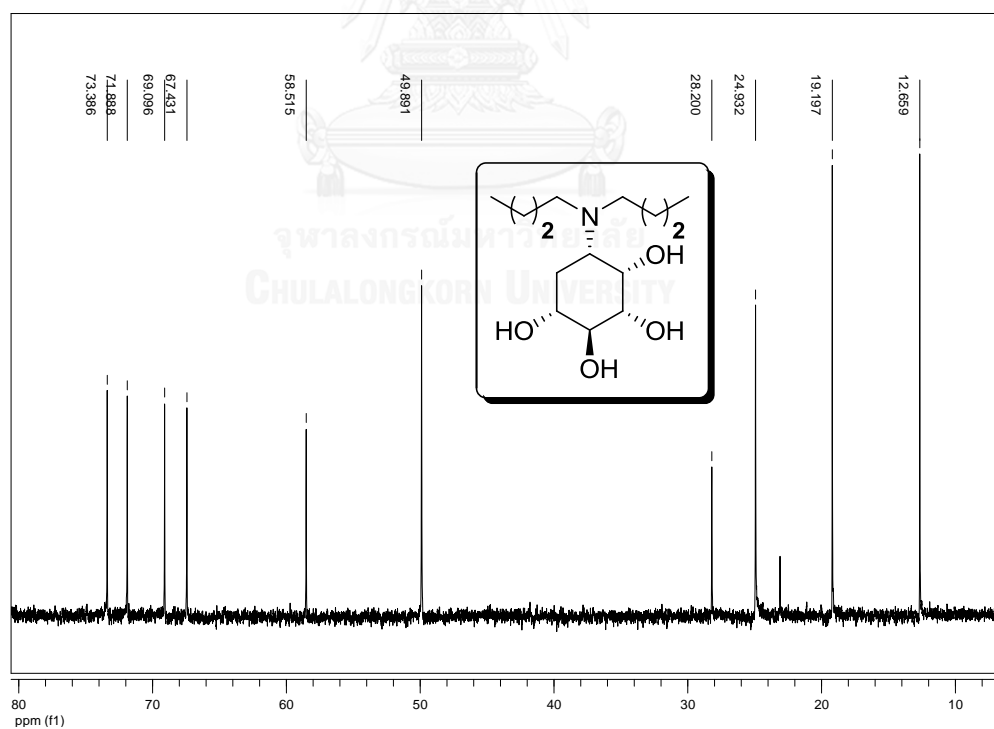


Figure 72. ^{13}C NMR spectrum of 3-38 (D_2O)

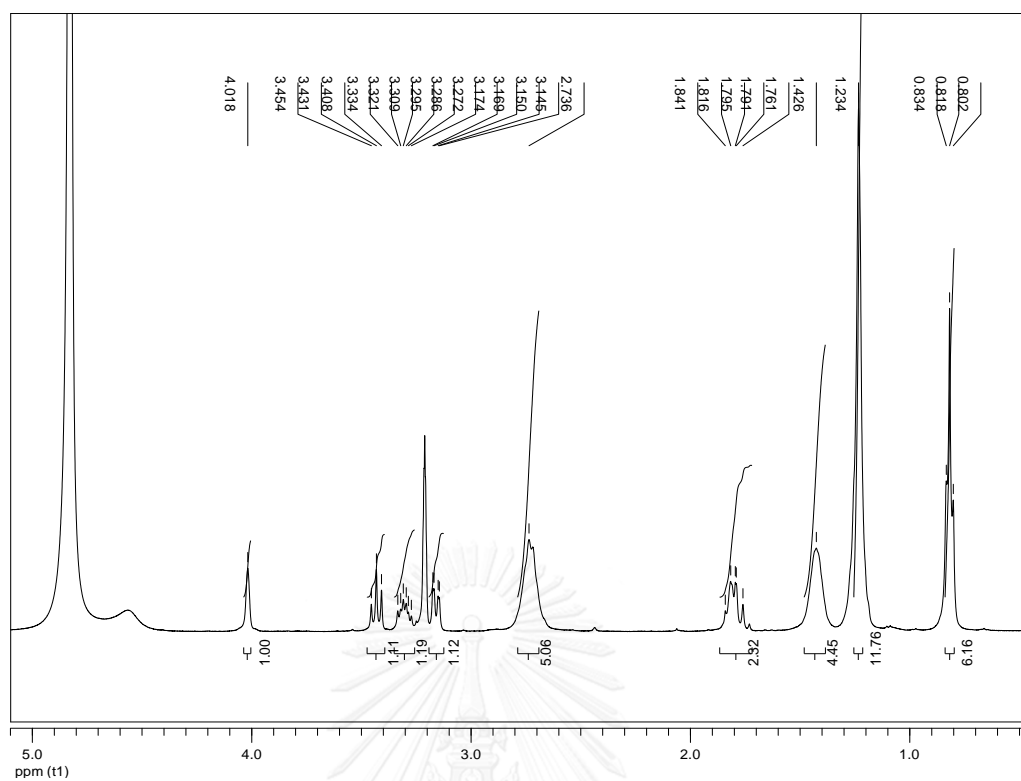


Figure 73. ^1H NMR spectrum of 3-39 (CD_3OD)

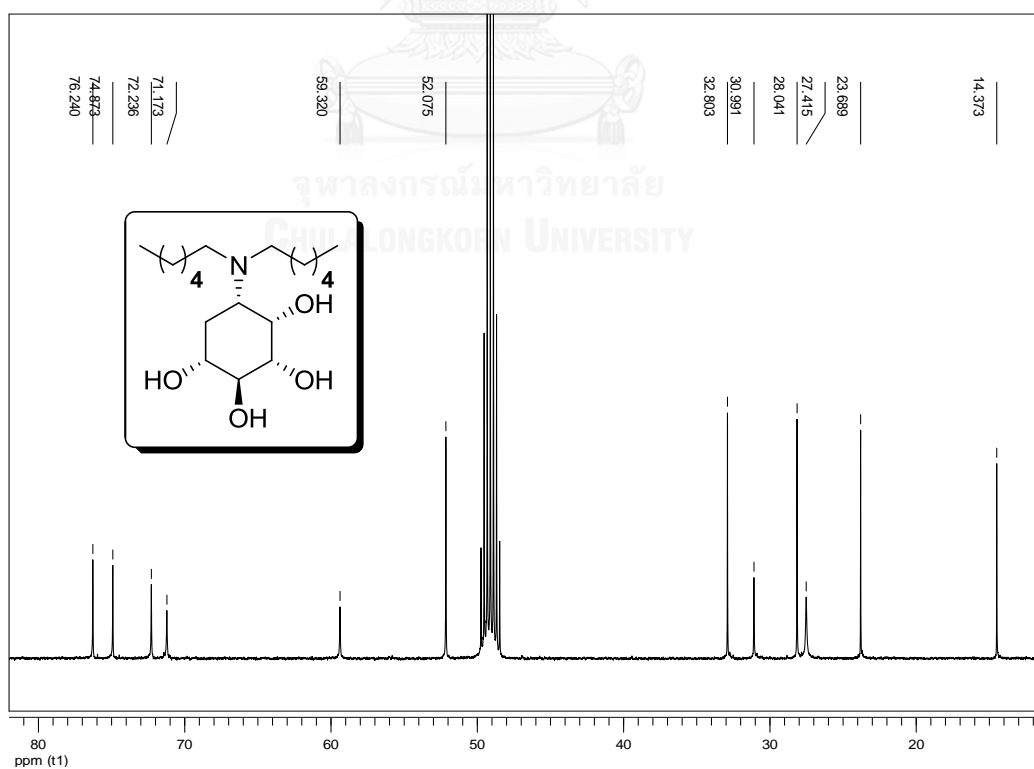


Figure 74. ^{13}C NMR spectrum of 3-39 (CD_3OD)

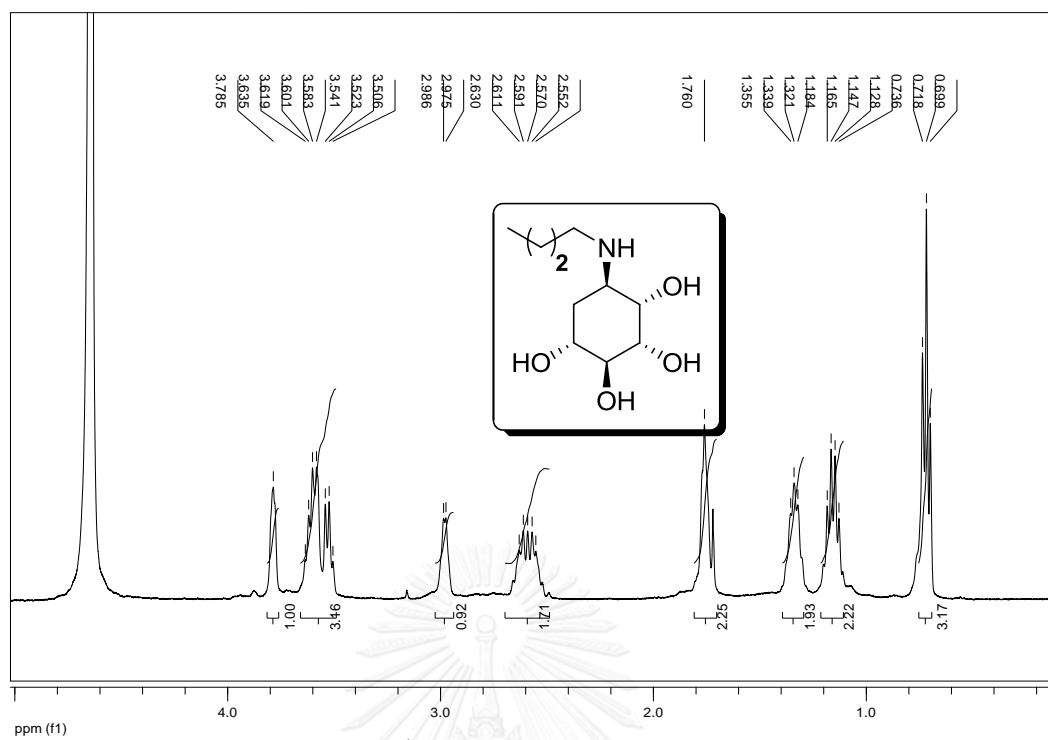


Figure 75. ^1H NMR spectrum of 3-33 (D_2O)

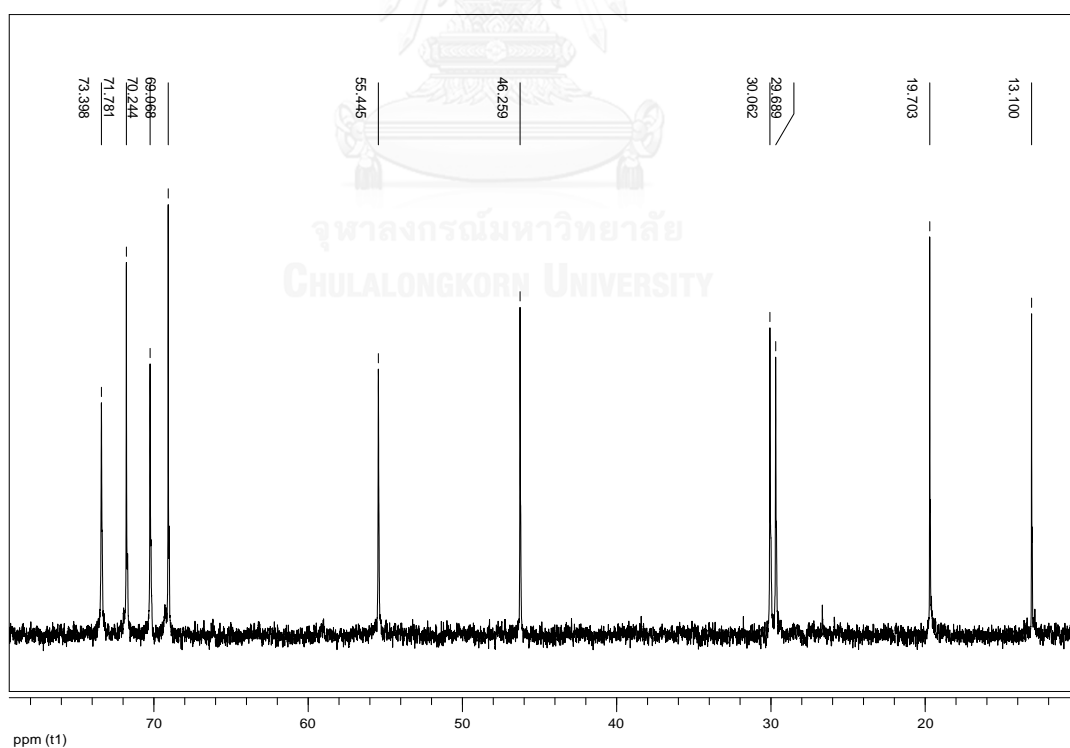
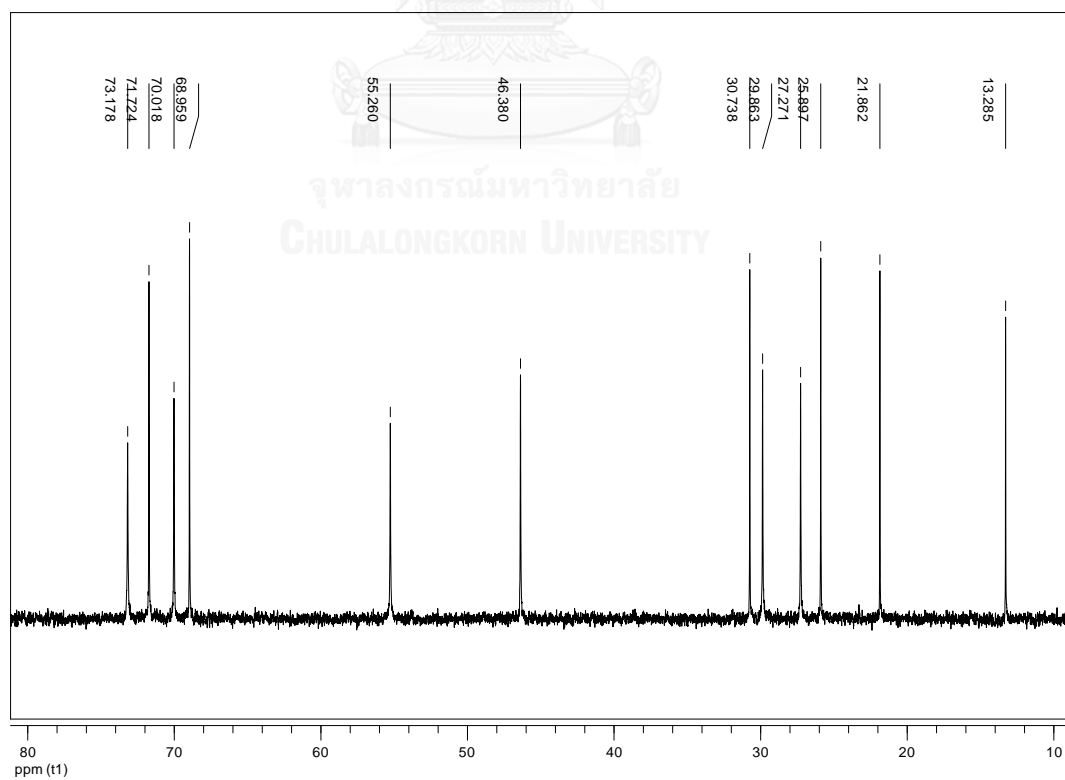
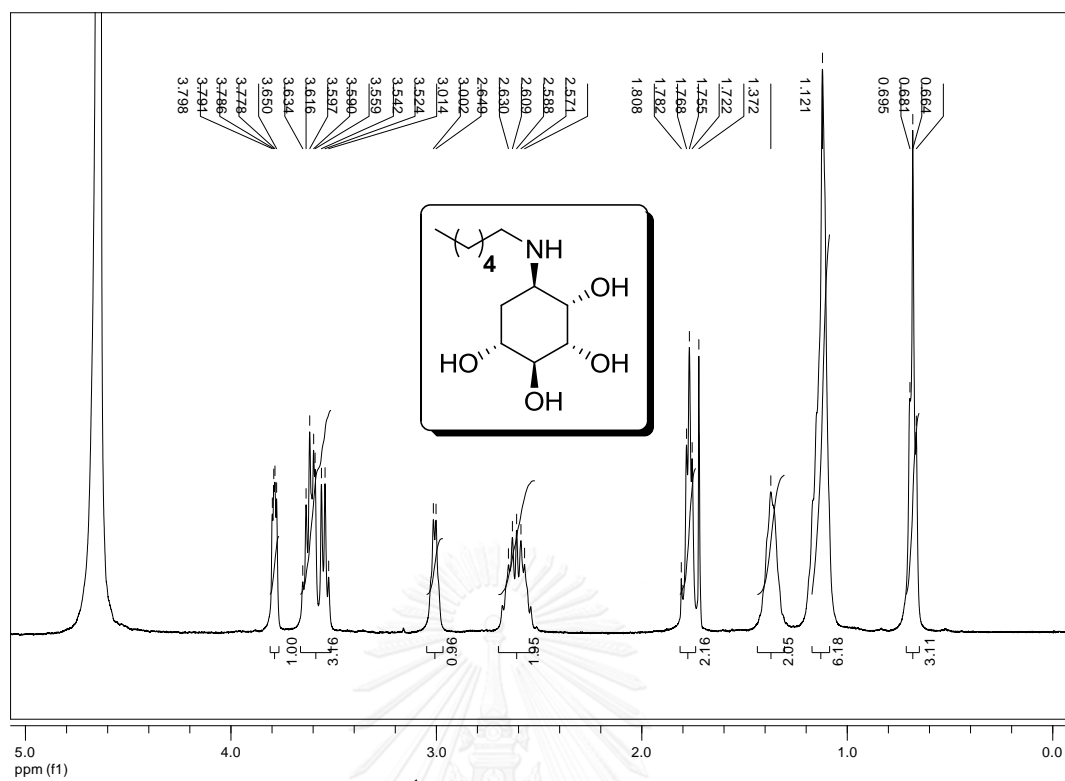


Figure 76. ^{13}C NMR spectrum of 3-33 (D_2O)



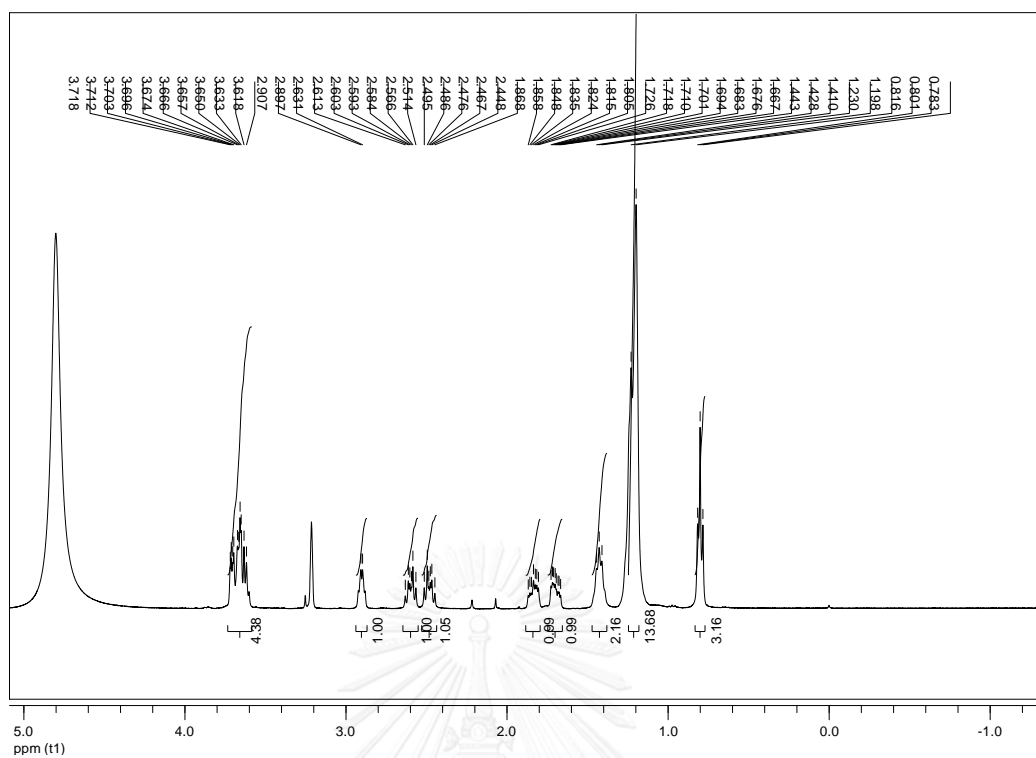


Figure 79. ¹H NMR spectrum of 3-35 (CD₃OD)

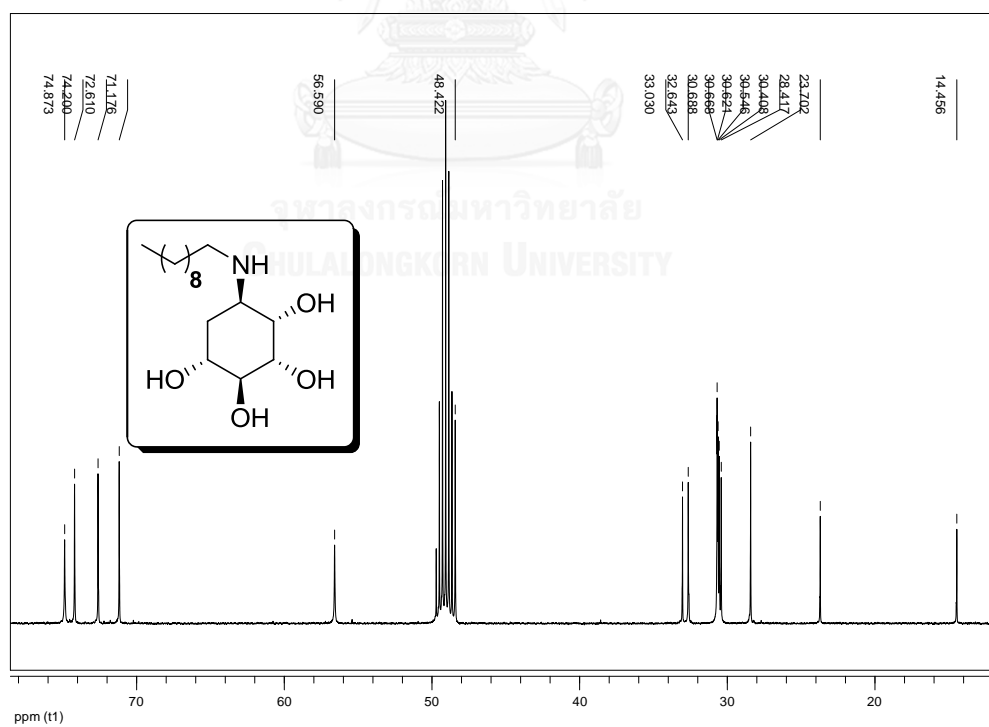


Figure 80. ¹³C NMR spectrum of 3-35 (CD₃OD)

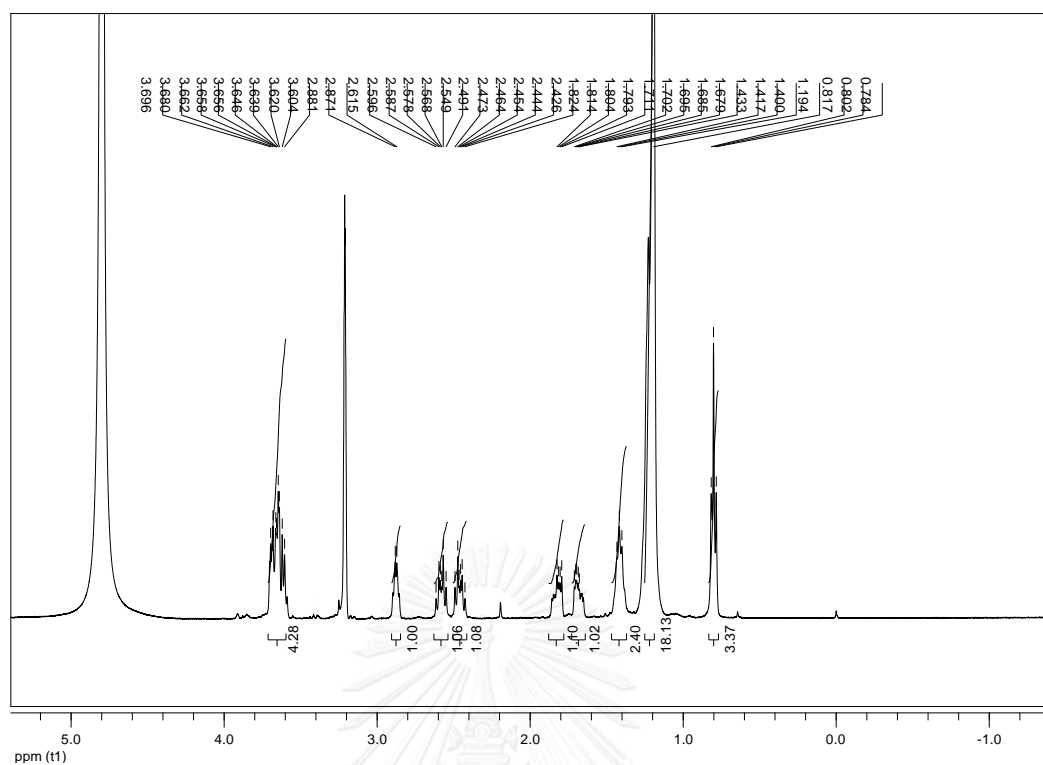


Figure 81. ^1H NMR spectrum of 3-36 (CD_3OD)

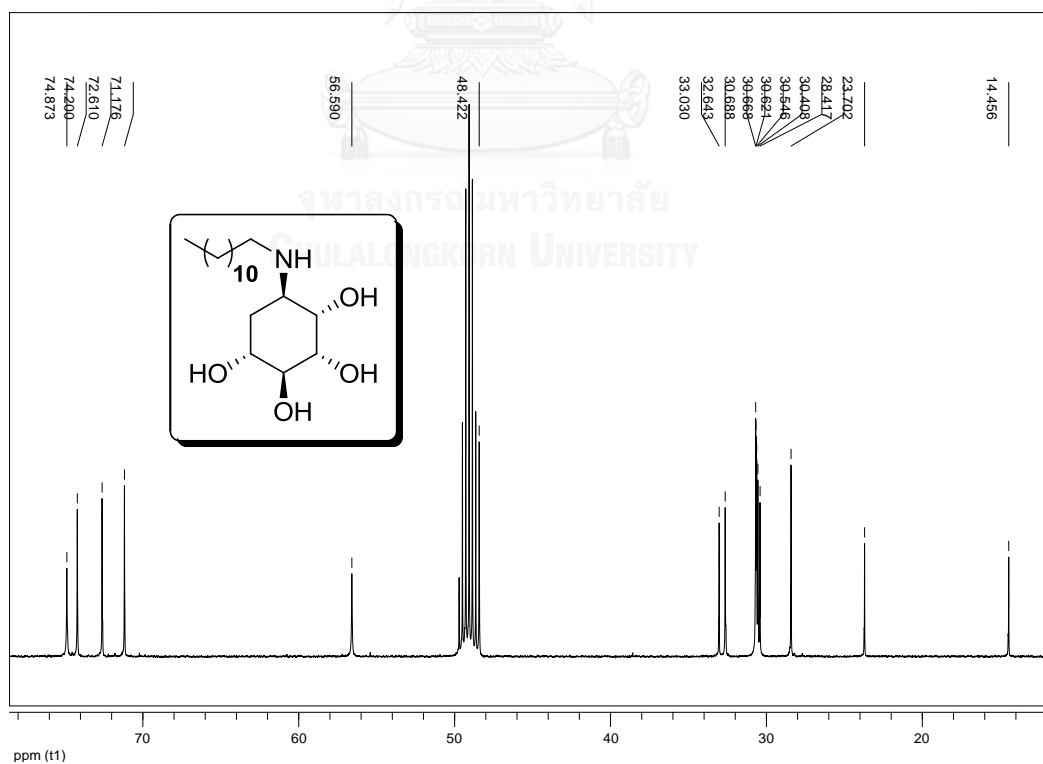
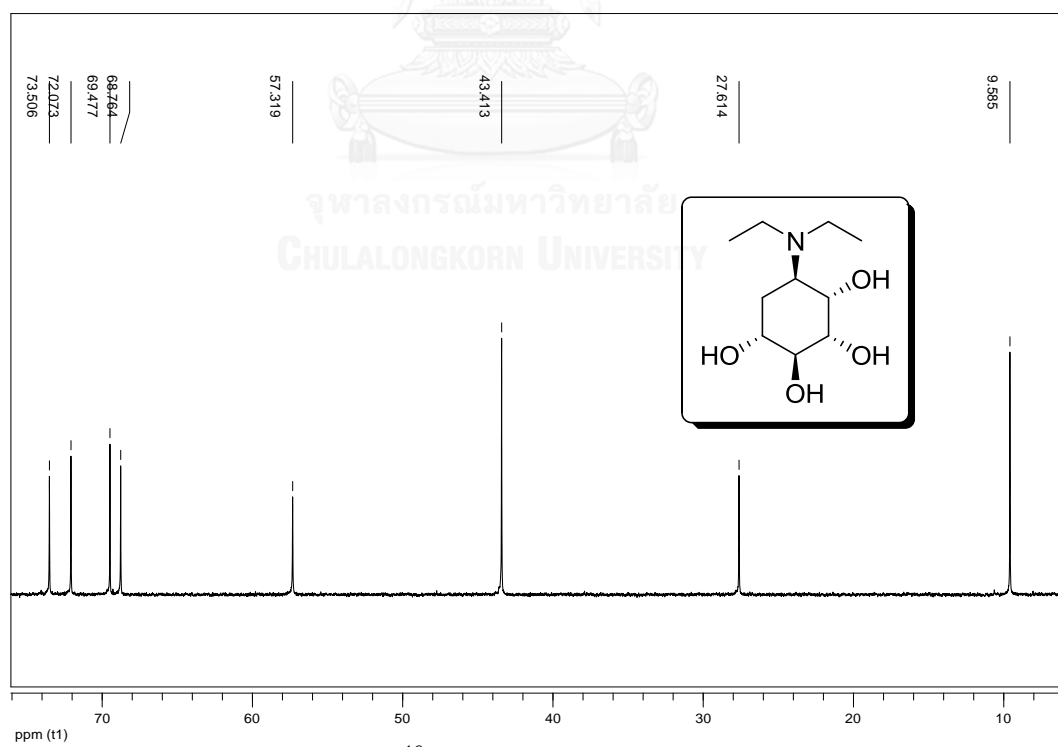
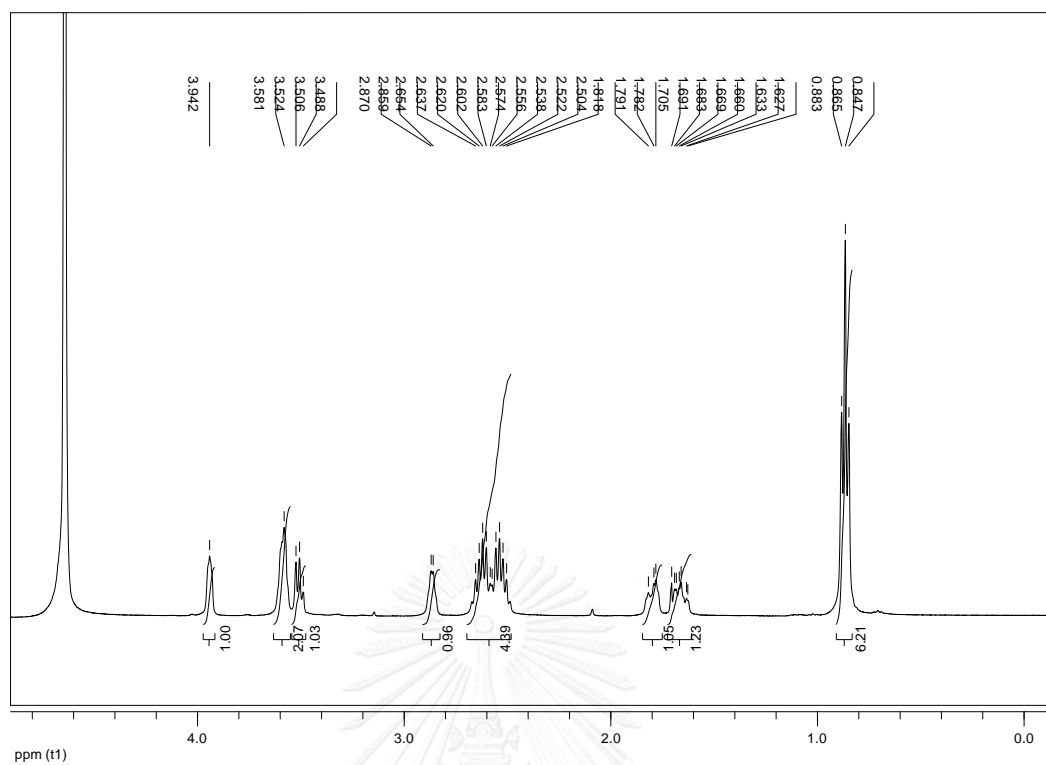


Figure 82. ^{13}C NMR spectrum of 3-36 (CD_3OD)



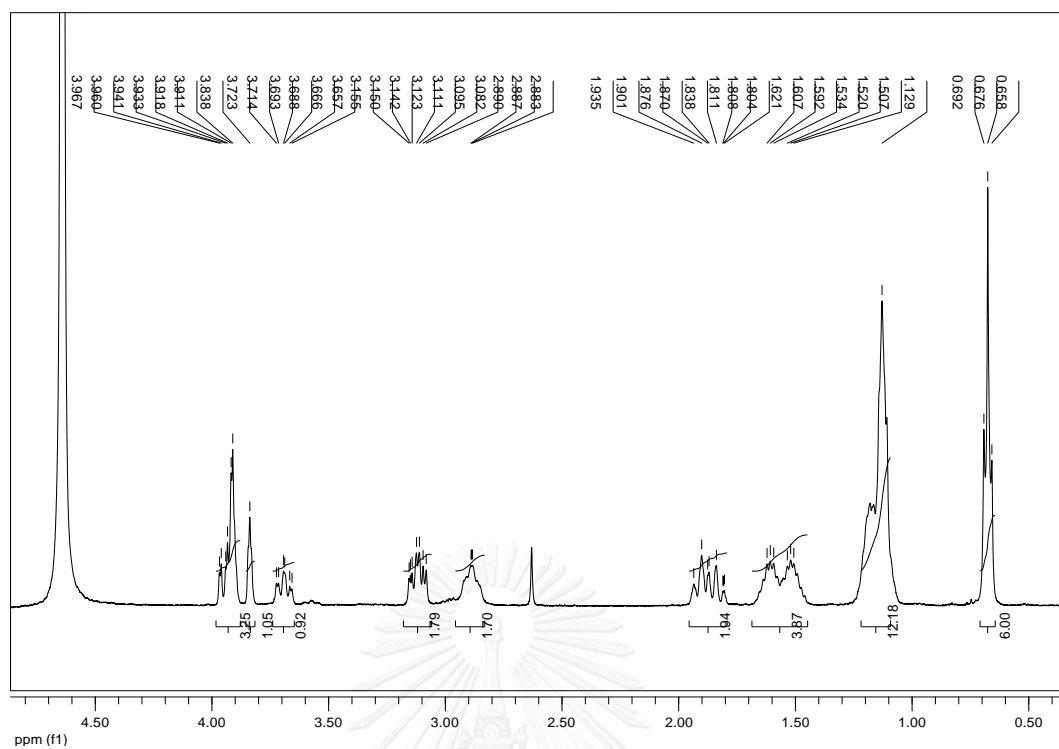


Figure 87. ^1H NMR spectrum of 3-42 (D_2O)

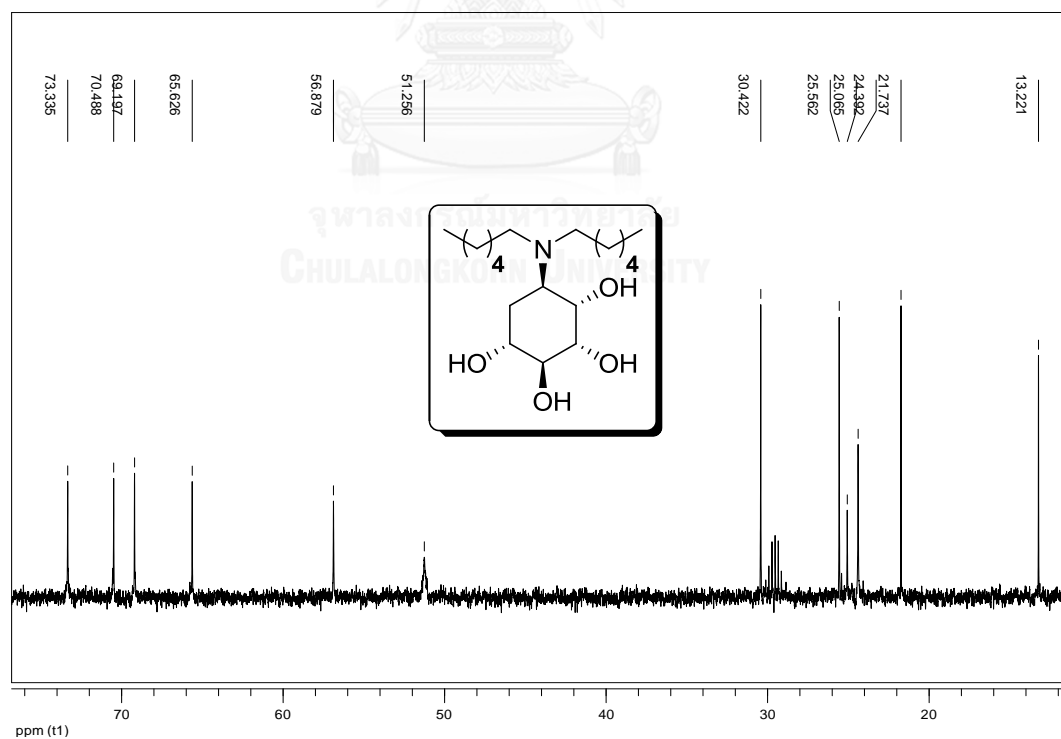


Figure 88. ^{13}C NMR spectrum of 3-42 (D_2O)

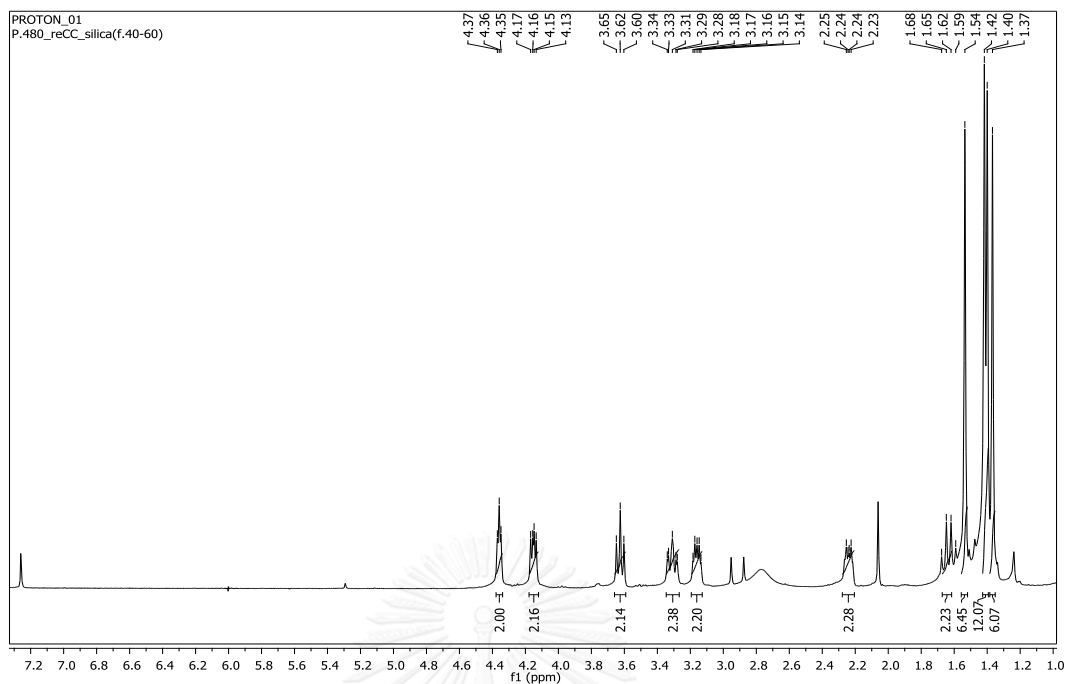


Figure 89. ^1H NMR spectrum of **4-4** (CDCl_3)

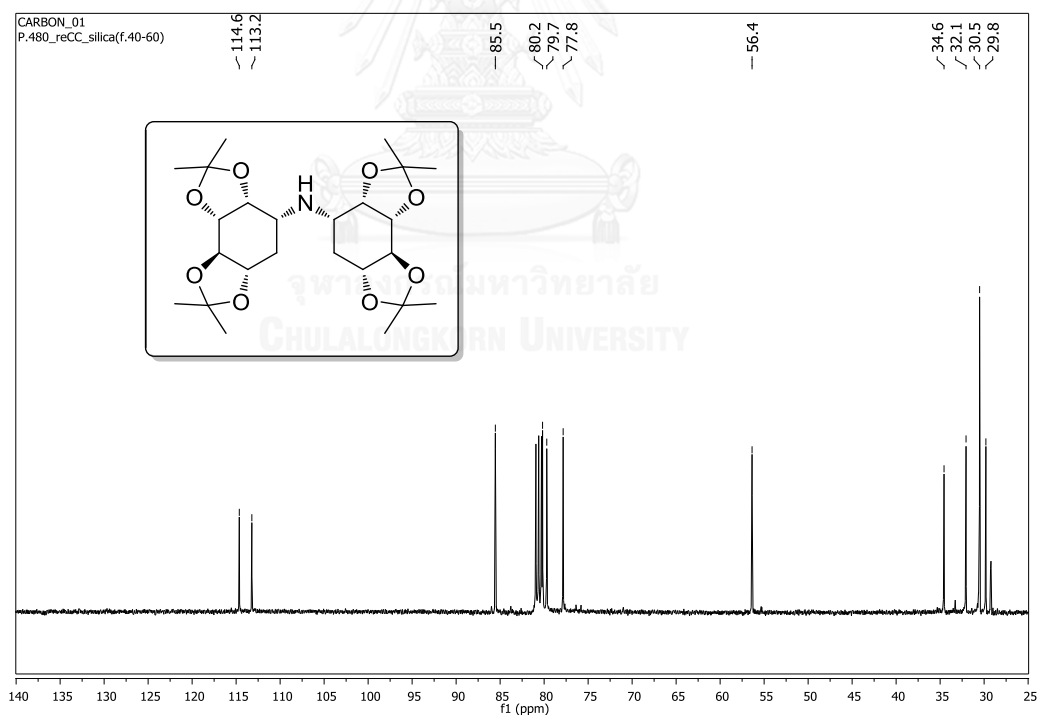


Figure 90. ^{13}C NMR spectrum of **4-4** (CDCl_3)

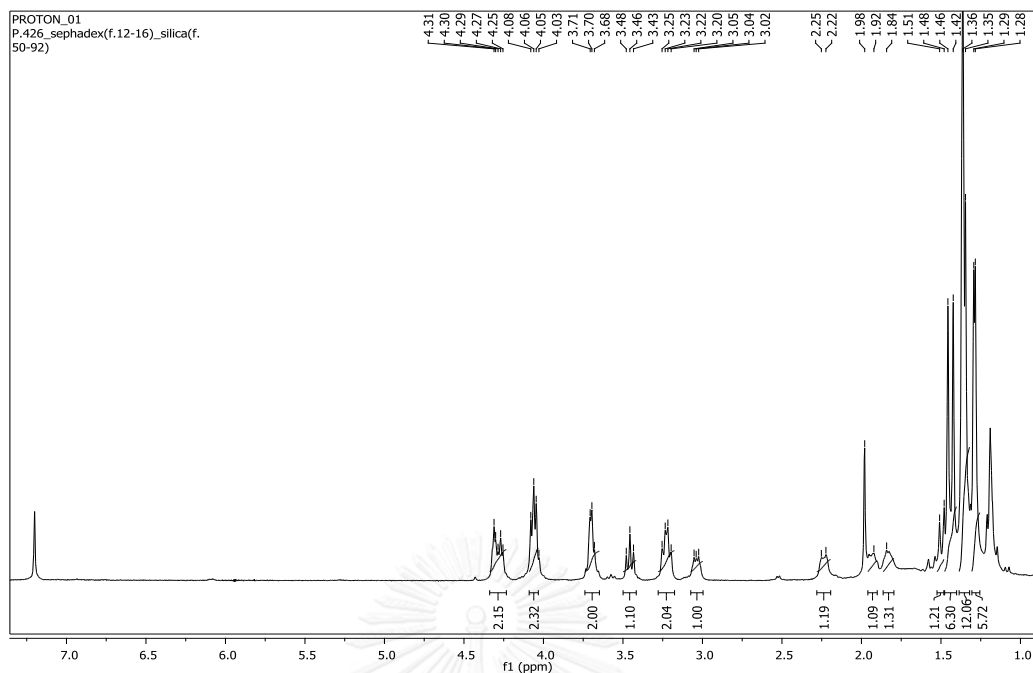


Figure 91. ^1H NMR spectrum of 4-6 (CDCl_3)

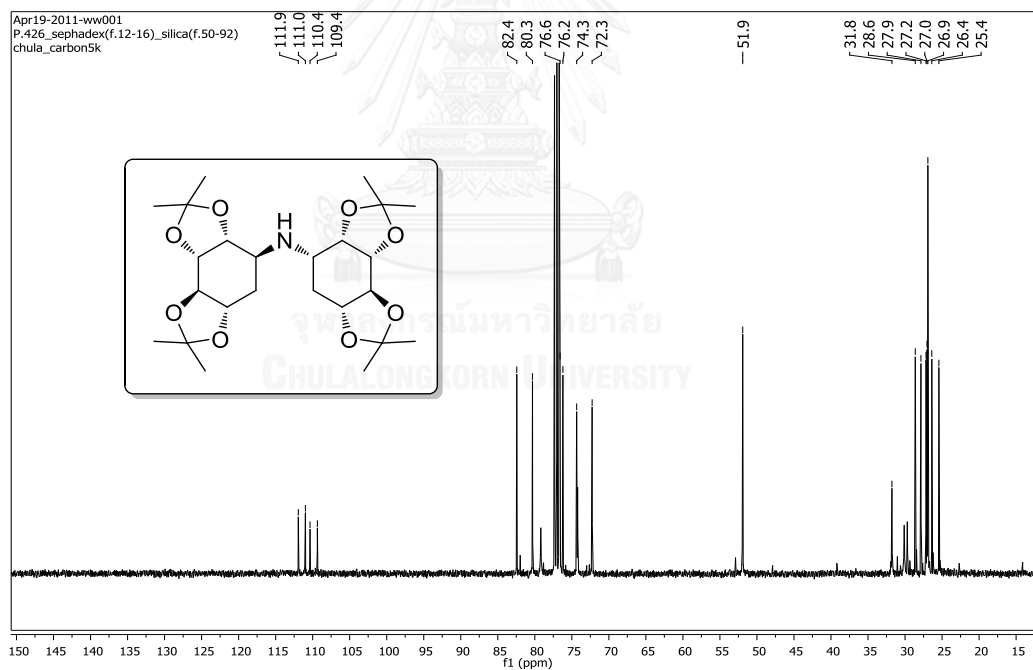


Figure 92. ^{13}C NMR spectrum of 4-6 (CDCl_3)

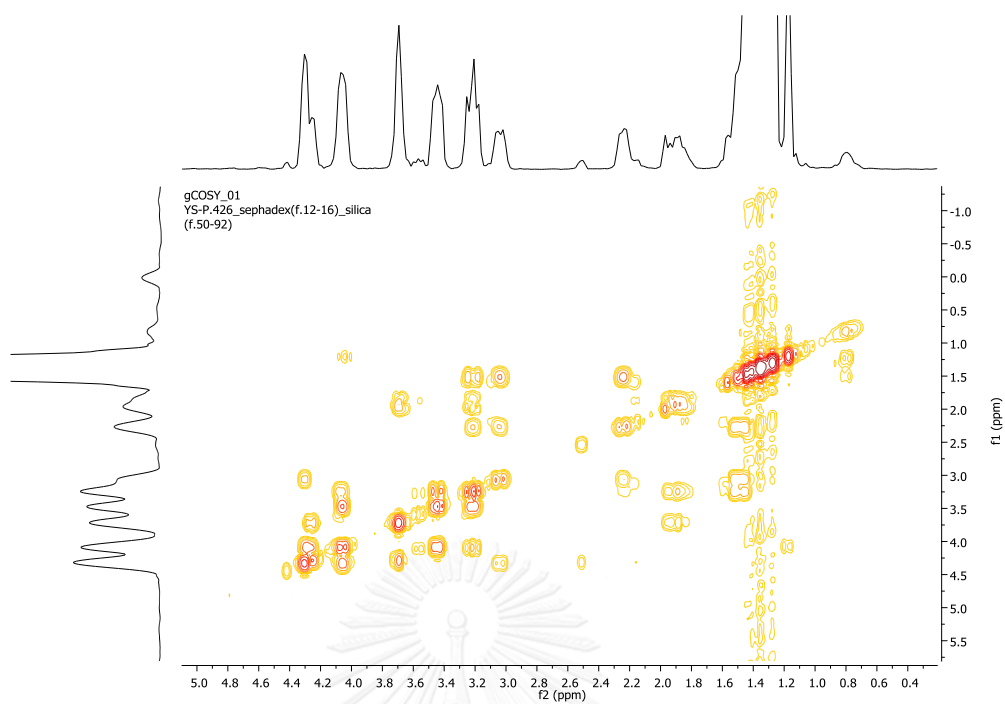
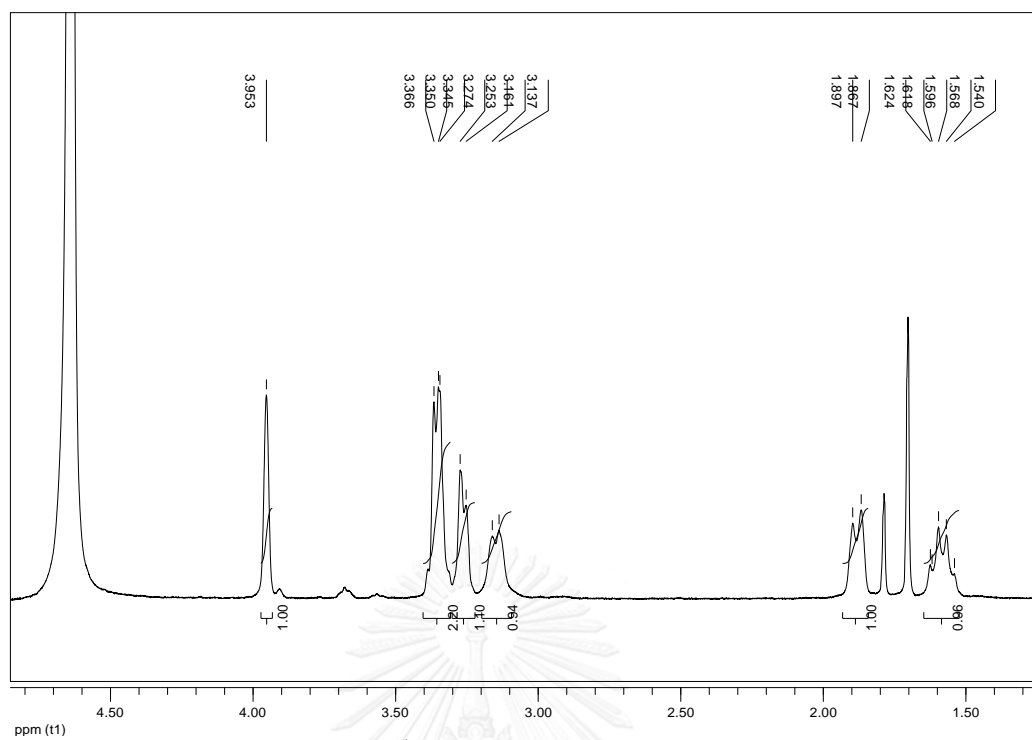
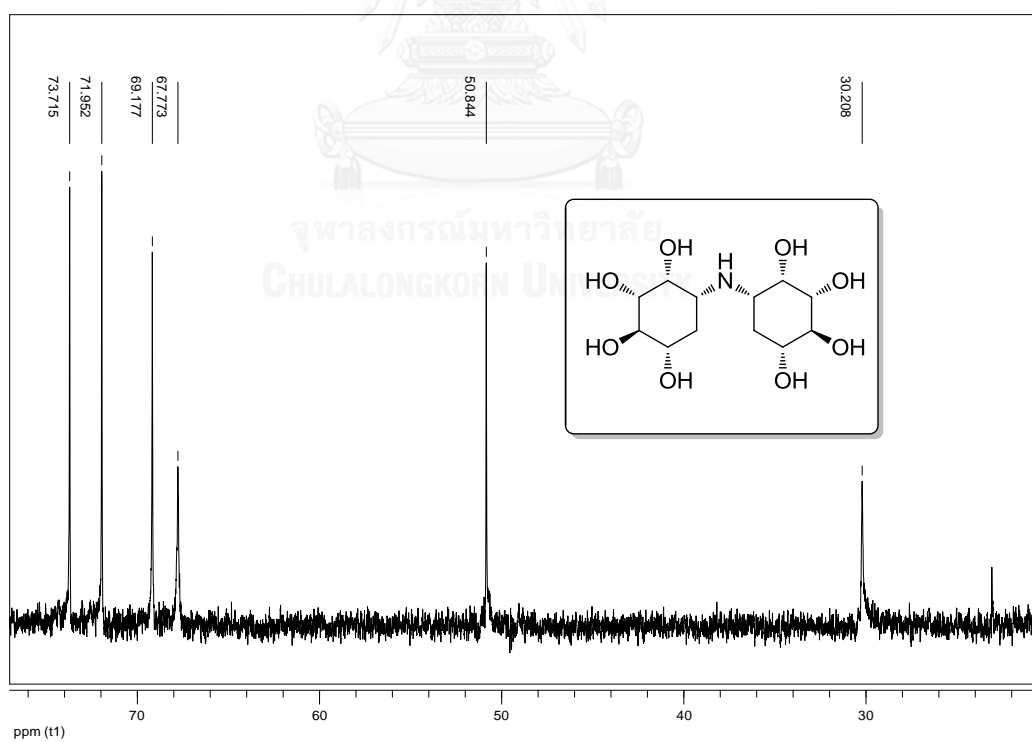


Figure 93. COSY NMR spectrum of 4-6 (CDCl_3)

Figure 94. ^1H NMR spectrum of 4-5 (D_2O)Figure 95. ^{13}C NMR spectrum of 4-5 (D_2O)

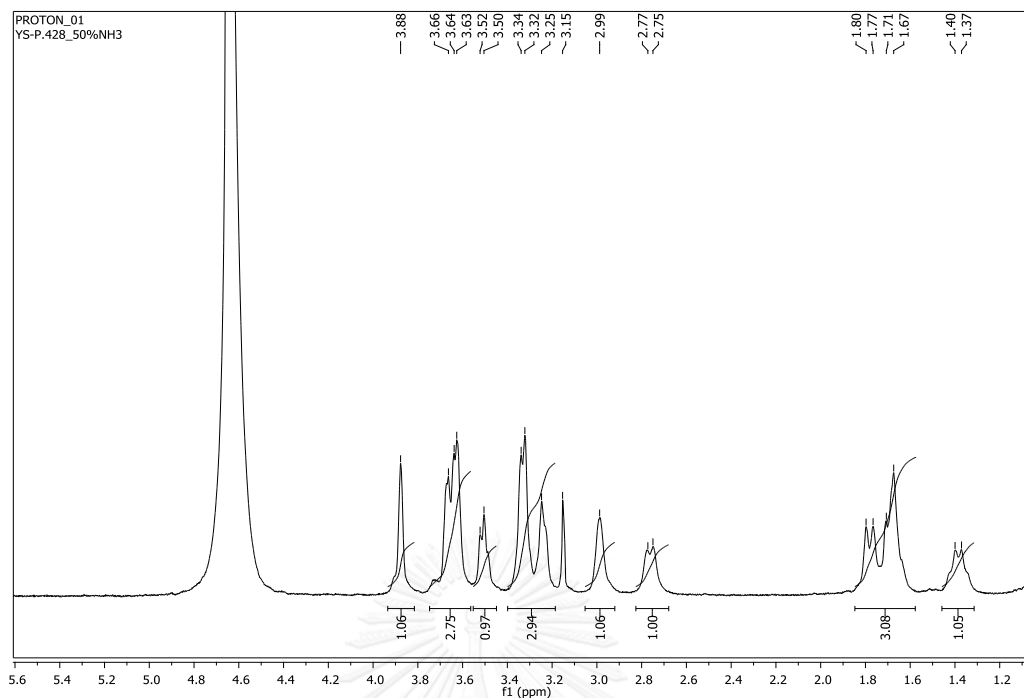


Figure 96. ^1H NMR spectrum of 4-7 (D_2O)

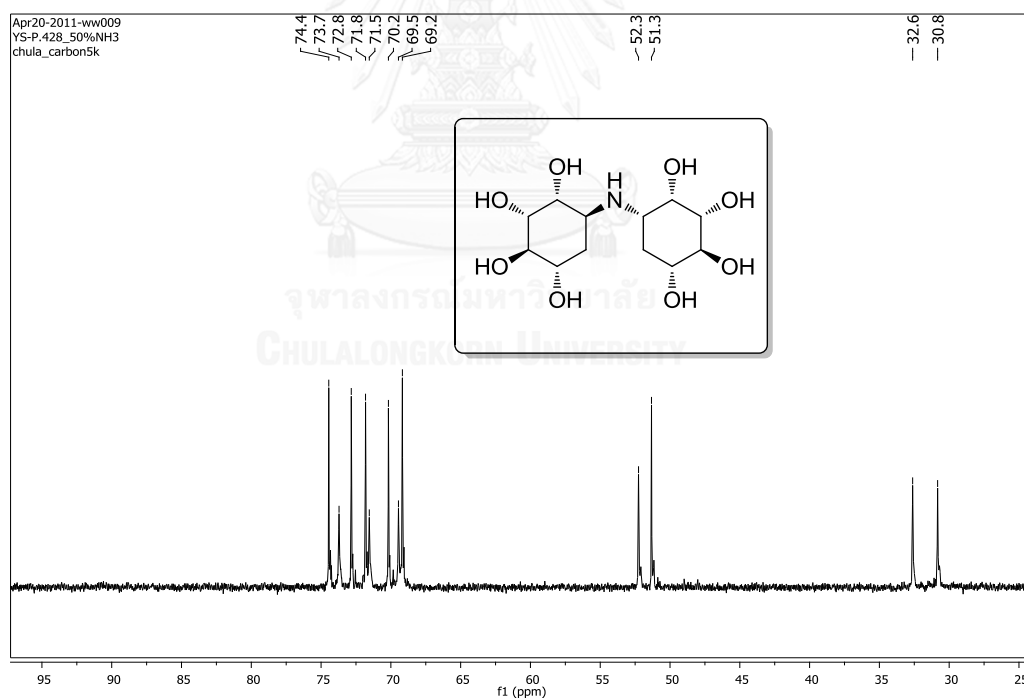


Figure 97. ^{13}C NMR spectrum of 4-7 (D_2O)

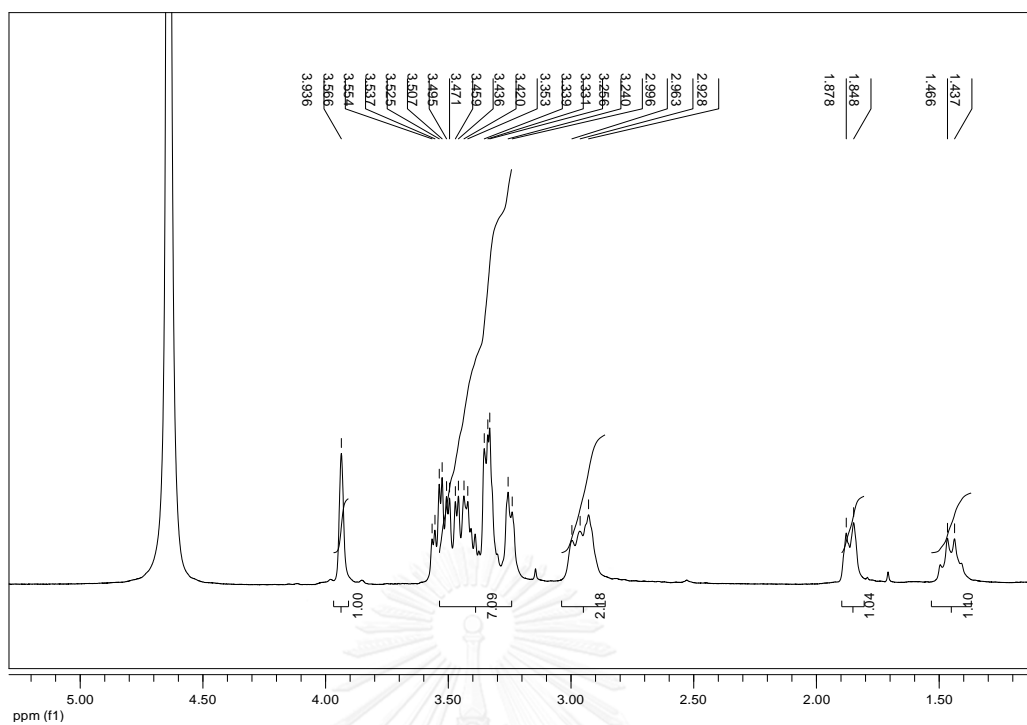


Figure 98. ^1H NMR spectrum of 5-1 (D_2O)

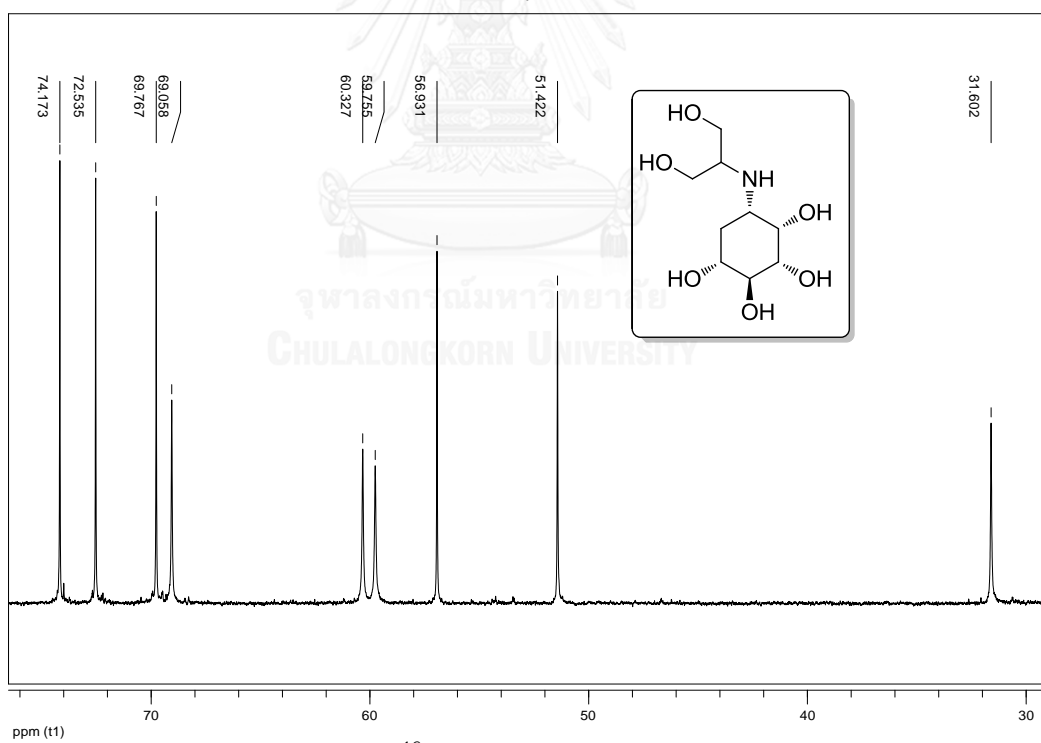


Figure 99. ^{13}C NMR spectrum of 5-1 (D_2O)

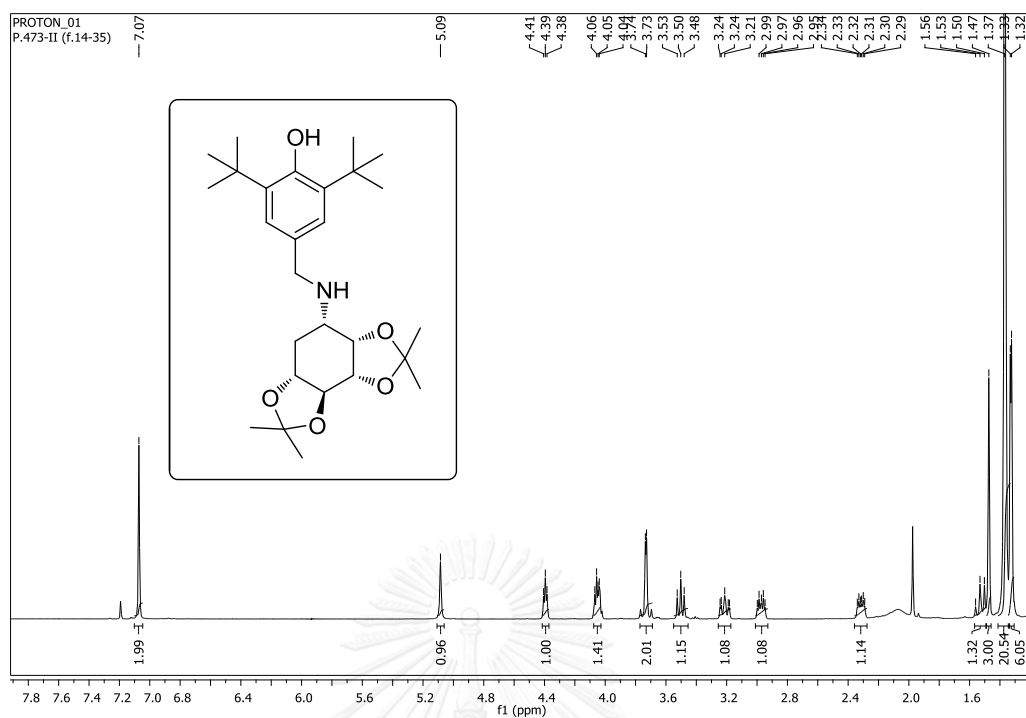


Figure 100. ¹H NMR spectrum of 5-2 (CDCl₃)

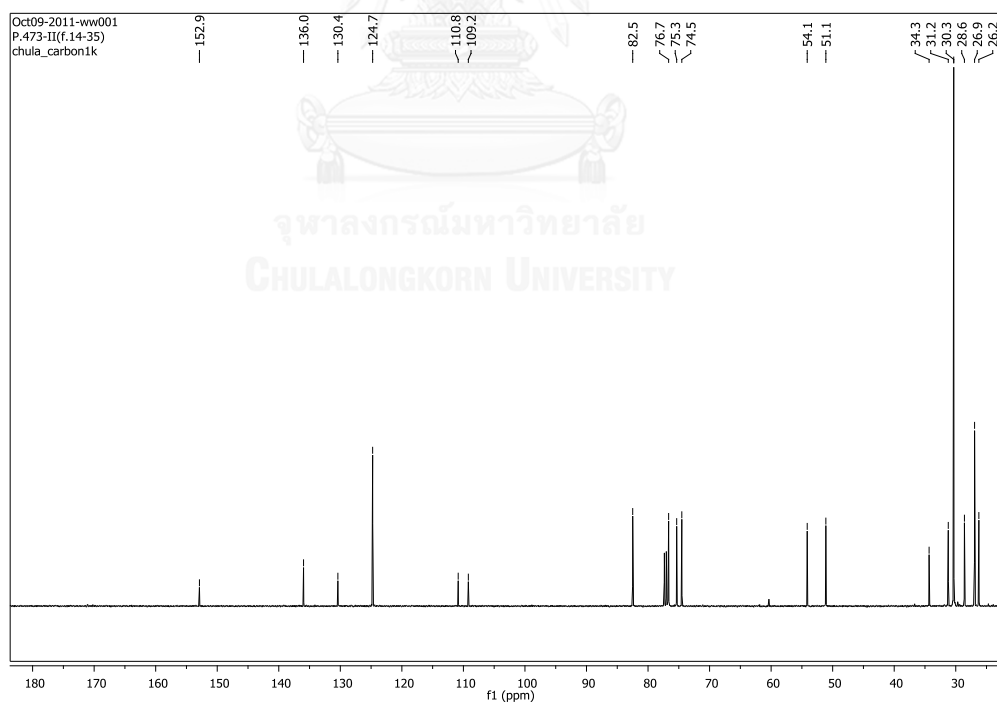


Figure 101. ¹³C NMR spectrum of 5-2 (CDCl₃)

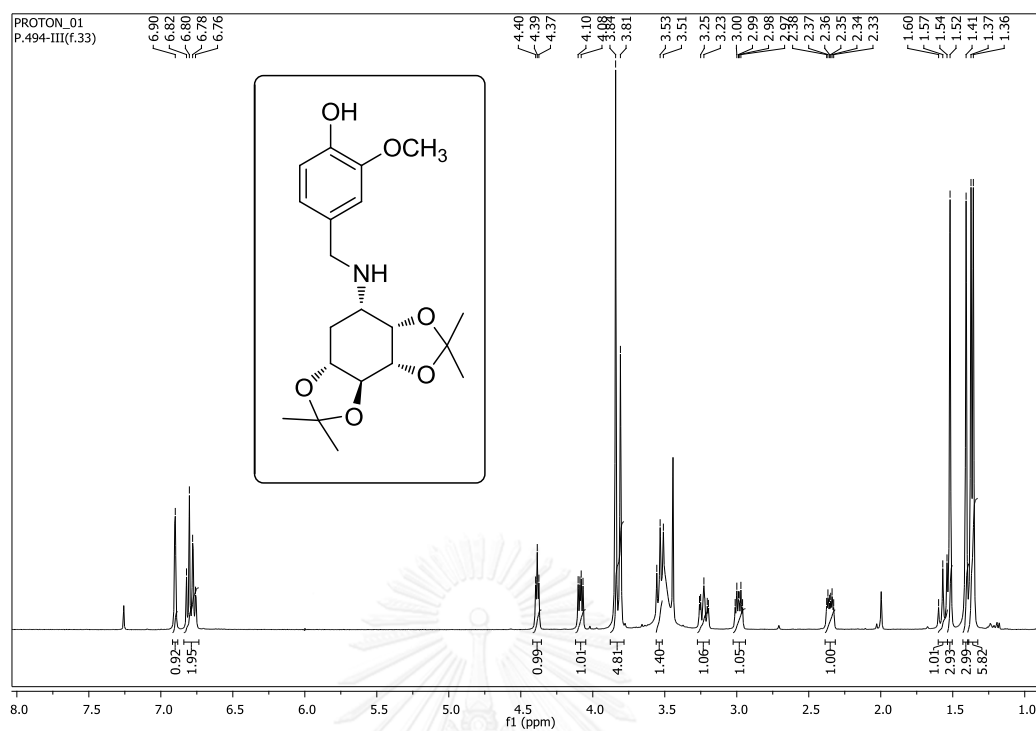


Figure 102. ¹H NMR spectrum of 5-3 (CDCl₃)

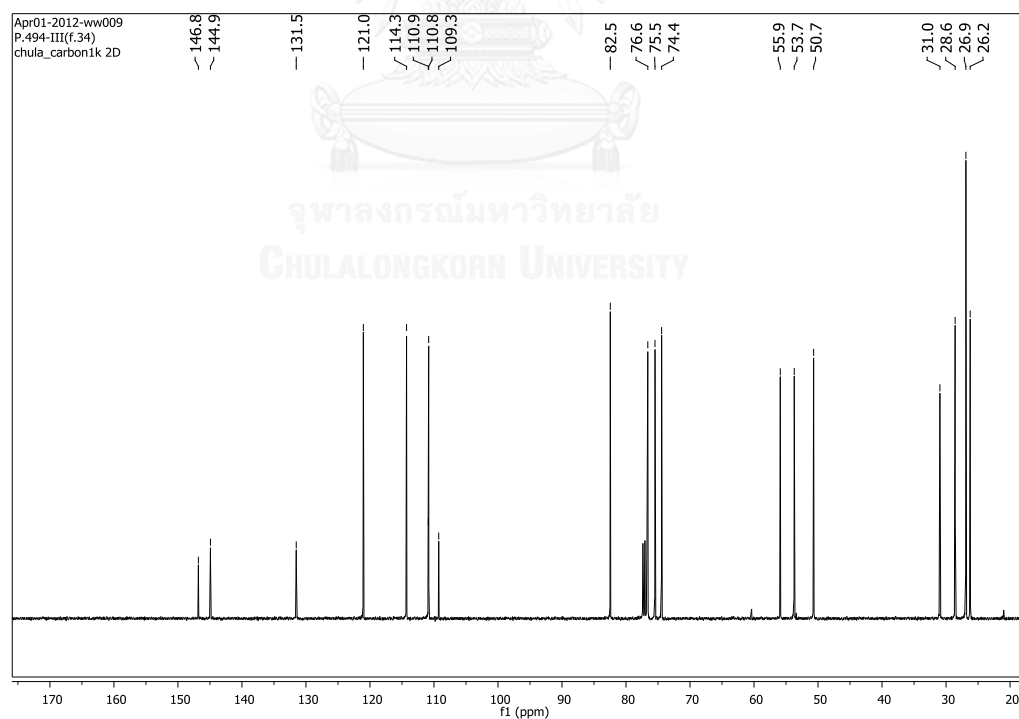


Figure 103. ¹³C NMR spectrum of 5-3 (CDCl₃)

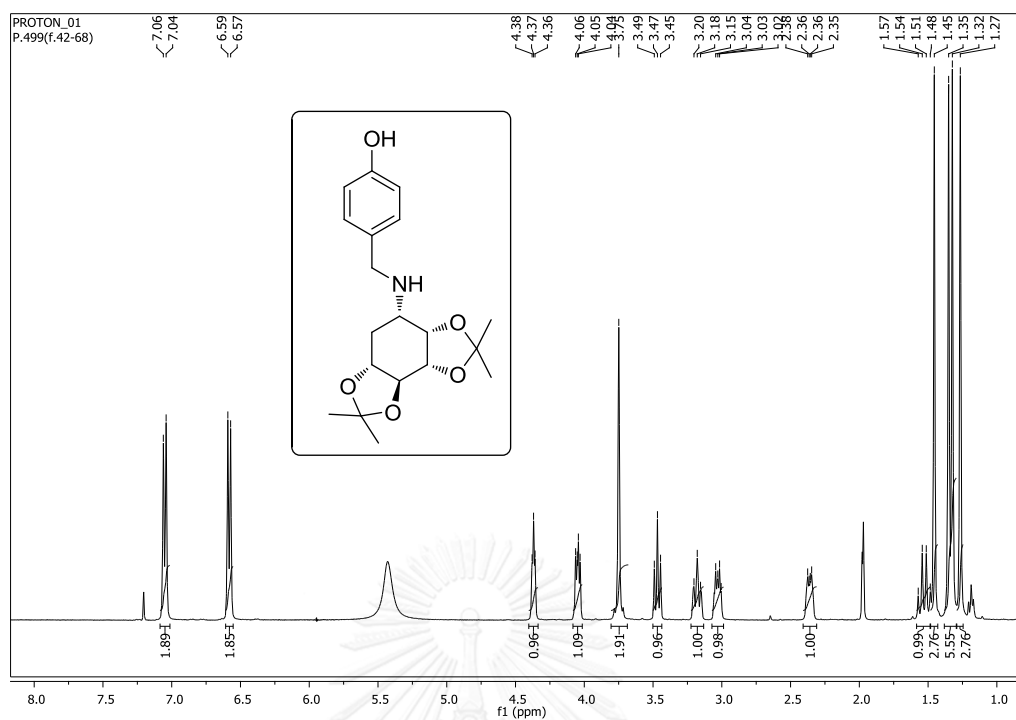


Figure 104. ^1H NMR spectrum of **5-4** (CDCl_3)

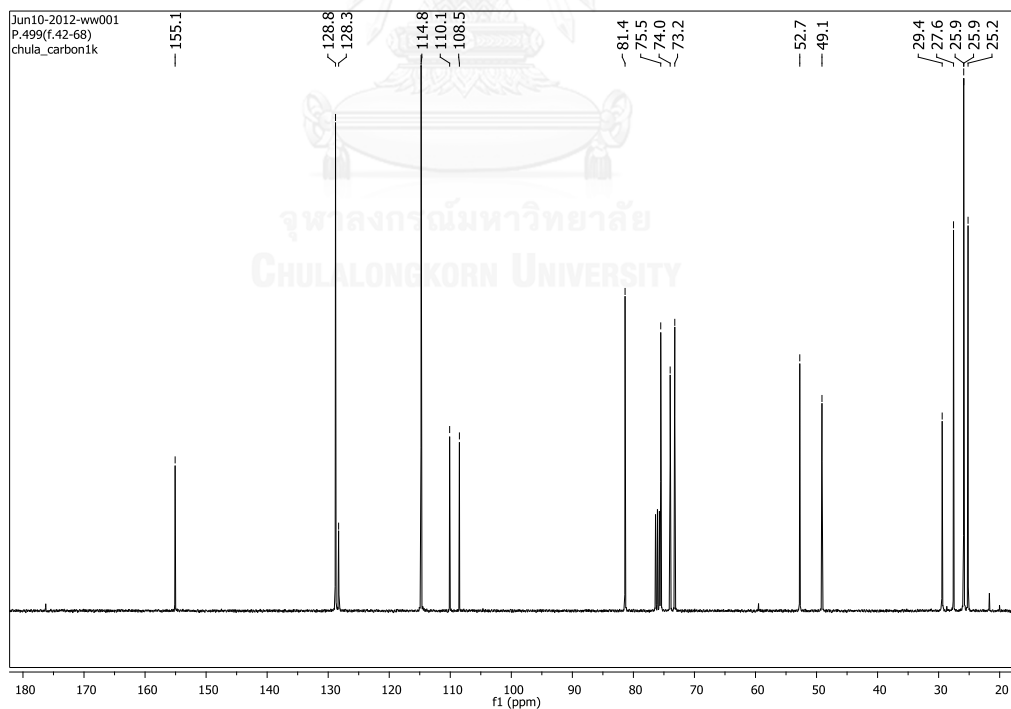


Figure 105. ^{13}C NMR spectrum of **5-4** (CDCl_3)

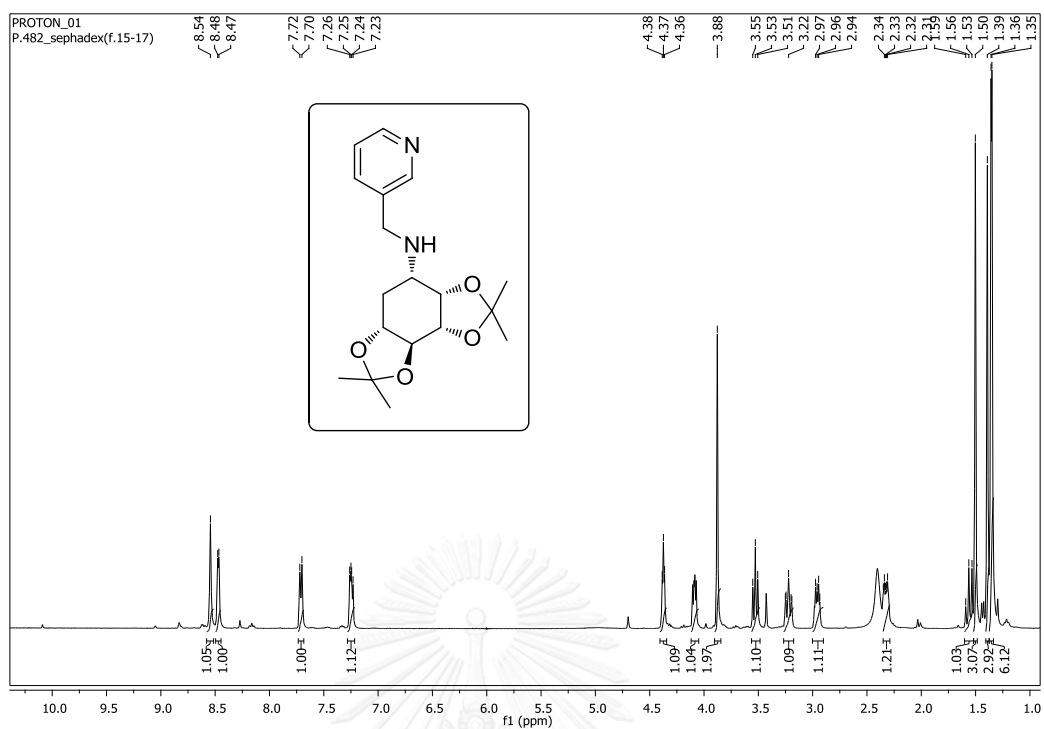


Figure 106. ^1H NMR spectrum of 5-5 (CDCl_3)

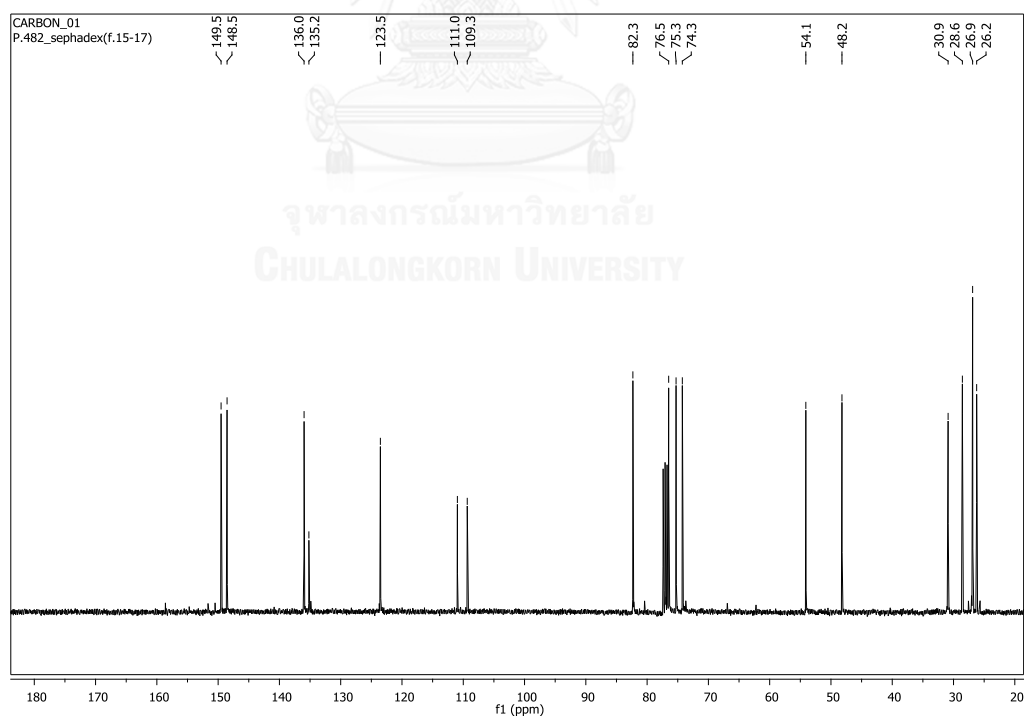


Figure 107. ^{13}C NMR spectrum of 5-5 (CDCl_3)

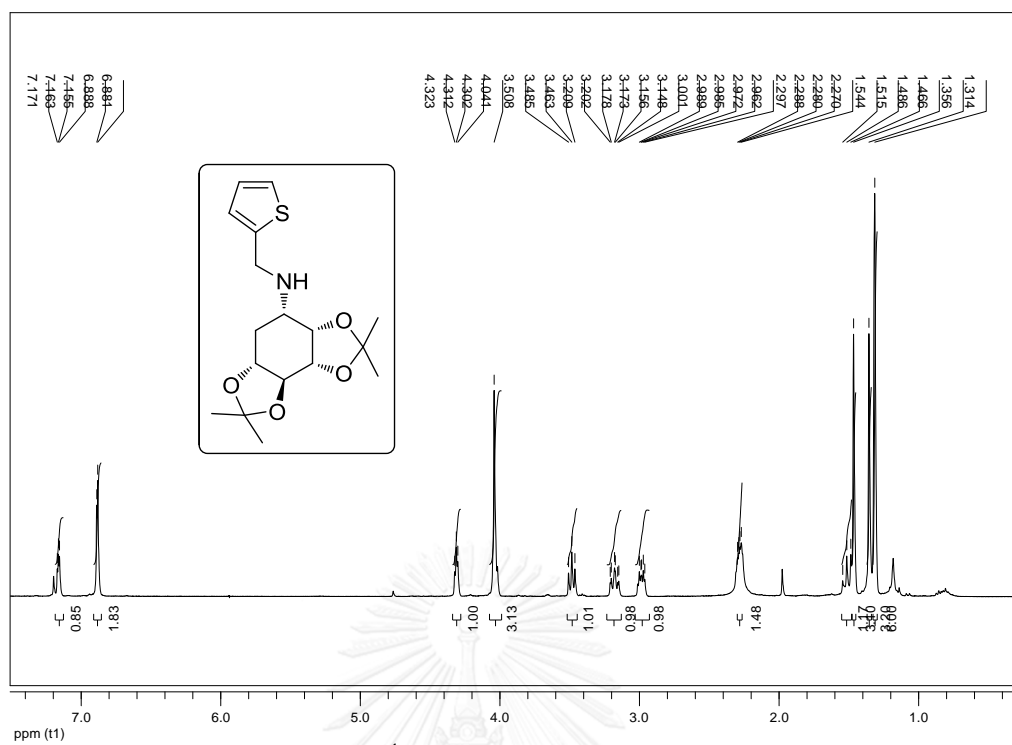


Figure 108. ^1H NMR spectrum of 5-6 (CDCl_3)

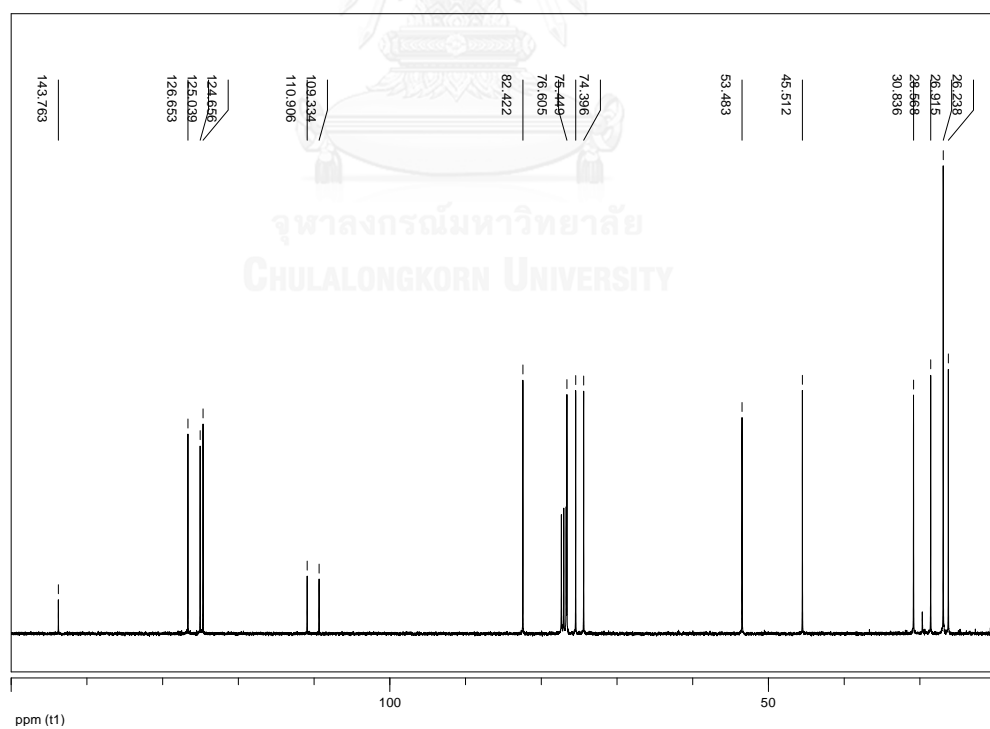


Figure 109. ^{13}C NMR spectrum of 5-6 (CDCl_3)

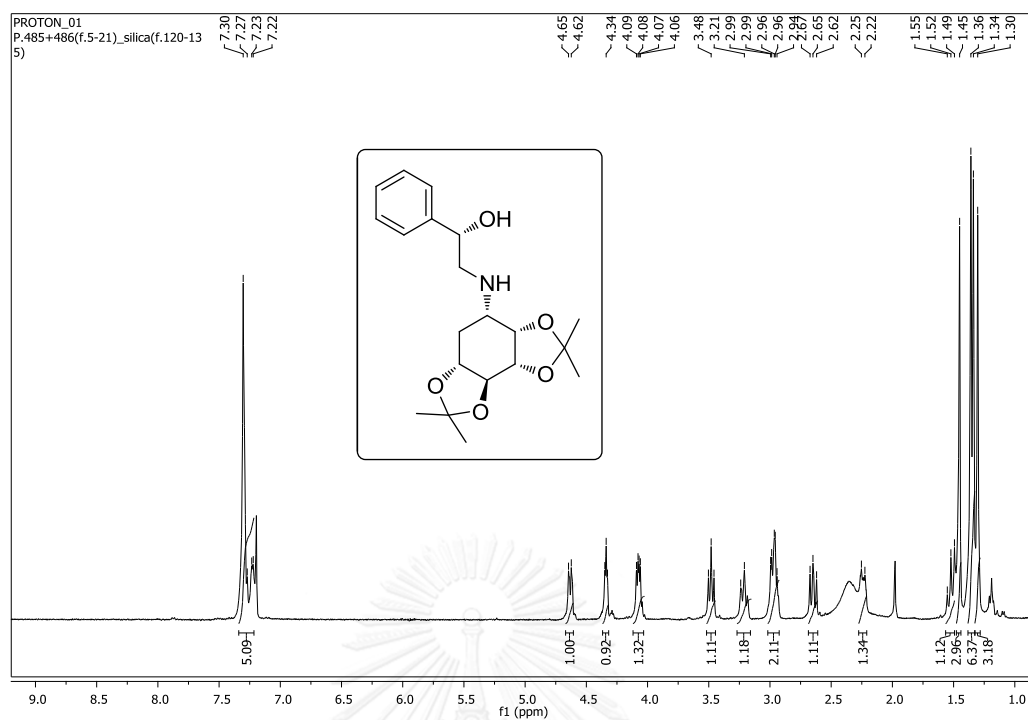


Figure 110. ^1H NMR spectrum of **5-7** (CDCl_3)

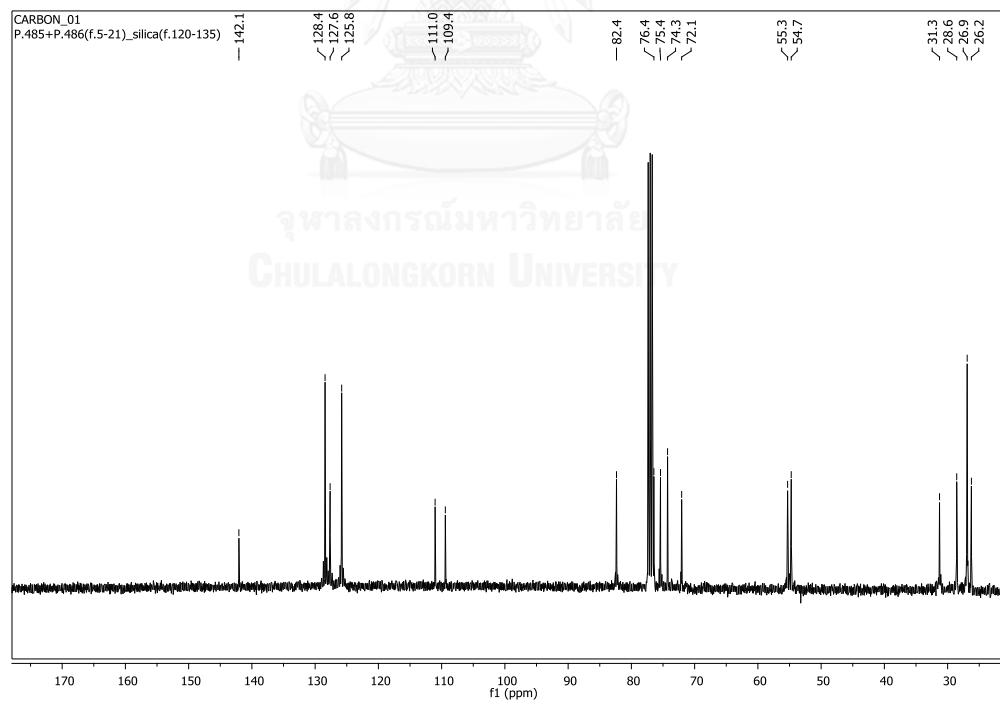


Figure 111. ^{13}C NMR spectrum of **5-7** (CDCl_3)

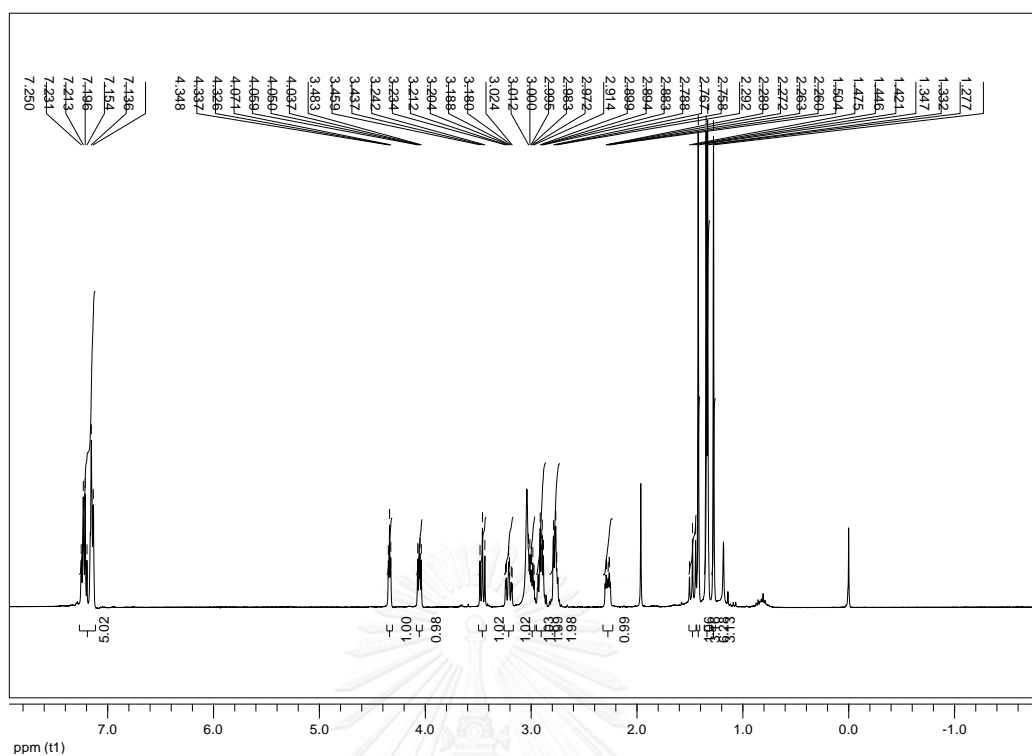


Figure 112. ^1H NMR spectrum of 5-8 (CDCl_3)

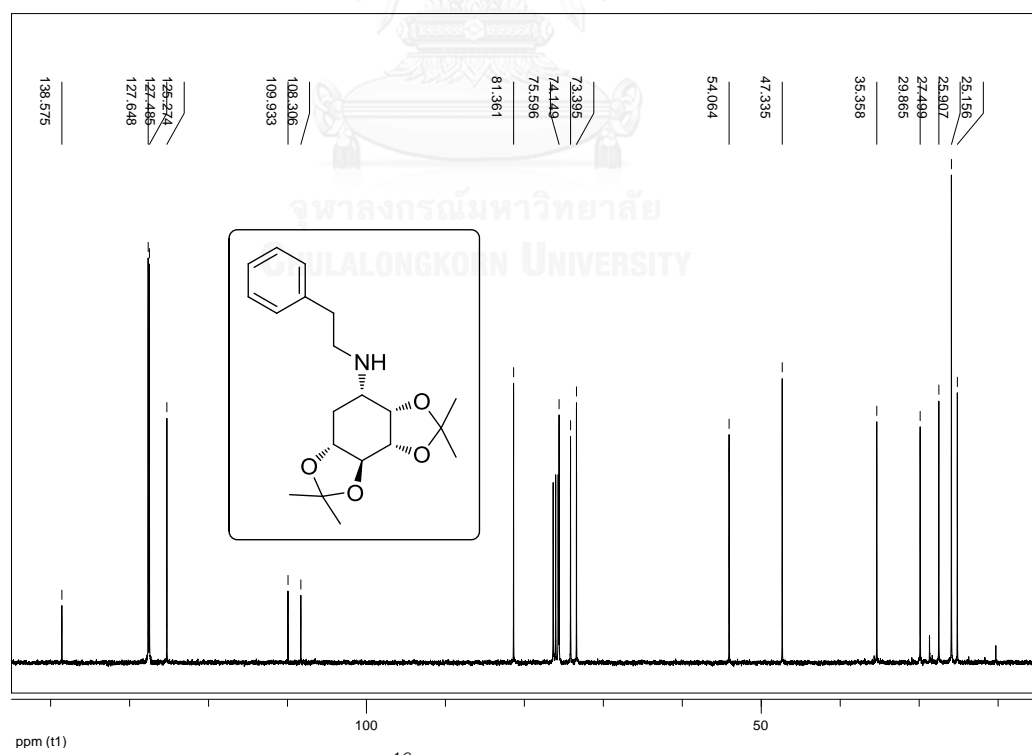
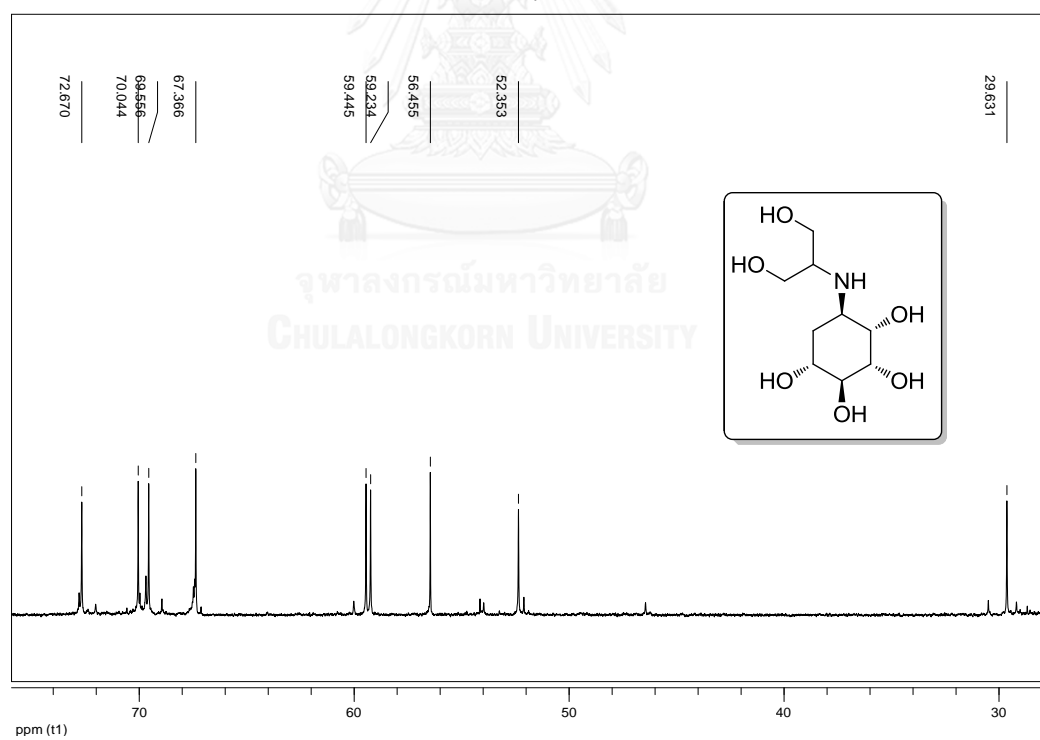
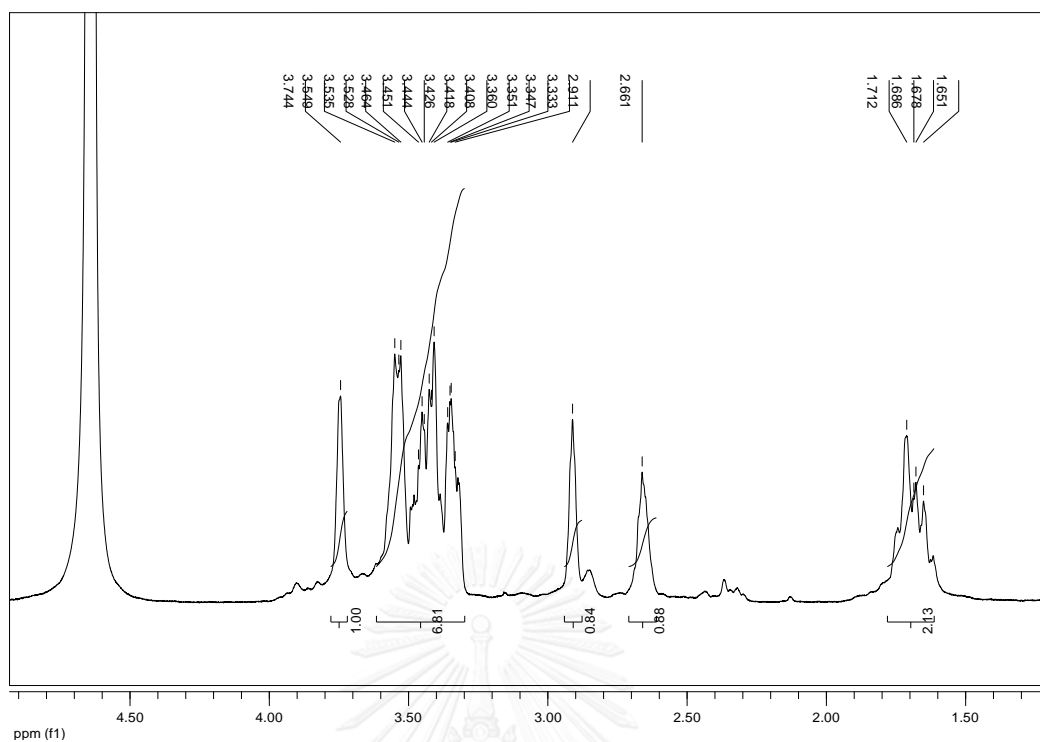


Figure 113. ^{13}C NMR spectrum of 5-8 (CDCl_3)



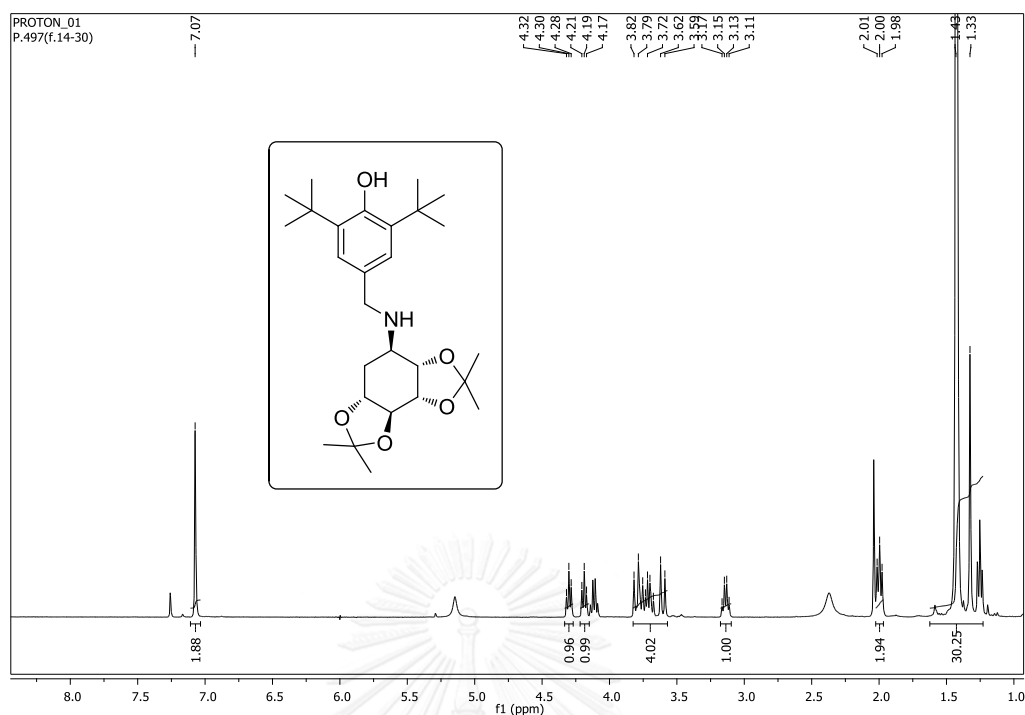


Figure 116. ^1H NMR spectrum of 5-10 (CDCl_3)

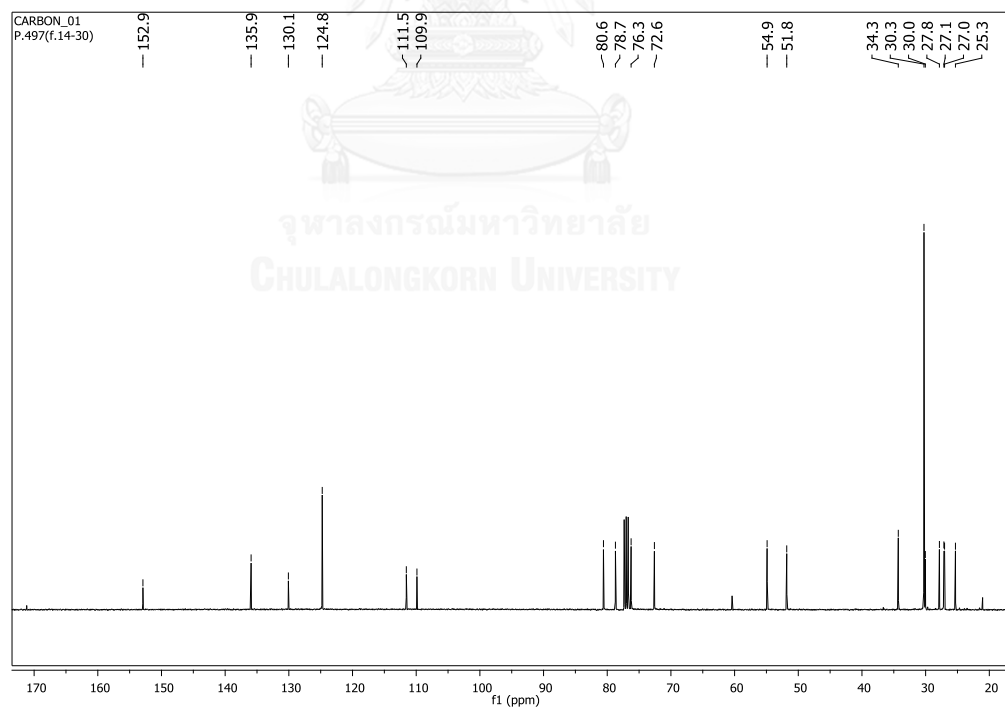


Figure 117. ^{13}C NMR spectrum of 5-10 (CDCl_3)

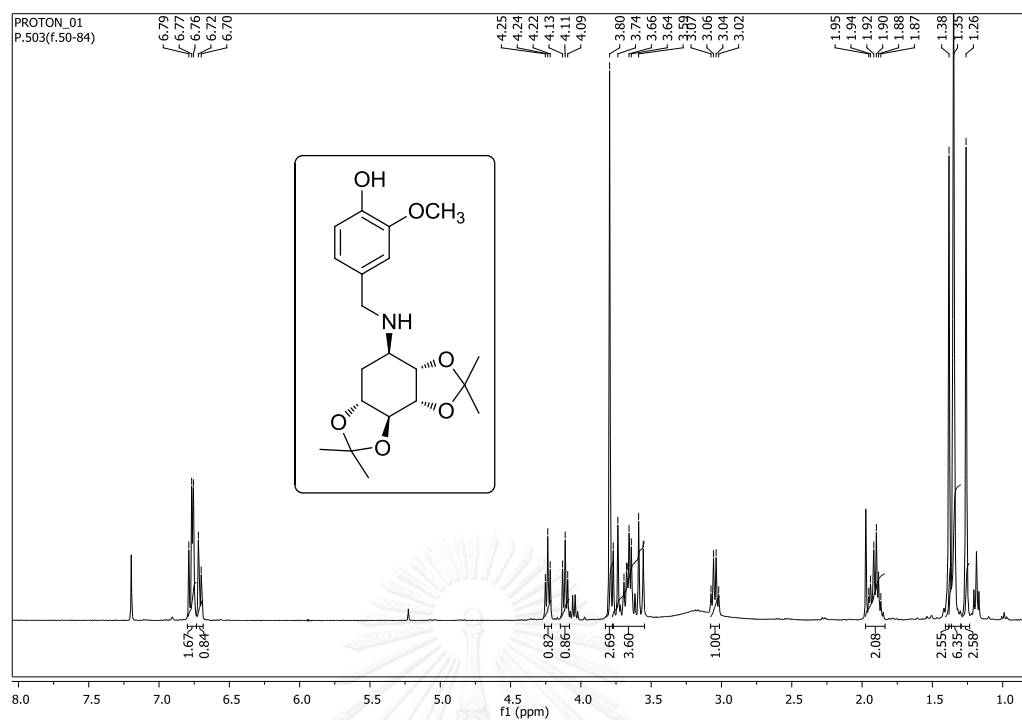


Figure 118. ¹H NMR spectrum of 5-11 (CDCl₃)

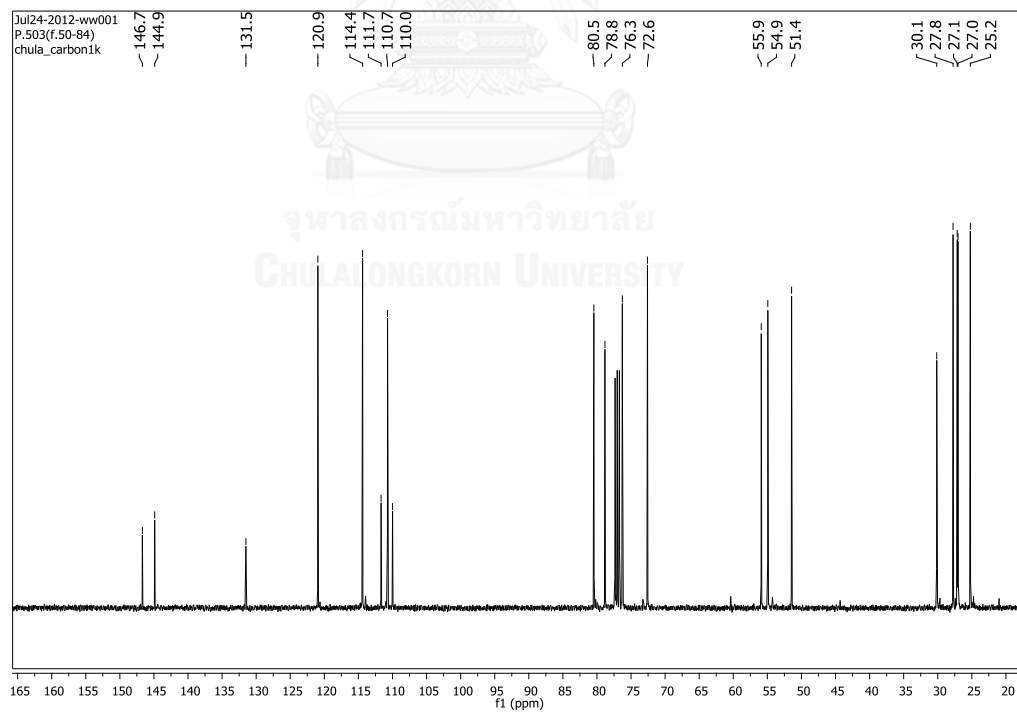


Figure 119. ¹³C NMR spectrum of 5-11 (CDCl₃)

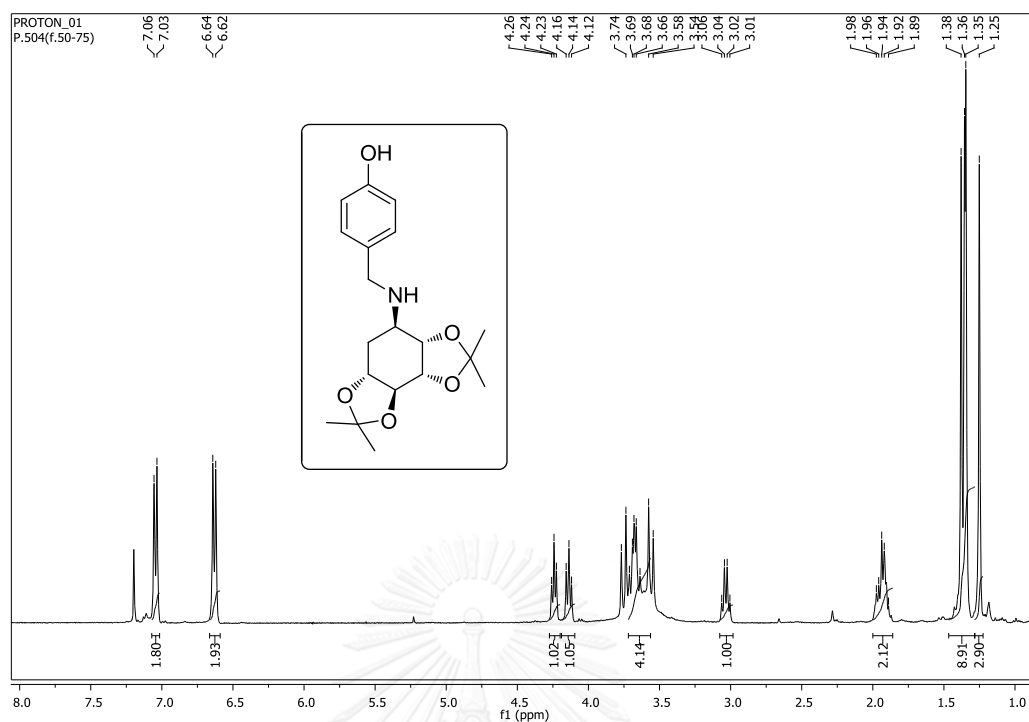


Figure 120. ^1H NMR spectrum of 5-12 (CDCl_3)

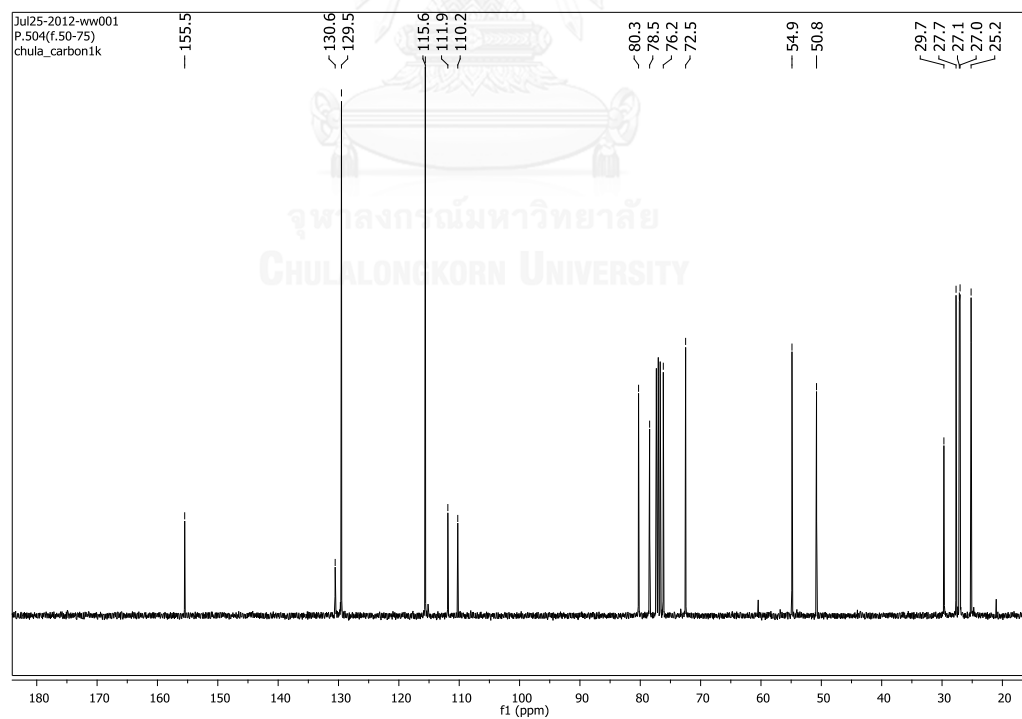


Figure 121. ^{13}C NMR spectrum of 5-12 (CDCl_3)

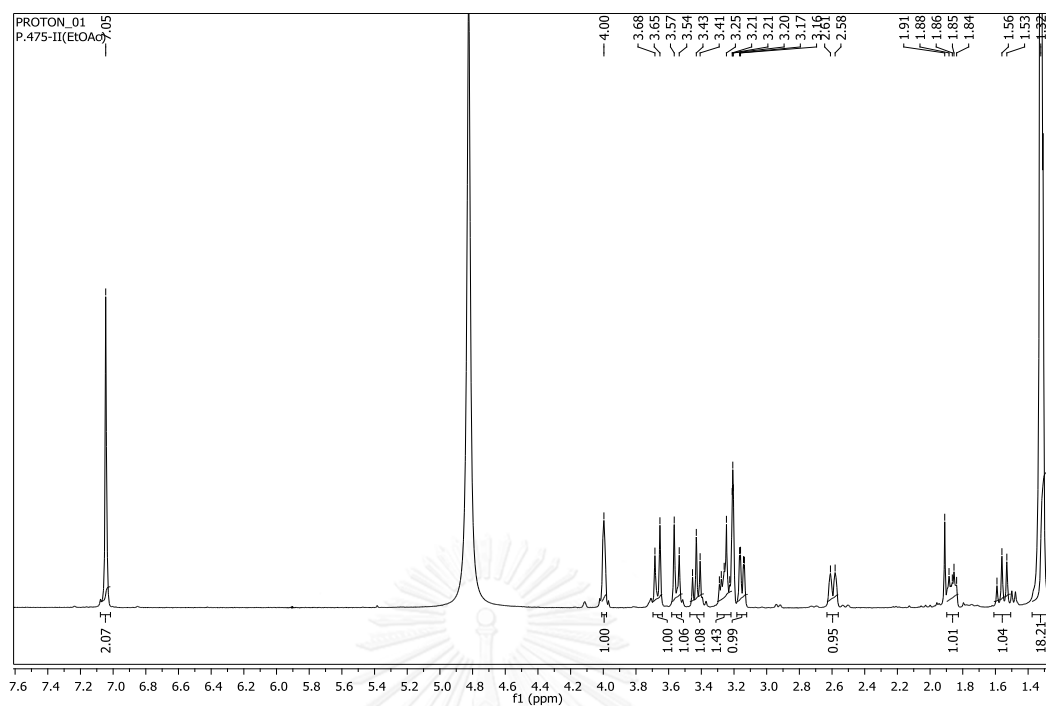


Figure 122. ^1H NMR spectrum of **5-13** (CD_3OD)

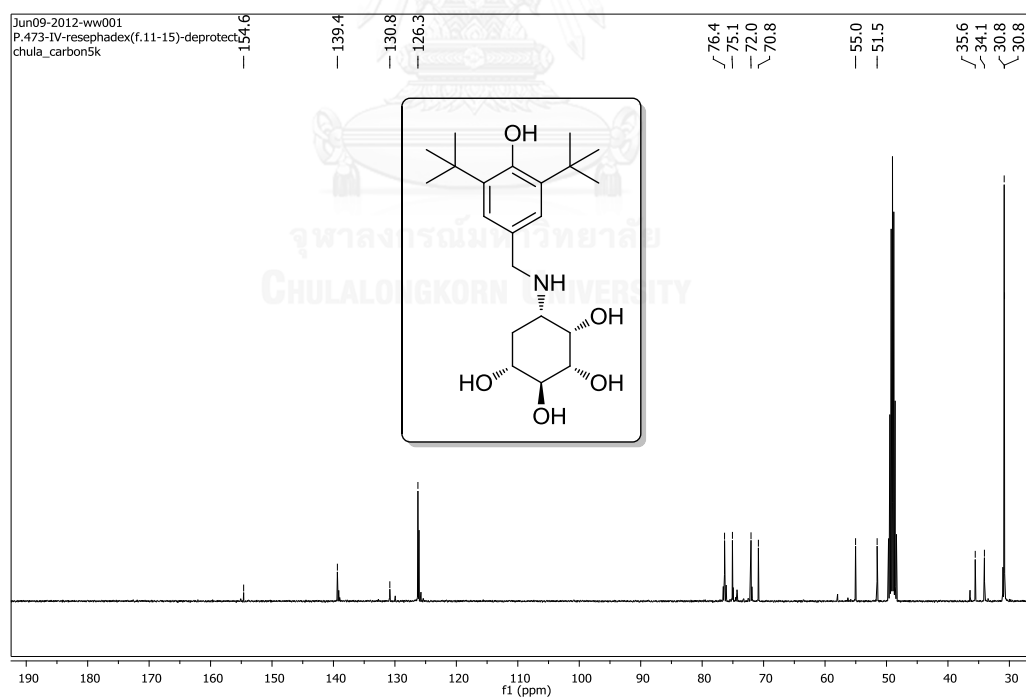


Figure 123. ^{13}C NMR spectrum of **5-13** (CD_3OD)

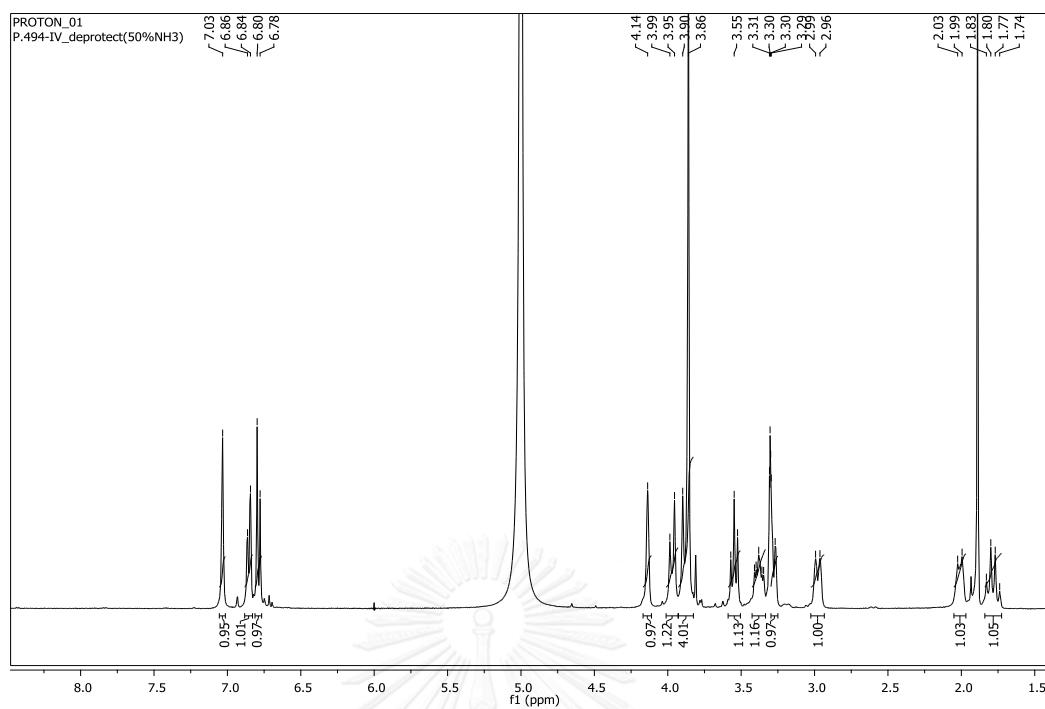


Figure 124. ^1H NMR spectrum of 5-14 (CD_3OD)

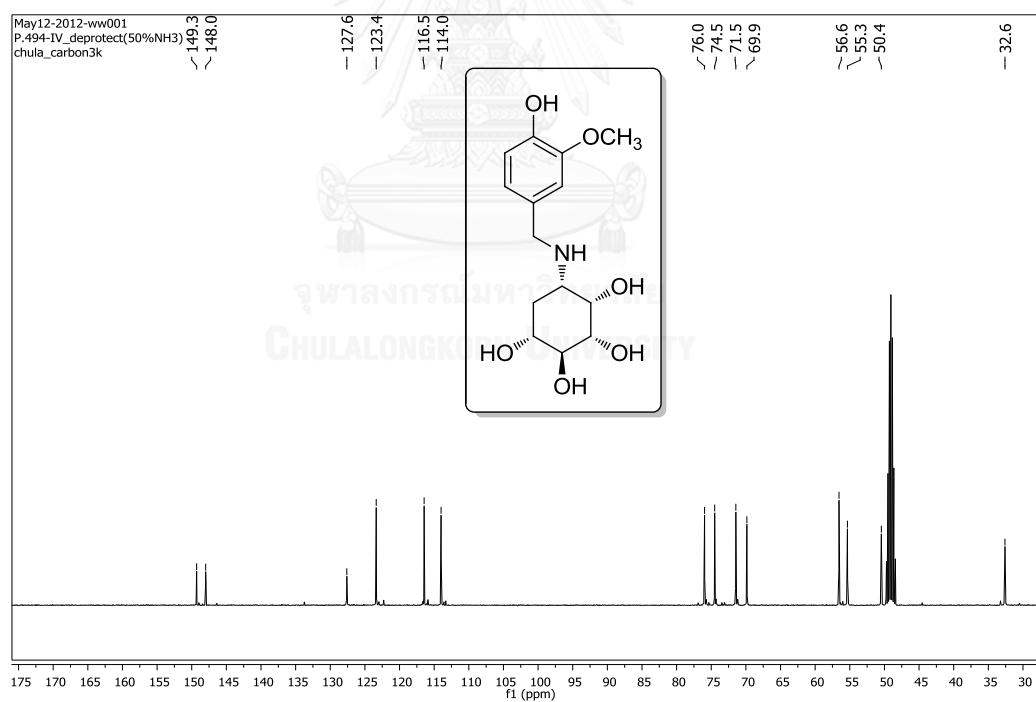


Figure 125. ^{13}C NMR spectrum of 5-14 (CD_3OD)

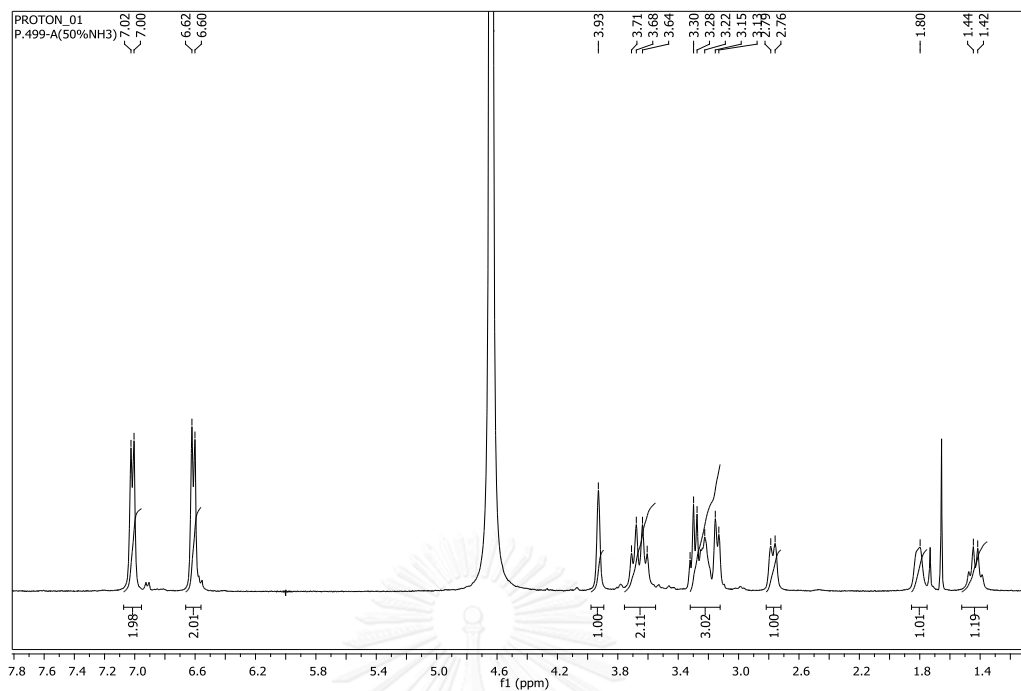


Figure 126. ^1H NMR spectrum of 5-15 (D_2O)

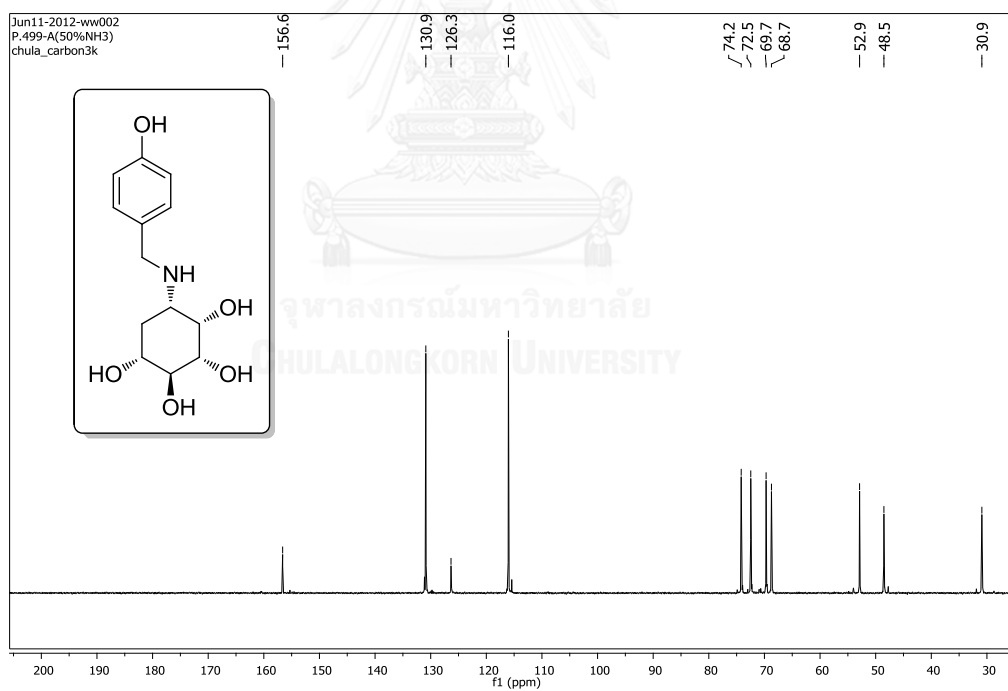


Figure 127. ^{13}C NMR spectrum of 5-15 (D_2O)

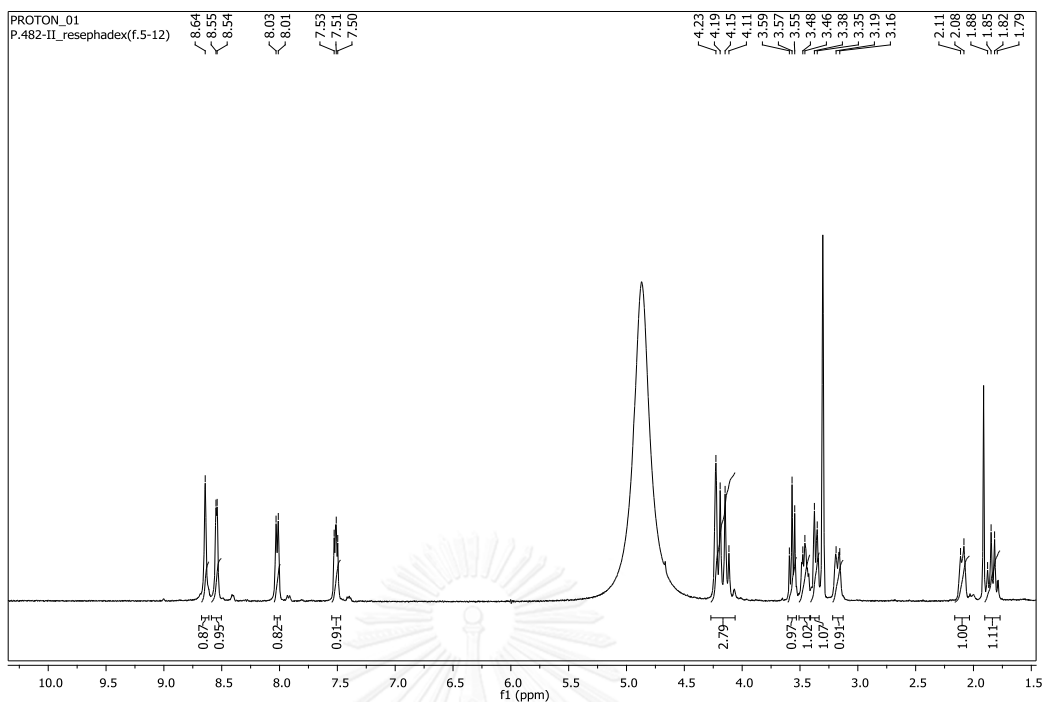


Figure 128. ^1H NMR spectrum of **5-16** (CD_3OD)

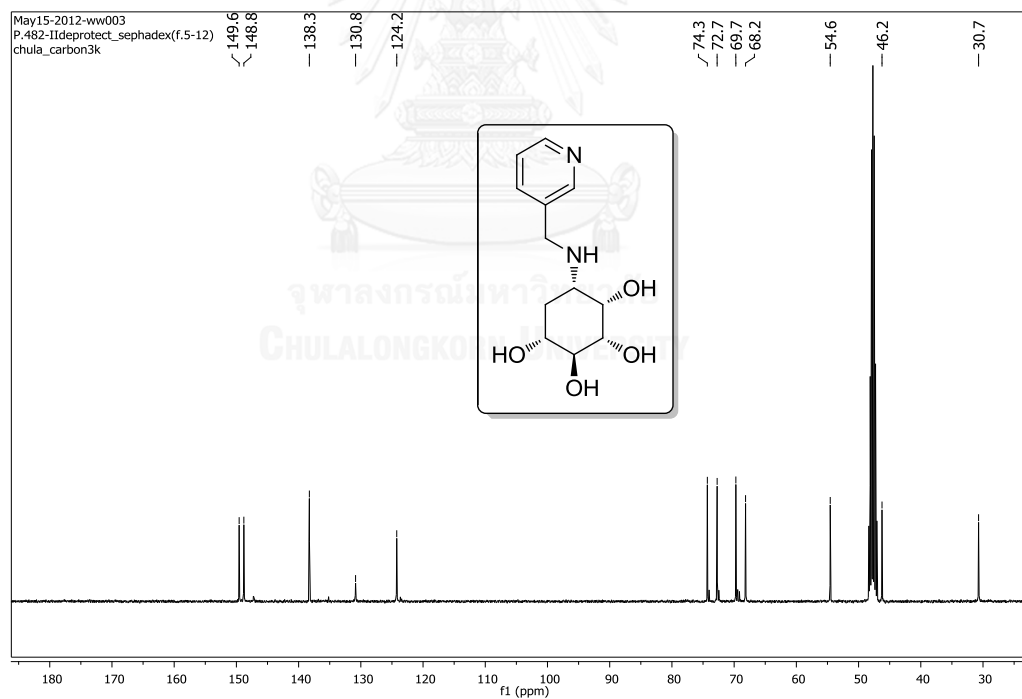


Figure 129. ^{13}C NMR spectrum of **5-16** (CD_3OD)

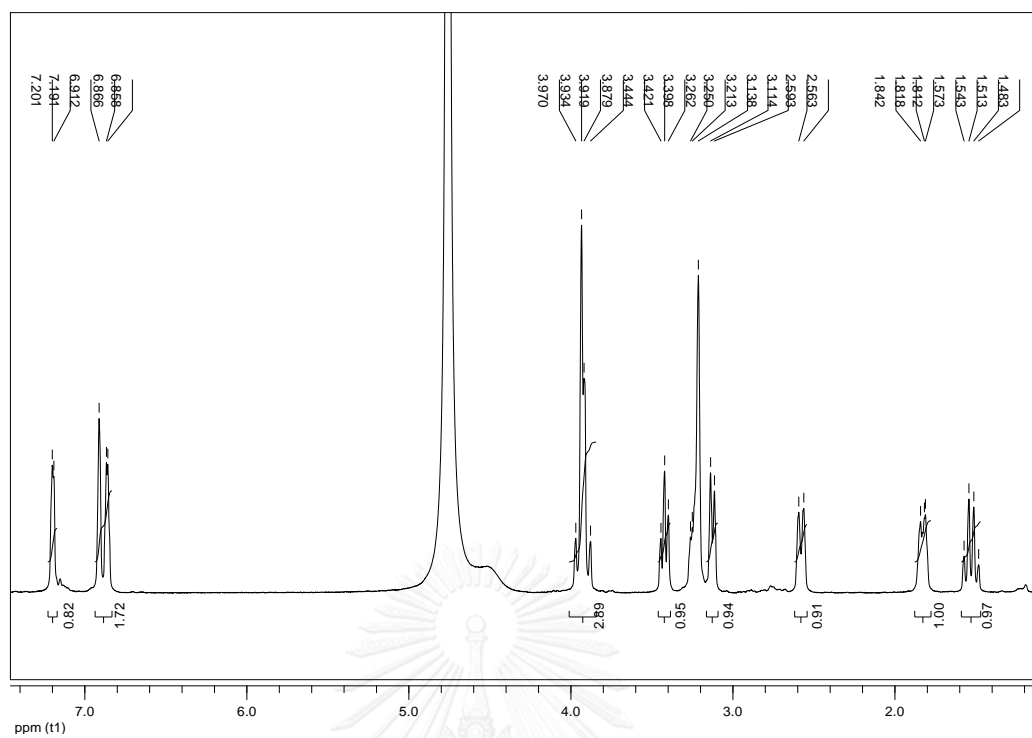


Figure 130. ¹H NMR spectrum of 5-17 (CD₃OD)

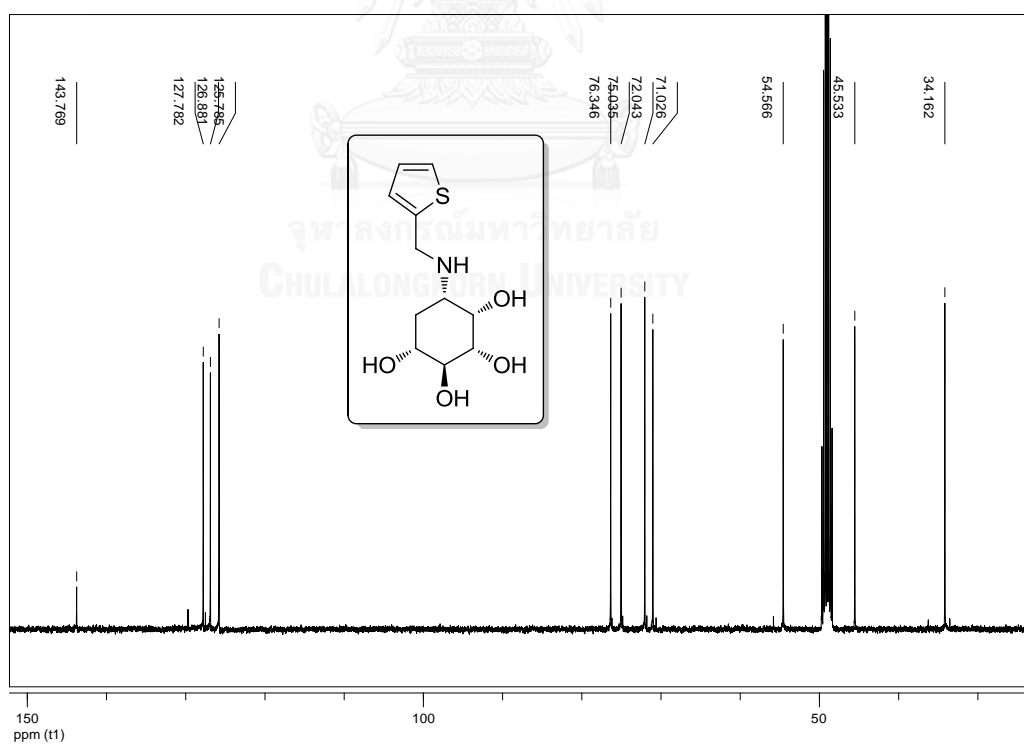
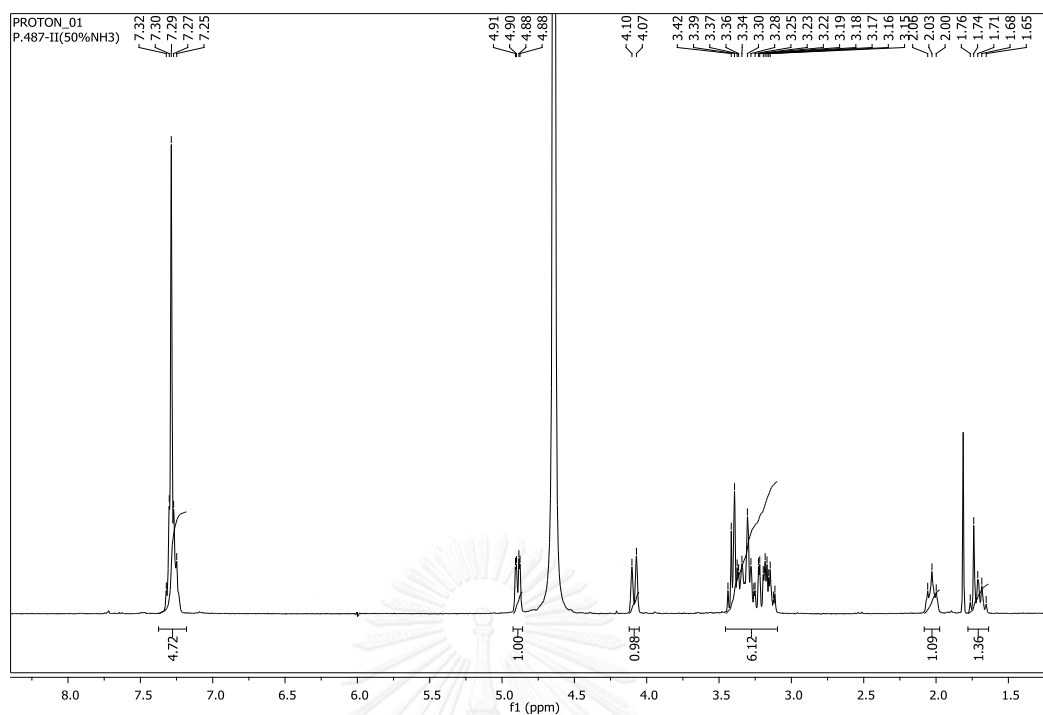
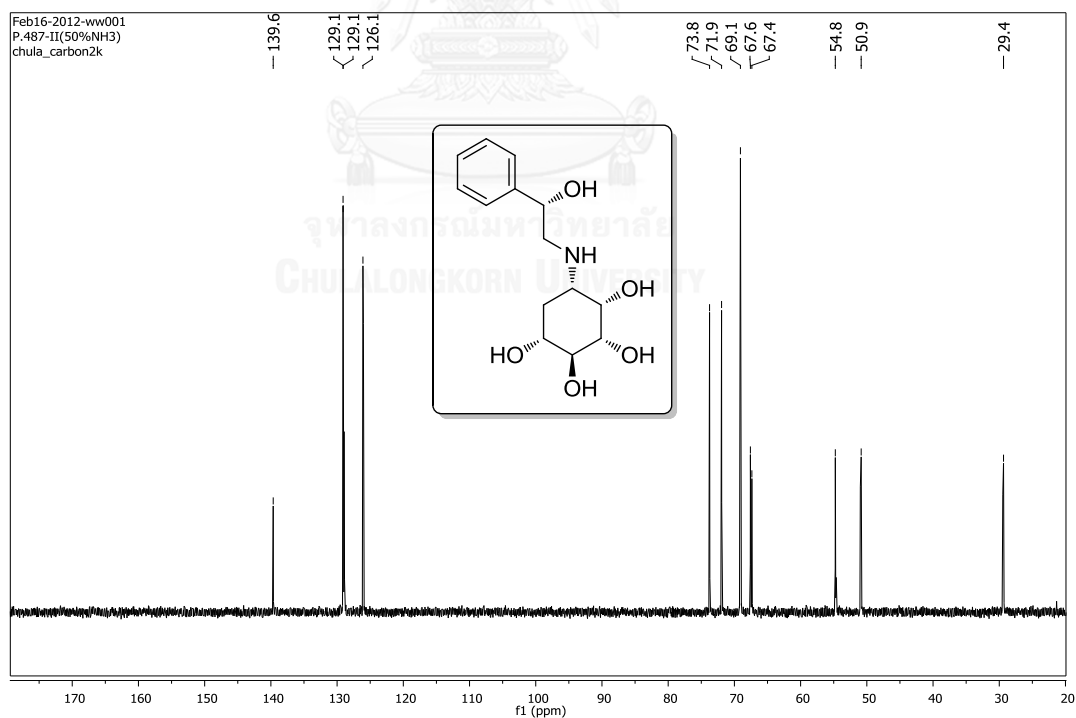


Figure 131. ¹³C NMR spectrum of 5-17 (CD₃OD)

Figure 132. ^1H NMR spectrum of 5-18 (D_2O)Figure 133. ^{13}C NMR spectrum of 5-18 (D_2O)

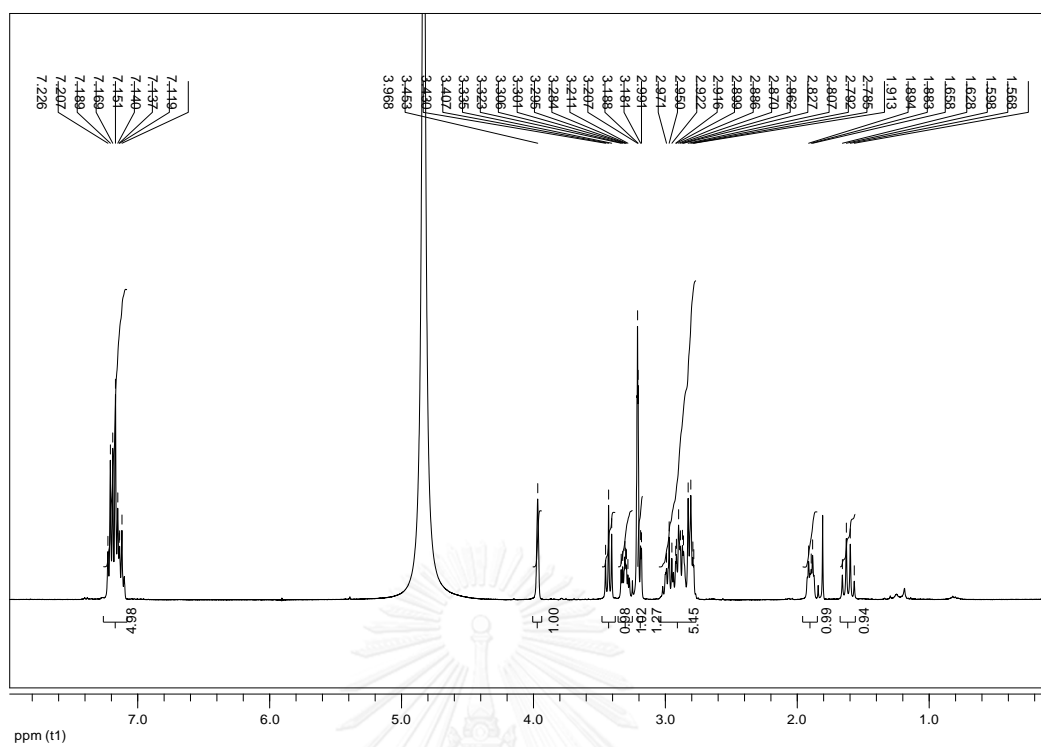


Figure 134. ^1H NMR spectrum of 5-19 (CD_3OD)

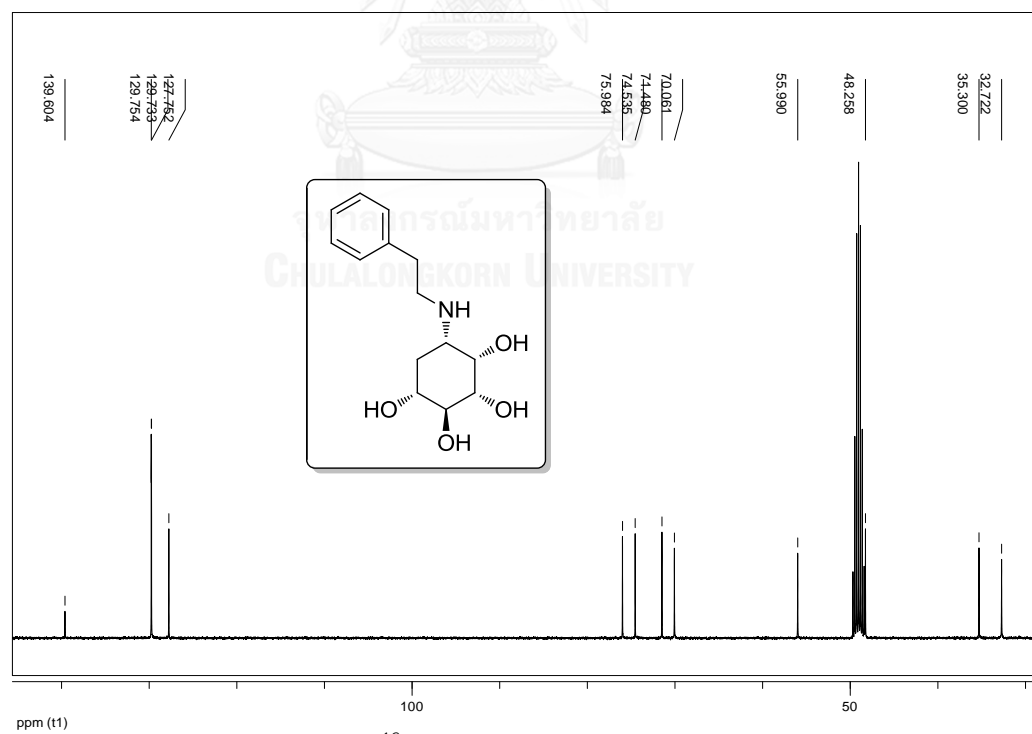


Figure 135. ^{13}C NMR spectrum of 5-19 (CD_3OD)

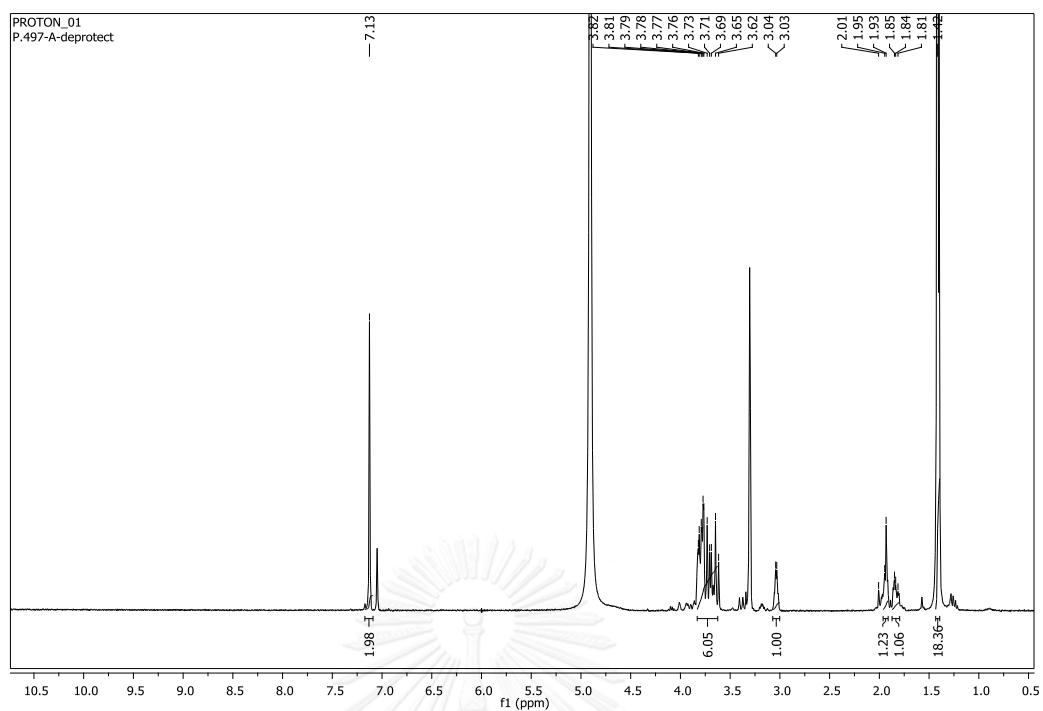


Figure 136. ^1H NMR spectrum of 5-20 (CD_3OD)

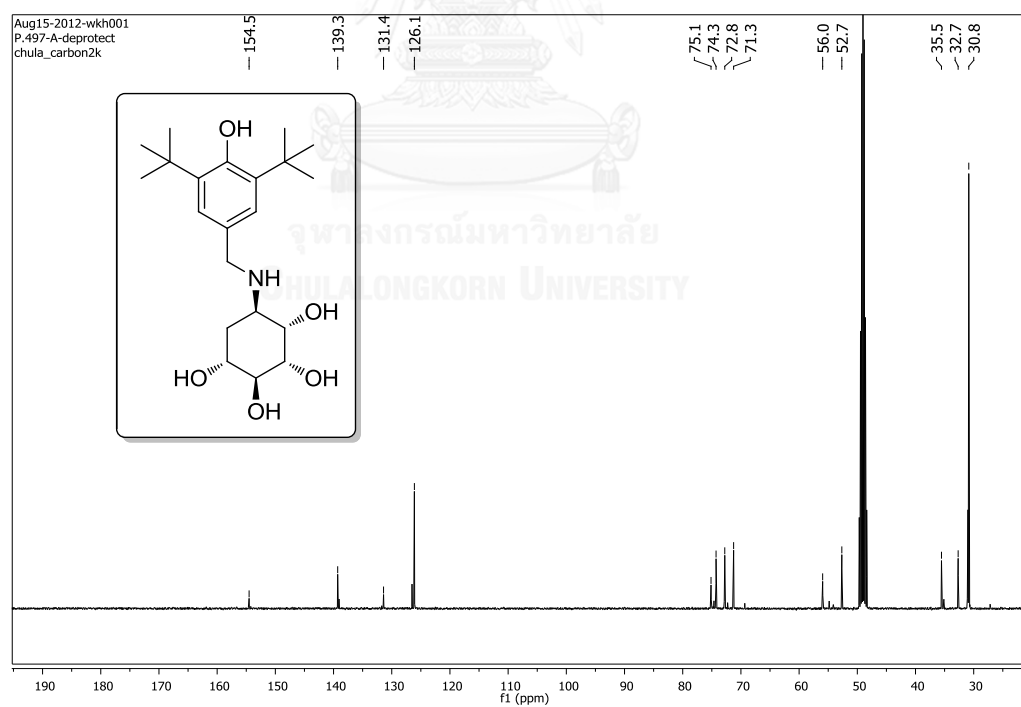
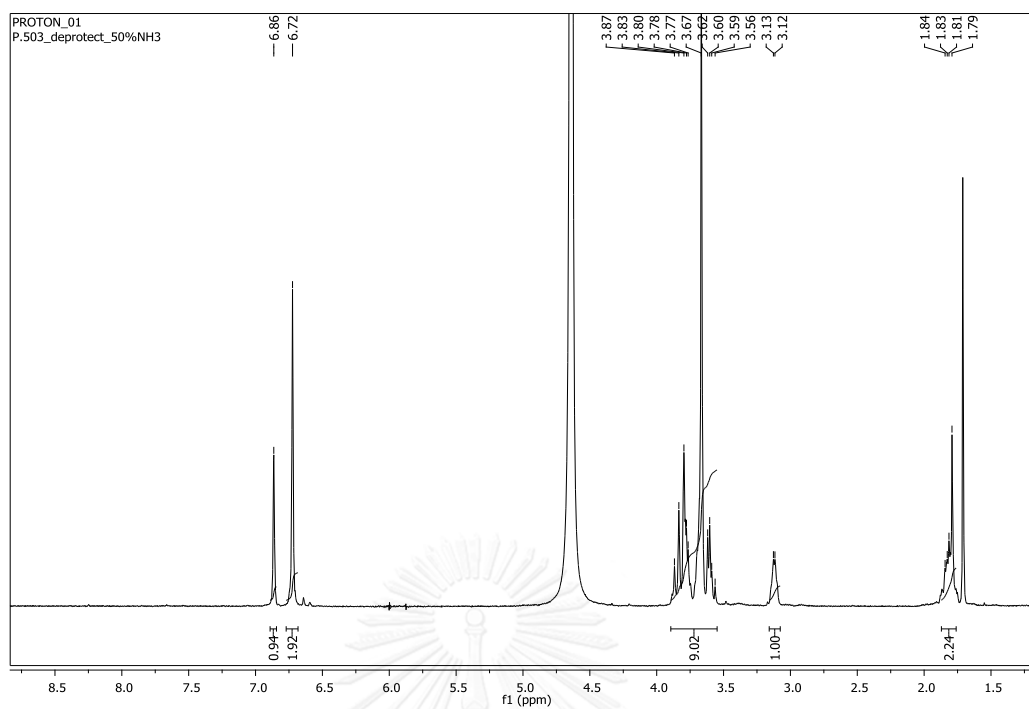
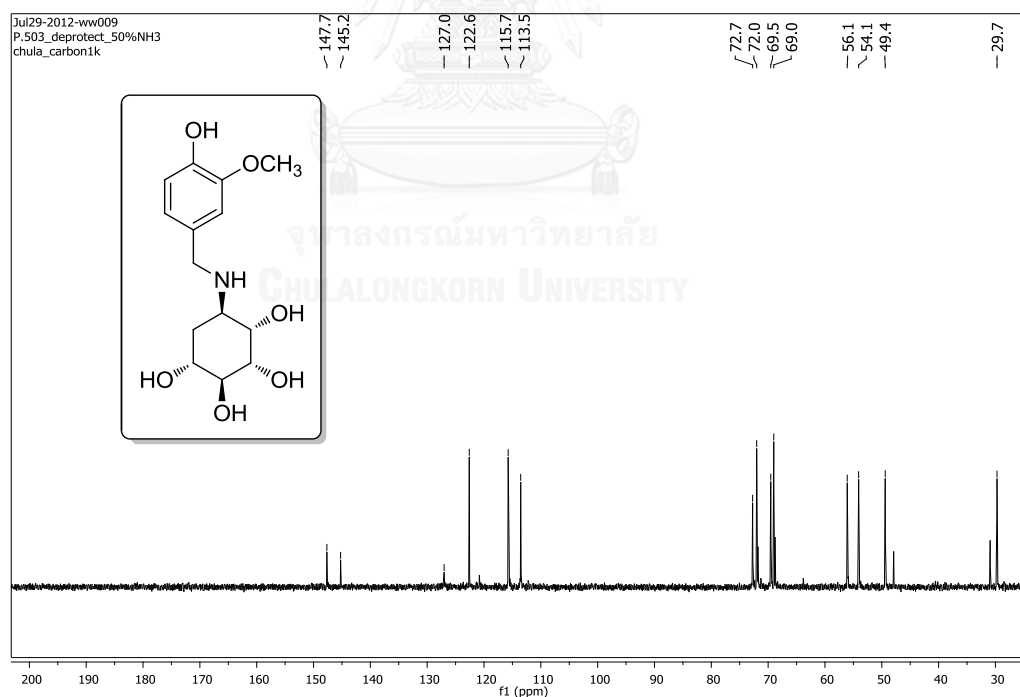
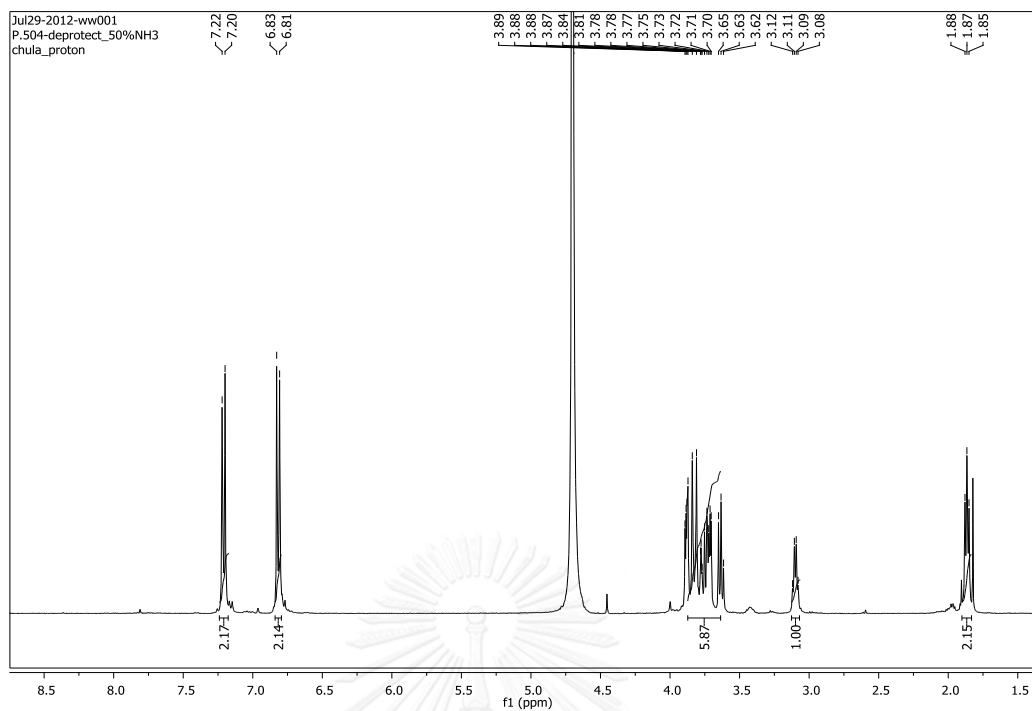
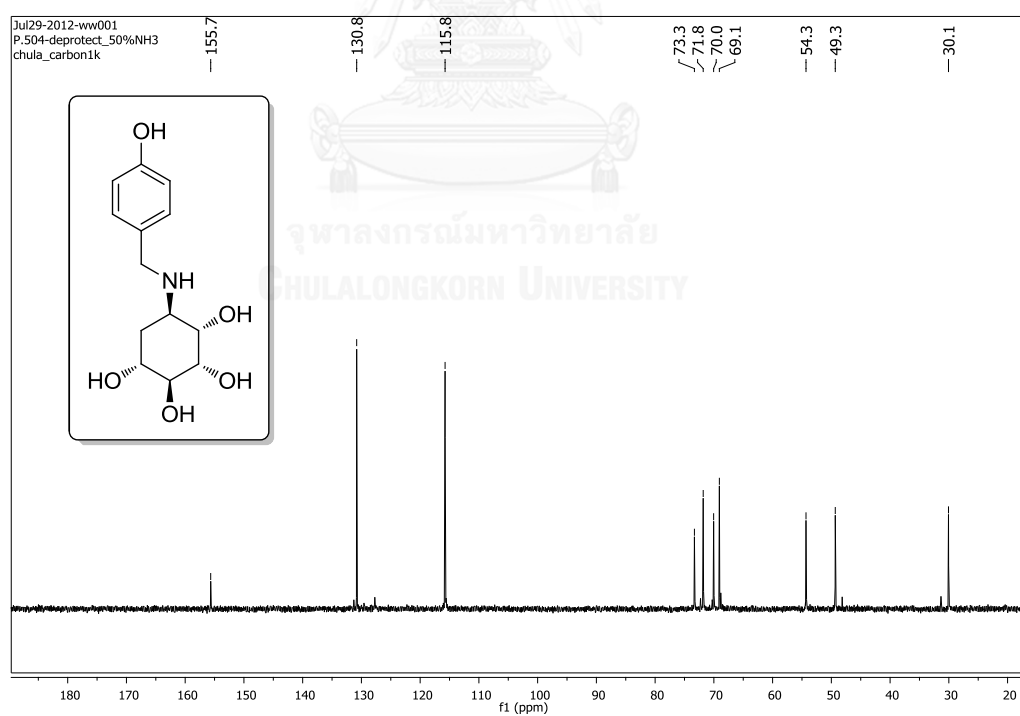
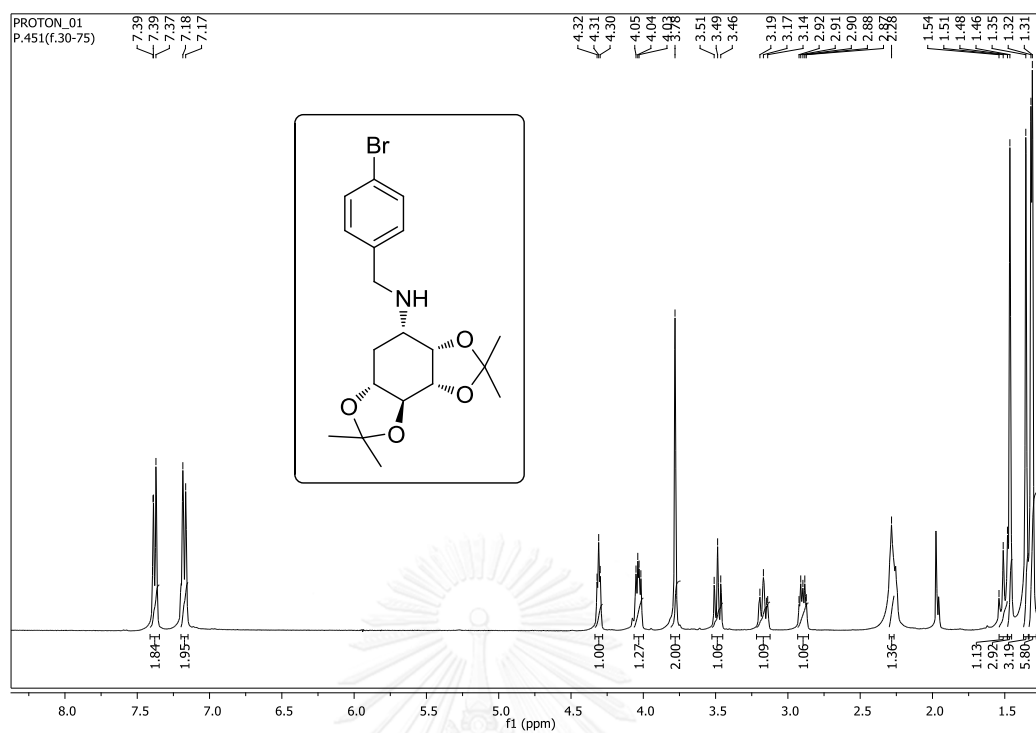
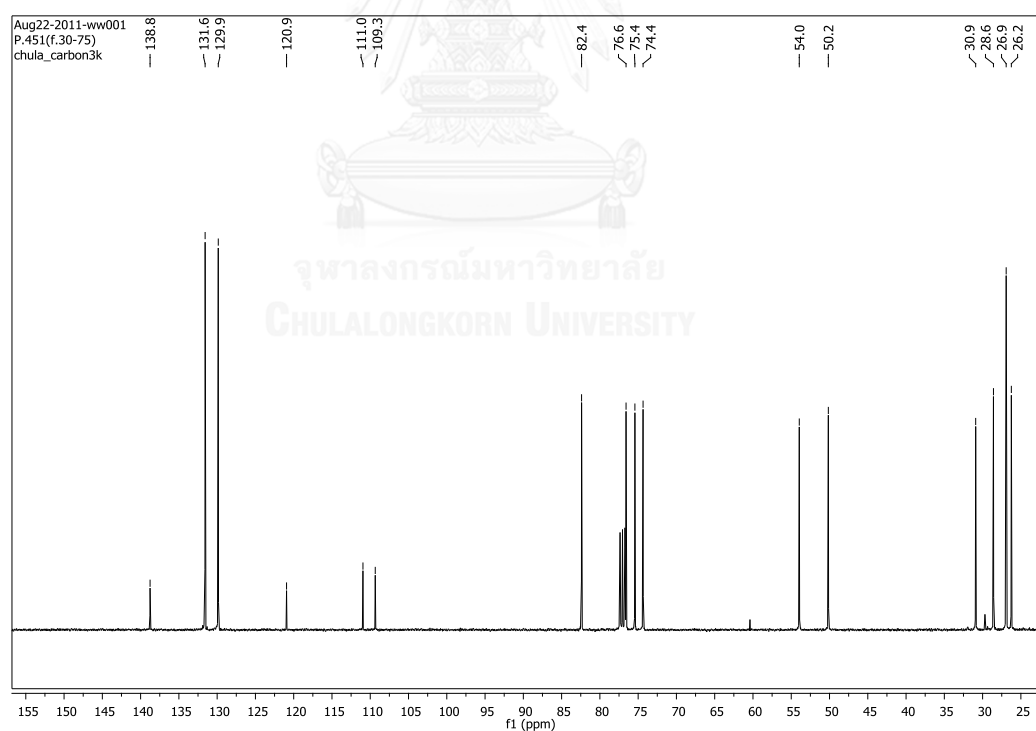


Figure 137. ^{13}C NMR spectrum of 5-20 (CD_3OD)

Figure 138. ^1H NMR spectrum of 5-21 (D_2O)Figure 139. ^{13}C NMR spectrum of 5-21 (D_2O)

Figure 140. ^1H NMR spectrum of 5-22 (D_2O)Figure 141. ^{13}C NMR spectrum of 5-22 (D_2O)

Figure 142. ¹H NMR spectrum of 5-23 (CDCl₃)Figure 143. ¹³C NMR spectrum of 5-23 (CDCl₃)

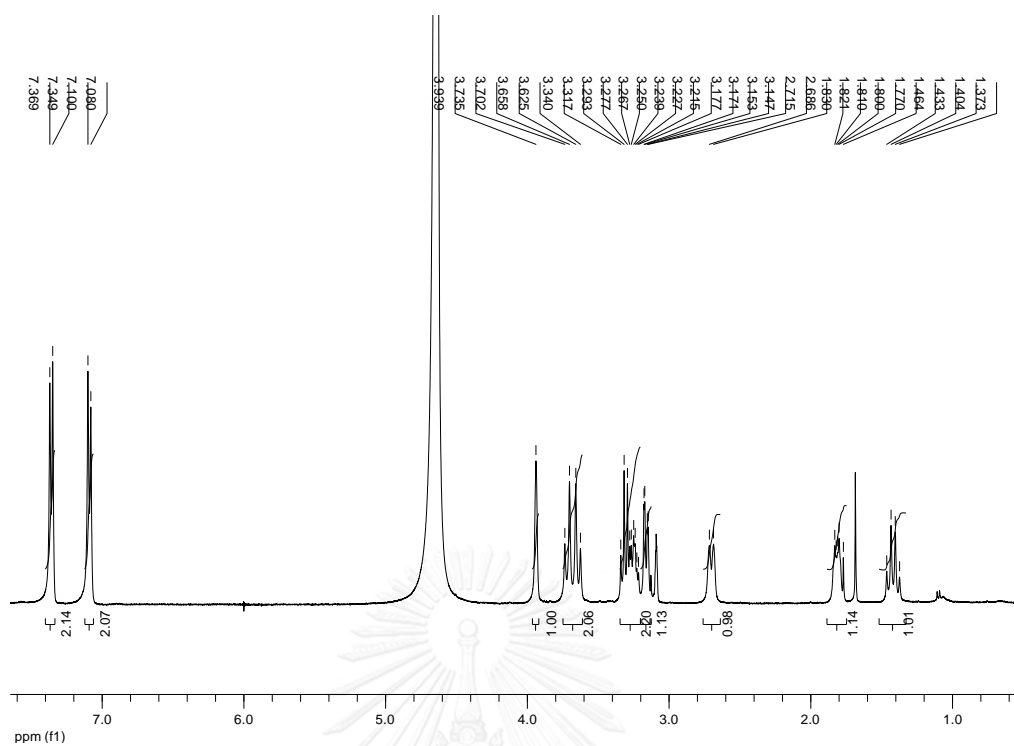


Figure 144. ^1H NMR spectrum of 5-24 (D_2O + 2 drops MeOD)

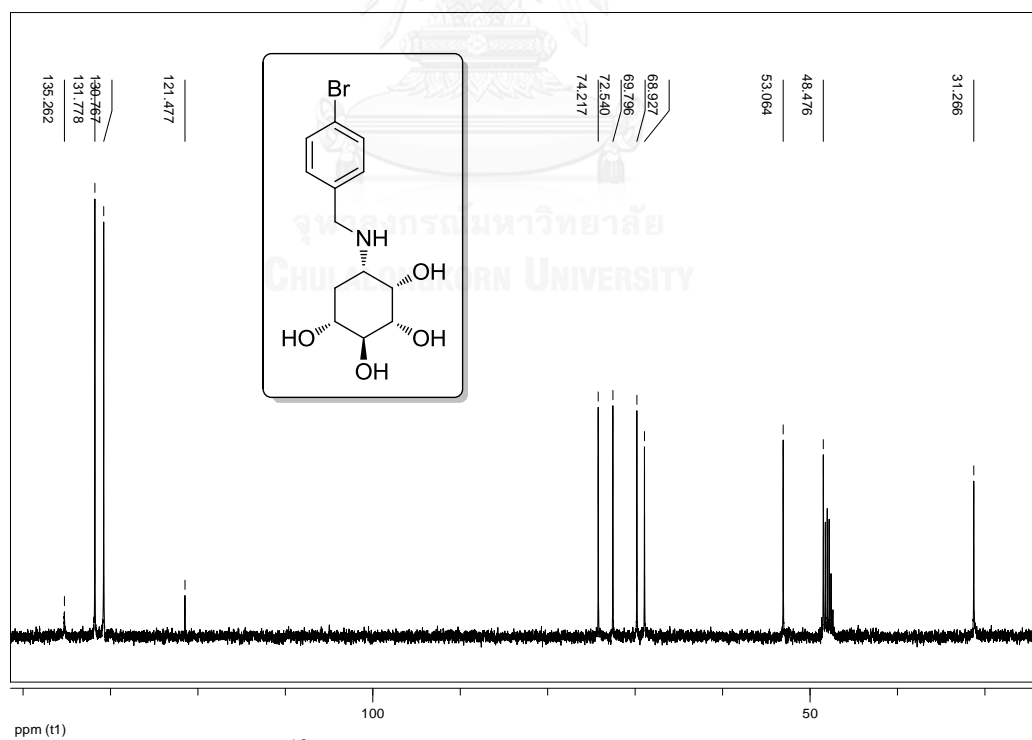


Figure 145. ^{13}C NMR spectrum of 5-24 (D_2O + 2 drops MeOD)

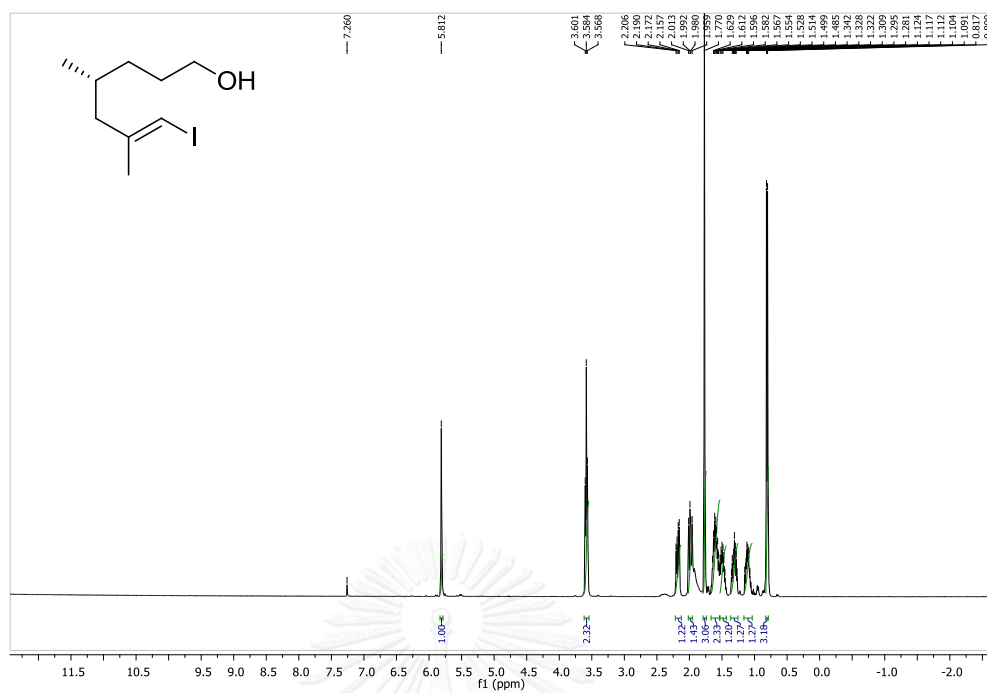


Figure 146. ^1H NMR spectrum of 6-20 (CDCl_3)

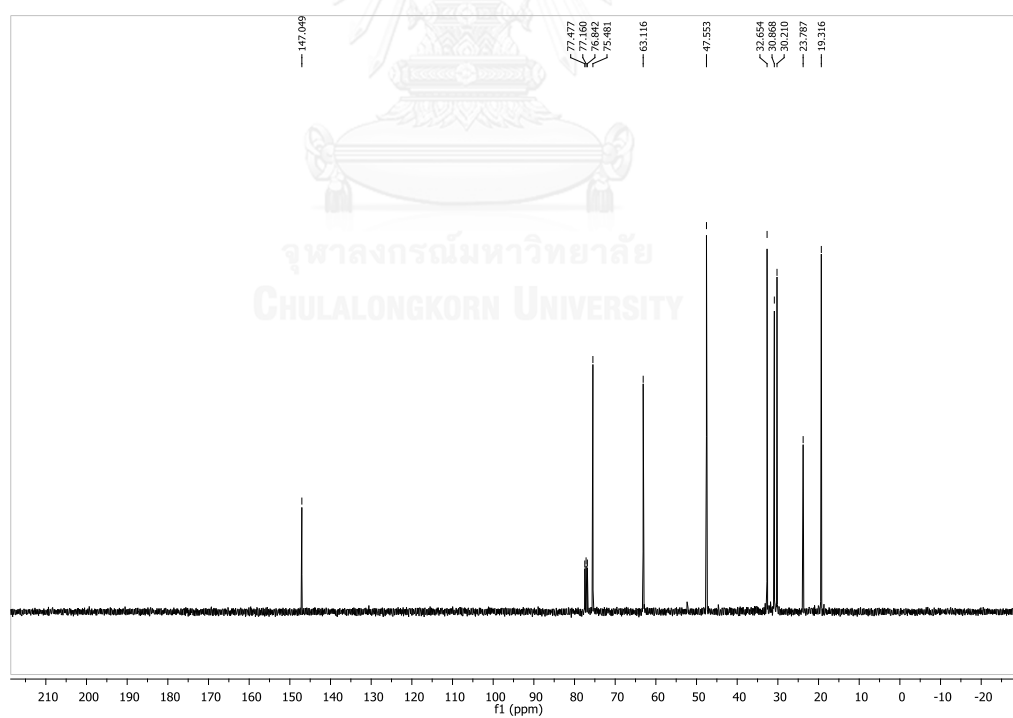


Figure 147. ^{13}C NMR spectrum of 6-20 (CDCl_3)

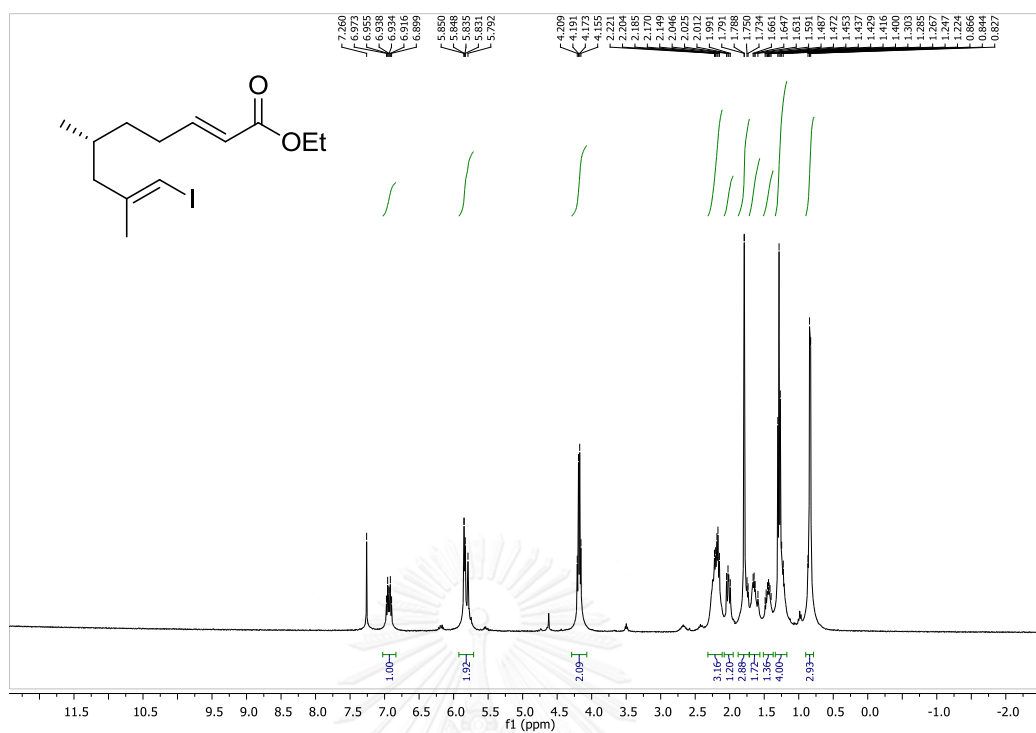


Figure 148. $^1\text{H NMR}$ spectrum of 6-21 (CDCl_3)

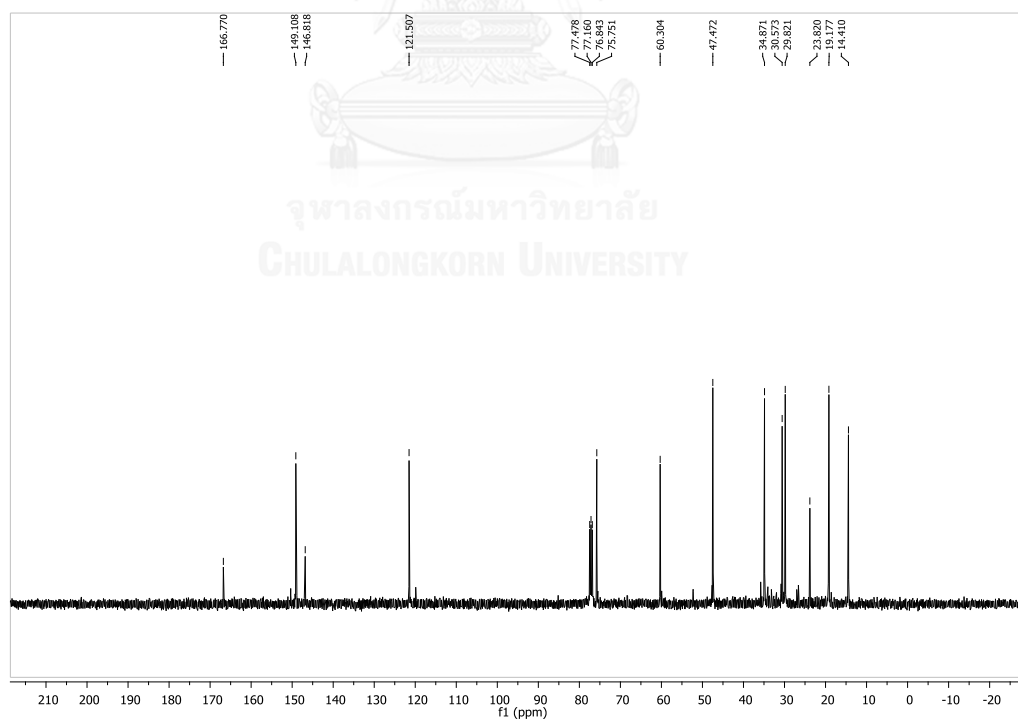


Figure 149. $^{13}\text{C NMR}$ spectrum of 6-21 (CDCl_3)

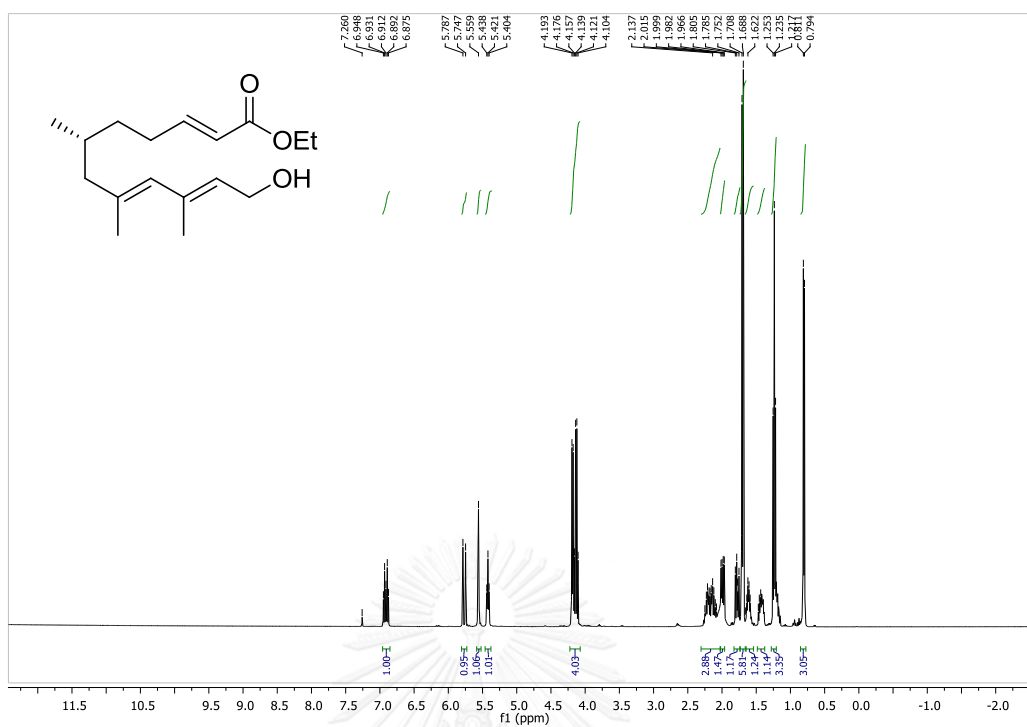


Figure 150. ^1H NMR spectrum of **6-23** (CDCl_3)

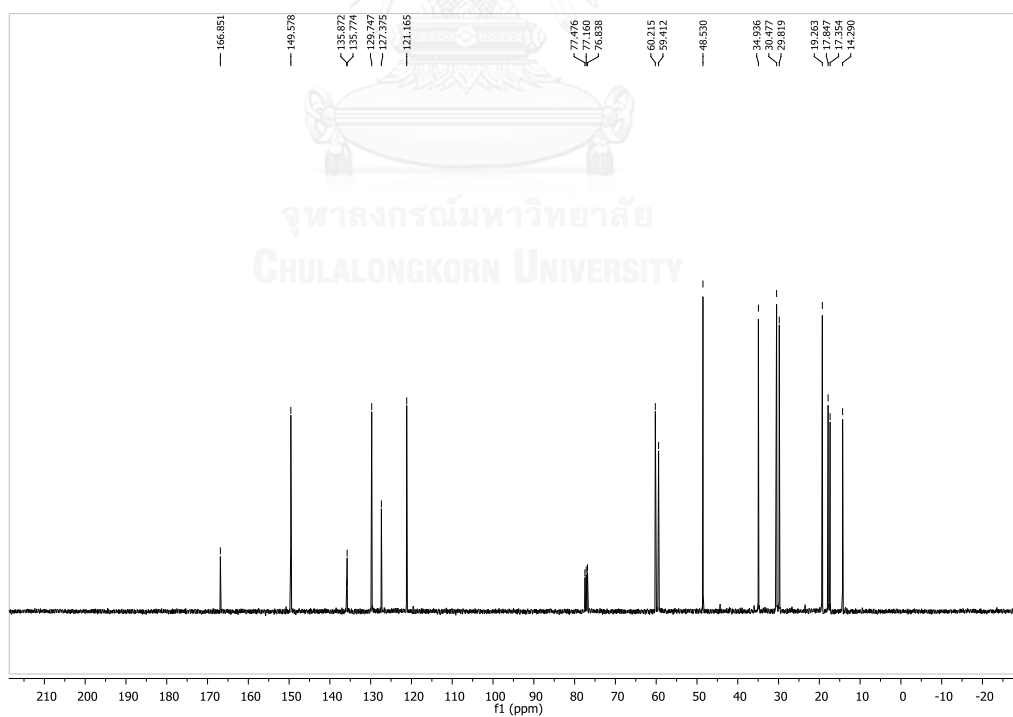


Figure 151. ^{13}C NMR spectrum of **6-23** (CDCl_3)

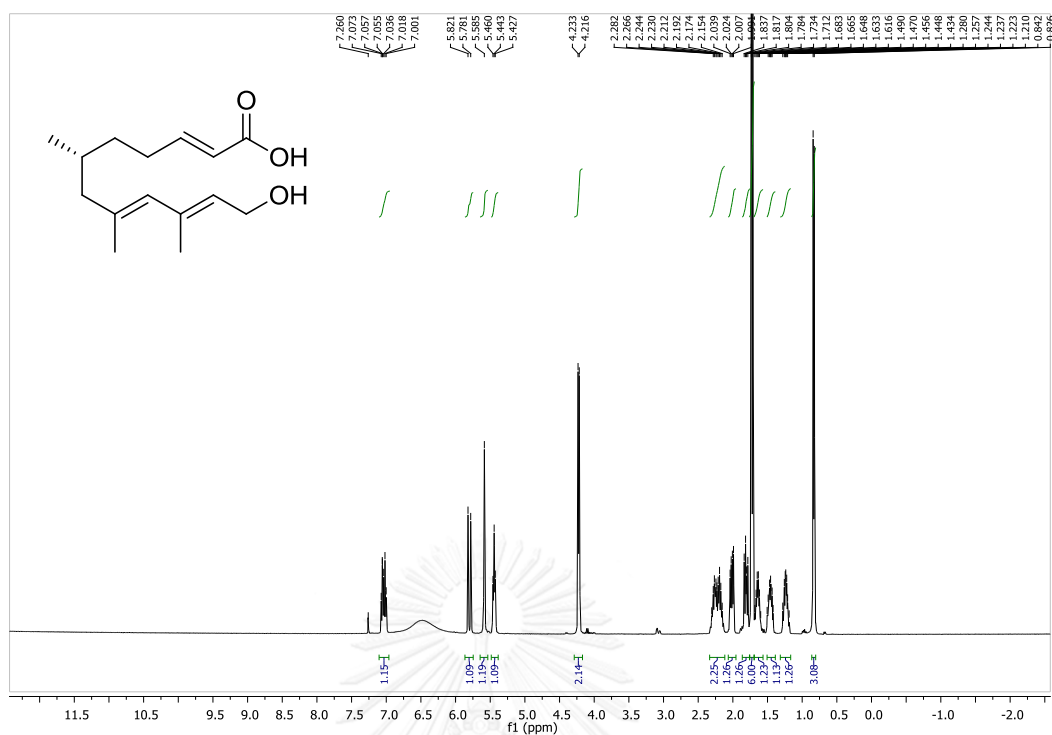


Figure 152. ^1H NMR spectrum of 6-24 (CDCl_3)

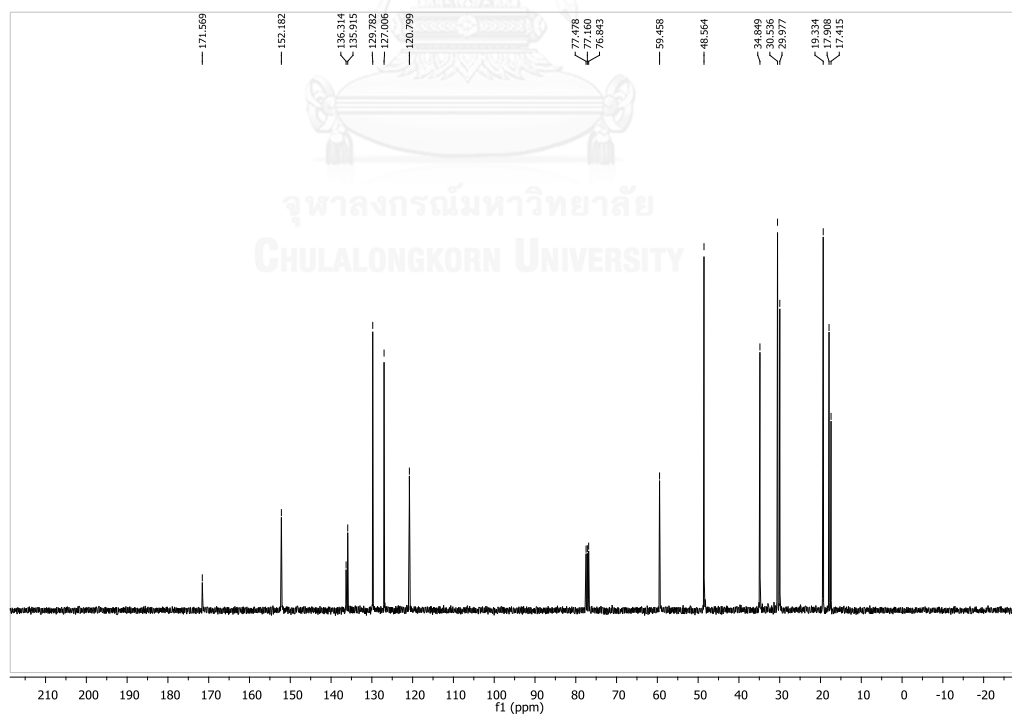
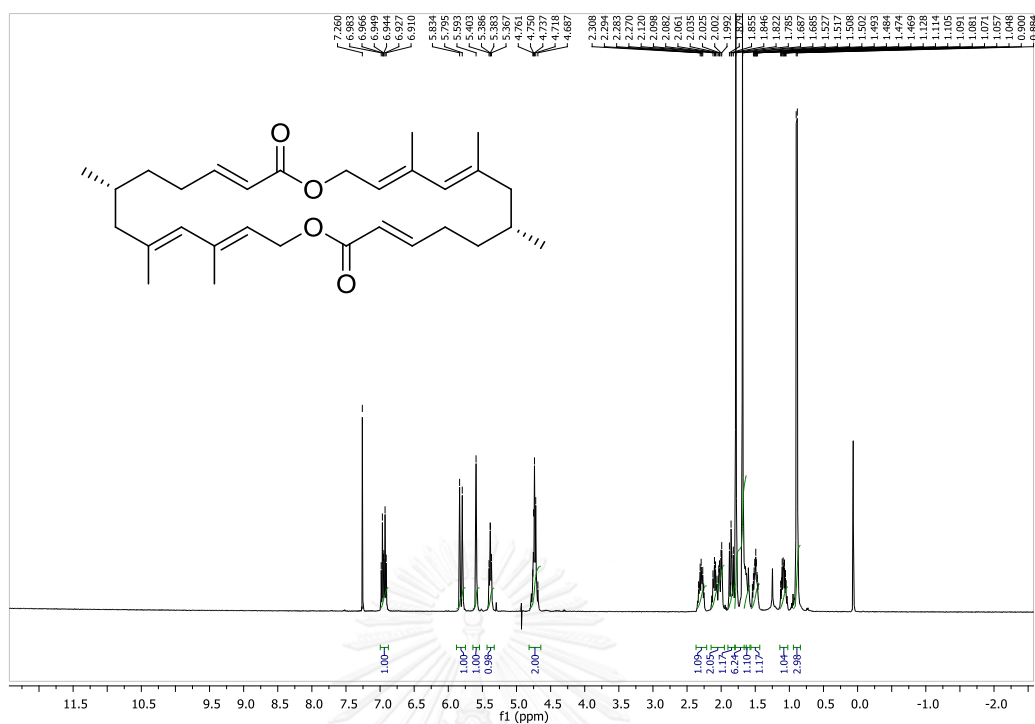
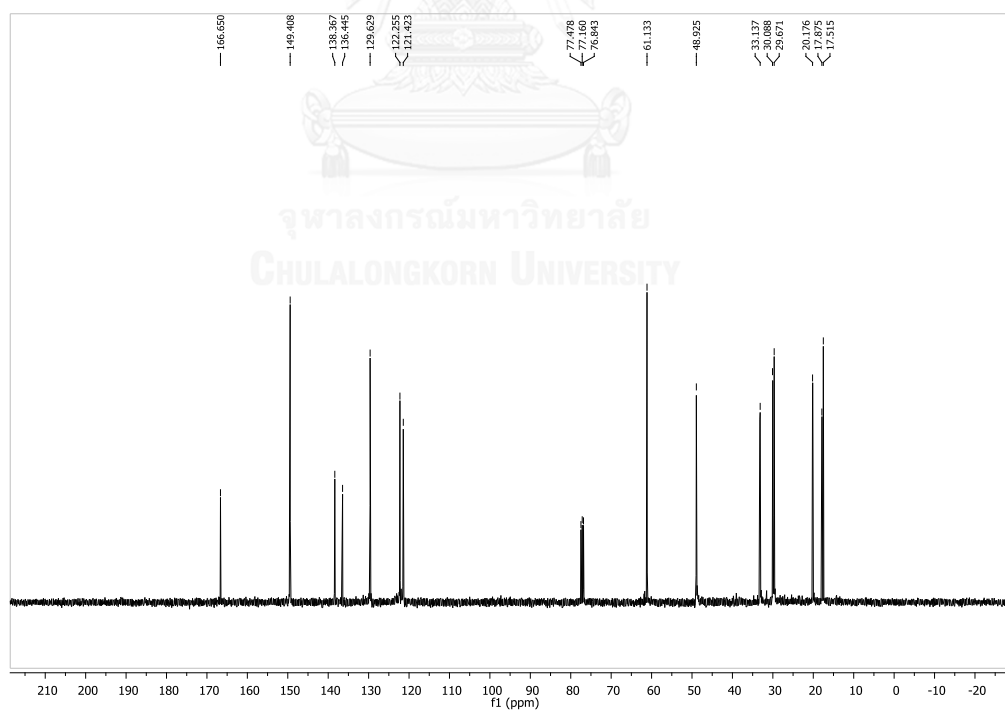


Figure 153. ^{13}C NMR spectrum of 6-24 (CDCl_3)

Figure 154. ^1H NMR spectrum of 6-25 (CDCl_3)Figure 155. ^{13}C NMR spectrum of 6-25 (CDCl_3)

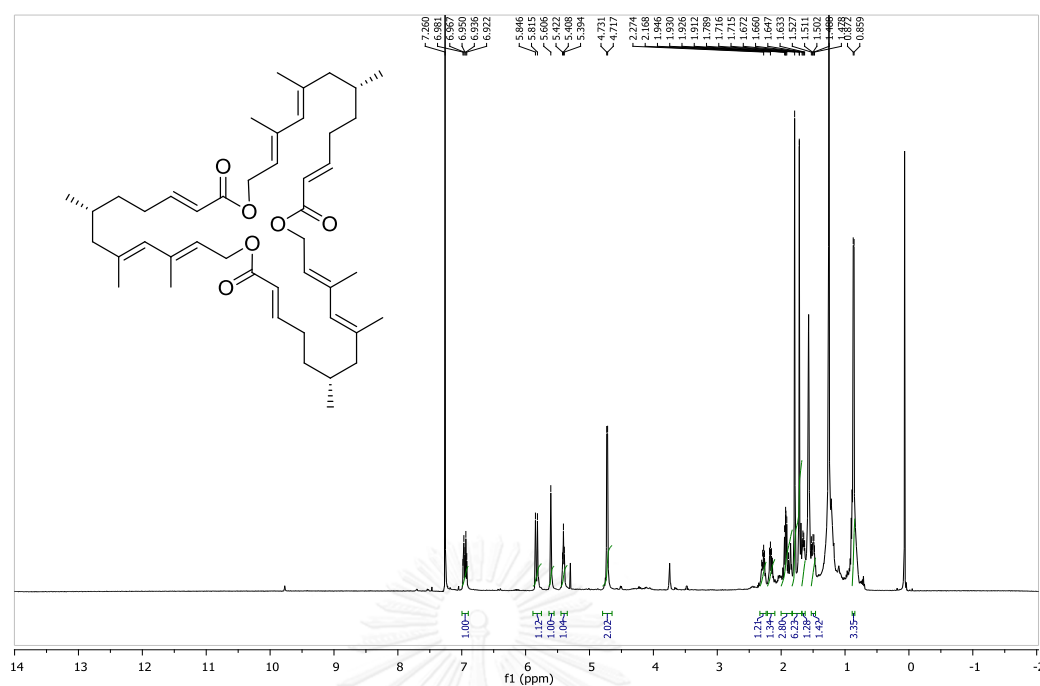


Figure 156. ^1H NMR spectrum of **6-43** (CDCl_3)

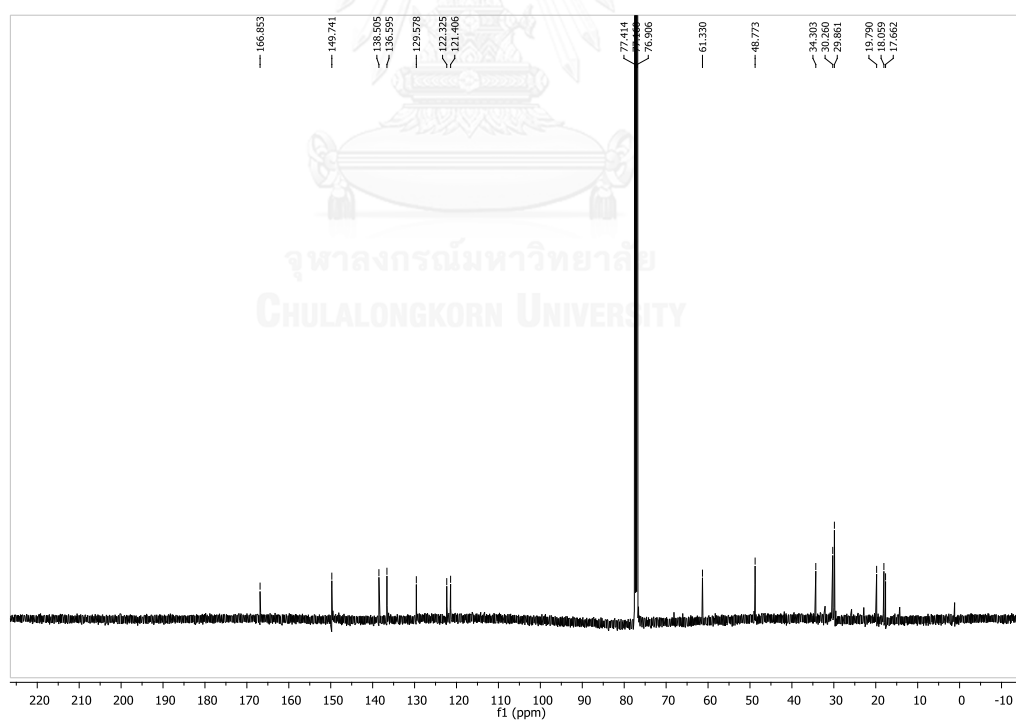


Figure 157. ^{13}C NMR spectrum of **6-43** (CDCl_3)

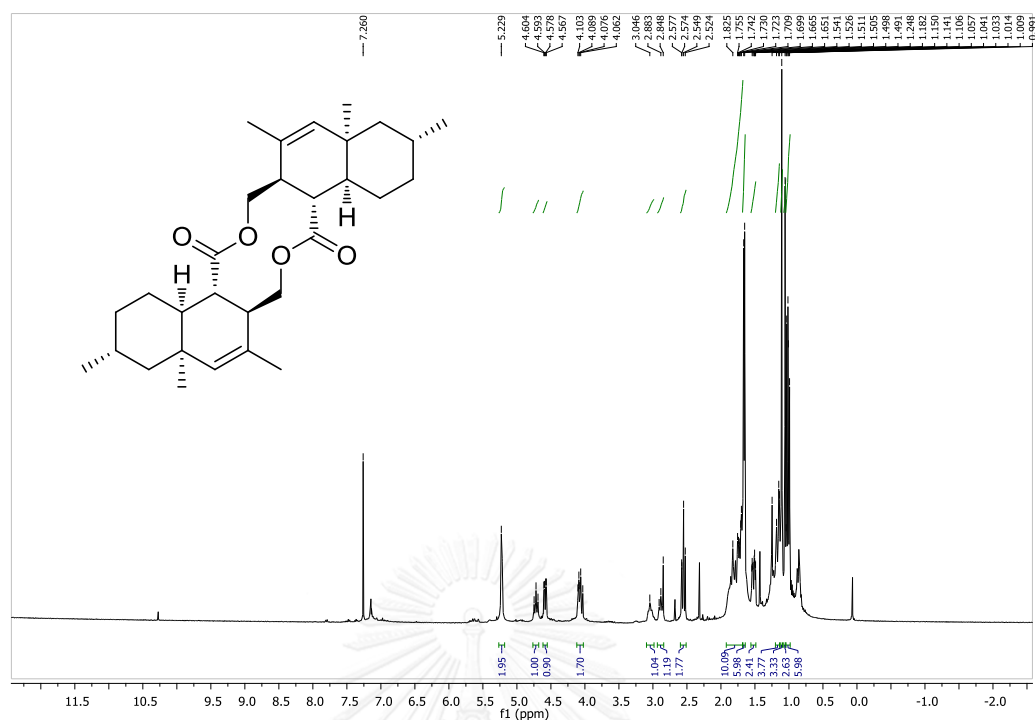


Figure 158. $^1\text{H NMR}$ spectrum of 6-26 (CDCl_3)

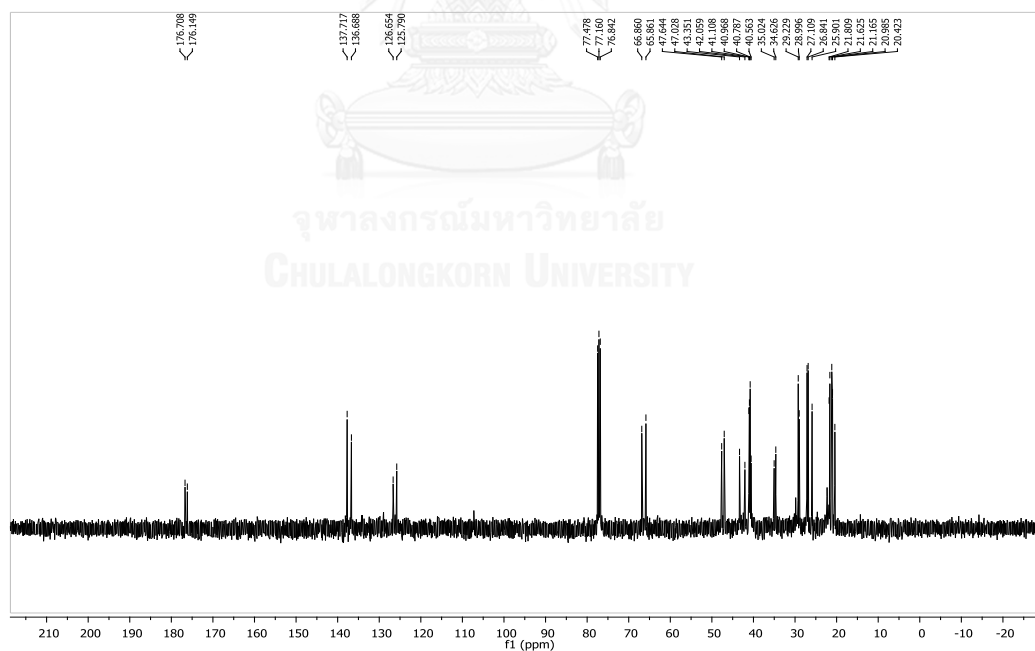
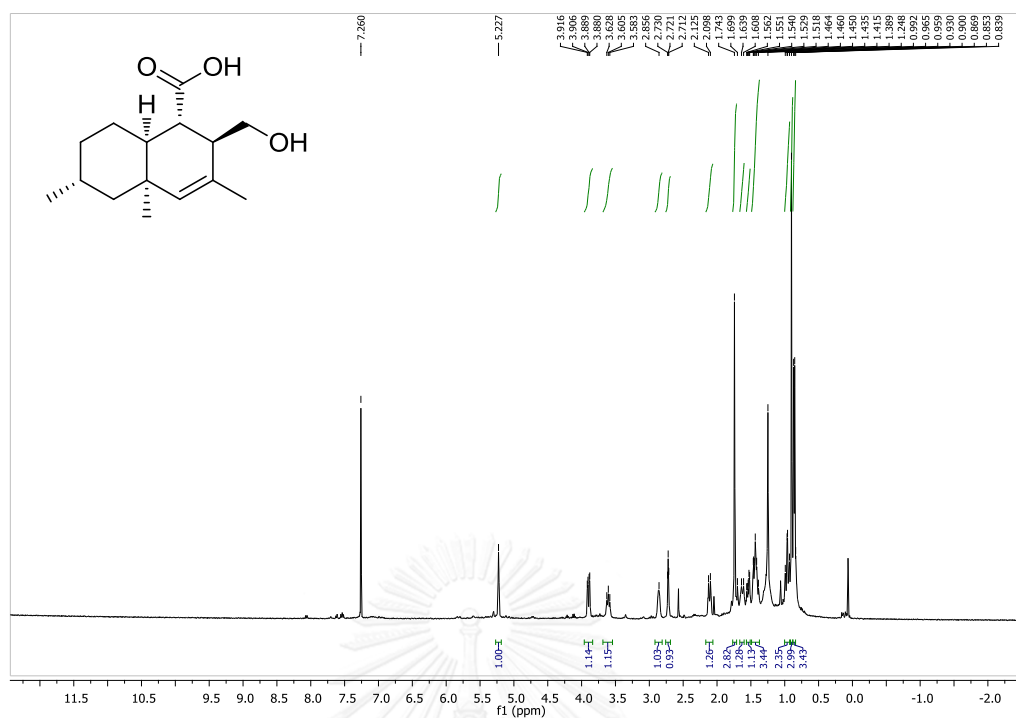
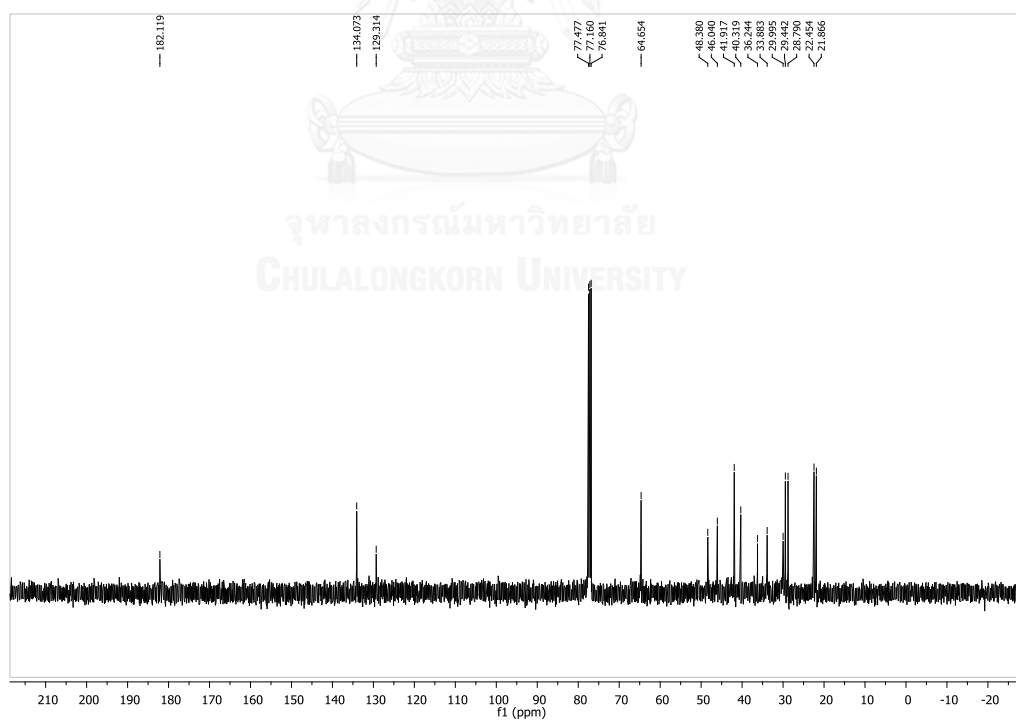


Figure 159. $^{13}\text{C NMR}$ spectrum of 6-26 (CDCl_3)

Figure 160. $^1\text{H NMR}$ spectrum of 6-27 (CDCl_3)Figure 161. $^{13}\text{C NMR}$ spectrum of 6-27 (CDCl_3)

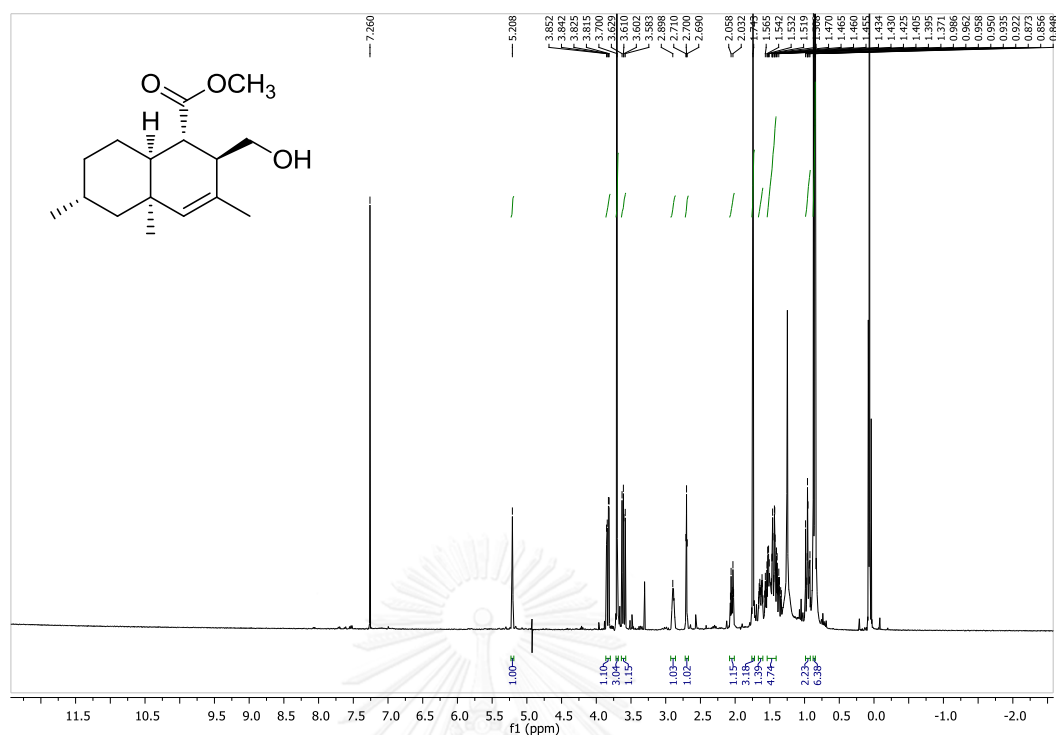


Figure 162. ^1H NMR spectrum of 6-28 (CDCl_3)

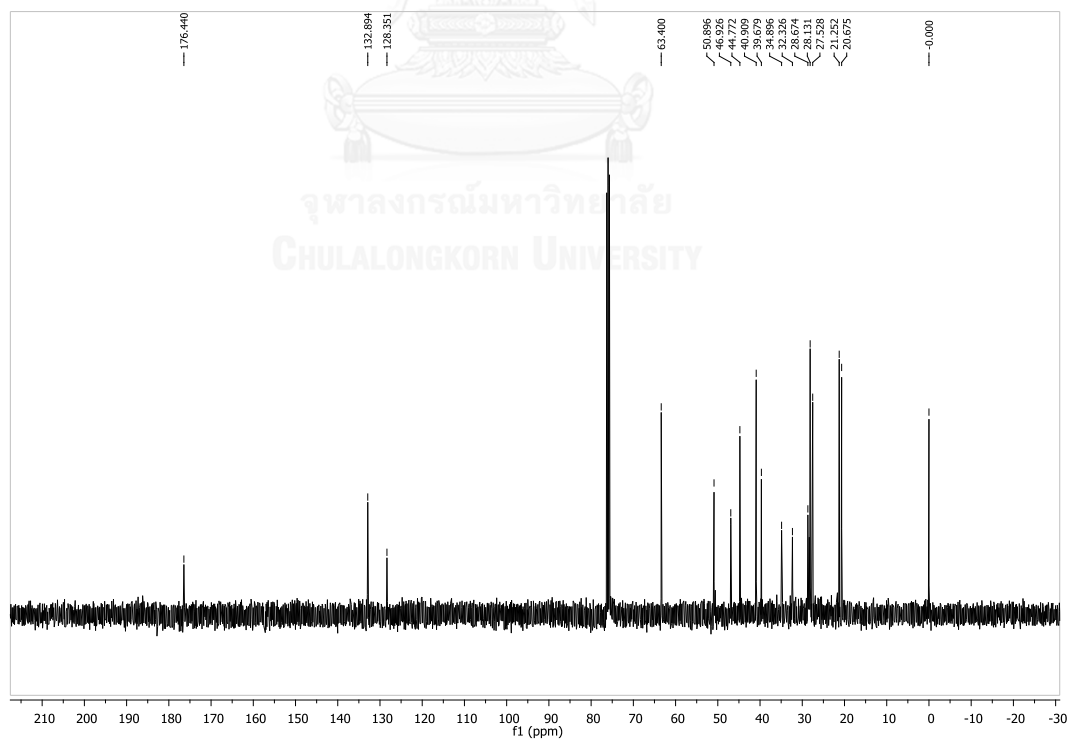


Figure 163. ^{13}C NMR spectrum of 6-28 (CDCl_3)

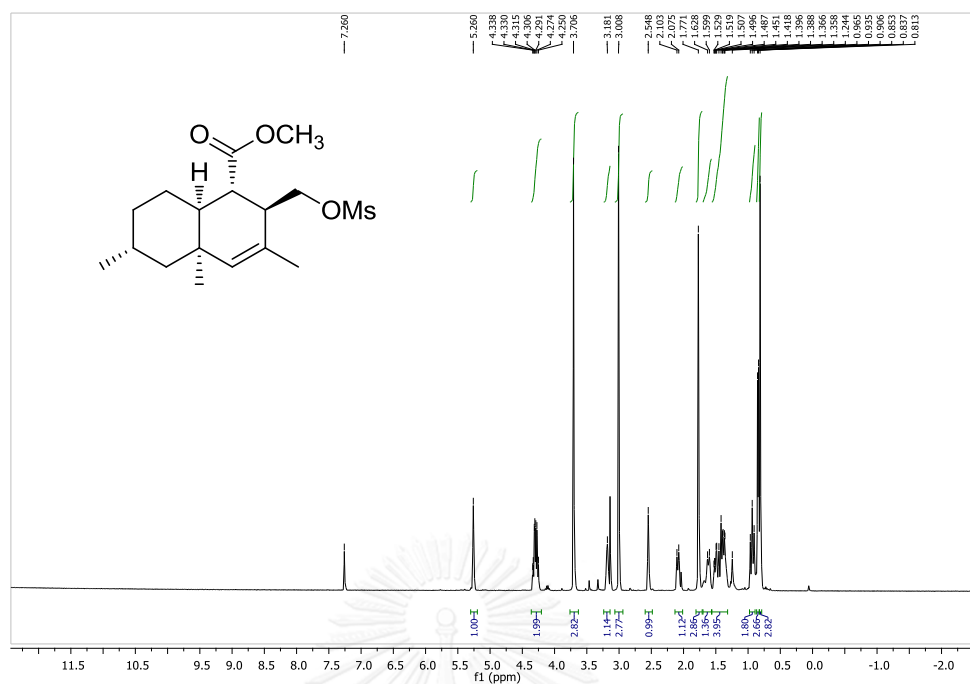


Figure 164. ¹H NMR spectrum of 6-29 (CDCl₃)

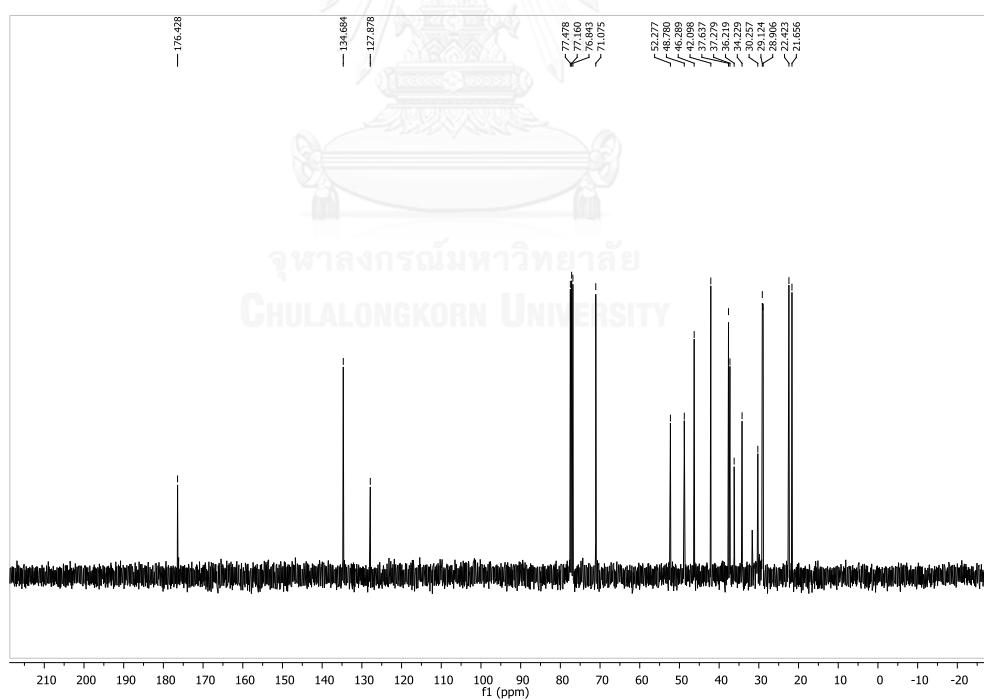


Figure 165. ¹³C NMR spectrum of 6-29 (CDCl₃)

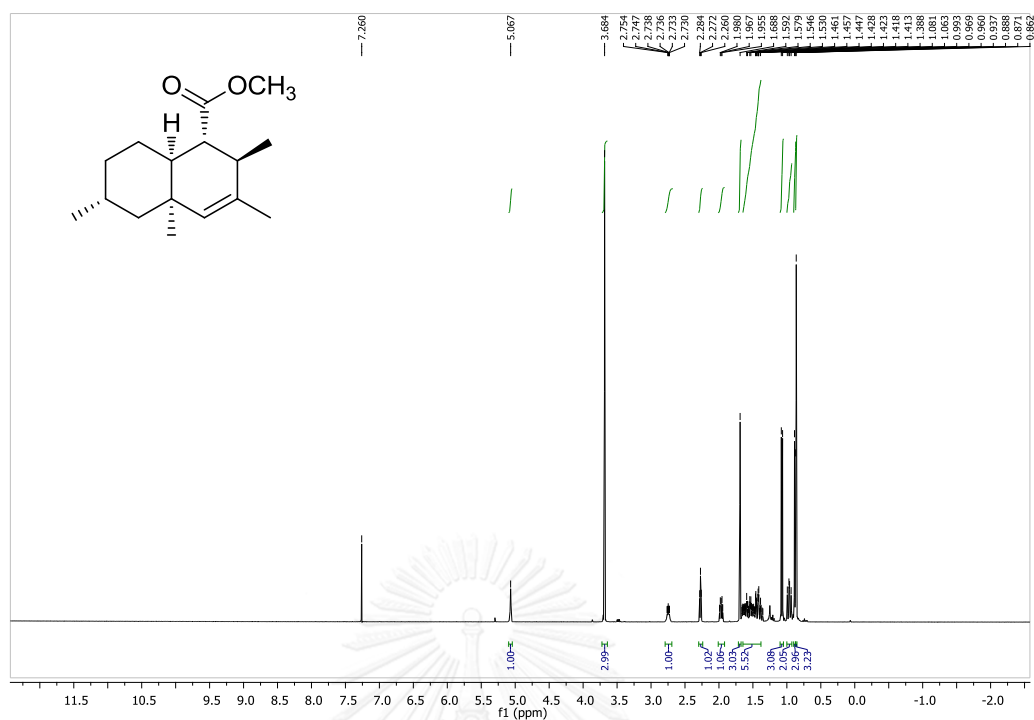


Figure 166. $^1\text{H NMR}$ spectrum of 6-30 (CDCl_3)

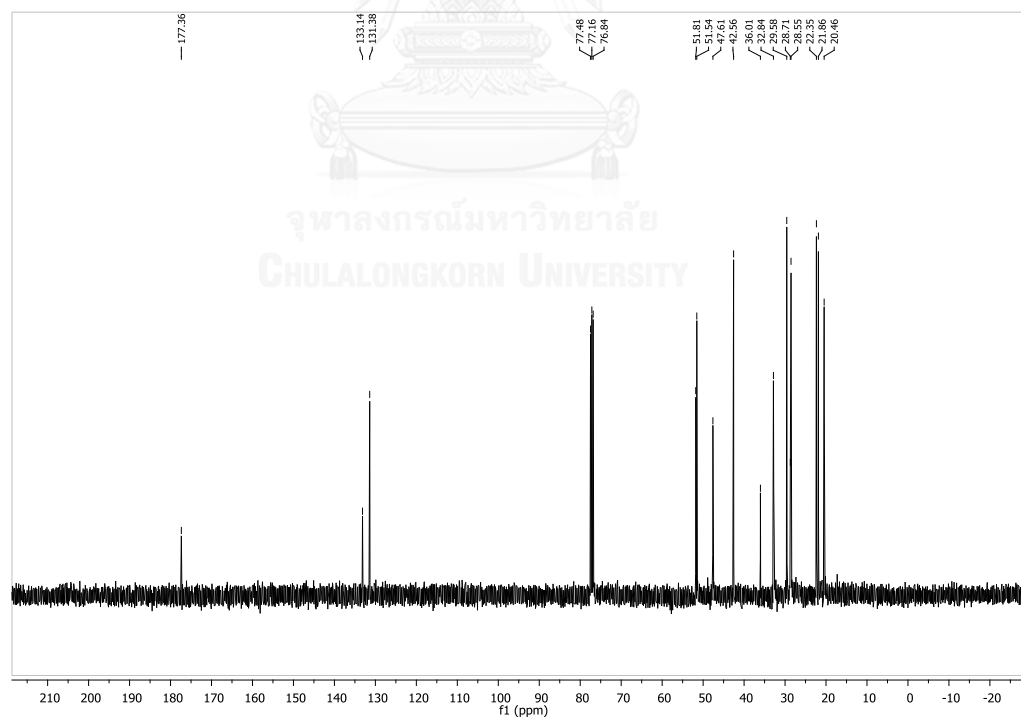


Figure 167. $^{13}\text{C NMR}$ spectrum of 6-30 (CDCl_3)

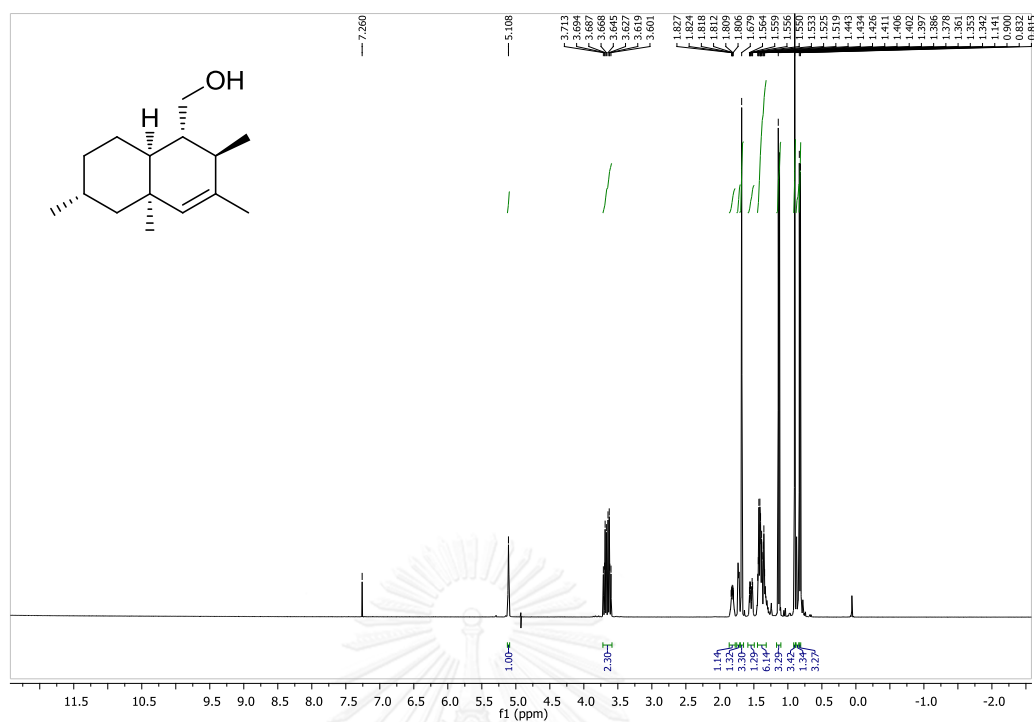


Figure 168. ^1H NMR spectrum of 6-31 (CDCl_3)

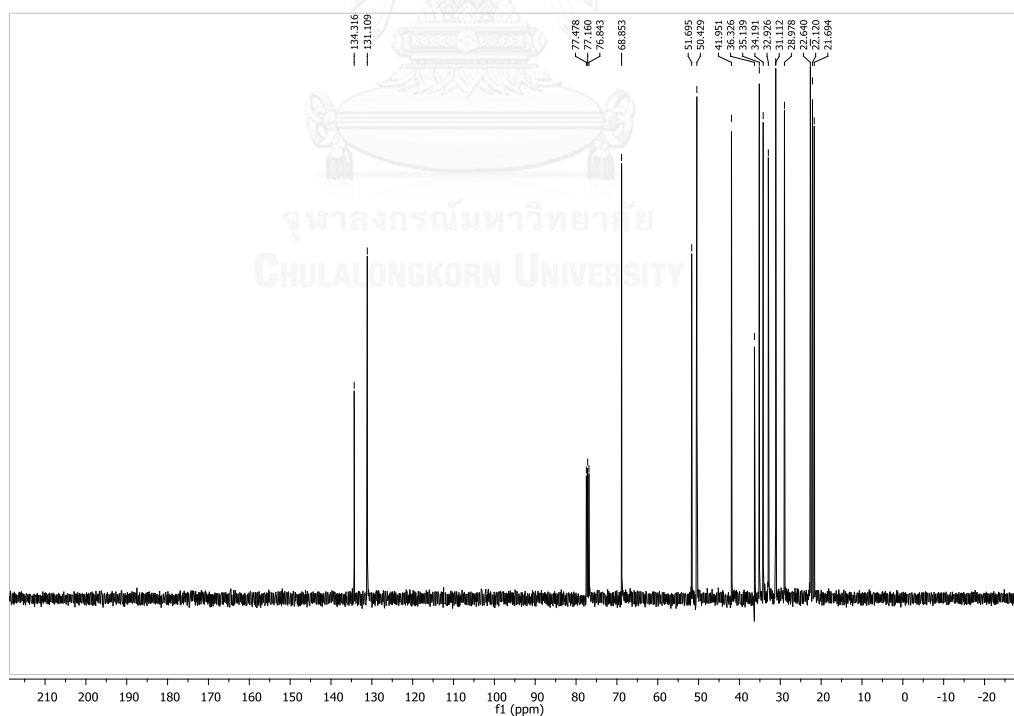


Figure 169. ^{13}C NMR spectrum of 6-31 (CDCl_3)

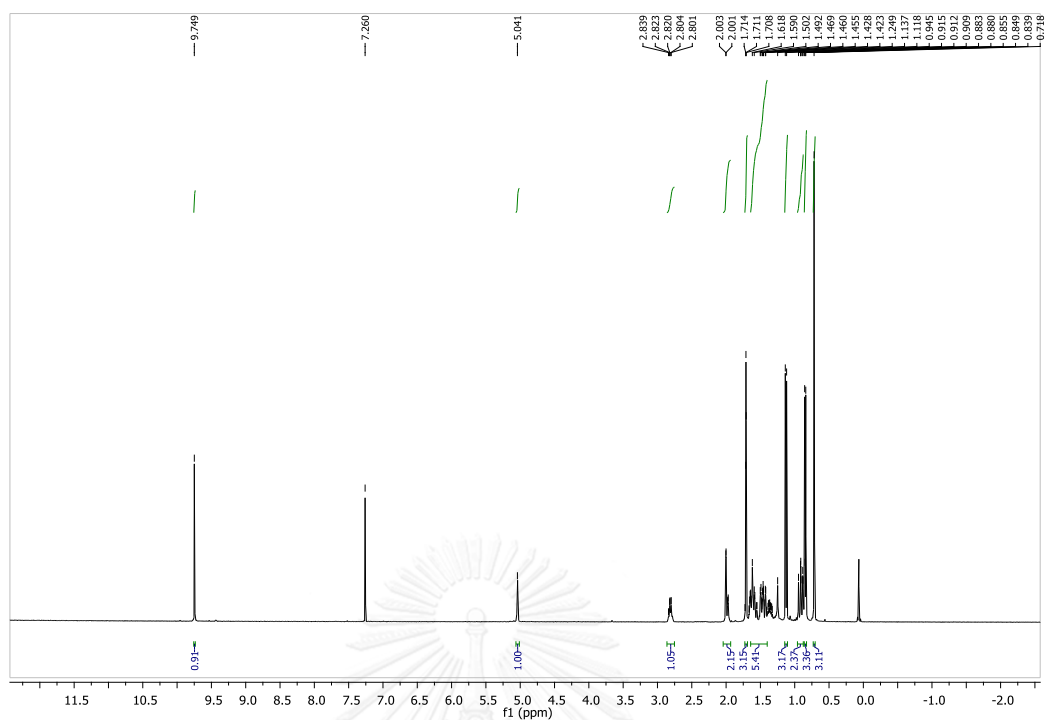


Figure 170. ^1H NMR spectrum of **6-10** (CDCl_3)

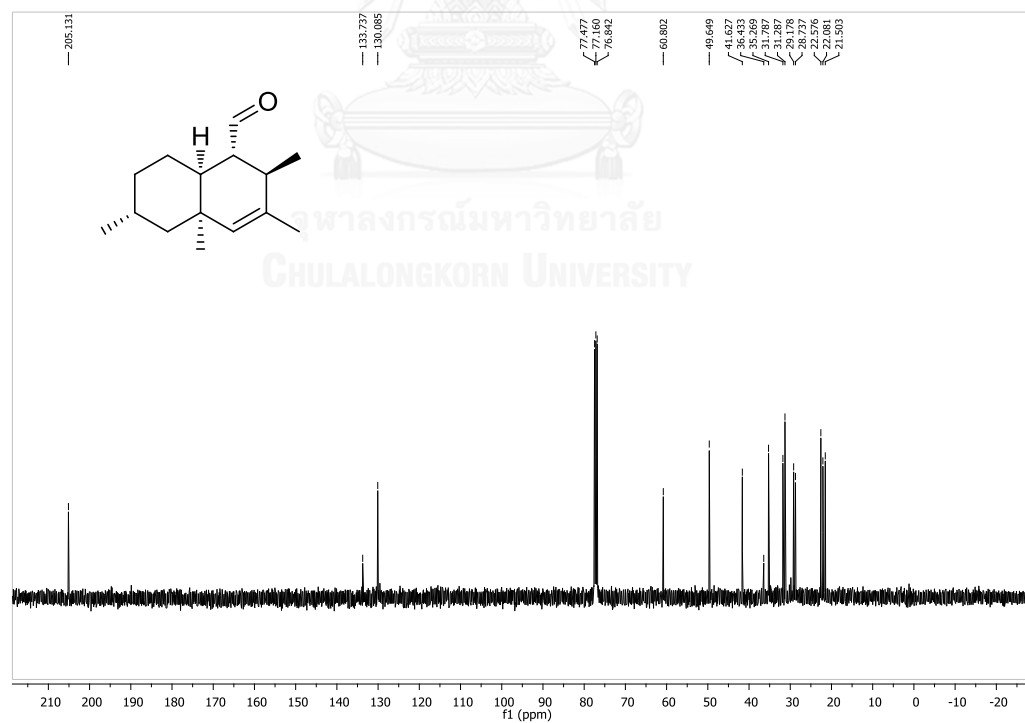
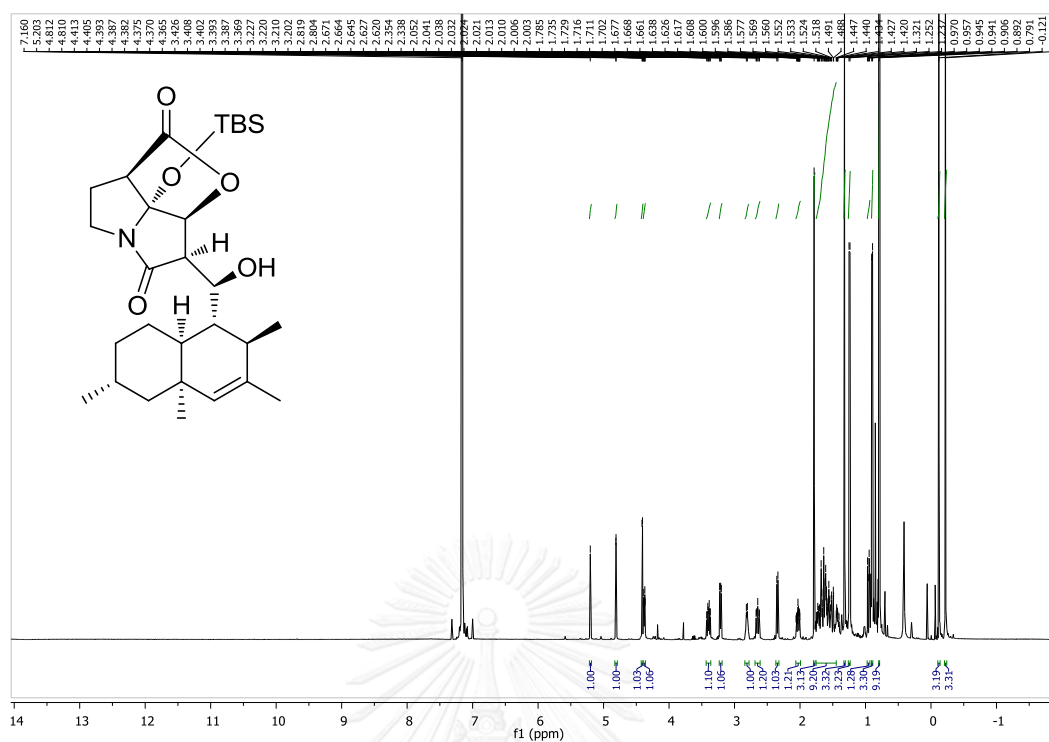
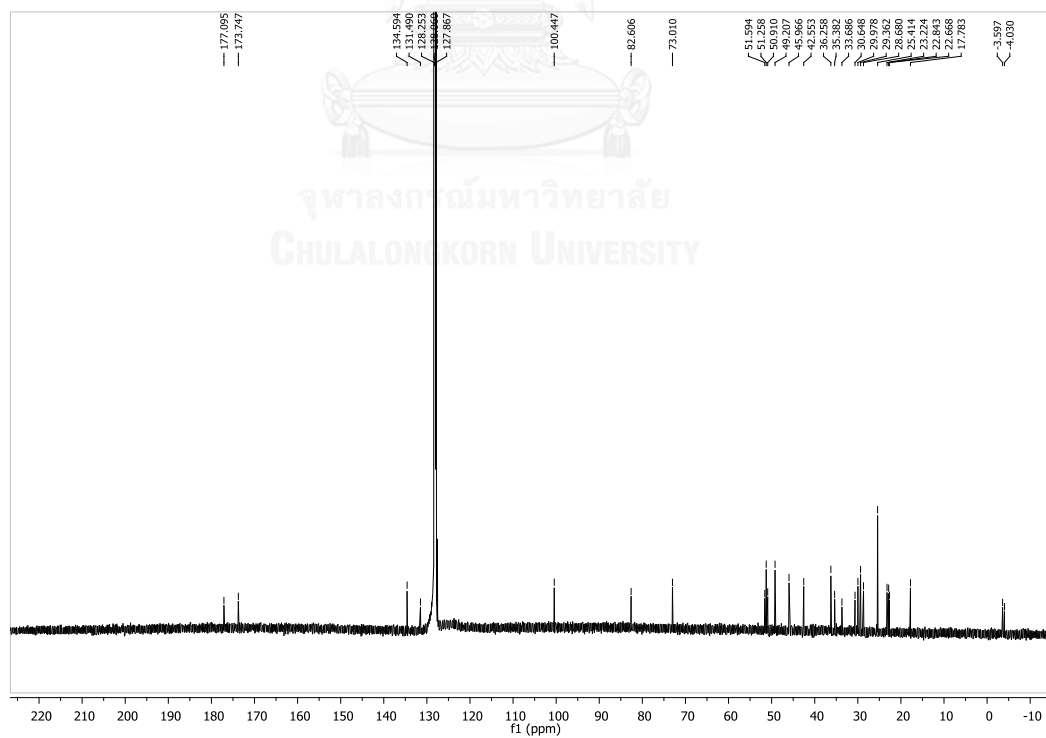


Figure 171. ^{13}C NMR spectrum of **6-10** (CDCl_3)

Figure 172. ^1H NMR spectrum of 6-32 (C_6D_6)Figure 173. ^{13}C NMR spectrum of 6-32 (C_6D_6)

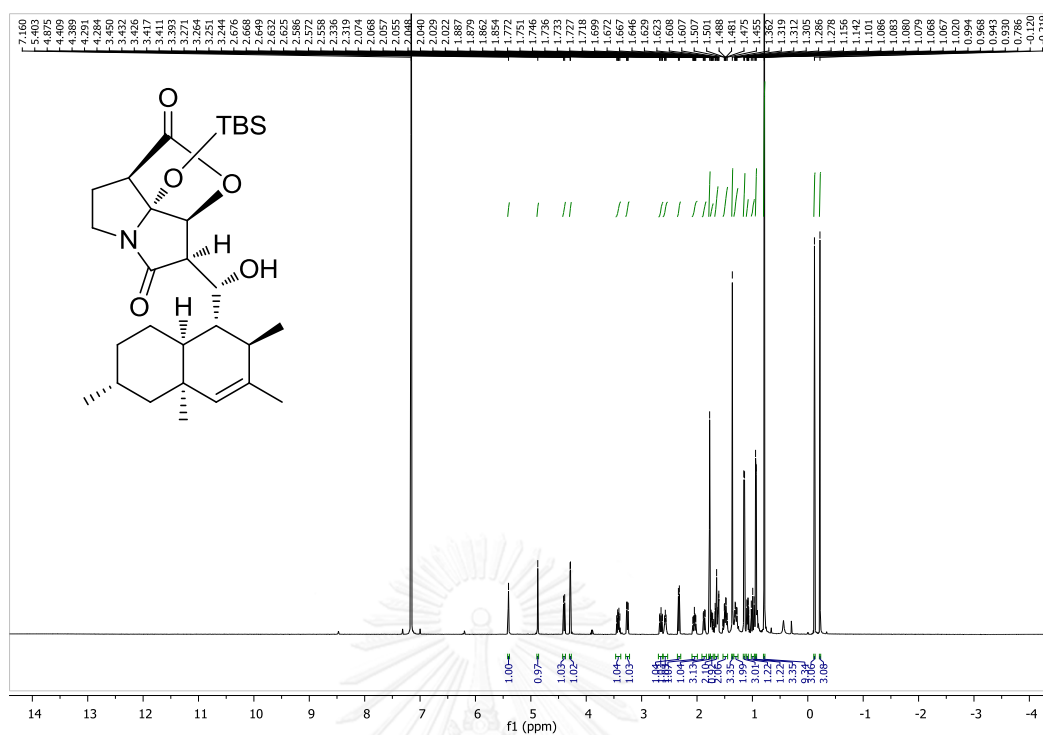


Figure 174. ^1H NMR spectrum of 6-33 (C_6D_6)

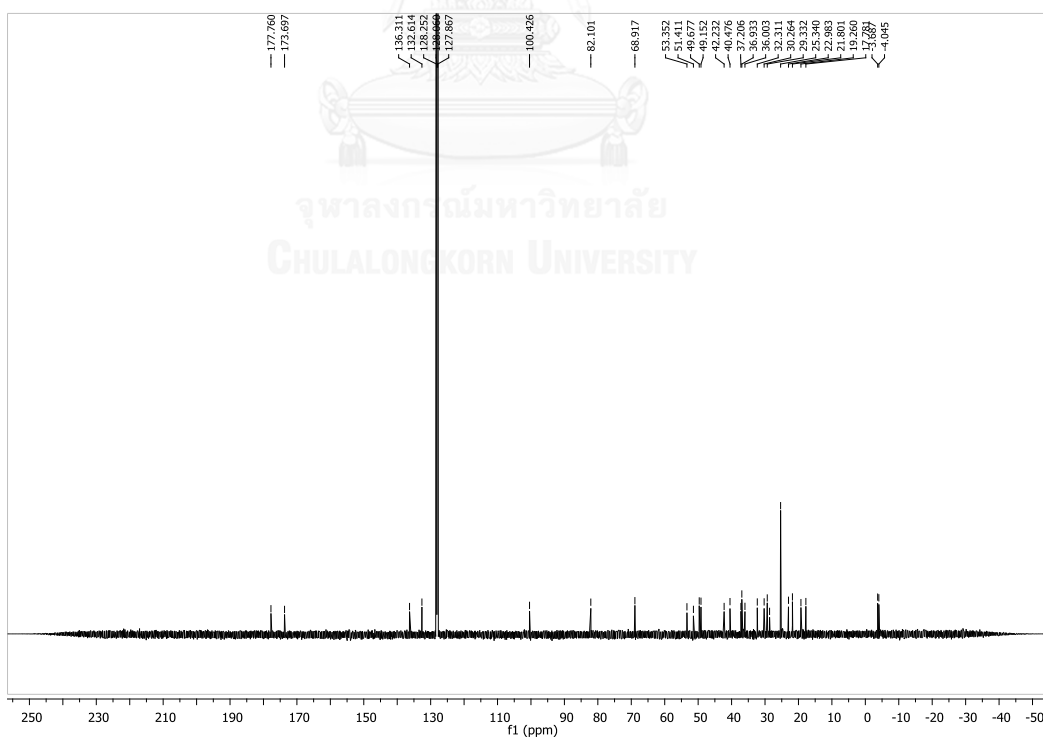


Figure 175. ^{13}C NMR spectrum of 6-33 (C_6D_6)

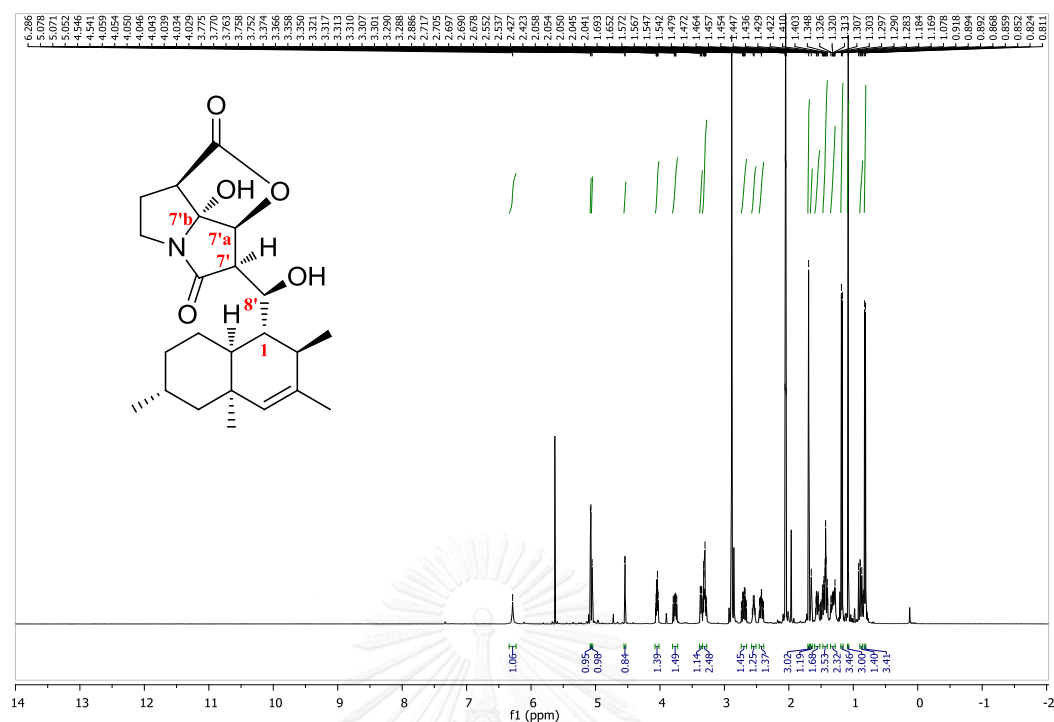


Figure 176. ^1H NMR spectrum of **6-34** (acetone- d_6)

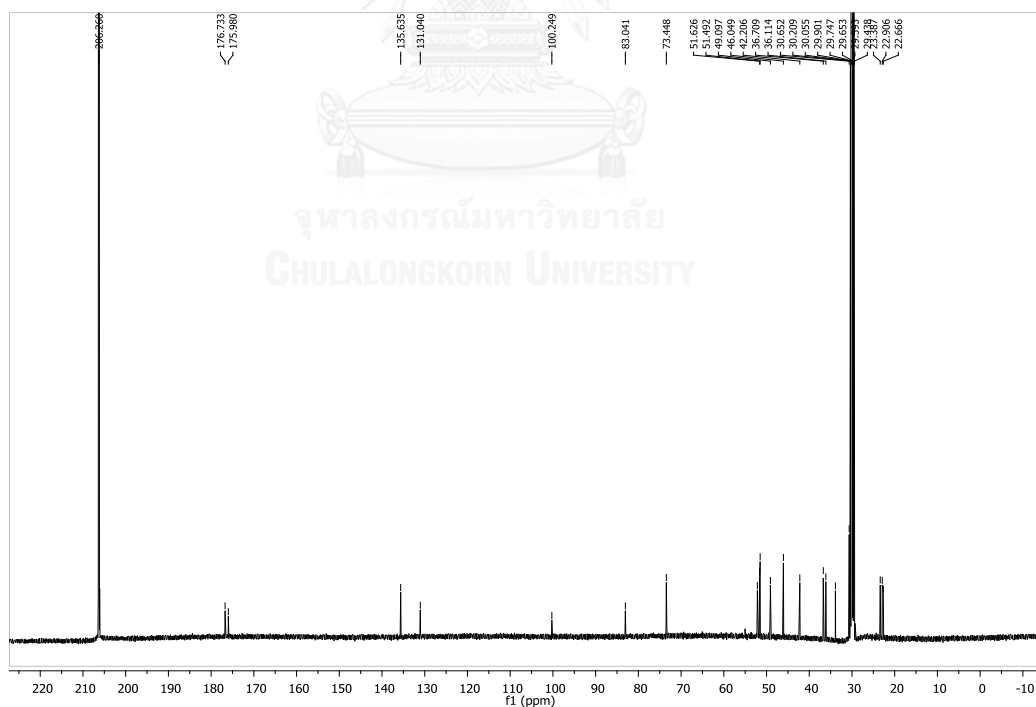


Figure 177. ^{13}C NMR spectrum of **6-34** (acetone- d_6)

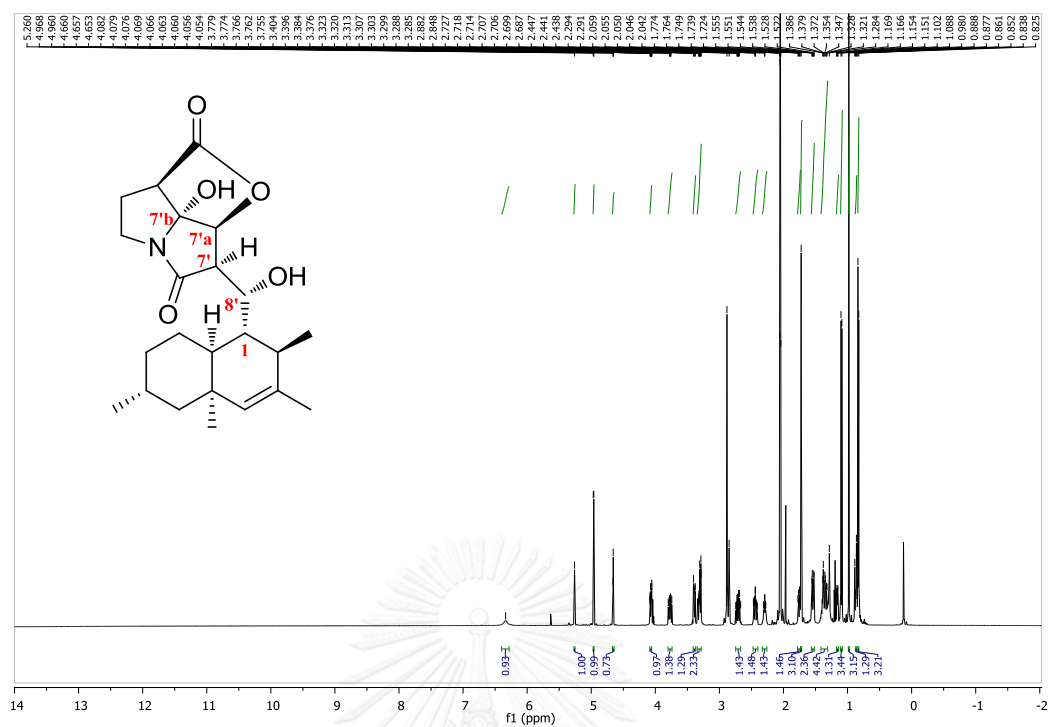


Figure 178. ^1H NMR spectrum of 6-35 (acetone- d_6)

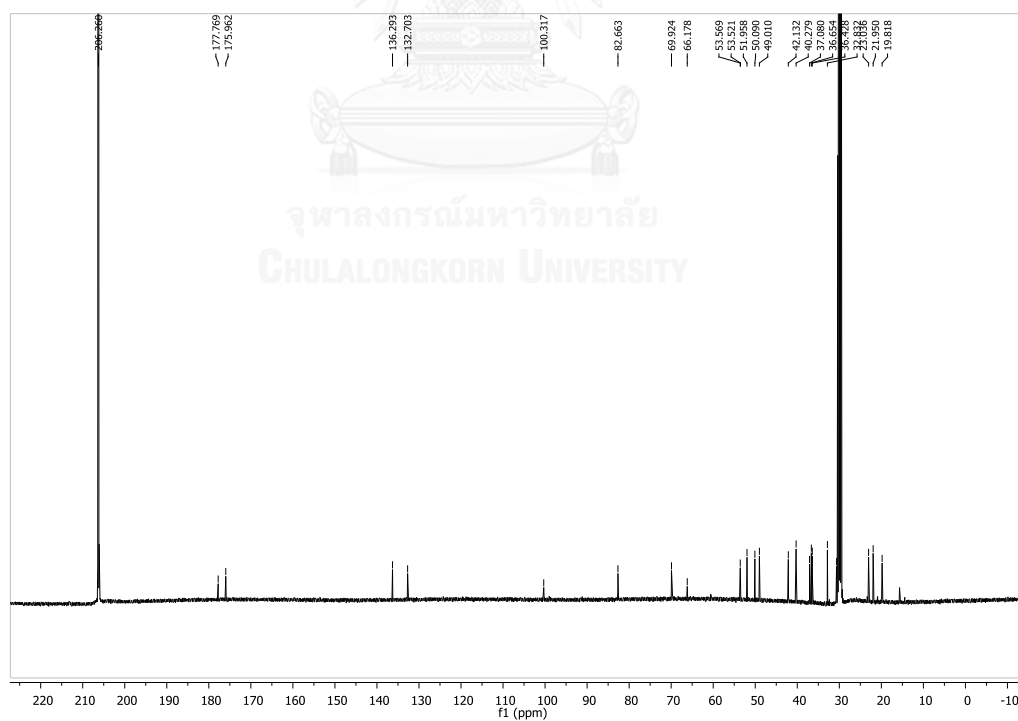


Figure 179. ^{13}C NMR spectrum of 6-35 (acetone- d_6)

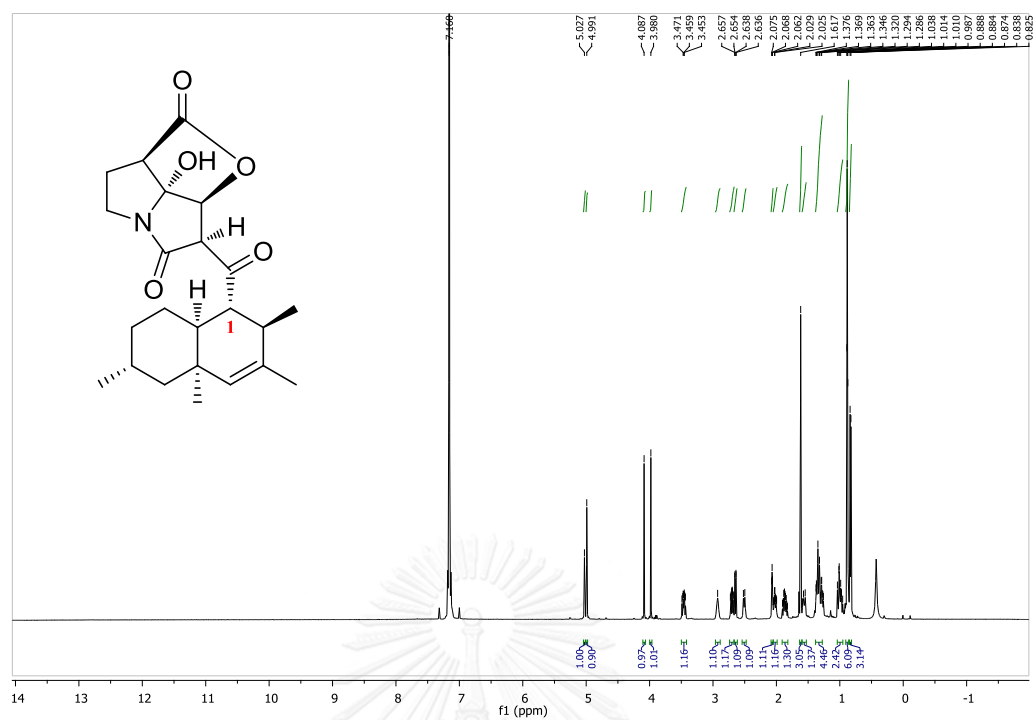


Figure 180. ^1H NMR spectrum of 6-1a (C_6D_6)

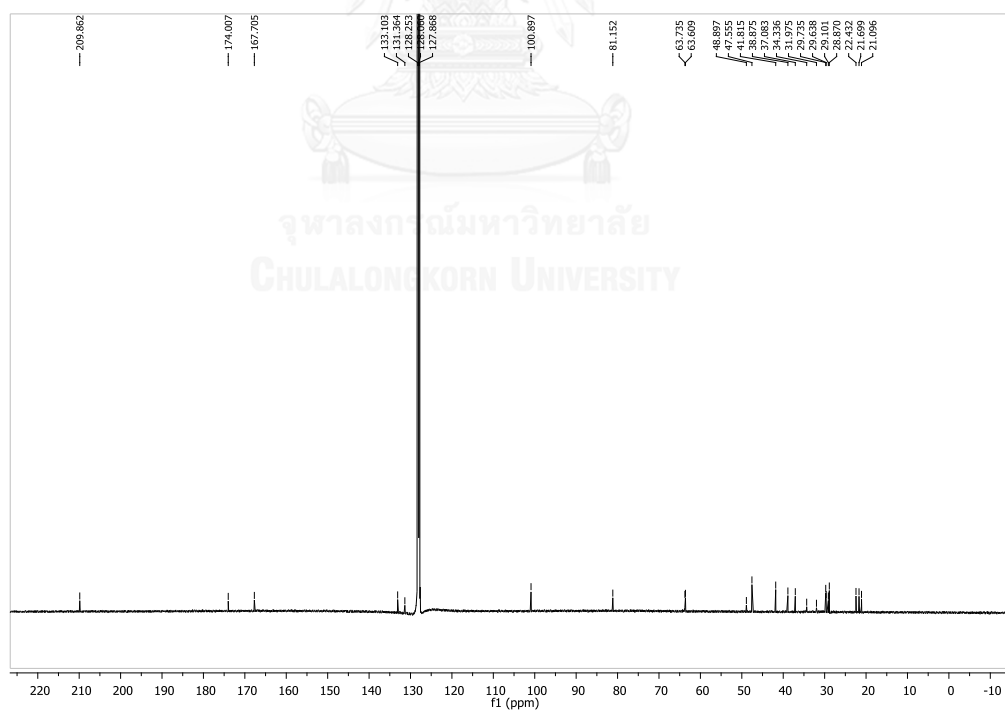


Figure 181. ^{13}C NMR spectrum of 6-1a (C_6D_6)

VITA

Education:

2014 Ph.D. (Organic Chemistry, Chulalongkorn University)

2009 M.Sc. (Organic Chemistry, Chulalongkorn University)

2007 B.Sc. (Chemistry, Chulalongkorn University)

Scholarships:

2010-2014 The Royal Golden Jubilee Ph.D. Program

2007-2009 The Graduate School of Chulalongkorn University

Publications:

1. Worawalai, W.; Wacharasindhu, S.; Phuwapraisirisan, P. Amine-liked diquercitols as new α -glucosidase inhibitors. *Bioorganic and Medicinal Chemistry Letters*. DOI: 10.1016/j.bmcl.2014.09.064.
2. Worawalai, W.; Wacharasindhu, S.; Phuwapraisirisan, P. Synthesis of new N-substituted aminoquercitols from naturally available (+)-proto-quercitol and their α -glucosidase inhibitory activity. *Med. Chem. Commun.* 2012, 3, 1466-1470.
3. Worawalai, W.; Rattanangkool, E.; Vanitcha, A.; Phuwapraisirisan, P.; Wacharasindhu, S. Concise synthesis of (+)-conduritol F and inositol analogues from naturally available (+)-proto-quercitol and their glucosidase inhibitory activity. *Bioorganic and Medicinal Chemistry Letters* 2012, 22, 1538-1540.
4. Wacharasindhu, S.; Worawalai, W.; Rungprom, W.; Phuwapraisirisan, P. (+)-proto-Quercitol, a natural versatile chiral building block for the synthesis of the α -glucosidase inhibitors, 5-amino-1,2,3,4-cyclohexanetetrols. *Tetrahedron Letters* 2009, 50, 2189-2192.
5. Sichaem, J.; Worawalai, W.; Tip-Pyang, S. Chemical constituents from the roots of *Nauclea orientalis*. *Chemistry of Natural Compounds* 2012, 48, 827-830.
6. Sichaem, J.; Ruksilp, T.; Worawalai, W.; Siripong, P.; Khumkratok, S.; Tip-Pyang, S. A new dimeric aporphine from the roots of *Artabotrys spinosus*. *Fitoterapia* 2011, 82, 422-425.